Control of agent swarms in random environments

THÈSE N^{O} 6946 (2016)

PRÉSENTÉE LE 15 AVRIL 2016
À LA FACULTÉ DES SCIENCES ET TECHNIQUES DE L'INGÉNIEUR
LABORATOIRE DE PRODUCTION MICROTECHNIQUE
PROGRAMME DOCTORAL EN ROBOTIQUE, CONTRÔLE ET SYSTÈMES INTELLIGENTS

ÉCOLE POLYTECHNIQUE FÉDÉRALE DE LAUSANNE

POUR L'OBTENTION DU GRADE DE DOCTEUR ÈS SCIENCES

PAR

Guillaume Adrien SARTORETTI

acceptée sur proposition du jury:

Prof. A. Martinoli, président du jury
Prof. M.-O. Hongler, directeur de thèse
Prof. R. Filliger, rapporteur
Prof. M. A. Hsieh, rapporteuse
Prof. C. Pfister, rapporteur

ÉCOLE POLYTECHNIQUE
FÉDÉRALE DE LAUSANNE
Suisse
2016

Coming together is a beginning;
keeping together is progress;
working together is success.

— Henry Ford.

To Anna, my Parents and Julie.

Abstract

The collective dynamic behavior of large groups of interacting autonomous agents (*swarms*) have inspired much research in both fundamental and engineering sciences. It is now widely acknowledged that the intrinsic nonlinearities due to mutual interactions can generate highly collective spatio-temporal patterns. Moreover, the resulting self-organized behavior cannot be simply guessed by solely investigating the elementary dynamic rules of single individuals. With a view to apply swarm collective behaviors to engineering, it is mandatory to thoroughly understand and master the mechanism of emergence to ultimately address the basic question: *What individual dynamics and what type of interactions generate a given stable collective spatio-temporal behavior ?* The present doctoral work is a contribution to the general common effort devoted to give an engineering operational answer to this simple and yet still highly challenging question.

Swarms modeling is based on the dynamic properties of multi-agents systems (MAS). Methodological approaches for studying MAS are i) mathematics, ii) numerical simulation and iii) experimental validation on physical systems. While in this work we strive to construct and analytically solve new classes of mathematical MAS models, we also make a very special effort to develop new MAS modeling platforms for which one is simultaneously able to offer exact analytical results, corroborate these via simulation and finally implement the resulting control mechanism on swarms of actual robots.

In full generality, MAS are formed by mutually interacting autonomous agents evolving in random environments. The presence of noise sources will indeed be unavoidable in any actual implementation. This drives us to consider coupled sets of stochastic nonlinear differential equations as being the natural mathematical modeling framework. We first focus on the simplest situations involving homogeneous swarms. Here, for large homogeneous swarms, the mean-field approach (borrowed from statistical physics) can be used to analytically characterize the resulting spatio-temporal patterns from the individual agent dynamics. In this context, we propose a new modeling platform (the so-called mixed-canonical dynamics) for which we are able to fully bridge the gap between pure mathematics and actual robotic implementation.

In a second approach, we then consider heterogeneous swarms realized either when one agent behaves either as a leader or a shill (i.e as an infiltrated agent), or when two different sub-swarms compose the whole MAS. Analytical results are generally very hard to find for heterogeneous swarms, since the mean-field approach cannot be used. In this context, we use recent results in rank-based Brownian motions to approach some heterogeneous MAS models. In particular, we are able to analytically study i) a case of soft control of the swarm by a shill agent, and ii) the mutual interactions between two different societies (i.e., sub-groups) of homogeneous agents. Finally, the same mathematical framework enables us to consider a class of MAS where agents mutually interact via their environment (stigmergic interactions). Here, we can once again simultaneously present analytical results, numerical simulations and to ultimately implement the controller on a swarm of robotic boats.

Keywords: multi-agent system, Brownian agent, homogeneous swarm, heterogeneous swarm, leader-based control, soft control, analytical results, numerical simulation, experimental validation.

Résumé

La dynamique collective de sociétés d'agents autonomes (*essaims* d'agents) suscite un grand intérêt du point de vue de la recherche en sciences fondamentales et appliquées. Il est avéré que les non-linéarités dues aux interactions mutuelles entre les agents peuvent engendrer des motifs collectifs au niveau de l'essaim. Cependant, le comportement auto-organisé qui en résulte ne peut pas être simplement deviné ou déduit par l'analyse seule des comportements individuels. Afin d'utiliser ces comportements émergents dans le domaine de l'ingénierie, il est nécessaire de maîtriser le concept d'émergence afin d'être en mesure de déduire : *Quelle dynamique individuelle, associée à quel type d'interactions, permet-elle de créer un motif stable souhaité au niveau de la société ?* La présente thèse contribue à l'effort dédié à la résolution de ce défi.

La modélisation d'essaims est basée sur les propriétés dynamiques des systèmes multi-agents (MAS). Les différentes approches utilisées dans l'étude des MAS sont i) l'appel aux mathématiques, ii) l'utilisation de simulations numériques et iii) la validation expérimentale sur des systèmes physiques. Dans ce travail, nous nous efforçons de construire et d'étudier analytiquement de nouvelles classes de MAS, tout en mettant l'accent sur la construction de nouveaux modèles pour lesquels il est possible de simultanément obtenir des résultats analytiques, corroborer ceux-ci par des simulations numériques, et finalement implémenter le méchanisme de contrôle résultant sur un essaim de robots.

En toute généralité, les MAS sont formés d'agents autonomes, qui interagissent et évoluent dans un environnement aléatoire. La présence de bruit est propre à tout système physique. Un cadre naturel consiste à modéliser nos MAS en termes de systèmes d'équations différentielles stochastiques couplées. Par simplicité, nous considérons d'abord de larges essaims homogènes, pour lesquels l'approche en champ moyen (*mean-field approach*, inspirée de la physique statistique) nous permet de caractériser analytiquement les motifs au niveau de l'essaim à partir de la connaissance de la dynamique d'un agent. Dans ce cadre, nous construisons une nouvelle plateforme de modélisation (dynamique mixte canonique-dissipative), pour laquelle nous sommes en mesure de conduire simultanément l'analyse théorique et l'implémentation robotique sur des robots mobiles.

Nous étudions ensuite des systèmes hétérogènes plus généraux, à savoir ceux comprenant soit i) un agent prenant le rôle de *leader* ou de *shill* (i.e., agent infiltré), soit ii) deux différentes sous-sociétés formant le MAS. Ici, l'obtention de résultats analytiques est en général plus complexe – l'approche en champ moyen ne pouvant en effet pas être utilisée. Des résultats récents obtenus dans le contexte des systèmes de mouvements Browniens ordonnés (*ranked-based Brownian motions*) nous permettent d'approcher analytiquement certains MAS hétérogènes. En particulier, nous sommes en mesure d'étudier i) un cas de *soft control* (contrôle d'un essaim par l'utilisation d'un agent infiltré), et ii) un modèle d'interactions mutuelles entre deux sociétés (i.e., sous-groupes) différentes d'agents homogènes. Le même cadre formel nous permet enfin de considérer une classe de MAS avec interactions mutuelles via l'environnement (interactions stigmergiques). Là encore, nous sommes en mesure de présenter à la fois des résultats analytiques, des simulations numériques et une validation expérimentale du modèle sur un essaim de bateaux robotiques.

Mots clefs : système multi-agents, agent Brownien, essaim homogène, essaim hétérogène, contrôle par leader, soft control, résultats analytiques, simulation numérique, validation expérimentale.

Zusammenfassung

Das kollektive dynamische Verhalten großer Gruppen (*Schwärme*) interaktiver, autonomer Alleinvertreter (Individuen) erweckt heuttzutage ein grosses Interesse in Forschungtätigkeit sowohl in den Grundlagen- als auch in den Ingenieurwissenschaften. Es ist nun allgemein akzeptiert, dass intrinsische Nichtlinearitäten aufgrund gegenseitiger Wechselwirkungen kollektive raum-zeitliche Muster erzeugen können. Allerdings kann das resultierende selbstorganisierte Verhalten nicht einfach durch Untersuchen der elementaren dynamischen Regeln der einzelnen Individuen erraten werden. Hinsichtlich technischer Anwendung des schwarmkollektiven Verhaltens ist es zwingend notwendig den Mechanismus hinter dessen Entstehens gründlich zu verstehen und zu beherrschen, um schließlich die grundlegende Frage beantworten zu können: *Welche individuelle Dynamik und welche Art von Wechselwirkungen ermöglichen das Erzeugen des gewünschten stabilen Verhalten?* Die vorliegende Doktorarbeit versteht sich als Beitrag zu den Anstrengungen welche allgemein unternommen werden, um eine Ingenieur-operative antwort auf diese einfache und doch sehr herausfordernde Frage zu erhalten.

Schwarmmodellierung basiert sich auf den dynamischen Eigenschaften von Multiagentsystemen (MAS). Methodische Ansätze für das Studium von MAS beinhalten i) mathematische Methoden, ii) numerische Simulationen und iii) experimentelle Validierung auf Grund physikalischer Systemen. In der vorliegenden Arbeit bemühen wir uns neue Klassen mathematischer MAS-Modelle zu konstruieren und analytisch zu lösen. Ebenso konzentrieren wir uns darauf neue MAS-Modellierungsplattformen zu entwickeln, welche uns erlauben sollten simultan exakte analytische Ergebnisse zu erhalten, diese mittels Simulationen zu bestätigen und schließlich den resultierenden Steuermechanismus auf Schwärme von Robotern anzuwenden.

Ganz allgemein bilden sich MAS durch wechselwirkende autonome Alleinvertreter die sich in zufälliger Umgebungen entwickeln. Rauschquellen sind in einer realistischen Implementierung zu berücksichtigen. Dieser Umstand bedeutet gekoppelte stochastische, nichtlineare Differentialgleichungen als den geeignete Rahmen für die mathematische Modellierung zu bevorzugen. Wir konzentrieren uns zunächst auf den einfachsten Fall homogener Schwärme. In diesem Fall kann für große homogene Schwärme der Ansatz der gemittelten Felder (*mean-field approach*, aus der statistischen Physik entlehnt) angewandt werden, um das raumzeitliche Muster, welches sich aus der Dynamik der einzelnen Alleinvertreter ergibt, analytisch zu charakterisieren. In diesem Rahmen schlagen wir einen neuen Modellierungsansatz vor

(die sog. gemischt kanonische Dynamik) welche es uns ermöglicht ein Brücke zwischen reiner Mathematik und tatsächlich robotischer Implementation zu schlagen.
In einem zweiten Fall betrachten wir heterogene Schwärme in welchen entweder ein Alleinvertreter als *Führer* oder als *shill* (d.h. als infiltrierter Agent) auftritt, oder zwei Unterschwärme einen vollständigen MAS bilden. In der Regel sind analytische Ergebnisse für heterogene Schwärme sehr schwierig zu finden, da der Ansatz der gemitteltem Felder nicht verwendet werden kann. In diesem Zusammenhang nutzen wir jüngste Ergebnisse aus der *rank based Brownschen Bewegungen* Theorie, um sich einigen heterogenen MAS-Systemen anzunähern. Insbesondere sind wir in der Lage i) einen Fall *schwacher Steuerung* des Schwarms durch einen shill Agenten und ii) die gegenseitigen Wechselwirkungen zwischen zwei verschiedenen Gesellschaften (das heißt, Untergruppen) von homogenen Alleinvertreter analytisch zu studieren. Schließlich ermöglicht uns derselbe mathematische Rahmen eine Klasse von MAS zu betrachten, in welcher die Agenten gegenseitig über ihre Umwelt (stigmergic interaction) in Wechselwirkung treten. Für diesen Fall können wir ebenfalls gleichzeitig analytische Resultate, numerische Simulationen und die Implementation der Steuerung auf einem Schwarm von Roboter-Booten präsentieren.

Stichwörter: Multiagentensystem, Brownscher Agent, homogener Schwarm, heterogener Schwarm, Führer-basierte Steuerung, Soft-Steuerung, Analyseergebnisse, numerische Simulation, experimentelle Validierung.

Sommario

La dinamica collettiva di società di agenti autonomi (*sciami di agenti*) suscita un grande interesse dal punto di vista della ricerca nelle scienze fondamentali e applicate. Si è verificato che le non-linearità in seguito alle interazioni mutuali tra gli agenti possono provocare dei motivi collettivi a livello dello sciame. Nel frattempo, il comportamento auto-organizzato risultante non può essere facilmente indovinato o dedotto solo dall'analisi dei comportamenti individuali. Per utilizzare comportamenti emergenti nel campo dell'ingegneria, è necessario controllare il concetto di emergenza per essere in grado di dedurre: *Quale dinamica individuale e quale tipo di interazioni permette di creare un motivo stabile desiderato a livello della società?* La presente tesi contribuisce allo sforzo dedicato alla risoluzione di questo quesito.

La modellazione di sciami si basa sulle proprietà dinamiche dei sistemi multi-agenti (MAS). I diversi approcci utilizzati nello studio dei MAS sono i) il ricorso alla matematica, ii) l'uso di simulazioni numeriche e iii) la validazione sperimentale sui sistemi fisici. In questo lavoro, ci sforziamo di costruire e studiare analiticamente nuove classi di MAS, mettendo l'accento sulla costruzione di nuovi modelli per i quali è possibile simultaneamente ottenere risultati analitici, corroborarli con simulazioni numeriche, e finalmente implementare il modello su uno sciame di robot.

In generale, i MAS sono formati da agenti autonomi che interagiscono mutualmente ed evolvono in un ambiente aleatorio. La presenza di rumore è propria a qualsiasi sistema fisico. Un contesto naturale consiste nel modellizzare i nostri MAS in termini di sistemi di equazioni differenziali stocastiche. Per semplicità, consideriamo innanzitutto larghi sciami omogenei, per i quali l'approccio del campo medio (*mean-field approach*, ispirata dalla fisica statistica) ci permette di caratterizzare analiticamente i motivi a livello dello sciame a partire dalla conoscenza della dinamica di un agente. In questo contesto, costruiamo une nuova piattaforma di modellazione (la cosiddetta dinamica mista canonica-dissipativa), per la quale siamo in grado di condurre simultaneamente l'analisi teorica e l'implementazione robotica su robot mobile.

Studiamo poi sistemi eterogeni più generali, vale a dire quelli che includono i) un agente nel ruolo di *leader* o *shill* (cioè, agente infiltrato), o ii) due sotto-società differente formando il MAS. In questo caso, l'ottenimento di risultati analitici é in generale più complessa, dato che l'approccio del campo medio non puo' essere utilizzata Risultati recenti ottenuti nel contesto dei sistemi di moti Browniani ordinati (*ranked-based Brownian motions*) ci permettono di avvicinare analiticamente certi MAS eterogeni. In particolare, siamo in grado di studiare i) un caso di *soft control* (controllo di uno sciame per l'utilizzazione di un agente infiltrato), e ii) la mutua interazione tra due differenti sotto-gruppi che formano il MAS. Infine, lo stesso contesto formale ci permette di considerare una classe di MAS dove gli agenti interagiscono mutualmente attraverso l'ambiente (interazioni stigmergiche). Di nuovo, siamo in grado di presentare sia risultati analitici che simulazioni numeriche e una validazione sperimentale del modello su uno sciame di navi robotiche.

Parole chiave: sistema multi-agenti, agente Browniano, sciame omogeno, sciame eterogeno, controllo da un leader, soft control, risultati analitici, simulazione numerica, validazione sperimentale.

Acknowledgments

A thesis is never the work of a single person and I would like to thank here the people who helped me make this incredible journey possible and enjoyable.

First and foremost, I would like to express my special thanks to Max-Olivier Hongler, without whom none of this would have been possible. Max offered me the opportunity of this thesis around a very nice meal (at Copernic's) four years ago, and I will never forget this day. Since then, he has always been there for me, to share his ideas and to listen to mine, to criticize my work but also to congratulate my achievements, and most of all to help me succeed. I was once advised to choose a thesis advisor over choosing a thesis subject, since you can always change your subject but are stuck with your advisor for four years. Max has proven to be a first class choice in this sense. I spent four amazing years collaborating with Max, slightly changing the thesis' direction multiple times, but never getting tired of learning from and with him. Thank you very much for being there for me during all these years and for everything you taught me! I will miss our passionate discussions very much!

I would also like to extend my gratitude to some of Max's former PhD students, whom I had the chance of meeting, and who helped me during my thesis. I would like to warmly thank Roger Filliger, with whom Max and I had so many work sessions, talking about our current research, or discussing possible future works. Roger has always been extremely positive towards my work, and has greatly helped me believe in myself and in what I was doing. He proofread everything that I wrote, has given excellent critics and remarks, and has often offered very interesting new directions for our research. Thank you very much for your presence and your help Roger!
I also would also like to thank Julio Rodriguez with whom I shared an office for the first year of my thesis. I valued all the many discussions we had about work, personal matters, as well as every piece of advice he gave me (and that helped me since then). Finally, I only met Olivier Gallay a couple of times, but his own thesis, which is exceptionally well written and presented, has been an important source of inspiration for my own work.

I would like to warmly thank Professor M. Ani Hsieh, from Drexel University, for her precious help during the course of my thesis. Thank you for inviting me into your laboratory, for all the excellent advice you gave me and for your help during the research that led to the writing (and publication) of Chapter 8! These weeks in Pennsylvania were an amazing experience, and

I would also like to thank her students at the Scalable Autonomous System laboratory, who made me feel welcome and always helped me: Dhanushka, Dan, Hadi and Hyunjoo. An extra special thank you is in order for Sam, a visiting student at the SAS lab, who helped me with the experimental implementation, running experiments during countless hours over the course of several months!

When I joined the laboratory, I was immediately welcomed by the people working here. I would like to personally thank Professors Jacques Jacot and Peter Ryser for their support during my thesis, and Miss Karine Genoud for her help with the administrative matters related to my work. I would like to warmly thank the member of my thesis jury: Professors Roger Filliger, M. Ani Hsieh, Charles Pfister and Alcherio Martinoli, for their careful proofreading of my manuscript. Their detailed comments and remarks, along with the discussions we had about my work, helped improve the quality of this thesis.

Next, I would like to thank each person I shared an office with over the years: Julio, Nao, Jérémy, David, Csaba, Karim and Eric. At first, I was happy to be able to work quietly, alone in my office, but quickly learned to enjoy the presence of other people. We had many discussions about my work, and I discovered how much explaining things to people unfamiliar with what we do can really help. I would like to especially thank David, Jérémy and Csaba for all those moments they lent me their full attention, leading to several important results in my thesis. Huge thanks to my coworkers here at the lab (aka “Team Castor”) for all the fun times we had over the years, either “apéros” here at the office or at Sat’, or lunch breaks watching YouTube videos.

These four years at EPFL also allowed me to meet amazing people from other labs. I would like to thank the people from the LSRO lab for all the fun tea times we shared: Christophe, Philippe, Frank, Florian, Michael and Mariza. My best encounter in the university was without any doubt Fanny, whom I owe many mind-blowing discoveries, such as Bollywood movies, absurd YouTube videos and crazy food, to cite only a couple of them. Fanny, I hope I have been able to support you throughout your thesis as much as you did during mine. Thank you very much for your friendship and support!

Outside from the university, my warmest gratitude goes to my closest family and to Anna. My parents have supported me and pushed me forward since I was little; they helped me achieve great things, by not forcing great goals onto me. They made me curious about the world, about maths and sciences, and trusted me to make the best from this curiosity. They are the source of that sound advice that encouraged me to do a thesis under Max’s supervision, and I am eternally grateful for their wisdom, in this matter and in so many more. My thanks go to my sister Julie too, on whom I can always count, and who knows how to cheer me up no matter what happened. My family has helped me achieve my goals and has been there either to celebrate my successes, or to support me when things did not go my way. Thank you for your unconditional love and support!

Anna is the best thing that ever happened to me, and that is continuing to happen every single day since nearly seven years. Despite her background being very different to mine (medicine), she has always found both the time and the pleasure to listen to my focus of the moment, and has very often come up with new ideas and even solutions to my problems. She has permanently supported me during this thesis, driving me to the lab on weekends, joining me for conferences, proofreading my papers, providing moral support or “kicking my butt” (depending on what I needed). Thank you for being there, and for being so important!

I would also like to extend my warmest thanks to her parents, András and Erzsi, who welcomed me in their family with open arms. Thank you for supporting me, proofreading some of my papers and general writing, and for your amazing cooking!

As additional moral supporters, I would like to thank my closest friends from my school years: Sarah, Johanna, Géraldine, Jonathan, Alexandre, Bruno, Antoine, Flavio, Quentin, Marisa and Jeremy. Those friends have seen me grow throughout the years, and I am extremely grateful for their never-ending friendship and presence. Thank you for all the good memories together, and for all the trips we took together!

A special extra thank you to Flavio for his help with the calculation of Eq.(7.9) in Chapter 7!

An other extra thank you to Bruno and his father Giacomo, for the translation of the thesis' abstract in Italian! Thank you very much to Oskar Steiner, for the translation of the thesis' abstract in German!

Finally, on an unrelated and more personal note, I would like to grant virtual thanks to famous figures (whom I sadly do not know personally (yet?)), who have also brought me some sort of moral support throughout my life. I would like to thank Natalie Portman (Baird et al. (2002)), Emilia Clarke, Deepika Padukone, Alia Bhatt, Mila Kunis, Shauna Coxsey and Ashley Eckstein. Mainly for their voices, which have supported me throughout the thesis, I would also like to extend my gratitude to Ashleigh Ball, Tara Strong, Andrea Libman, Kazumi Evans, Britt McKillip and Rebecca Schoichet.

Lausanne, March 8th, 2016 Guillaume Sartoretti

Contents

Abstract (English/Français) i

Acknowledgments ix

List of figures xvii

List of tables xxiii

I Introduction 1

Introduction 3

- United We Stand 3
- Modeling a Group 4
  - What is an Agent ? 5
  - Multi-Agent Systems 7
  - Brownian Agents 8
- Controlling a Group 9
  - Planned Control 10
  - Real-Time Control 10
- State of the Art 12
  - Homogeneous Swarms of Agents 12
  - Hard Control of Swarms 14
  - Soft Control of Swarms 15
- Thesis Outline 15
  - Original Contributions of the Thesis 16

II Planned Control 19

1 Self-Organized Mixed Canonical-Dissipative Dynamics for Brownian Planar Agents 21

- 1.1 Introduction 21
- 1.2 Interacting Brownian Agents Driven by Canonical-Dissipative Dynamics and White Gaussian Noise 23
- 1.3 Numerical Experiments 29

1.4 Generalization 29
1.5 Conclusions and Perspectives 31
1.6 New Contributions of Chapter 1 33

2 Decentralized Self-Selection of Swarm Trajectories: From Dynamical Systems Theory to Robotic Implementation 35
2.1 Introduction 35
2.2 Mathematical modeling 39
  2.2.1 Single agent dynamics 39
  2.2.2 Multi-agent dynamics 41
2.3 Robotic implementation 44
  2.3.1 Braitenberg control mechanism 44
  2.3.2 Physical implementation on e-puck robots 47
  2.3.3 Dictionary theoretical model-robotic implementation 51
  2.3.4 Experimental validation 52
  2.3.5 Experiment Results 53
  2.3.6 Comparison with the theoretical results 55
  2.3.7 Generalization to other Hamiltonian functions 56
2.4 Conclusion 58
2.5 New Contributions of Chapter 2 58

III Leader-Based (Hard) Control 59

3 Leader-Follower Control Mechanism for Planar Robots Evolving in Formation 61
3.1 Problem Statement 61
3.2 Introductory Example: Robotic Train 62
  3.2.1 Braitenberg Control Mechanism 62
  3.2.2 Numerical Simulations 63
  3.2.3 Stability Analysis 64
3.3 Triangular Formation 65
  3.3.1 First Layer - 4 Robots 65
  3.3.2 Extra Layers 66
3.4 New Contributions of Chapter 3 69

4 Nonlinear filtering and heterogeneous swarms of autonomous agents - An exactly solvable model 71
4.1 Introduction 71
4.2 Multi-Agent Dynamics and Feedback Particle Filtering 73
4.3 Finite Dimensional Filtering with Weber Parabolic Functions 76
4.4 Numerical Results 79
4.5 Conclusion 80
4.6 New Contributions of Chapter 4 82

IV Shill-Based (Soft) Control 83

5 Soft Control of Self-Organized Locally Interacting Brownian Planar Agents 85
5.1 Introduction . . . 85
5.2 Interacting Diffusion Processes on $\mathbb{R}^2$ . . . 86
5.3 Swarm Soft Controlling - Harmonic oscillator Hamiltonian . . . 89
5.3.1 Inhomogeneous swarm - Shill soft controlling mode . . . 90
5.4 Conclusion . . . 93
5.5 New Contributions of Chapter 5 . . . 94

6 Soft Control of Swarms - Analytical Approach 95
6.1 Introduction . . . 95
6.2 Rank-Based Brownian Motions - Atlas Model . . . 96
6.3 How Does a Super-Diffusive Fellow Smash Tightness . . . 98
6.3.1 Spatial Dispersion of the Agents . . . 101
6.3.2 Distance Between Successive Agents . . . 102
6.4 Using a Shill to Guide the Collective Crossing of Obstacles . . . 103
6.4.1 Optimal Barycentric Driving for Suitable Choice of β . . . 104
6.4.2 Adjusting the Spatial Dispersion Resolution for a Given Drift g . . . 105
6.4.3 Multi-slots Configurations . . . 106
6.5 Conclusion . . . 107
6.6 New Contributions of Chapter 6 . . . 108

V Strongly Heterogeneous Swarms 109

7 Interacting Brownian Swarms: Some Analytical Results 111
7.1 Introduction . . . 111
7.2 Flocking of Interacting Brownian Agents . . . 113
7.2.1 Rank-Based Brownian Motions (RBMs) . . . 114
7.3 Heuristic Characterization of the Observation Threshold Leading to Cooperative Dynamics . . . 115
7.4 Interactions between Collinear Colliding Swarms . . . 117
7.4.1 Colliding Swarms Driven by Hybrid Atlas Models . . . 118
7.4.2 Colliding Swarms Driven by Modified Hybrid Atlas (MHAM) Dynamics . 120
7.4.3 Numerical Simulations . . . 121
7.5 Conclusions and Perspectives . . . 123
7.6 New Contributions of Chapter 7 . . . 123

8 Distributed Planar Manipulation in Fluidic Environments 125
8.1 Introduction . . . 125
8.2 Problem Statement . . . 126
8.3 Planar Manipulation Under Conditional Forced Caging . . . 127
8.3.1 Distributed Approach and Grasp . . . 127

8.3.2 Computation of the Manipulation Trajectories 131
8.3.3 Numerical Results 135
8.4 Results 137
8.4.1 Experimental Setup 137
8.4.2 Experimental Results 138
8.5 Conclusions and Perspectives 139
8.6 New Contributions of Chapter 8 140

VI Conclusion and Perspectives 143

Conclusion and Perspectives 145

VII Appendices 147

A Chapter 2 - Multi-agent tracking tool 149

B Chapter 4 - Details of Calculations 151
B.0.1 Collection of useful formulas 151
B.0.2 Quadratures 152

VIII Bibliography and Index 155

Bibliography 157

Index 168

Curriculum Vitae 173

List of Figures

1 1941 second world war American propaganda poster. Image in the Public Domain. 3

2 Emergence of strength in a group by self-organization. Art piece from Banksy. . 5

3 Left: Pack of wild dogs, driven by the leading dog. Here the leader is clearly apparent. Right: Robotic shill used to control the decisions of a group of cockroaches in Halloy et al. (2007). Here also the shill is apparent (i.e., easily recognizable by an external observer). 12

1.1 The cylindrical symmetry characterizing the stationary regime implies that the agents probability distribution is rotationally invariant with respect to **O**. Accordingly, there will be on average N/M agents located in a sector with an opening angle $2\pi/M$. For large γ/σ^2, these agents will be confined in the direct proximity of the circle of radius $\mathscr{L}_{s,\rho}$. Let us consider an arbitrary agent located at **A** with a stationary observation range of radius $\rho =$ **AC**. This range exactly encompasses the circular arc with aperture $2\pi/M$ thus ensuring that the agent at **A** has M/N neighboring fellows. The cosine theorem in the triangle **OAC** implies that $\mathscr{L}^2_{s,\rho} = 2\rho^2/[1-\cos(\pi/M)]$ $2\mathscr{L}^2_{s,\rho} = \rho^2/[1-\cos(\pi/M)]$. 28

1.2 For a collection of $N = 200$ agents with $M = 4$, $\rho = 1$ and $\sigma = 0.07$, we explicitly draw the trajectory of a randomly chosen agent. We observe that this agent indeed follows the consensual limit cycling orbit with analytically predicted radius $\mathscr{L}_{s,\rho} = \sqrt{2}\rho = \sqrt{2}$. The observation range of the considered agent (red circle) encompasses exactly the sector of aperture $\pi/4$ to determine the size of the self-generated limit cycle (see the construction given in Figure 1.1). 29

1.3 For a collection of $N = 200$ agents with $M = 4$, $\rho = 1$ and $\sigma = 0.07$, we explicitly draw the trajectory of a randomly chosen agent. We observe that this agent indeed follows the consensual limit cycling orbit with analytically predicted radius $\mathscr{L}^2_{s,\rho} = 2/[1-\cos(\pi/50)] \simeq (50/\pi)^2 \simeq (17)^2$. The observation range of the considered agent encompasses exactly the narrow sector of aperture $\pi/50$ to determine the size of the self-generated limit cycle (see the construction given in Figure 1.1). The High value $M = 50$ is responsible for the sometimes erratic behavior of the agent, as its observation range only encompasses a very small sector of the consensual circle. 30

1.4 Typical shapes of the Cassini's ovals determined by the equation $\mathscr{H}(x_1, x_2) = \left[(x_1-a)^2 + x_2^2\right]\left[(x_1+a)^2 + x_2^2\right] = b^4$ for b-values ranging from $b = 0.6a$ to $1.6a$. Image courtesy of Wikimedia under CC BY-SA 3.0. 32

1.5 Left: Selection of a couple of limit cycling orbits obtained from the Cassini Hamiltonian Eq.(1.21) when the control parameters are set to $M = 4$ and $\rho = 0.4$. In red, the observation range of a randomly picked representative agent. Right: Single limit cycling trajectory for the Cassini Hamiltonian Eq.(1.21) but here with the control parameters set to $M = 4$ and $\rho = 0.8$. 32

1.6 Left: Orbit generated by the $\left(\frac{2\pi}{3}\right)$-symmetric Hamiltonian function: $\mathscr{H}(x_1, x_2) = \left[(x_1-1)^2 + (x_2)^2\right] \cdot \left[(x_1+\frac{1}{2})^2 + (x_2 - \frac{\sqrt{3}}{2})^2\right] \left[(x_1+\frac{1}{2})^2 + (x_2 + \frac{\sqrt{3}}{2})^2\right]$. Here we have $N = 200$ and the control parameters are set to $M = 4$ and $\rho = 0.5$. In red, the observation range of a randomly picked representative agent. Right: Here, all parameters are identical, except for the interaction range which is $\rho = 1$. . . 33

2.1 "Ring"-shaped probability density on the plane, for $\sigma = 0.07$ and $\sigma = 0.35$. These simulations were run with $N = 5000$ agents, up to time $T = 10[s]$, with $\gamma = 1$. . . 41

2.2 Numerical simulation for $N = 200$ agents, $\rho = 1$, $\sigma = 0.07$ and $M = 4$. The black dots show the final position of the agent at time $T = 50[s]$, while the blue line gives the trajectory of one arbitrary agent (with its observation range in red). The black circle (hidden below the swarm of agents) gives the theoretically computed limit cycle. This shows the exactitude of Eq.(2.10), even for finite swarms.
Left: Harmonic oscillator Hamiltonian function $H(X,Y) = \frac{X^2+Y^2}{2}$.
Center: Cassini ovals Hamiltonian function $H(X,Y) = ((X-1)^2+Y^2)\cdot((X+1)^2+Y^2)$, with $\rho = 0.4$, showing closed ovals without connections (see Yates (1947)).
Right: Same Hamiltonian function as the center figure, with $\rho = 0.8$, presenting one connected orbit around both attractors. 44

2.3 Numerical simulation for $N = 200$ agents, $\rho = 1$, $\sigma = 0.07$ and $M = 4$, until time $T = 25[s]$ (left) or $T = 50[s]$ (center and right). In red, the observation range of a randomly picked representative agent.
Left: Hamiltonian function with three attracting poles $H(X,Y) = ((X-1)^2+Y^2)\cdot((X+\frac{1}{2})^2+(Y-\frac{\sqrt{3}}{2})^2)\cdot((X+\frac{1}{2})^2+(Y+\frac{\sqrt{3}}{2})^2)$.
Center: Asymmetric Hamiltonian function $H(X,Y) = (((X-\frac{1}{2})^2+Y^2)\cdot((X+\frac{1}{2})^2+(Y-\frac{\sqrt{3}}{2})^2)\cdot((X+\frac{3}{4})^2+(Y+\frac{\sqrt{27}}{4})^2))^{\frac{1}{3}}$.
Right: Hamiltonian function $H(X,Y) = (((X-1)^2+Y^2)\cdot((X+1)^2+Y^2)\cdot(X^2+(Y-4)^2))^{\frac{1}{3}}$, resulting in two disconnected orbits. 45

2.4 Left: Theoretical robot, seen from above. Note the 8 sensors evenly distributed on the perimeter of the robot's body and the two motors L and R. The point S (resp. U) shows the stable (resp. unstable) facing direction of the light source in the BCM. Right: Actual e-puck robot in the same position; the 8 proximity sensors (ps0,ps1,...,ps7) are nearly evenly distributed on the perimeter. 46

2.5 Schematic of the robot's main programming loop. 50

2.6 Initial positions and headings of the eight robots in each of the 25 experiments. Each circle corresponds to a robot, and the corresponding line denotes the heading. The center cross represents the position of the light source. 53

2.8 Full extracted trajectories of the eight robots through the duration of experiments, for initial conditions 1 (left) and 6 (right). 55

2.9 Average radius/angular speed in the last 15% of each experiment. Left: For each robot. Right: Averaged for the whole swarm. 56

2.10 Order parameter $\mathscr{R}$ of the swarm for each initial situation, averaged over the last 15% of each experiment. 57

2.11 Numerical simulation of the BCM on a swarm of 100 robots, with two light sources located at $(\pm 100, 0)$.
With an observation range of $\rho = 100$, the swarm consensually rotates around both light sources (left), whereas a smaller range of $\rho = 10$ lets the swarm split into two sub-swarms rotating around each light source (right). The trajectory of 10 randomly selected robots are shown, along with the final position of all robots as black dots. 57

3.1 a: Initial state of a swarm of 10 robots (1 leader [in red] and 9 followers) following the dynamics of Eq.(3.2). All robots are initially facing upward. b-d: Selected consecutive states of the swarm through time. During this run, the leader follows a horizontal scripted figure eight, while the rest of the train follows in its path. Distances are displayed in millimeters. 64

3.2 End state of a swarm of 10 robots (1 leader [in red] and 9 followers) following the dynamics of Eq.(3.2) at $T = 60[s]$. During this run, the leader follows a horizontal scripted figure eight, while the rest of the train follows in its path. The choice of $\beta = 32 < 43.19 = \beta_c$ does not enable all robots to remain in formation while they follow the leader. Three robots (red, blue and green lines) ultimately leave the swarm. Distances are displayed in millimeters. 65

3.3 Triangular one-layered formation for 4 robots: 1 leader (in red) and 3 followers (in black). The blue lines represent the angle at which each follower wishes to keep the leader from its heading. All robots are facing upward. 66

3.4 a: Initial state of a swarm of 4 robots (1 leader (in red) and 3 followers) in a one-layered triangular formation. All robots are initially facing upward. b-d: Selected consecutive states of the swarm through time. During this run, the leader follows a horizontal scripted figure eight, while the rest of the train follows in its path. The forward speed of the leader is 12.19 [cm/s], and $\beta = 40 > \beta_c = 32.3$. Distances are displayed in millimeters. 67

3.5 Triangular two-layered formation for 9 robots: 1 leader (in red) and 8 followers (in black). The blue lines represent the angle at which each follower wishes to keep its leading robots from its heading. All robots are facing upward. 68

3.6 a: Initial state of a swarm of 9 robots (1 leader [in red] and 8 followers) in a two-layered triangular formation. All robots are initially facing upward. b-d: Selected consecutive states of the swarm through time. During this run, the leader follows a horizontal scripted figure eight, while the rest of the train follows in its path. The forward speed of the leader is 12.19 [cm/s], and $\beta = 40 > \beta_c = 32.3$. Distances are displayed in millimeters. 69

4.1 Shape of $\mathscr{Y}_B(y)$ (left) and $f_B(y)$ (right) for $B = 0$ (plain line), $B = 0.01$ (stripped line), $B = 0.5$ (stripped-dotted line) and $B = 1$ (dotted line). For $B = 0$, the filtering problem is linear and the dynamics are stable. For $B = 1$, the filtering problem is again linear but with unstable dynamics. In between, we have a nonlinear filtering problem and the conditional probability density changes – with increasing B – from unimodal to bimodal and back to unimodal. 77

4.2 Leader's position $Y(t)$ from Eq.(4.10) (black), along with its unveiled position $\mathscr{Z}(t)$ (red), for $B = 0$, $\sigma = h = 1$ and $t \in [0;5]$. In blue the mean value $\langle Y \rangle_t$ measured from a swarm of $N = 1000$ agents. The particles start with $Y_i(0) = x_0 = 1\ \forall i$, while $Z(0) = Y(0) = x_0$. 80

4.3 Leader's position $Y(t)$ from Eq.(4.10) (black), along with its unveiled position $\mathscr{Z}(t)$ (red), for $B = 1$, $\sigma = h = 1$ and $t \in [0;5]$. In blue the value $\langle Y \rangle_t$ measured from a swarm of $N = 1000$ agents. The particles start with $Y_i(0) = x_0 = 0.1\ \forall i$, while $Z(0) = Y(0) = x_0$. 80

4.4 Leader's position $Y(t)$ from Eq.(4.10) (black), along with its unveiled position $\mathscr{Z}(t)$ (red), for $B = 0.49$, $\sigma = h = 1$ and $t \in [0;8]$. In blue the value $\langle Y \rangle_t$ measured from a swarm of $N = 1000$ agents. The particles start with $Y_i(0) = x_0 = 0.2\ \forall i$, while $Z(0) = Y(0) = x_0$. 81

4.5 Leader's position $Y(t)$ from Eq.(4.10) (black), along with its unveiled position $\mathscr{Z}(t)$ (red), for $B = 0.49$, $\sigma = 5$, $h = 1$ and $t \in [0;8]$. In blue the value $\langle Y \rangle_t$ measured from a swarm of $N = 1000$ agents. The particles start with $Y_i(0) = x_0 = 0.2\ \forall i$, while $Z(0) = Y(0) = x_0$. 81

5.1 Left: An example run with $N = 100$ agents, and a range $\rho = 1$. In black, the theoretic limit cycle, and in blue the positions through time of one agent. Right: Geometric explanation of the computation of $\mathscr{L}_{s,\rho}$: In the stationary regime, each agent has in average $\frac{N}{M}$ agent in her neighborhood. Since the agents are uniformly distributed on the limit cycle, the number of neighbors is directly correlated with the arc length contained within the neighborhood of each agent. Thus, each agent's range exactly encompasses an arc of $\frac{2\pi}{M}$, and the rule of cosine in the triangle OAC leads to the result of Eq.(5.11). 89

5.2 Computation of the time intervals T_1 and T_2 spent by the agents in each of the states of Eq.(5.16). The state 1 starts when SH enters the agent's range (that is when their phase differs by $\frac{\pi}{M}$ in one direction), and lasts until they differ by $\frac{\pi}{M}$ in the other direction. Then, the time interval T_2 lasts until SH re-enters the agent's range, that is when their phases differ of $\frac{2M-1}{M}\pi$. 92

5.3 Top left: In blue, the average angular speed of the regular agents, with in red its average over the period $t \in [50;100]$. In black, the expected value $\omega_{ave} = 0.4$. right: Individual angular speeds of each agent as a function of time. Bottom left: In blue the average radius of the regular agents, and in red the radius of SH. In black, the expected value $\mathscr{L}_{s,\rho} \simeq 1.31$. right: Individual radii of each agent as a function of time. 93

6.1 Probability of spatial repartition of the agents at $t_{end} = 10$, numerical computation over 10^3 runs, with $N = 3$, $g = 1$, $\beta = 1.1 < \beta_c = \frac{3}{2}$. 102

6.2 Left: End position distribution at $t_{end} = 10$, with $N = 3$, $g = 1$, $\beta = 2 > \beta_c$.
Right panel: Probability density of the position at $t_{end} = 10$ for $N = 3$, $g = 1$, $\beta = 4 > N \cdot g$. Both numerical computations include 10^3 runs. 102

6.3 Initial configuration for the soft control problem. The agents start their diffusion at $\left(t_0, y_0\right) = (0,0)$. 104

6.4 Left panel: $N = 10$ agents, $W = 20$ and $D = 10$. Right panel: $N = 20$ agents, $W = 20$ and $D = 50$. 105

6.5 Trajectories for β and g optimal, with $N_d = 3$ doors, under different conditions for the position/width of the doors. 107

7.1 End probability distribution $P(x, T)$ at time $T = 200 > \tau_{\text{relax}} = \frac{\mu_s}{\sigma^2} = \frac{13.58}{1^2}$ of swarms of $N = 500$ agents, with respect to U. Here, all agents initially start at $x_0 = -15$. **(a): tight swarm for $U = 3U_c = 3\mu_S$ (red) and "diffusive evaporating" swarm for $U = \frac{U_c}{3}$ (blue). (b): tight swarm for $U = 2U_c$ (red) and "diffusive evaporating" swarm for $U = \frac{U_c}{2}$ (blue). The respective observation ranges U are depicted at the top of each figure.** 116

7.2 End probability distribution $P(x, T)$ at time $T = \tau_{\text{relax}} = 13.58$ of a swarm of $N = 500$ agents, initially starting at $x_0 = -15$. The observation range $U = U_c = \mu_S$ is depicted at the top of the figure. Notice that the evaporation (*i.e.*, destruction of swarm tightness) does not start before the relaxation time τ_{relax}. 117

7.3 Value of the critical threshold ρ_c, with regard to the swarm size N of the HAM, when $N_1 = N_2$. The asymptotic value $N \to \infty$ of $\rho_c = 3$ is depicted in red. 121

7.4 Value of the critical threshold ρ_c, with regard to the proportion N_1/N of fast agents in the HAM, when $N \to \infty$. 121

7.5 Final distributions $P_{1,2}(x, T)$ and average barycentric speeds $v_{1,2}(t)$ for one realization, in which both societies that start at $x_{0,\{1,2\}} = \mp 15$ achieve flocking. Here, $\rho = 2.5 < \rho_c$, $U = 20 > U_c = 5.4$, $\sigma = 1$ and $N_1 = N_2 = 250$ agents. **(a): distribution of the agents from $\mathscr{S}_1$ (blue) and $\mathscr{S}_2$ (red), at ending time $T = 100$. (b): average barycentric speed of each society, with respect to time.** 122

7.6 Final distributions $P_{1,2}(x, T)$ and average barycentric speeds $v_{1,2}(t)$ for one realization, in which both societies that start at $x_{0,\{1,2\}} = \mp 15$ do not achieve flocking. Here, $\rho = 6 > \rho_c$, $U = 20 > U_c = 2.26$, $\sigma = 1$ and $N_1 = N_2 = 250$ agents. **(a): distribution of the agents from $\mathscr{S}_1$ (blue) and $\mathscr{S}_2$ (red), at ending time $T = 100$. (b): average barycentric speed of each society, with respect to time.** 122

8.1 Example of conditional closure (CC), where the pushing ASVs (black dots) are able to translate and rotate the vessel, with constraints on the translation direction and the rotation pivot. The target points are depicted as blue crosses, and the ASVs' heading vectors as red segments). 127

8.2 Illustration of the system and the relevant quantities needed for the Braitenberg control mechanism. Here, $T = \mathbf{O} = (0,0)$. The vessel (blue rectangle) and an ASV (black dot) located at position (x, y). The heading h of the ASV is illustrated in red, and its angular position α in black. A desired angle ϕ, defining the desired difference between α and h, is depicted in blue. 128

8.3 Typical shape of the spiral of Eq.(8.4), with $r_\pi = 1$. Here, we make the substitution $\theta = arcmin(\alpha, \frac{\pi}{2})$, meaning that both axes are simply switched. 130

8.4 Initial (left) and final (right) positions, and trajectories, of a swarm of $N = 10$ agents following Eq.(8.8) without noise. Here, $\sigma^2 = \frac{1}{2}$. Notice the trajectories following the spiral-shape of Eq.(8.4). 132

8.5 Example trajectory where α_1 must be corrected (left), and the corrected trajectory using Eq.(8.15) (right). The initial and final states of the vessel are shown in black. 134

8.6 Selected successive states of the system during a numerical simulation of the approach and push phases. Here, a swarm of $N = 4$ ASVs (black dots) push the large vessel (black rectangle) towards the final position $\{x_f, y_f, h_f\} = \{55, -95, 0.1\}$ (red rectangle). 136

8.7 Complete trajectories of a swarm of $N = 8$ ASVs (back dots), moving a vessel to its final position (red rectangle). The vessel is initially positioned at $\{x_0, y_0, h_0\} = \{0, 0, 0\}$. The two circles' centers, and the intermediate switching point, are depicted as black crosses. 137

8.8 Key successive states during an experimental run of the presented control mechanism with $N = 4$ boats. The trajectories (colored lines) of the boats (black dots), are depicted, along with the plank's current position (black rectangle) and its final desired state (red rectangle). During the approach phase, the boats' targets along the plank's side are plotted as colored crosses. During the push phases, the circle centers and intermediate switching points are illustrated as black crosses. 139

8.9 Key successive states during an experimental run of the presented control mechanism with $N = 4$ boats. Initial position of the boat (black rectangle); final desired state (red rectangle). The circles centers, and the intermediate switching point, are depicted as blue crosses. Caging position obtained by the boats after the approach phase (8.9a). Start of the pushing phase (8.9b), switch between both circles (8.9c), and stopping point of the boats (8.9d). 140

8.10 Minimal error on the position (red) and corresponding error on the orientation (blue) during the 12 experimental trials. The respective mean errors are depicted as dotted lines. 141

List of Tables

1 Structure of the thesis. 16

2.1 Theoretical and robotics implementations of the main control mechanisms in our model, and their respective control parameter(s). 51

Introduction Part I

Introduction

United We Stand

"*United we stand*" is a historical saying, having been often used as a motto by nations/states or political causes. It means that groups of individuals can achieve more together than what single individuals can on their own. The full expression is usually quoted as "*United we stand, divided we fall*": only by working together can individuals achieve critical goals. The power of coherent groups – where individuals work together toward the same goal(s) – is well known, and has been repetitively demonstrated throughout history and in the scientific literature. For example, Figure 1 shows a 1941 second world war American propaganda poster, featuring the full expression of the saying. Like always, collective power can either be used to do good or evil. In the subsequent sections, we warn the reader that we will only consider group control neutrally, as a way of enhancing a group's performance (i.e., regardless of the nature of the group's objective).

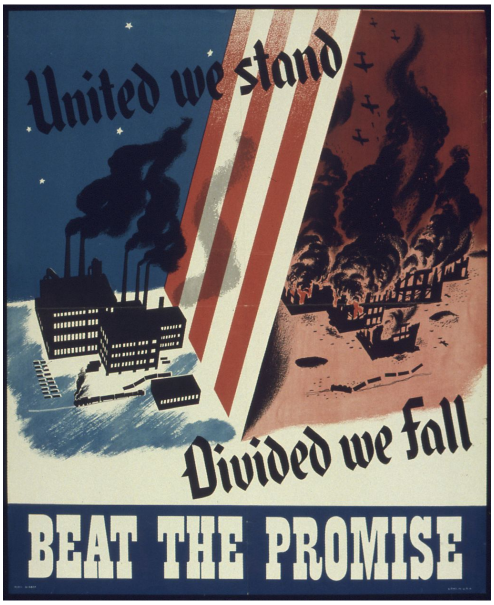

Figure 1 – 1941 second world war American propaganda poster. Image in the Public Domain.

Groups dynamics – i.e., how a group acts, with regard to the behavior of its individuals – is an active research topic. Group dynamics have often been studied theoretically using a variety of tools, such as those offered by stochastic theory and dynamical systems. Other more recent approaches include numerical and experimental simulations. Theoretical models are either constructed based on actual observations or measurements, or devised to obtain relevant group behaviors. The theory of group behavior is strongly tied with other sciences, to cite a restricted selection:

- In ethology, the dynamics of groups of social animals are studied. Theoretical models, constructed from observations of actual animals, are constructed and then validated against data obtained from real populations. Each animal society has its own hierarchy and rules, making each population singular in its essence. Interactions between groups of animals can also be considered, for example, in situations of predation or territorial concurrence. The case of a pride of lions attacking a herd of wildebeest can be studied by considering one global group encompassing both types of individuals. In this heterogeneous group, the two types of individuals – namely, the lions and the wildebeests – obviously have opposite goals.

- In sociology, human groups are the main focus. Humans, are social primates, but have remained strongly individualist. It is more difficult for them than for animals to be part of a coherent group. Humans feel that they need to sacrifice a part of their self to let the group's needs stand before their own, even though they know the power of standing united. Human crowds are often studied with that essential individuality in mind, which differs from animal groups. Researches in crowd behavior have, for example, been used to help optimize public spaces by studying the trajectories of pedestrians. One can use the knowledge obtained from the study of a given crowd in order to control it. Crowd control is a powerful tool, which can be constructively used, for example to help define and test emergency scenarios. It can also be used destructively to break cohesion in crowds or influence voting pools unnoticed.

- In robotics, swarm robotics in particular, many control mechanisms are devised to allow a group of robots to work together on completing a given task. Swarm robotics often takes its inspiration from the fields of ethology or crowd study/control. Recent studies, at the frontier between robotics and ethology, study the possibility to infiltrate (and sometimes control) animal groups by using robots, recognized as fellows by the animals. Contrary to sociology and ethology, robotics control mechanism, defining the behavior of the individuals, are usually constructed (i.e., not modeled after observed behaviors). This allows to test individual behaviors, and discover if they lead to interesting behaviors at the group level. This can sometimes help validate theoretic models of ethology or sociology.

Modeling a Group

To begin the theoretic study of groups of individuals, we need a way to represent those groups. Two different approaches can be followed: the macro- and microscopic representations of groups. Macroscopically, a group is effectively simplified to a single entity. This entity is obtained by grouping the individuals contained within. This aggregation is similar to a complex solid, which can sometimes be simplified to a single point in physics. The main drawback with this simplified approach is the fact that we lose information about each individual in the group, in particular the swarm's distribution.

This is the reason why, in this thesis, we will systematically follow the **microscopic representation** of groups.

In this representation, a group is built upon the behaviors of its individuals. This approach allows a more faithful representation of reality, taking into account each individual's contribution into the group's dynamic.

However, since we have chosen to represent a group at the level of its most basic constituents – the individuals –, it is more difficult to discuss the whole group's dynamic. In the microscopic representation, we are interested in determining a group's behavior from the knowledge of its constituents' behavior. In other words, we are looking for emerging patterns that may arise from the individuals' behaviors, at the group level. **Emergence** is defined by the possibility that a group exhibits a property that the individuals contained within do not. Emergence is a perfect example of "*United we stand*": no individual possesses a property on its own, but working together the whole group does.

These emergent properties come from the fact that the individuals are able to work together. Interactions between the individuals allow them to synchronize and create a coherent group dynamic. Figure 2 shows a street art from Banksy, illustrating how self-organization within a group can effectively lead to greater strength. The capability to interact with the other individuals is the foundation of the concept of **agent**.

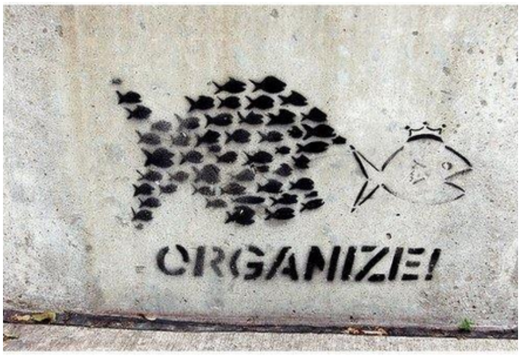

Figure 2 – Emergence of strength in a group by self-organization. Art piece from Banksy.

In this thesis, we will systematically consider groups of agents, capable of interacting with one another, creating emergent group properties.

What is an Agent ?

An agent is an individual of a group, that has an autonomous decision capability, and which can communicate with his fellow agents. The concept of agent is opposed to that of **particle**, which is an individual which simply follows a given dynamic. A particle does not take any decision, and does not communicate with other particles. An important capacity of an agent is that of being able to make decisions, based on the other agents' states and on the environment.

As an illustration of this critical difference, consider a portion of the ocean, where fish and plankton live. In this illustration, the plankton can be simplified as particles, whereas fishes are better modeled as agents. Fish and plankton are influenced by the movement of the mass of water, and can feel the influence of tides or underwater currents. But whereas the plankton can only derive, driven by their environment, fishes have a capability to decide in which direction to swim. Ultimately, a strong enough current cannot be countered by the fishes, but in general, they will enjoy a far greater freedom of movement than plankton. Contrary to the plankton, the fishes will also be able to interact with their fellows, for example to remain schooled with them. For example, each fish can adapt its direction and speed to remain with its fellows, effectively creating a group that will give him a greater chance for survival.

Two large families of agents exist, namely, the **deliberative** and **reactive** agents. A deliberative agent has a planned behavior, which results from its thorough examination of the environment and the task at hand. After constructing its plan, it simply carries it out. A reactive agent, on the other hand, does not have a fully planned behavior, but a set of rules defining how to react to external stimuli. It will follow a nominal dynamic, and mainly react to environmental changes or interactions with its fellows.

Imagine that you are working for a delivery company, and that your task for the day is the delivery of packages to different addresses in a city. You could follow a deliberative planning: you would take some time and come up with a perfect itinerary for the delivery. This itinerary would be based on a thorough study of the city map, and on information received from other drivers in the city. You would finally stick to your carefully planned journey, only deviating from it if you encounter bad traffic or an accident for example. On the other hand, the reactive planning would be to directly start driving to the first address. You would then adapt your itinerary as you drive, based on the traffic conditions you encounter and on the information you receive from other drivers.

In general, you cannot prove than one behavior performs better than the other (with regard to the underlying swarm objective function), and the choice between the two must be made depending on the task at hand and the variability of the environment. If the environment is unpredictable, reactivity will let you better deal with it, whereas in more stable environment, following a carefully planned behavior can be more suitable. The difference between deliberative and reactive agents embodies the dichotomy between strategy (i.e., planned behavior) and tactic (i.e., a set of reaction rules). Helmuth von Moltke the Elder is known for his quote "*No plan survives contact with the enemy*", meaning that it does not matter how good your strategy is, you must always also have a tactic to fall back on. This is why agents rarely are only reactive or only deliberative, but they generally tend to embody one behavior more than the other.

In this thesis, we will systematically consider mostly reactive agents, which better model the groups we study.

We let agents follow a nominal dynamic, defining their behavior in the absence of interactions with their fellows. This nominal dynamic encompasses the possible influences of the environment on each agent, and their individual behavior. On top of this dynamic, we then characterize the influence of their interactions with other agents. A group of agents is called a **swarm**. A swarm of such agents, following their individual dynamic and capable of interacting with each other, is called a **Multi-agent system** (MAS).

Multi-Agent Systems

In a MAS, each agent is defined by its **state**, which can change through time. The state of an agent is the value of its internal variables – discrete or continuous. For example, one such variable can define its position in space (i.e., a vector in d dimensions to represent a point in $\mathbb{R}^d$). Variables can also be tags, defining how the agent is behaving. For instance, a tag $A \in \{1,0\}$ can respectively define whether or not an agent is active. In this particular case, an agent with $A = 0$ cannot move, at least until its tag value changes back to 1. The **dynamic** of an agent defines how its state changes with respect to time, depending on the environment, its current state and its interactions with the other agents.

As mentioned previously, each agent in a MAS has a nominal dynamic and can interact with its fellows. Agents interact by exchanging information, similarly to the exchange of messages. Restrictions can exist, defining which agents can directly interact. In general, a virtual interaction network can be defined in the system. Two agents are connected in this virtual network if and only if they can interact. This network can either be time-dependent or not.

In the case of a time-independent network, a fixed hierarchy exists within the system. Some agents may not be able to directly interact with others, and must go through intermediate agents to pass their messages along. As an example, systems with **global** interactions possess time-independent interaction networks. In those systems, all agents are always able to interact with all other agents. In such cases, agents share a global consciousness, and share the same information at all time. When global interactions are involved, **centralized** systems have a time-independent network. In those systems, one agent (acting as a base station) receives all messages, and either routes them to their destination, or broadcasts them to all agents in the system. These systems possess a star-shaped interaction network, with the base station at the center.

In systems with time-dependent interactions networks, the interactions depend on the state of the agents. For instance, in systems with **local** interactions, two agents are only able to interact if they are close enough. Local interactions mean that the agents get information only from their close neighbors. In those systems, two agents far from each other could possess very different information at a given time. For example, **decentralized** systems only let agents gather information locally (by interactions with their close neighbors, or from their local environment). Agents in decentralized systems are more autonomous, but are often harder to synchronize and to keep flocked together. Systems with local interactions are generally harder to analyze, but describe more accurately the variability of the knowledge between individual agents, therefore better reflecting reality.

To provide an almost perfect model of the reality, one may wish to define very complex agents, with a large number of state variables. This representation of these agents would be very close to the real world, but the resulting MAS would be nearly impossible to study. For this reason, one generally tries to simplify agents by reducing their number of state variables. A MAS is always an oversimplified model of the reality. But a well simplified MAS can give useful insights into the real world situation it models.

In this thesis, we systematically try to consider analytically tractable MAS's, i.e., MAS's which can be theoretically studied.

In those systems, agents follow dynamics which enable an analytical investigation. Our main aim is to obtain **analytical results**, which can then be confirmed and illustrated through numerical simulations. Analytical results are time-independent, and far more reliable than empirical results. However, they are more difficult to obtain, and often require a specific kind of agent dynamics in order to use the analytical tools at our disposal. We feel that the restrictions brought by this choice do not reduce the usability of the results presented in this thesis. To obtain such MAS's, we follow a widely used approach Schweitzer (2003), and consider **Brownian agents**.

Brownian Agents

Brownian agents are driven by a Gaussian Noise source, usually a **White Gaussian Noise** (WGN) source. Concretely, a random component is added to each agent's state, generally to its position in the state space. The noise source reflects the sum of the variations due to the complexity levels that were lost during the simplification. This random noise source effectively simplifies the agent's dynamic, while still reflecting the full complexity it should possess to provide a model closer to reality.

Mathematically, each agent's state is modeled as a **diffusion process** on its continuous state space. Each agent's dynamic is then expressed as a set of stochastic differential equations (SDE), defining how it changes through time. The state variables are all continuous, and the speed at which they change is quantified as a function of their actual state.

We let $\vec{A}_i(t)$ be the state vector, containing the value of all state variables, of agent i at time t. We then express agent i's dynamic by giving an update function $f(\vec{A}_i(t))$, defining how its state changes, with regard to its current state. A second function $\mathscr{I}\left[\vec{A}_i, \vec{A}\right]$ (with $\vec{A} = \left(\vec{A}_1, ..., \vec{A}_N\right)$) characterizes the interactions of agent i with its fellows. The values of the functions f and $\mathscr{I}$ express the instantaneous speeds of the agent in the state space. In particular, we call the instantaneous speed of an agent in the position state space its **drift**. Since we consider Brownian agents, WGN sources $d\vec{W}_i(t)$ are also added to the dynamic of each agent. In general, we say that agent i diffuses on its state space, following the dynamic:

$$d\vec{A}_i(t) = \underbrace{f(\vec{A}_i(t))\cdot dt}_{\text{indiv. behavior}} + \underbrace{\mathscr{I}[\vec{A}_i,\vec{A}]\cdot dt}_{\text{interactions}} + \underbrace{\sigma\, d\vec{W}_i(t)}_{\text{WGN source}} . \tag{1}$$

The WGN source $dW(t)$ is a statistical noise with a known probability distribution function: a Normal distribution with mean 0 and variance 1 (i.e., $\mathcal{N}(0,1)$). As a consequence of the Central Limit Theorem, the WGN effectively models the sum of a large number of different independent noise sources. This is the reason why this noise source is successfully used to model the internal complexity of an agent.

Dynamical systems theory provides us with tools to analytically investigate stochastic processes, especially those driven by WGN sources. Since the dynamic is stochastic, we must represent the position of an agent as a probability distribution, expressing the probability of finding the agent in a global area at a given time. For particles, the **Fokker-Planck Equation** (FPE) provides us with a way of estimating the future position of a particle, with regard to its dynamic. The FPE effectively propagates in the future the probability distribution of the position of a particle, knowing its nominal dynamic and the variance of its noise source. For agents, we can use the FPE for the nominal dynamics' propagation, but we need a tool to investigate the influence of interactions. The **mean-field** (MF) approach allows, for a homogeneous MAS (i.e., where all agents follow the same dynamic), to characterize the agents interactions. For large homogeneous swarms, the MF approach states that any randomly selected agent is representative of the whole swarm. The influence of all agents on a representative agent can be expressed as one external interaction field. From the nominal dynamic of the representative agent and the effects of this field, the whole swarm dynamic can finally be derived. The results given by the MF approach are exact for swarm of $N \to \infty$ agents, but remain very accurate for large enough swarms ($N \approx 1000$).

In this thesis, we systematically consider the **heterogeneity** of a group at the behavioral level, i.e., heterogeneous agents have different dynamics Eq.(1). In robotics terms, we therefore consider software heterogeneity (as opposed to hardware heterogeneity).

Controlling a Group

When attempting to control a swarm of agents, we will here consider two different approaches, that we will refer to as **planned** or **real-time** control. Similarly to the difference between reactive and deliberative agents, these two approaches respectively embody the concepts of "strategy" and "tactic". Planned control lets us define a swarm strategy, which the agents will then follow. Real-time control is usually more difficult to implement. It lets the agents follow a nominal dynamic, but allows to externally regain control of the swarm at will.

Planned Control

In robotic swarms, the dynamic of each agent can be constructed. If the swarm's dynamic is homogeneous, it allows the use of the MF approach. One can therefore hope for analytical results in those situations. For general heterogeneous swarms, no general analytical approach exists, and analytical results are far more difficult to obtain.

Planned control (of homogeneous swarms) is easier to define and study, but behaves poorly when faced with real-time changes. Once the strategy (i.e., the dynamic) has been defined, the agents will blindly follow it, and will not be able to react to unexpected situations. If one robot in a homogeneous swarm fails, the overall dynamic of the swarm most likely becomes unstable. A homogeneous swarm dynamic performs well, as long as it is only used under exactly the conditions it was designed for.

Real-Time Control

To obtain real-time control of a swarm, one must be able to control each agent continually. For large swarms of agents, one wishes not to control each agent separately, but to defer the control of the swarm to a few selected special agents. These special agents can be externally controlled, effectively enabling the control of the whole swarm.

[1] *[...]The first type of real-time swarm control can be achieved by using a number of* **leader** *agents (possibly only one). In this case, all regular agents must be aware of the presence of the special agents. Accordingly, the dynamics of the regular agents must incorporate the role of the leader agents a priori. The result is a heterogeneous swarm, where regular agents simultaneously follow their own nominal dynamics, and feel the influence of the leader agents. By adequately controlling the leader agents, one can therefore control the whole group.*

Within leader-controlled swarms, we further differentiate two classes of models. The difference lies in whether the special agents can be identified as such by an **external observer** *of the swarm's behavior. This observer would be aware of the presence of special agents, but would not be allowed access to the underlying swarm's dynamics. Whether a leader can be externally recognized defines its* **visibility***, and can help us to assess its vulnerability. Since a small number of leader agents control the entire swarm, leaders are the main liability of the group. Leaders are single points of failure in a swarm, and could be targeted by external forces wishing to break the swarm's cohesion and dynamic. Depending on the application, hiding the leaders' identity can therefore effectively protect the swarm.*

---

[1] Italic text in the present section is reproduced from the conference paper Sartoretti (2015).

Apparent leaders usually stand out in the swarm by their positioning. They act as general landmarks for the regular agents, either stationary or moving, and can therefore easily be identified by an external observer. Hidden leader agents are intrinsically less vulnerable than apparent leaders. Hidden leaders are often encountered in swarms of social animals; a prime example is swarms of bees. When swarming, either moving or resting, regular bees regroup around the queen bee (which acts as the leader). Even when the swarm is moving (and thus less tightly packed around the queen), an external observer will not be able to tell the queen from the regular bees. This allows the swarm to safely move to a new hive location, led by a leader hidden within the swarm and following a similar dynamics.

The second controlling mechanism consists of inserting **shill** *agents in a swarm. These infiltrated agents are recognized by the other agents as regular agents. Control of these infiltrated agents can lead to the control of the whole swarm, provided one possesses extensive knowledge of the regular agents' dynamics. This type of control is often referred to as* **soft control***, since the swarm is not aware of being infiltrated. The influence of the shill agents is not explicitly included in the dynamic of each agent. Shills control the other agents only by taking advantage of the agents' interactions.*

In this thesis, we introduce the term **hard control**, that we will use indistinctively from **leader-based control**, in contrast with the term **soft control**.

Since shills are infiltrated within an unwitting swarm, their actions can positively influence the swarm's dynamics. This constructive soft control can help the swarm fulfill its objectives, by adding the possibility of a real-time external control. Alternatively, soft control can also be used destructively – for example, it may break the swarm cohesion or drive the swarm toward an incorrect direction.

We introduce a similar distinction between apparent and hidden shill agents. An example in which shills must be apparent to an **external observer***, to control a swarm, can help assess the robustness of the swarm's dynamics. In those cases, an infiltrated swarm can be immediately recognized as such from the outside, precluding destructive shills to quietly take control of the swarm. Cases in which the soft control can be achieved using hidden shills help protect the special agent's identity. In the same manner as the leaders, shill agents can be a liability since the whole swarm can be controlled through their single influence. However, since agents in a soft-controlled swarm do not recognize their shills, the swarm can resume functioning on its own (uncontrolled) in their absence.[...]*

Figure 3 illustrate an actual case of hard and soft control. Leader-controlled groups of animals are often encountered in nature, where leaders are often visible. Soft control of animal swarms have been studied, usually with ties in robotics to supply the actual shills.

State of the Art

In this section, we present the reader with a brief review of the literature associated with multi-agent systems. We mainly focus on homogeneous MAS and their applications to other topics, and on cases of soft control. Leader-based control is discussed only briefly, mainly for the completeness of the present thesis.

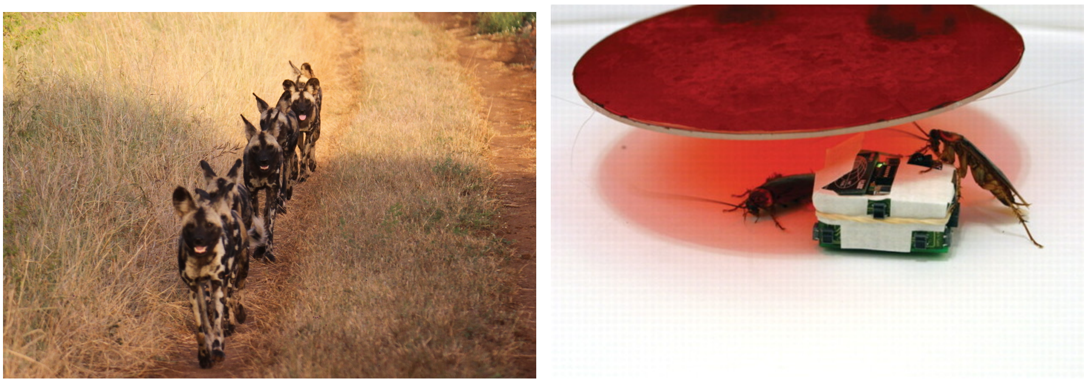

Figure 3 – Left: Pack of wild dogs, driven by the leading dog. Here the leader is clearly apparent. Right: Robotic shill used to control the decisions of a group of cockroaches in Halloy et al. (2007). Here also the shill is apparent (i.e., easily recognizable by an external observer).

Homogeneous Swarms of Agents

Scalar and Planar Brownian swarms

In this subsection, we only list the type of analytical approaches that we plan to adopt in this thesis (i.e., simulation experiments are not reported here). The seminal contribution of F. Schweitzer Schweitzer (2003) sets several basic elements of interacting agent dynamics including some inertial features. Gazi and Fidan (2007) provides us with a comprehensive review of the different MAS construction mechanisms, and of their control.

In parallel, the monograph by T. D. Frank Frank (2005) and the recent contribution Chavanis (2008) offer comprehensive frameworks devoted to nonlinear Fokker-Planck equations. It is of direct use for the mean-field approach that can be used for Brownian interacting agents. Zola et al. (2008) recently studied solvable nonlinear FPEs which can be interpreted as a mean-field dynamics for interacting agents. More recent analytically solvable models stylizing some aspects of reality are becoming scarce Hongler et al. (2014); Bertin et al. (2006).

A large family of dynamics encompasses all **potential-based** dynamics. In this family, each agent's dynamics directly depends on a potential landscape $V(\vec{x})$, attributing an altitude to each point $\vec{x}$ in the state space. Agents are naturally driven towards the lower sections of this landscape, and naturally follow a gradient approach. Their instantaneous speed is then usually obtained by deriving the potential function at their current position: $-\frac{\partial V}{\partial \vec{x}}(\vec{x})$. In the large family of potential-ruled algorithms, we can cite for example Gazi and Passino (2004); Paley et al. (2007) where global attractive/repulsive potentials are used to obtain a cohesive swarm. Local potentials, constructed separately by each agent, are used to devise the dynamics of robotic swarms in Hsieh et al. (2008); Sepulchre et al. (2008).

In economy, MAS have been used to model the and analyze the movement of stocks or portfolio management Fernholz (2002). A large family of models let agent have **rank-based dynamics** Chatterjee and Pal (2010); Pal and Pitman (2008). In other words, the agents' behaviors change according to a ranking of their position (i.e., the price of the stock they are modeling). The first famous model of this kind was the Atlas model, where agents only had a rank-based drift Banner et al. (2005). An extension to this model was then introduced in Ichiba et al. (2011), creating the *Hybrid Atlas Model*, where agents have a nominal drift, a rank-based drift and a global swarm drift. These rank-based swarms are effectively heterogeneous, but some analytical results can still be expressed.

Ethological Models

Many ethological studies focus on the emergence and hold of flocking in swarm of animals Aldana et al. (2007). **Flocking** occurs when a swarm comes together and creates a **cohesive group**, where all individuals can remain together through movement and even direction changes. The first attempt at characterizing flocking was done in Reynolds (1987), where the first rules to obtain a flocking swarm were devised: the *rules of Reynolds*. Nowadays, most dynamics are proven to create flocking in a system by showing that they obey to the rules of Reynolds Olfati-Saber (2006); Dosseti (2012). Fundamental papers like Cucker and Smale (2007a,b) offer a synthesized and now almost classical view on emergent flocking behaviors and relevant modeling issues for MAS.

Decentralized models, where agents only rely on locally gathered information, and local interactions with neighbors, to create flocking patterns, have been pioneered by Viczek et al. (1995). The famous Viczek model has then been extended in Chate et al. (2008), but where no noise source is considered in the dynamic. Leonard (2013) discusses how decentralized ethological models can positively influence the construction of powerful MAS. In Bialek et al. (2012), the flocking of birds is studied, and a model using non metrics interactions is proposed and tested against real life data.

Eftimie (2012) provides a good review of the aggregation mechanisms in biological systems. In Yates et al. (2009), the importance of the noise in the dynamics of flocking herds in movement is shown, leading to the conclusion that noise is needed in order to let a swarm remain flocked through changes in direction. A small survey of (human) crowd modeling can finally be found in Bellomo and Dogbe (2011).

Agent Circulation in Production and Service Networks

In recent contributions Filliger and Hongler (2005); Gallay and Hongler (2008b,a), an agent character has been introduced in elementary queueing models allowing analytical treatment. These models show that interactions between autonomous agents traveling in queueing networks may give rise to the emergence of dissipative spatio-temporal flow patterns. In Gallay and Hongler (2009a), several simple queueing networks involving agents with *smart parts* features have been analytically discussed. More particularly, we have considered situations where autonomous agents select, at a given time and at a given vertex location, their routing in the network, according to (individual) historical data (such as waiting times) collected during their past progression in the network. For several simple network configurations and despite the intrinsically non-Markovian character of the dynamics, we have been able to discuss analytically the emerging collective dynamics that such a circulation of autonomous agents generates. Feedback loops in the network topology coupled with the presence of delays in the routing selection mechanisms produce a wealth of dynamical phenomena like self-sustained generically stable oscillations, spatio-temporal patterns, stabilization by noise phenomena and oscillator synchronization that are explicitly discussed. Very recently, the idea that the emergence of spatio-temporal patterns could actually be used to produce optimal flow control has been explored in Gallay and Hongler (2009b).

Homogeneous Robotic Swarms

For the state of the art in homogeneous robotics swarm, we refer the reader to the introduction of Chapter 2, where we present a comprehensive state of the art for homogeneous MAS applied to swarm robotics.

Hard Control of Swarms

Leader-based control is often encountered in animal swarms, where some individuals may have a special knowledge and should be able to guide a whole group toward the correct direction. Couzin et al. (2005) discusses how the proportion of leader agents, having a correct information, can affect the course of a large moving group of animals. Their result is very interesting, as well as counter-intuitive: it states that the larger the group, the less the number of leaders is needed to achieve the best decision making.

Analytical study of Brownian swarm controlled by a leader is presented in Aureli and Porfiri (2010). In this paper, the leader can be shown to induce different aggregation states to the whole swarm. In Nourian et al. (2010), the case of a swarm flocking around a group of leaders is studied from the point of view of game theory. An analytical approach can even be applied, using the MF approach on both the group of leaders and of followers.

In robotics, leader-based control have been extensively studied to control swarms of mobile robots. In Desai et al. (1998), authors give the first ideas toward a leader-follower dynamic, allowing to synchronize the motion of multiple robots behind a few leading robots. Tanner et al. (2004) further discusses the stability of leader-follower type formations, with regard to the leader's behavior. The possible issues with decentralized leader-follower models are discussed, and conditions on the interaction graph within the swarm are presented in Ji et al. (2009). Recently, in Michini et al. (2014), a decentralized leader-follower dynamic is devised to successfully allow a swarm of sub-aquatic mobile robots to track a given manifold.

Soft Control of Swarms

Soft Control of Brownian Swarms

Soft control of swarms, via the use of shill agents, is a fairly recent topic of study. As mentioned previously, the heterogeneity of the group generally precludes the use of the MF approach. In Han et al. (2006), the authors constructed, for a specific model at hand, a control law for the shill and showed numerically that the shill can synchronize the whole group to a given objective. In a recent contribution, a different strategy of the shill is then studied Jing and Lin (2010).

Constructive soft control, allowing the swarm to remain cohesive or to reach a consensus, have been studied in Wang et al. (2011); Wang and Guo (2008). In Wang et al. (2009), soft control of a swarm via the use of potential functions is achieved.

Robotic Soft Control of Animal Swarms

Recently, the soft control of actual animal groups has been achieved, by introducing robotic shills in societies of animals. Animals societies are very complex decentralized MAS, and the journey from biological systems to artificial models is discussed in Bonabeau et al. (1999). Mondada et al. (2011) discusses the approach and methodology needed to design a robotic shill, and to devise its dynamic.

A robotic shill has been successfully recognized as their mother by hatching chicks in Gribovskiy et al. (2010). External influence of internal decision mechanisms has been managed by a robotic shill inserted within a colony of cockroaches in Halloy et al. (2007). *Robofish*, a robotic fish, has also been developed to soft control schools of fishes in Faria et al. (2010). In Vaughan et al. (2000), a robotic shill is used to soft control a swarm of ducklings, after a potential-based model is devised to theoretically investigate the soft control of the swarm.

Thesis Outline

In this thesis, we present different examples of planned and real-time swarm controls. After this introduction, we provide the reader with a short review of literature on the subject of MAS's, and their planned and real-time control, concluding Part I. The outline of the thesis is summarized in Table 1, where the chapters are separated along the two main axes. The first axis is the type of control used, and the second the visibility of the special agent used (if the swarm is controlled in real-time).

Table 1 – Structure of the thesis.

Introduction (Part I)

Planned Control (Part II)
Chapter 1 Chapter 2

Control Type Control Visibility	Real-Time Control	
	Hard control (Part III)	Soft control (Part IV)
Apparent	Chapter 3	Chapter 6
Hidden	Chapter 4	Chapter 6 Chapter 5

Strongly Heterogeneous Swarms (Part V)	Chapter 7 Chapter 8

Conclusion (Part VI) Appendices (Part VII) Bibliography (Part VIII)

In Part II, we focus on planned control of homogeneous swarms. Part III and IV consider real-time swarm control using special agents. Part V presents strongly heterogeneous systems. In Part VI, we present concluding remarks to this thesis, and perspectives for future research. Appendices are featured in Part VII, while Part VIII provides the reader with the bibliography and the index. The author's CV and publications are presented after the index, at the end of the present thesis.

Original Contributions of the Thesis

Innovative contributions to the state of the art, in the field of multi-agent systems, are featured in Chapters 1-2, part of Chapter 3 and Chapters 4-8. More specifically, those chapters are detailed as follows:

- In Chapter 1, we present a homogeneous swarm dynamics, where planar agents follow a distributed mixed canonical-dissipative (MCD) dynamics. Using only locally gathered information, agents are able to consensually select a closed curve within a given family of curves and circulate on it. For circular orbits, the radius of the limit cycle can be explicitly expressed.

- In Chapter 2, we present a natural extension of the MCD dynamics to other closed curves. We then present a robotic control mechanism, allowing a swarm of mobile robots to follow the circular MCD dynamics of Chapter 1. We experimentally validate our model by implementing the robotic control mechanism on actual mobile robots, and run 25 experiments.

- In Chapter 3 we present simple examples of leader-controlled robotic swarms, with a visible leader. The control of the swarm is derived from Braitenberg-inspired dynamics, similar to the robotic adaptation of the MCD dynamic of Chapter 2. Since visible leaders have been extensively studied in the literature, these examples are presented here mainly for completeness.

- In Chapter 4, we present an analytically tractable swarm dynamics, where agents are controlled by a leader, which remains hidden in the swarm. The example is taken from the field of nonlinear estimation problems. The swarm of regular agents follow the dynamic of a feedback particle filter, whereas the leader acts as the noisy signal to filter.

- In Chapter 5, we present an extension of the circular MCD dynamic of Chapter 1. Now, the agents also self-select their angular speed on the circular limit cycle by local interactions. A shill agent, with a constant angular speed, is then able to soft control the global swarm's angular speed while remaining hidden.

- In Chapter 6, we present the soft control of a swarm of Brownian agents following a Hybrid Atlas Model on $\mathbb{R}$. A shill agent, driven by a ballistic noise source, is able to drive an initially stationary swarm toward one direction. Depending on the shill's level of turbulence, it can either remain hidden within the swarm or become apparent.

- In Chapter 7, we present a case of interactions between societies of agents. In each society, agents achieve flocking by mutual interactions, and the whole society propagates in one direction as a soliton wave. When two societies of agents meet, interactions between their agents can either allow them to remain flocked together, as the faster society pulls the slowest one, or both societies reach asymptotically freedom.

- In Chapter 8, we consider the case of a MAS with stigmergic agent interactions. With this type of interactions, agents interact indirectly, by influencing the global state of their environment. In this chapter, the control of a swarm of robotic boats is devised, in order to collaboratively approach, grasp and manipulate a floating object in a distributed manner. Analytical results on the object trajectory are presented, and numerical simulations confirm our theoretical findings. Finally, the experimental validation of our distributed control mechanism is performed using a swarm of $N = 4$ robotic boats.

Planned Control Part II

1 Self-Organized Mixed Canonical-Dissipative Dynamics for Brownian Planar Agents

Summary

We consider a collection of N homogeneous interacting Brownian agents evolving on the plane. The time continuous individual dynamics are jointly driven by mixed canonical-dissipative (MCD) type dynamics and White Gaussian noise sources. Each agent is permanently at the center of a finite size observation disk D_ρ. Steadily with time, agents count the number of their fellows located in D_ρ. This information is then used to re-actualize control parameters entering into the MCD. Dissipation mechanisms together with the noise sources ultimately drive the dynamics towards a consensual stationary regime characterized by an invariant measure P_s on an appropriate probability space. A mean field approach enables to analytically calculate P_s. For each agent, our dynamics naturally implement: i) a trend to not be isolated, ii) a trend to avoid strong proximity, and iii) an overall trend to be attracted to a polar point. The MCD drift is derived from a Hamiltonian function $\mathscr{H}$ and drives the agents to follow one consensual orbit coinciding with a level curve of $\mathscr{H}$. When $\mathscr{H}$ is the harmonic oscillator, we are able to analytically derive the consensual orbit as a function of the size of D_ρ. Generalizations involving more complex $\mathscr{H}$ are explicitly worked out. Among these illustrations, we study a Hamiltonian whose level curves are the Cassini's ovals. A selection of simulations experiments corroborating the theoretical findings are presented.

1.1 Introduction

The emergence of structured collective dynamical patterns from simple agent level behaviors as observed in nature for fishes, birds, insects and the like inspires a sustained research activity in management and control of complex systems, and particularly in the domain of swarm robotics. The capability of agents to act asynchronously to determine specific trajectories by relying only on local sensing is definitely attractive when a centralized control becomes unfeasible - for example to coordinate large assemblies of autonomous robots or other agents. One possibility to address these difficult global control issues is by implementing adaptive strategies where identical robots are programmed with elementary features requiring limited on-board real time sensing and computational resources. This general and truly simple idea triggers a strong interdisciplinary research activity which, as emphasized in the recent review Gazi and Fidan (2007), encompasses a relatively wide spectrum of perspectives ranging from ethology to swarm robotics. Focusing here on the dynamical system and control perspectives, we study a collection of asynchronously interacting point Brownian agents obeying elementary coordination algorithms. The basic ingredients of our modeling are: i) a Hamiltonian function $\mathscr{H}$ which provides a parametric family of non-intersecting level curves defining closed orbits, ii) a mixed conservative and gradient vector field constructed from $\mathscr{H}$ involving one (or several) control parameters, iii) a stochastic driving stylized by WGN's sources and iv) for each agent, a circular observation range D_ρ with radius ρ, centered at each agent location. The agents mutual interactions directly depend on the size of D_ρ. Interactions produce an adaptive mechanism which drives the agents to ultimately adopt one (or several) consensual value(s) of the control parameter(s). The consensual parameter(s) value selects one specific orbit among the Hamiltonian parametric family. For such mixed canonical-dissipative stochastic dynamics, connected with models discussed in Hongler and Ryter (1978), we are able to explicitly write the resulting invariant probability measure solving the associated time-independent non-linear *Fokker-Planck* equation (NLFP). We can therefore analytically investigate the influence of the radius ρ of the observation range D_ρ on the emerging dynamics achieved by the agents. While our class of dynamics presents similarities with potential-ruled algorithms as those used for example in Gazi and Passino (2004); Gazi and Fidan (2007); Hsieh et al. (2008); Sepulchre et al. (2008), it however keeps a decentralized mechanism stylized in the basic agents models pioneered by Reynolds (1987); Viczek et al. (1995) and more recently by Cucker and Smale (2007a).

Mathematically speaking, our modeling relies on a set of N continuous time, coupled non-linear stochastic differential equations (SDE) driven by White Gaussian noise (WGN). In this context, the basic formal question, first raised first by H. McKean McKean Jr. (1966), is to calculate the limit of the probability distribution which describes a large agent collection (i.e. formally the thermodynamic limit $N \to \infty$) and then fluctuations around this limit for finite N. Considering that all agents have random identically distributed independent initial conditions, one mathematically expects (this can be rigorously proved under somehow restricting technical hypothesis) that in the thermodynamic limit, all finite number of agents behaves independently of the others and they can all be described by the same probability distribution (this is known as *propagation of chaos*). The common probability distribution solves a Markovian evolution described by a nonlinear Chapman-Kolmogorov type partial differential equation. Accordingly, when propagation of chaos holds, we may characterize the dynamic behavior of the global population by only studying the dynamics of a single, randomly chosen, agent subject to an effective external *mean-field* generated by its surrounding fellows. In presence of WGN's sources, the single representative agent follows a diffusion process and its probability measure obeys to a NLFP, Frank (2005).

1.2 Interacting Brownian Agents Driven by Canonical-Dissipative Dynamics and White Gaussian Noise

We consider a swarm of N mutually interacting dynamical planar agents a_k for $k = 1,2,\cdots,N$ evolving on the plane $\mathbb{R}^2$ with state variables $\vec{X}(t) = (X_1(t), X_2(t),\cdots,X_N(t))$. In this section, we assume the homogeneous situation in which all individual isolated agents a_k are dynamically identical. The collective dynamics is assumed to obey an N-dimensional diffusion process on $\mathbb{R}^2$ given by a set of stochastic differential equations (SDE):

$$\begin{cases} d\mathbf{X}_k(t) = \mathbb{A}_k(t)\mathbf{X}_k(t)\,dt + \gamma \overbrace{\left[\mathscr{L}^2_{k,\rho}(t) - \|\mathbf{X}_k(t)\|_2^2\right]\mathbf{X}_k(t)}^{\mathscr{C}_k(\mathbf{X}_k(t))}\,dt + \sigma\, d\mathbf{W}_k(t), \\[2ex] \mathbf{X}_k(0) = \mathbf{X}_{0,k}, \qquad \text{and} \qquad \mathbf{X}_k(t) \in \mathbb{R}^2, \qquad\qquad k = 1,2,\cdots,N. \end{cases} \tag{1.1}$$

In Eq.(1.1), the following notations are used: $\mathbf{X}_k(t) = \left(x_{k,1}(t), x_{k,2}(t)\right) \in \mathbb{R}^2$, the usual norm $\|\mathbf{X}_k(t)\|_2^2 := \left(x^2_{k,1}(t) + x^2_{k,2}(t)\right)$, γ and σ are positive constants common to all a_k (i.e. homogeneity assumption) and $\mathbf{W}_k(t) = \left(W_{k,1}, W_{k,2}\right)_{t\geq 0}$ are independent standard Brownian Motions (BM) and hence the formal differentials $dW_k(t)$ are White Gaussian Noise (WGN) processes. The agents interactions will be defined via the scalars $\mathscr{L}^2_{k,\rho}(t)$ and the matrices $\mathbb{A}_k(t)$ which both will depend on $\mathscr{D}_{k,\rho}(t)$ the set of instantaneous neighboring fellows surrounding agent a_k at time t. For a given observation range ρ, the a_k-*instantaneous observation neighborhood* $\mathscr{D}_{k,\rho}(t)$ is the disk:

$$\mathscr{D}_{k,\rho}(t) = \left\{\mathbf{X} \in \mathbb{R}^2 \mid \|\mathbf{X} - \mathbf{X}_k(t)\|_2 \leq \rho\right\} \tag{1.2}$$

and we define the indices set

$$V_{k,\rho}(t) = \left\{i \mid \mathbf{X}_i(t) \in \mathscr{D}_{k,\rho}(t)\right\}. \tag{1.3}$$

which identifies the a_k-neighboring agents present in the disk $\mathscr{D}_{k,\rho}(t)$. We shall write $N_{k,\rho}(t) := |V_{k,\rho}(t)|$ the cardinality of the set $V_{k,\rho}(t)$. The dynamic elements contained in Eq.(1.2) and Eq.(1.3) are now used to characterize the agents' mutual interactions via a couple of contributions:

i) **Canonical-dissipative matrix** $\mathbb{A}_k(t)$. The skew symmetric dynamic matrix $\mathbb{A}_k(t)$ associated with agent a_k can be defined as:

$$\mathbb{A}_k(t) := \begin{pmatrix} \frac{N_{k,\rho}(t)}{N} - \frac{1}{M} & \frac{N_{k,\rho}(t)}{N} \\ -\frac{N_{k,\rho}(t)}{N} & \frac{N_{k,\rho}(t)}{N} - \frac{1}{M} \end{pmatrix}, \tag{1.4}$$

with $1 \leq M \leq N$ and $N_{k,\rho}(t)/N$ is the fraction of the total swarm that agent a_k detects in $\mathscr{D}_{k,\rho}(t)$ (we shall adopt the convention that agent a_k systematically detects itself, implying that $N_{k,\rho}(t) \geq 1, \forall\, t$). As $\mathbf{X}_k = 0$ is a singular point of the deterministic dynamics (i.e. obtained for $\sigma = 0$ in Eq.(1.1)) the matrix $\mathbb{A}_k(t)$ formally stands for the linear mapping of the dynamics in the neighborhood of the origin. The associated couple of eigenvalues of $\mathbb{A}_k(t)$ read:

$$\lambda_{k,\pm}(t) = \underbrace{\left[\frac{N_{k,\rho}(t)}{N} - \frac{1}{M}\right]}_{:=\mathscr{R}_{k,\rho}(t)} \pm (\sqrt{-1}) \underbrace{\left[\frac{N_{k,\rho}(t)}{N}\right]}_{:=\mathscr{I}_{k,\rho}(t)}. \tag{1.5}$$

Hence, at a given time t, the real part in Eq.(1.5) expresses the non-conservative type of the dynamics (i.e. the divergence part of the vector field (VF)). The singular point $\mathbf{0} \in \mathbb{R}^2$ is an attractive (respectively repulsive) node when $\mathscr{R}_{k,\rho}(t) < 0$ (resp. $\mathscr{R}_{k,\rho}(t) > 0$). Moreover, the component $\mathscr{I}_{k,\rho}(t)$ expresses the rotational nature of the VF. In particular, when $\mathscr{R}_{k,\rho}(t) = 0$, the dynamics are conservative; it expresses the *Hamiltonian* component of the a_k-VF.

ii) **Adaptive limit cycle radius**. The scalar quantity

$$\mathscr{L}^2_{k,\rho}(t) := \frac{1}{|V_{k,\rho}(t)|} \sum_{j \in V_{k,\rho}(t)} \|X_j(t)\|_2^2 \tag{1.6}$$

defines the (square) of the radial position of the barycenter of the agents belonging to $\mathscr{D}_{k,\rho}$.

Proposition 1. *Consider the* **mixed-canonical dissipative diffusive dynamics** *Eq.*(1.1). *Asymptotically with times, the dynamics propagates chaos and the MF representative agent obeys to* *the couple of diffusion equations :*

$$\begin{cases} dX_1(t) = +\frac{1}{M}X_2(t) + \gamma\left[\mathscr{L}_{s,\rho}^2 - (X_1^2(t) + X_2^2(t))\right]\cdot X_1(t)\,dt + \sigma dW_1(t), \\ \\ dX_2(t) = -\frac{1}{M}X_1(t) + \gamma\left[\mathscr{L}_{s,\rho}^2 - (X_1^2(t) + X_2^2(t))\right]\cdot X_2(t)\,dt + \sigma dW_2(t). \end{cases} \tag{1.7}$$

For weak noise (i.e. large values of γ/σ^2*), the radius approximately reads* $\mathscr{L}_{s,\rho} \simeq \frac{\rho}{\sqrt{2(1-\cos(\pi/M))}}$ *and the associated stationary probability density* $P_s(\mathbf{x})$ *reads:*

$$P_s(\mathbf{x})dx_1dx_2 = \frac{\exp\left\{\frac{2\gamma}{\sigma^2}\left[\mathscr{L}_{s,\rho}^2 - (x_1^2 + x_2^2)\right]\right\}dx_1dx_2}{\mathcal{Z}}, \tag{1.8}$$

with $\mathbf{x} = (x_1, x_2) \in \mathbb{R}^2$*, and* $\mathcal{Z}$ *being the probability normalization factor.*

Proof of Proposition 1.

The Fokker-Planck equation associated with the diffusion process of Eq.(1.1) can be written in the form:

$$\partial_t P(\vec{\mathbf{x}}, t|\vec{\mathbf{x}}_\mathbf{0}) = -\nabla\cdot\left\{\frac{1}{2}\left[\mathbb{A}_a(t)\nabla\|\vec{\mathbf{x}}\|^2 - \nabla V_\rho(t,\vec{\mathbf{x}})\right]P(\vec{\mathbf{x}}, t|\vec{\mathbf{x}}_\mathbf{0}) + \frac{\sigma^2}{2}\nabla P(\vec{\mathbf{x}}, t|\vec{\mathbf{x}}_\mathbf{0})\right\}, \tag{1.9}$$

where $\mathbb{A}_a$ is the $(2N \times 2N)$ block-simplectic matrix:

$$\mathbb{A}_a(t) := \begin{pmatrix} B_1(t) & & 0 \\ & \ddots & \\ 0 & & B_N(t) \end{pmatrix},$$

$$\text{with } B_k(t) = \begin{pmatrix} 0 & \frac{N_{k,\rho}(t)}{N} \\ -\frac{N_{k,\rho}(t)}{N} & 0 \end{pmatrix}$$

and the *time-dependent* generalized potential $V_\rho(t,\vec{\mathbf{x}})$ from which the dissipative component of the drift is derived, can be written as:

$$V_\rho\left(t,\vec{\mathbf{x}}\right) = \sum_{k=1}^{N}\left\{\frac{1}{2}\overbrace{\left[\frac{N_{k,\rho}(t)}{N}-\frac{1}{M}\right]}^{:=\mathscr{R}_{k,\rho}(t)}\|\vec{\mathbf{x}}\|^2+\frac{\gamma}{2}\left[\mathscr{L}^2_{k,\rho}(t)-\|\vec{\mathbf{x}}\|^2\right]^2\right\}. \tag{1.10}$$

The potential parameterization $\mathscr{R}_{k,\rho}(t)$ and $\mathscr{L}^2_{k,\rho}(t)$ in Eq.(1.10) explicitly depends on the agents' configurations implying that Eq.(1.9) is effectively a NLFP. The potential $V_\rho\left(t,\vec{\mathbf{x}}\right)$ is globally attractive on $\mathbb{R}^{2N}$, (i.e $V_\rho\left(t,\vec{\mathbf{x}}\right) \to \infty$ for $\|\vec{\mathbf{x}}\| \to \infty$). Global attraction together with the WGN driving sources imply that the diffusive dynamic Eq.(1.1) is *ergodic* on $\mathbb{R}^{2N}$. Accordingly, it exists a unique invariant measure $P_s(\vec{\mathbf{x}})$ and therefore both $\mathscr{R}_{k,\rho}(t)$ and $\mathscr{L}^2_{k,\rho}(t)$ asymptotically converge to stationary (i.e time-independent) values $\mathscr{L}^2_{k,s,\rho}$ and $\mathscr{R}_{k,s,\rho}$. Eqs.(1.9) and (1.10) being explicitly invariant under permutations in the agents labeling, we shall also have $\mathscr{L}^2_{k,s,\rho} = \mathscr{L}^2_{s,\rho}$ and $\mathscr{R}_{k,s,\rho} = \mathscr{R}_{s,\rho}$. Finally, in the stationary regime, the system is driven to its minimal energy configuration implying here that $\mathscr{R}_{s,\rho} \equiv 0$. This in turn yields that $\lim_{t\to\infty}\mathbb{A}_a(t) = \mathbb{A}_{a,s}$ with:

$$\mathbb{A}_{a,s} := \begin{pmatrix} \mathbb{A}_s & & 0 \\ & \ddots & \\ 0 & & \mathbb{A}_s \end{pmatrix}, \qquad \mathbb{A}_s = \begin{pmatrix} 0 & \frac{1}{M} \\ -\frac{1}{M} & 0 \end{pmatrix}.$$

The gradient $\nabla V_\rho\left(t,\vec{\mathbf{x}}\right)$ is systematically orthogonal to the antisymmetric component $\frac{1}{2}\mathbb{A}_a(t)\nabla\|\mathbf{x}\|^2$ (this remains true for the stationary regime $A_{a,s}$). It enables to write the stationary solution of Fokker-Planck Eq.(1.9) in the *product-form* $P_s(\vec{\mathbf{x}})$:

$$P_s(\vec{\mathbf{x}}) = \left[P_s(\mathbf{x})\right]^N = \left[\mathscr{N}^{-1}e^{\{V_{s,\rho}(\mathbf{x})\}}\right]^N, \qquad V_{s,\rho}(\mathbf{x}) = +\frac{\gamma}{2}\left[\mathscr{L}^2_{s,\rho}-\|\mathbf{x}\|^2\right]^2 \tag{1.11}$$

with the notation $\vec{\mathbf{x}} = (\mathbf{x}_1,\mathbf{x}_2,\cdots,\mathbf{x}_N) \in \mathbb{R}^{2N}$, $\mathbf{x}_k \in \mathbb{R}^2$ and $\mathbf{x} \in \mathbb{R}^2$ stands for one representative agents among the collection of the $\mathbf{x}_k$'s. The product form of the invariant measure explicitly shows that our dynamics propagates chaos, validating the use of a MF approach where a single agent behavior effectively reflects the global dynamics.

Taking the MF approach, and focusing on the stationary regime, from the point of view of a single representative planar agent $\mathbf{X}(t) = (x_1(t), x_2(t))$, we have:

$$0 = \triangledown\Big\{\frac{1}{2}\left[\mathbb{A}_s \triangledown \|\mathbf{x}\|^2 - \triangledown V_{s,\rho}(\mathbf{x})\right] \cdot P_s(\mathbf{x})\Big\} - \frac{\sigma^2}{2} \triangle P_s(\mathbf{x}), \tag{1.12}$$

where $P_s(\mathbf{x})$ is the invariant probability density.

Within the stationary regime, auto-consistency implies

$$\frac{N_{s,\rho}}{N} = \int_{(\mathbf{x})\in D_\rho} P_s(\mathbf{x})\, dx_1\, dx_2 \left(= \frac{1}{M}\right) \tag{1.13}$$

and

$$\mathscr{L}^2_{s,\rho} = \int\limits_{(x_1,x_2)\in D_\rho} \left(x_1^2 + x_2^2\right) P_s(\mathbf{x})\, dx_1\, dx_2, \tag{1.14}$$

where D_ρ is the representative agent's neighborhood.

From a uniformly rotating coordinates' frame with angular velocity M^{-1}, the stationary regime dynamics becomes purely gradient and the resulting probability density $P_s(\mathbf{x})$ solving Eq.(1.12) enjoys microscopic reversibility (i.e. *detailed balance*). It explicitly reads, Hongler and Ryter (1978):

$$P_s(\mathbf{x}) dx_1 dx_2 = P_s(r) dr\, d\theta = \mathcal{N}^{-1}(\mathscr{L}_{s,\rho})\, e^{\left[-\frac{\gamma}{\sigma^2}(r^2 - \mathscr{L}^2_{s,\rho})^2\right]} d(r^2)\, d\theta. \tag{1.15}$$

with $\mathcal{N}^{-1}(\mathscr{L}_{s,\rho}) = \sqrt{\frac{\pi^3\sigma^2}{\gamma}}\,\mathrm{Erfc}\left(-\frac{\sqrt{\gamma}(\mathscr{L}^2_{s,\rho})}{\sigma})\right)$ being the normalization factor.

In this stationary regime, the stationary observation neighborhood of each agent exactly encompasses a circular sector with aperture $\varphi(M)$ and radius $\mathscr{L}^2_{s,\rho}(M)$. Both $\varphi(M)$ and $\mathscr{L}_{s,\rho}(M)$ are adjusted to ensure that N/M agents are located in $\mathscr{D}_{s,\rho}$. For large ratio $\frac{\gamma}{\sigma^2}$ (i.e. essentially a large signal-to-noise ratio), Eq.(1.15) exhibits a sharply peaked "Mexican hat" shape with its maximum on the circle $r = \mathscr{L}_{s,\rho}$ (i.e. almost all agents stay confined in the direct neighborhood of the circle $r = \mathscr{L}_{s,\rho}$).

As detailed in Figure 1.1's caption, an elementary trigonometric argument enables to derive the compact relation:

$$\mathscr{L}_{s,\rho} = \frac{\rho}{\sqrt{2-2\cos(\pi/M)}}. \tag{1.16}$$

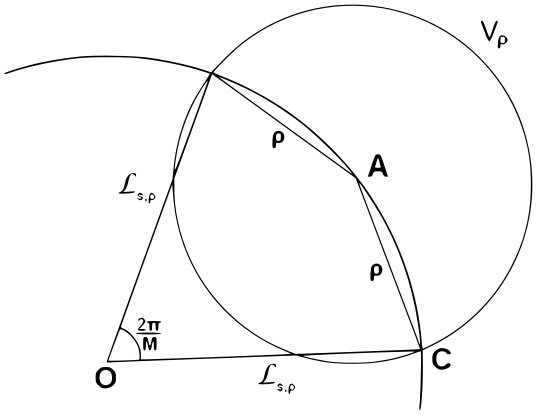

Figure 1.1 – The cylindrical symmetry characterizing the stationary regime implies that the agents probability distribution is rotationally invariant with respect to **O**. Accordingly, there will be on average N/M agents located in a sector with an opening angle $2\pi/M$. For large γ/σ^2, these agents will be confined in the direct proximity of the circle of radius $\mathscr{L}_{s,\rho}$. Let us consider an arbitrary agent located at **A** with a stationary observation range of radius $\rho = \mathbf{AC}$. This range exactly encompasses the circular arc with aperture $2\pi/M$ thus ensuring that the agent at **A** has M/N neighboring fellows. The cosine theorem in the triangle **OAC** implies that $\mathscr{L}^2_{s,\rho} = 2\rho^2/[1-\cos(\pi/M)]$ $2\mathscr{L}^2_{s,\rho} = \rho^2/[1-\cos(\pi/M)]$.

$\square$

Additional remarks. Observe that besides γ and σ which define an overall time scale, there are two additional control parameters in the dynamics Eq.(1.1):

a) **Hamiltonian parameter** M. The sector angle M into the canonical-dissipative matrix $\mathbb{A}(t)$. This parameter fixes the angular velocity $\omega = M^{-1}$ of the swarm and adjusts the size of the consensual limit cycle (i.e., a limit cycle whose value is consensually determined by the swarm) radius $\mathscr{L}_{s,\rho}$. For a given size of the observation disk with radius ρ and for large M, we have $\mathscr{L}_{s,\rho} \simeq \rho M/\pi$ and the angular velocity tends to vanish.

b) **Interaction range parameter** ρ. The radius of the observation disk ρ which directly determines the consensual size of the limit cycle radius $\mathscr{L}_{s,\rho}$.

1.3 Numerical Experiments

In all numerical experiments performed, we observe a truly remarkable agreement with the theoretical predictions (see Figure 1.2 for a specific illustration). According to Eq.(1.16), by reducing the sector opening angle (i.e by increasing the values of the M), the resulting limit cycle radius $\mathscr{L}_{s,\rho}$ increases and the number of agents present in $\mathscr{D}_{s,\rho}$ is reduced thus somehow invalidating the large population required for MF to be used. Even when $M = 50$, the couple of orbits realizations shown in Figure 1.3 show that analytical results, in particular Eq.(1.16), remain valid in this large M limit.

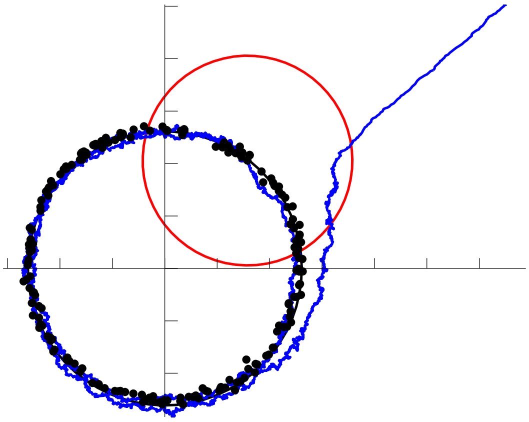

Figure 1.2 – For a collection of $N = 200$ agents with $M = 4$, $\rho = 1$ and $\sigma = 0.07$, we explicitly draw the trajectory of a randomly chosen agent. We observe that this agent indeed follows the consensual limit cycling orbit with analytically predicted radius $\mathscr{L}_{s,\rho} = \sqrt{2}\rho = \sqrt{2}$. The observation range of the considered agent (red circle) encompasses exactly the sector of aperture $\pi/4$ to determine the size of the self-generated limit cycle (see the construction given in Figure 1.1).

1.4 Generalization

By using the class of mixed-canonical dissipative dynamics Hongler and Ryter (1978) and following the same lines as those given in Proposition 1, we now can relax the cylindrical symmetry and write:

Proposition 2. *Consider the class of functions* $\mathscr{H}(x_1, x_2) : \mathbb{R}^2 \mapsto \mathbb{R}^+$ *for which the family of planar curves defined by* $[\mathscr{H}(x_1, x_2) - R] = 0$ *are closed* $\forall\ R > 0$ *and do not intersect for different values of* R*'s. Introduce a functional* $\mathcal{V}(\mathscr{H}) : \mathbb{R}^+ \mapsto \mathbb{R}$ *with* $\lim_{\mathscr{H}\to\infty} \mathcal{V}(\mathscr{H}) = \infty$ *(here, we shall use* $\mathcal{V}(\mathscr{H}) = \gamma\left\{\mathscr{L}^2 H - \frac{1}{2}H^2\right\}$ *with* $\gamma > 0$*). Assume in addition that the values of the* $\mathscr{H}$*-derivatives* $\mathcal{V}'(0) < 0$ *and* $\mathcal{V}'(\mathscr{H})\mid_{\mathscr{H}=C} = 0$ *and* C *is the unique value for which it holds. Then*

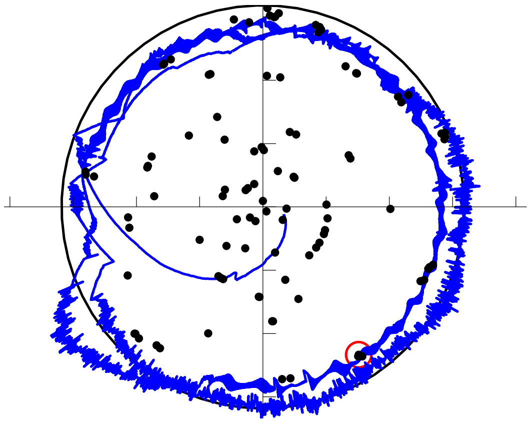

Figure 1.3 – For a collection of $N = 200$ agents with $M = 4$, $\rho = 1$ and $\sigma = 0.07$, we explicitly draw the trajectory of a randomly chosen agent. We observe that this agent indeed follows the consensual limit cycling orbit with analytically predicted radius $\mathscr{L}^2_{s,\rho} = 2/\left[1 - \cos(\pi/50)\right] \simeq (50/\pi)^2 \simeq (17)^2$. The observation range of the considered agent encompasses exactly the narrow sector of aperture $\pi/50$ to determine the size of the self-generated limit cycle (see the construction given in Figure 1.1). The High value $M = 50$ is responsible for the sometimes erratic behavior of the agent, as its observation range only encompasses a very small sector of the consensual circle.

Eqs.(1.1) *and* (1.7) *can be respectively generalized as:*

$$\begin{cases} d\mathbf{X}_k(t) = \mathbb{A}_k(\vec{\mathbf{X}})\,dt - \gamma\left\{\mathscr{V}'(\mathscr{H}(\mathbf{X}))\partial_{\mathbf{X}_k}\mathscr{H}(\mathbf{X}_k)\right\}dt + \sigma\,d\mathbf{W}_k(t), \qquad k = 1, 2, \cdots, N, \\ X_k(0) = X_{0,k}, \qquad \text{and} \qquad X_k(t) \in \mathbb{R}^2, \end{cases} \tag{1.17}$$

where

$$\mathbb{A}_k(\vec{\mathbf{X}}) = \begin{pmatrix} \frac{N_k(t)}{N} - \frac{1}{M} & \frac{N_k(t)}{N} \\ -\frac{N_k(t)}{N} & \frac{N_k(t)}{N} - \frac{1}{M} \end{pmatrix} \cdot \begin{pmatrix} \partial_{X_{1,k}}\mathscr{H}(\mathbf{X}_k) \\ \partial_{X_{2.k}}\mathscr{H}(\mathbf{X}_k) \end{pmatrix} \tag{1.18}$$

and

$$\begin{cases} dX_1(t) = \left[+\frac{1}{M}\partial_{X_2}\mathscr{H}(\mathbf{X}) - \gamma\left\{\left[\mathscr{V}'(\mathscr{H}(\mathbf{X})\right]\cdot\partial_{X_1}\mathscr{H}(\mathbf{X})\right\}\right]dt + \sigma dW_1(t), \\ dX_2(t) = \left[-\frac{1}{M}\partial_{X_1}\mathscr{H}(\mathbf{X}) - \gamma\left\{\left[\mathscr{V}'(\mathscr{H}(\mathbf{X})\right]\cdot\partial_{X_2}\mathscr{H}(\mathbf{X})\right\}\right]dt + \sigma dW_2(t). \end{cases} \tag{1.19}$$

The stationary measure Eq.(1.8) *here reads:*

$$P_s(\mathscr{H})\, d\mathscr{H} = \mathcal{Z}^{-1} \exp\left\{\frac{2\gamma}{\sigma^2}\,[V(\mathscr{H})]\right\} d\mathscr{H}, \tag{1.20}$$

where $\mathcal{Z}$ *is the normalization constant.*

□

Additional remarks.

a) Observe that Proposition 1 follows from the Proposition 2 in the rotationally symmetric case resulting when $\mathscr{H}(\mathbf{X}) = (1/2)\left[X_1^2 + X_2^2\right]$.

b) Contrary to Proposition 1, in Proposition 2, neither the limit cycle nor the invariant measure $P_s(\mathscr{H})$ generally have a cylindrical symmetry. This precludes the possibility to analytically determine the selected consensual limit cycle (i.e we do not have in the general case a simple expression like the one given by Eq.(1.16)).

c) As an illustration of Proposition 2, we may consider the Cassini Hamiltonian function given by

$$\mathscr{H}(\mathbf{X}) = \left[(x_1-1)^2 + x_2^2\right]\left[(x_1+1)^2 + x_2^2\right] = b^4, \tag{1.21}$$

with the level orbits sketched in Figure 1.4. According to the values of M and ρ which ultimately will fix the size of the parameter b, we are in this case able to generate two different regimes. For large b a single closed consensual limit cycle is generated. Alternatively, for small b, the agents are shared into two clusters and evolve on two separated consensual limit cycles (see Figure 1.5).

d) Generalizing the previous Cassini ovals construction, one may construct Hamiltonian generating agents circulation on even more complex orbits. We provide an additional example in Figure 1.6.

1.5 Conclusions and Perspectives

While agents with behavior-based interactions are relatively easy to implement, it is widely recognized that the underlying mathematical analysis of such models is generally difficult and often even impossible to perform completely. It is therefore quite remarkable that very simple

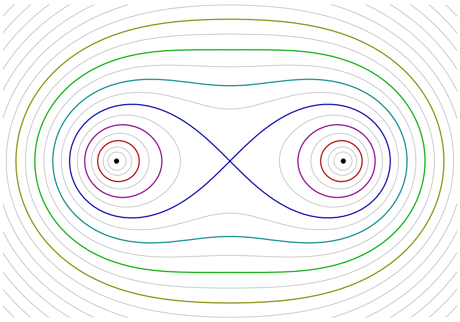

Figure 1.4 – Typical shapes of the Cassini's ovals determined by the equation $\mathcal{H}(x_1, x_2) = \left[(x_1-a)^2 + x_2^2\right]\left[(x_1+a)^2 + x_2^2\right] = b^4$ for b-values ranging from $b = 0.6a$ to $1.6a$. Image courtesy of Wikimedia under CC BY-SA 3.0.

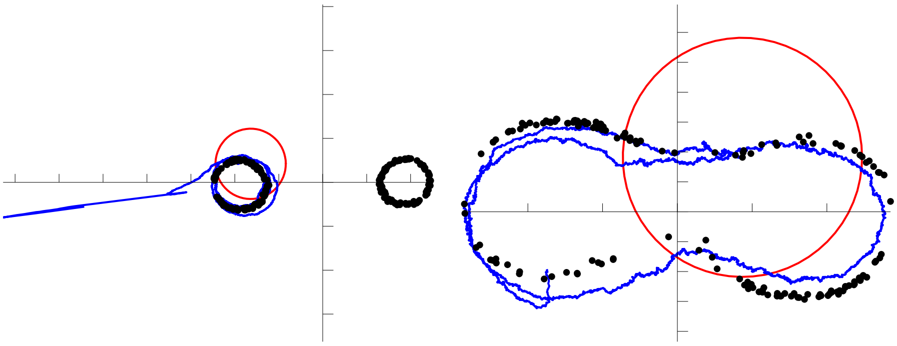

Figure 1.5 – Left: Selection of a couple of limit cycling orbits obtained from the Cassini Hamiltonian Eq.(1.21) when the control parameters are set to $M = 4$ and $\rho = 0.4$. In red, the observation range of a randomly picked representative agent.
Right: Single limit cycling trajectory for the Cassini Hamiltonian Eq.(1.21) but here with the control parameters set to $M = 4$ and $\rho = 0.8$.

analytical results can be derived for a whole class of dynamics which, due to its simplicity, offers potential for applications. Despite that for limited number of agents, typically one hundred in our present study, the mean-field approach can only be approximative, we nevertheless emphasize that all our numerical investigations still closely match the theoretical predictions. The resilience of our modeling approach opens several perspectives for implementations on actual agents. Several further research directions are naturally suggested by this contribution, among them:

a) *Extended MCD dynamics to higher dimensional spaces.* The role played here by the Hamiltonian function leading to a canonical motion on the plane can be extended. In particular one may consider, along the lines explained in Schweitzer et al. (2001), integrable canonical systems exhibiting additional constants of the motions. Using these extra constants of the motion, one will be able to stabilize the swarm motion along orbits in higher dimensions.

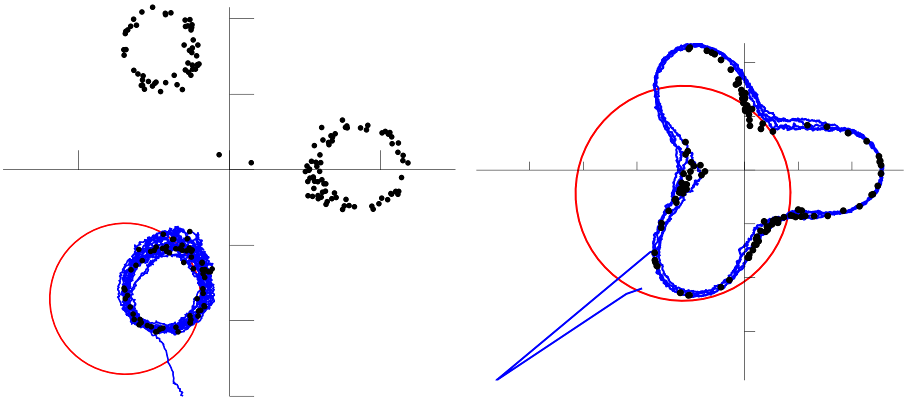

Figure 1.6 – Left: Orbit generated by the $\left(\frac{2\pi}{3}\right)$-symmetric Hamiltonian function: $\mathscr{H}(x_1,x_2) = \left[(x_1-1)^2+(x_2)^2\right] \cdot \left[(x_1+\frac{1}{2})^2+(x_2-\frac{\sqrt{3}}{2})^2\right]\left[(x_1+\frac{1}{2})^2+(x_2+\frac{\sqrt{3}}{2})^2\right]$. Here we have $N = 200$ and the control parameters are set to $M = 4$ and $\rho = 0.5$. In red, the observation range of a randomly picked representative agent.
Right: Here, all parameters are identical, except for the interaction range which is $\rho = 1$.

b) *Heterogeneity in agents and soft control of swarms.* Instead of focusing on homogeneous agents and by following the work Han et al. (2006), we intend to use the context of MCD to study the possibility to influence (i.e. *soft control*) the behavior by introducing into the society a single “fake” agent (i.e. a *shill*), which can be externally controlled.

c) *Resilience of the modeling.* In Eq.(1.2), we used the Euclidean norm to define $\mathscr{D}_{k,\rho}(t)$, the instantaneous neighboring agents in Eq.(1.3). To match specific applications, other type of norms could be used to redefine the interactions.

1.6 New Contributions of Chapter 1

- We present an analytically tractable decentralized mixed canonical-dissipative (MCD) dynamic for a homogeneous swarm of Brownian agents, in which agents self-select a control parameter by local interactions only. When cylindrical symmetry holds for the MCD, we are able to prove convergence of the swarm to a limit circular ring. The ring radius can be exactly calculated as a function of the interaction range and the interconnection strength. The method holds for more complex geometries, by relaxing the cylindrifcal symmetry.

- **Publication:** This chapter is reproduced from the published journal paper Sartoretti and Hongler (2013b), with slight modifications to fit the present dissertation. The initial research leading to the journal paper was published as a conference paper in Sartoretti and Hongler (2013a).

2 Decentralized Self-Selection of Swarm Trajectories: From Dynamical Systems Theory to Robotic Implementation

Summary

In this chapter, we present a distributed control strategy, enabling agents to converge onto and travel along a consensually selected curve among a class of closed planar curves. Individual agents identify the number of neighbors within a finite circular sensing range and obtain information from their neighbors through local communication. The information is then processed to update the control parameters and force the swarm to converge onto and circulate along the aforementioned planar curve. The proposed mathematical framework is based on stochastic differential equations driven by white Gaussian noise (diffusion processes). Using this framework, there is maximum probability that the swarm dynamics will be driven toward the consensual closed planar curve. In the simplest configuration where a circular consensual curve is obtained, we are able to derive an analytical expression that relates the radius of the circular formation to the agent's interaction range. Such an intimate relation is also illustrated numerically for more general curves. The agent-based control strategy is then translated into a distributed Braitenberg-inspired one. The proposed robotic control strategy is then validated by numerical simulations and by implementation on an actual robotic swarm. It can be used in applications that involve large numbers of locally interacting agents, such as traffic control, deployment of communication networks in hostile environments, or environmental monitoring.

2.1 Introduction

How can one trigger the self-emergence of desired spatio-temporal patterns via a collection of interacting autonomous agents? Can we analytically derive such collective behavior for scalable collections of agents? Is it possible to explicitly demonstrate how such collective behavior can possibly remain stable in the face of environmental noise? Progress in the engineering of swarm robotics relies on explicit and detailed answers to these questions, and that is the central goal of the present contribution. As no generic guidelines yet exist, engineering such collective behavior remains, in many respects, an open challenge. Bonabeau, Dorigo and Theraulaz illustrate how elementary, fully decentralized biological systems can achieve highly elaborate collective tasks Bonabeau et al. (1999). This pioneering work remains a rich and challenging source of inspiration for many further developments both in ethology (see the recent overview by Leonard Leonard (2013)) and in swarm robotics. Presently, serious effort is being made to import some basic features of these complex living systems into the engineering world of robotics. Obviously, animals remain intrinsically highly complex machines compared to actual robots and, therefore, direct applications remain rather limited. Nevertheless, recent attempts to combine artificial and natural collective systems by implementing the models observed in animal societies into that of robots shows promise Halloy et al. (2007); Mondada et al. (2011). Because of the complexity of the interactions taking place in such mixed societies, the models often remain partial and the link between them has not been fully established.

Several up-to-date reviews Kernbach (2013); Brambilla et al. (2013) summarize ongoing research in this area and the various engineering applications. Often the design of such robotic systems consists of a bottom-up trial-and-error exercise with no analytical link between the microscopic model (describing the single agent behavior) and the macroscopic one (describing the global result achieved). Microscopic and macroscopic models are then seen as separate approaches Brambilla et al. (2013), rather than steps in the engineering process. To bridge the gap between the micro- and macroscopic descriptions, Martinoli et al. Martinoli et al. (1999) constructed the first link between individual behavior and the statistical macroscopic model, which was successfully implemented on real robots. Along the same lines, Lerman et al. Lerman et al. (2005) exhibited the emergence of collective behavior from individual robot controllers using a class of stochastic Markovian mathematical models. The authors validated their approach by performing experiments using real robots. More recently, Hamann and Wörn Hamann and Wörn (2008) used an explicit representation of space together with methods of statistical physics to establish the link between microscopic and macroscopic models. Space heterogeneities are also considered by Prorok et al. Prorok et al. (2011), who derived, from diffusion-type evolutions, a collective inspection scenario implemented on real robots. Brambilla et al. Brambilla et al. (2012) proposed a top-down design process built on iterative model construction and based on Probabilistic Computation Tree Logic (Deterministic Time Markov Chains). Their design methods were further validated on a group of physical *e-puck* robots; their iterative construction potentially enables other types of swarming behavior, depending on the skills of the acting programmer. Berman et al. Berman et al. (2009) likewise proposed a top-down design methodology, but at a higher level (i.e., at the sub-swarm level). Their decentralized strategy allows dynamical allocation of a swarm of robots to multiple predefined tasks. The approach by Berman et al. Berman et al. (2009) is based on population fractions, which enable the design of stochastic control policies for each robot, and does not assume communication among robots. This strategy is analytically proven to achieve the desired allocation, and validation is made on a surveillance scenario involving 250 simulated robots distributed across four sites. More recently, Berman et al. Berman et al. (2011) have extended their work to spatially heterogeneous swarms. This control however, can only generate static patterns of robot sub-swarms Song and Kumar (2002). In the present work, we aim to generate self-organized dynamic patterns (i.e, circulation of robots along closed planar curves).

Closely related to the present research, Hsieh et al. Hsieh et al. (2007) synthesized controllers that allowed individual robots, when assembled in a swarm, to self-organize and circulate along a predefined closed curve. The system is fully distributed and relies only on local information, thus ensuring scalability. The controller can be analytically described, and does not require communication between the robots, thus simplifying its implementation. Hsieh et al. Hsieh et al. (2007) demonstrated convergence of the system for a certain class of curves and validated their theory with simulations. While the final behavior looks similar to what we are targeting here, we aim at directly deriving our controller from a stochastic dynamical model that can be analytically discussed. Our goal here is to allow the swarm to converge to a consensually selected curve among a given family (and not to a predefined curve as done in Hsieh et al.'s study). Conceptually, Hsieh et al.'s study belongs to the important family of potential field approaches . Within this family, Pimenta et al. Pimenta et al. (2013) proposed a decentralized hydrodynamics-inspired controller that drives the swarm into a preassigned arrangement using a static and/or dynamic obstacle avoidance mechanism. They also tested their approach on swarms of actual robots, including *e-puck* robots. More closely related to our research, Sabattini et al. Sabattini et al. (2012) developed a control strategy using decentralized time-dependent potential construction. Specifically, this mechanism allows a robotics swarm to track a closed curve (given by an implicit function, as in this research), while keeping a minimal safety distance between the robots. In Sabattini et al.'s study Sabattini et al. (2012), the robots are given a predefined curve, whereas in our approach, the swarm consensually selects the closed curve that will be tracked.

Amongst non-gradient-based approaches, Schwager et al. Schwager et al. (2011) demonstrated the stability and quantified the convergence rate of the control of a quad-rotors swarm. Their approach is based on a combination of decentralized controllers and mesh networking protocols. Moreover, the authors only used local information and validated their control on a group of three real robots. Schwager et al.'s controller needs to know the relative position of its neighbors with high precision, while our goal is to be noise-resistant. Sepulchre et al. Sepulchre et al. (2007) developed a methodology for the generation of stable circular motion patterns based on stabilizing feedbacks derived from Lyapunov functions. A very similar approach was also used in Paley and Leonard (2006); Zhang and Leonard (2007). This theoretical work was then used to design the control of mobile sensor networks for optimal data collection in environmental monitoring Leonard et al. (2007). The global patterns generated in Sepulchre et al's study exhibit similarities with those presented in the present research, but their control is "less" decentralized. Namely, Sepulchre et al. assume an all-to-all communication network between the robots, whereas in our work, we aim at using only local communication between neighbors within a given range. Given Sepulchre et al.'s assumption, the controller is also more sensitive to losses of communication between robots in the swarm. Finally, within non-gradient-based controls, it is worthwhile to mention Tsiotras et al. Tsiotras and Castro (2011), who devised a decentralized mechanism, leading to *Spirograph*-like planar swarm trajectories. Their approach only relies on individually gathered information on distance and angle to neighbors.

With respect to the state of the art, whereas most research in control theory aims at finding strong theoretical guarantees, the present work follows a very different approach. We aim at bridging the gap between the purely mathematical considerations and the implementation on actual robots, and approach the problem from a mathematical angle. The mathematical models are then implemented using a swarm of mobile robots. To some extent, our work is closer to that of biologists who use robotics as a validation tool for their theoretical models. Using this approach, we are able to achieve a decentralized consensual swarm control mechanism using only simple local information, such as the number of neighbors in a given range and their relative positions. In order to better link the model and the implementation, this article also includes a dictionary to help translation of the main concepts between the theoretical and the robotic control mechanisms. The developed controllers are not designed to achieve a fixed shape or trajectory, as often found in the state of the art, but to collectively choose one consensual shape. By tuning the control parameters, one can enable a given swarm to converge on different orbits without changing the behavior of each agent. Another important feature is the fact that the consensual orbit is not known by the agents, but is only determined by mutual interactions in a fixed range.

Although perfectly predictable analytically, this collective choice can be described as a *collective weakly emergent behavior*. Weak emergence is here understood in the S. and O. Kernbach's interpretation Kernbach et al. (2013); Kernbach (2013) (i.e., macroscopic swarm behavior due to interactions between agents but having its origin in the model that describes the system's behavior). Our model has a tractable complexity, enabling us to explicitly describe the resulting emergent collective behavior, which is controllable. Specifically, our class of models presents a distributed mechanism, enabling agents to select a parameter while fixing one consensual traveling orbit among the given family in a distributed manner, and this feature holds even if noise corrupts their movements.

The chapter is organized as follows: Section 2 exposes the basic mathematical formulation of agents' dynamics. Section 3 reports simulation experiments that fully match our theoretical finding even for finite N agents' populations (i.e., when the mean-field limit is not reached). Section 4 describes, in detail, how the actual implementation of our mathematical model was realized with a collection of e-puck autonomous robots.

2.2 Mathematical modeling

Our mathematical model consists of a set of N coupled stochastic differential equations (SDE) where the driving stochastic processes are White Gaussian Noise (WGN) representing a swarm of homogeneous Brownian agents Schweitzer (2003). The use of WGN in the dynamics implies that the resulting stochastic processes are Markovian. Accordingly, all probabilistic features of the model are known by solving the associated Fokker-Planck (FP) equation. A similar approach has already been used in several studies Berman et al. (2011); Hamann and Wörn (2008); Prorok et al. (2011). Agents' interactions are ruled by specifying the radius of an observation disk (i.e., metric interactions) and the strength of the attraction/repulsion control parameter. The specific form of agents' individual dynamics and their mutual interactions are constructed from a Hamiltonian function, from which one derives both a canonical and a dissipative drift force (i.e., *mixed canonical-dissipative vector fields* Hongler and Ryter (1978)). By imposing the orthogonality between the canonical and dissipative vector fields, we are able, in the N → ∞ mean-field limit, to explicitly calculate the stationary probability (i.e., invariant probability measure) characterizing the global agents' populations. For our class of models, we can analytically observe how a decentralized algorithm is able to generate a milling-type spatio-temporal pattern. In this pattern, all agents will circulate with constant angular velocity in the vicinity of a self-selected level curve from the input Hamiltonian function.

2.2.1 Single agent dynamics

Let us first consider the single agent Mixed Canonical-Dissipative (MCD) stochastic planar dynamics:

$$\begin{pmatrix} dX(t) \\ \\ dY(t) \end{pmatrix} = \mathbb{V} \begin{pmatrix} \partial_X H(X,Y) \\ \\ \partial_Y H(X,Y) \end{pmatrix} dt + \sigma \begin{pmatrix} dW_X(t) \\ \\ dW_Y(t) \end{pmatrix}, \qquad \begin{pmatrix} X(0) = X_0 \\ Y(0) = Y_0 \end{pmatrix} \tag{2.1}$$

where $\mathbb{V}$ stands for a skew symmetric (2×2) dynamical matrix defined by:

$$\mathbb{V} = \begin{pmatrix} U'[H(x,y)] & +\omega \\ \\ -\omega & U'[H(x,y)] \end{pmatrix} \tag{2.2}$$

where $(X,Y) \in \mathbb{R}^2$ are the positions of the planar agent, $H(X,Y) : \mathbb{R}^2 \mapsto \mathbb{R}^+$ and $U[H] : \mathbb{R}^+ \mapsto \mathbb{R}$ ($U'[H]$ stands for the derivative of $U[H]$ with respect to H) are differentiable functions, $\sigma > 0$ and $\omega \in \mathbb{R}$ are constant parameters. The inhomogeneous terms $dW_X(t)$ and $dW_Y(t)$ are two independent WGN sources. We shall assume that $H(X,Y) = E$, $\forall E > 0$ defines closed concentric curves and $H(0,0) = 0$. In addition, we require that $U[0] > 0$ and $\lim_{E\to\infty} U[H(E)] = -\infty$. When $\sigma = 0$, the (deterministic) dynamics Eq.(2.1) admits closed trajectories $\mathscr{C}$'s, which are defined by the solutions of the equation $U[H(X,Y)] = 0$. Depending on the sign of the curvature (i.e., second derivative) U'' taken at $\mathscr{C}$, one can either have attracting ($U'' < 0$) or repulsive ($U'' > 0$) limit orbits. An attracting $\mathscr{C}$ drives any initial conditions (X_0, Y_0) to $\mathscr{C}$ in asymptotic time. In Eq.(2.1), the antisymmetric part of $\mathbb{V}$ produces a rotation in $\mathbb{R}^2$ with angular velocity ω. This defines a canonical (conservative) part of the vector field (i.e., the Hamiltonian part of the dynamics). Concurrently, the diagonal elements of $\mathbb{V}$ model the non-conservative components of the dynamics (i.e., dissipation or supply of energy). From its structure, the non-conservative (deterministic) vector field of Eq.(2.1) is systematically perpendicular to the conservative one. This geometrical constraint reduces the dimensionality of the dynamics and allows the derivation of explicit and fully analytical results.

In the presence of WGN ($\sigma > 0$ in Eq.(2.1)), the resulting SDE describe a Markovian diffusion process, fully characterized by a bivariate transition probability density (TPD) measure

$$\begin{aligned}&P(x,y,t \mid x_0,y_0,0)\,dx\,dy = \\ &\qquad \text{Prob}\left\{x \le X(t) \le x+dx, y \le Y(t) \le y+dy \mid X(0)=x_0, Y(0)=y_0\right\}\end{aligned}$$

The TPD $P(x,y,t \mid x_0,y_0,0)$ is the solution of a FP equation:

$$\begin{cases} \partial_t P(x,y,t \mid x_0,y_0,0) = \mathscr{F}\left\{P(x,y,t \mid x_0,y_0,0)\right\}, \\ \\ P(x,y,0 \mid x_0,y_0,0) = \delta(x-x_0)\delta(y-y_0) \end{cases} \tag{2.3}$$

where $\delta(\cdot)$ stands here for the Dirac probability mass and the FP operator reads:

$$\mathscr{F}\{\cdot\} := -\partial_x\left[f_x(x,y)\{\cdot\}\right] - \partial_x\left[f_y(x,y)\{\cdot\}\right] + \frac{1}{2}\sigma^2\left[\partial_{xx} + \partial_{yy}\right]\{\cdot\} \tag{2.4}$$

with

$$\begin{cases} f_x(x,y) := +\partial_y\left[H(x,y)\right] + U[H(x,y)]\partial_x\left[H(x,y)\right] \\ \\ f_y(x,y) := -\partial_x\left[H(x,y)\right] + U[H(x,y)]\partial_y\left[H(x,y)\right] \end{cases}$$

For asymptotic time, the diffusion processes reach a stationary regime: $\lim_{t\to\infty} P(x,y,t \mid x_0,y_0,0) = P_s(x,y)$, solving the stationary FP Eq.(2.3), for which we obtain:

$$P_s(x,y) = \mathscr{N} e^{-(2/\sigma^2)\, U[H(x,y)]} \tag{2.5}$$

and $\mathscr{N}$ is the probability normalization factor yielding $\int_{\mathbb{R}^2} P_s(x,y)\,dx\,dy = 1$.

Example. Consider the Hamiltonian function $H(x,y) = x^2 + y^2$, $U[H] = \gamma\left\{\mathscr{L}^2 H - \frac{1}{2}H^2\right\}$ and $U'[H] = \gamma\left\{\mathscr{L}^2 - H\right\}$, width $\gamma > 0$. In this case, the deterministic dynamics coincides with the Hopf oscillator with an unique attracting $\mathscr{C}$ that is a circle with radius $\mathscr{L}$. In this situation, the measure Eq.(2.5) exhibits the shape of a circular "ring" with its maximum located on the circle $\mathscr{C}$ (see Figure 2.1).

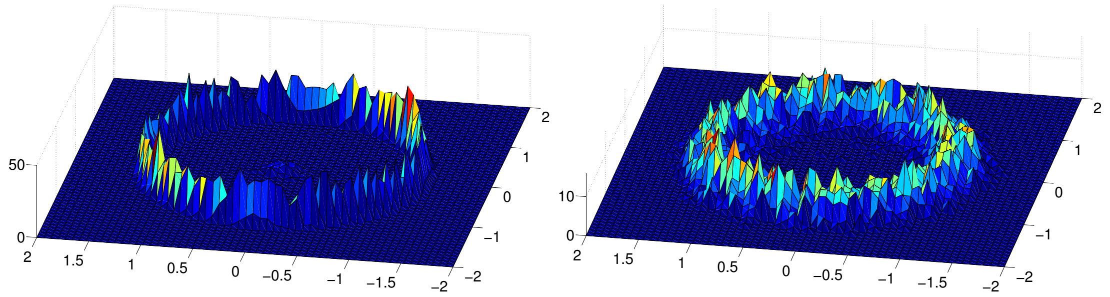

Figure 2.1 – "Ring"-shaped probability density on the plane, for $\sigma = 0.07$ and $\sigma = 0.35$. These simulations were run with $N = 5000$ agents, up to time $T = 10[s]$, with $\gamma = 1$.

2.2.2 Multi-agent dynamics

Let us now build on the dynamics presented in section 2.2.1 and consider a **homogeneous swarm** of N interacting agents exhibiting individual dynamics similar to the one described in Eq.(2.1). Specifically, for $k = 1, 2, .., N$, we now write:

$$\begin{pmatrix} dX_k(t) \\ \\ dY_k(t) \end{pmatrix} = \mathbb{V}_{k,\rho,M}(t) \begin{pmatrix} \partial_{X_k} H(X_k, Y_k) \\ \\ \partial_{Y_k} H(X_k, Y_k) \end{pmatrix} dt + \sigma \begin{pmatrix} dW_{X_k}(t) \\ \\ dW_{Y_k}(t) \end{pmatrix}, \quad \begin{pmatrix} X_k(0) = X_{0,k} \\ \\ Y_k(0) = Y_{0.k} \end{pmatrix} \tag{2.6}$$

where $\mathbb{V}_{k,\rho,M}$ stands for a (2×2) dynamical matrix defined by:

$$\mathbb{V}_{k,\rho,M} = \begin{pmatrix} \left[\frac{N_{k,\rho}(t)}{N} - \frac{1}{M}\right] + \overbrace{\gamma\left[\mathscr{L}_{k,\rho}(t) - \frac{1}{2}H(X_k, Y_k)\right]}^{U'[H,t]} & + \frac{N_{k,\rho}(t)}{N} \\ - \frac{N_{k,\rho}(t)}{N} & \left[\frac{N_{k,\rho}}{N}(t) - \frac{1}{M}\right] + \underbrace{\gamma\left[\mathscr{L}_{k,\rho}(t) - \frac{1}{2}H(X_k, Y_k)\right]}_{U'[H,t]} \end{pmatrix} \cdot M \cdot \omega, \tag{2.7}$$

where $M > 1$ and $\omega > 0$ are (time-independent) control parameters, $M \cdot \omega$ is a normalization factor and $dW_{(\cdot)}(t)$ are all independent standard WGN sources (homogeneity follows as we have $H_k(X_k, Y_k) \equiv H(X_k, Y_k)\ \forall\ k$). The mutual interactions enter via the term $N_{k,\rho}(t)$ present in the dynamic matrix $\mathbb{V}_{k,\rho,M}(t)$. To define $N_{k,\rho}(t)$, we assume that each agent $\mathscr{A}_k$ ($k = 1, 2, \cdots, N$) is located at the center of an (individual) observation disk $\mathscr{D}_{k,\rho}(t)$ with common constant radius ρ. We further assume that $\mathscr{A}_k$ is, in real time, able to count the number of neighboring fellows $N_{k,\rho}(t)$ that are contained in $\mathscr{D}_{k,\rho}(t)$. Finally, we introduce the instantaneous (geometric) inertial moment of the agents located in $\mathscr{D}_{k,\rho}(t)$, namely:

$$\mathscr{L}_{k,\rho}(t) := \frac{1}{N_{k,\rho}(t)} \sum_{j \in \mathscr{D}_{k,\rho}(t)} H\big(X_j(t), Y_j(t)\big) \geq 0. \tag{2.8}$$

To heuristically understand the collective behavior emerging from the set of SDE's given in Eq.(2.6), let us comment on the following features:

a) **Large population of homogeneous agents**. As we consider homogeneous populations, we may randomly tag one agent, say $\mathscr{T}$, and consider the actions of the others as an effective external field (often referred to as the **mean-field point approach**). This procedure reduces the nominal multi-agent dynamics to a single effective agent system, thus making the analytical discussion much easier while still taking into account interactions of the neighbors. The individual $\mathscr{T}$-diffusive dynamics on $\mathbb{R}^2$ are then assumed to be representative of the global swarm and follow from dropping the index k in Eqs.(2.6) and (2.7). The effective interactions terms $N_{\rho,M}$ and $\mathscr{L}_{\rho,M}$ are to be determined by auto-consistency from the TPD measure of $\mathscr{T}$. In the stationary regime, thanks to the orthogonal property between the canonical and the dissipative components of the vector fields, we obtain:

$$P_s(\vec{x}, \vec{y}) = \left[P_s(x, y)\right]^N = \left[\mathscr{N}^{-1} e^{\frac{2\gamma}{\sigma^2} U[H(x,y)]}\right]^N \qquad \vec{x} := (x_1, x_2, \cdots, x_N) \tag{2.9}$$

For $H(X,Y) = \frac{X^2+Y^2}{2}$, the harmonic oscillator Hamiltonian, and for large signal-to-noise ratio
$\mathscr{S} = 2\gamma/\sigma^2 \ll 1$, we can analytically express the value of the limit cycle's orbit:

$$\mathscr{L}_{\rho,M} = \frac{\rho}{\sqrt{2-2\cos(\pi/M)}}. \tag{2.10}$$

b) **Roles of the control parameters** M **and** ρ. The origin $\mathbf{O} := (0,0)$ is a singular point of the deterministic dynamics and its stability follows from linearizing the dynamics near $\mathbf{O}$. In the stationary regime, the linearization reads:

$$\mathbb{V}_{\rho,M}(\mathbf{0}) = \begin{pmatrix} \left[\frac{N_{\rho,M}}{N} - \frac{1}{M}\right] + \gamma\,\mathscr{L}_{\rho,M} & +\frac{N_{\rho,M}}{N} \\ -\frac{N_{\rho,M}}{N} & \left[\frac{N_{\rho,M}}{N} - \frac{1}{M}\right] + \gamma\,\mathscr{L}_{\rho,M} \end{pmatrix}$$

with eigenvalues:

$$\lambda_{\pm} = \underbrace{\left[N_{\rho,M}/N - 1/M\right]}_{\mathscr{RE}} \pm \sqrt{-1}\left[\sqrt{N_{\rho,M}/N}\right]. \tag{2.11}$$

When $\mathscr{RE} < 0$, (resp. > 0), $\mathbf{O}$ is attractive (resp. repulsive). The very existence of a stationary regime implies that $P_s(x,y)$ vanishes for large values of $|x|$ and $|y|$. For agents far from $\mathbf{O}$, both $N_{k,\rho,M}$ and $\mathscr{L}_{k,\rho,M}$ will vanish (with high probability, except the agent at the center, no agents will be found inside $\mathscr{D}_{k,\rho}$), implying $\mathbf{O}$ to be attractive as $\mathscr{RE} < 0$; conversely, agents close to $\mathbf{O}$ will be repelled. Ultimately, an equilibrium consensus will be reached when the diagonal part of $\mathbb{V}_{\rho,M}$ vanishes which is achieved when Eq.(2.10) is attained.

c) **Role of the dissipative terms** $U'[H,t]$ **and the parameter** $\mathscr{L}_{\rho,M}$. Observe that the regulating term $U'[H,t]$ is itself not necessary to reach a consensual behavior. However, for large γ's, it enhances the convergence rate toward equilibrium and reduces the variance around the mode of $P_s(x,y)$. This enables us to easily estimate the radius $\mathscr{L}_{\rho,M}$ given by Eq.(2.10).

According to Eqs.(2.9) and (2.10), we observe that, in the stationary regime, the swarm self-selects a consensual circular orbit with radius $\mathscr{L}_{\rho,M}$ that depends on both the observation range ρ and the effective attracting range M.

Numerical simulation results, obtained by applying the Euler method over discrete timesteps with
$dt = 5 \cdot 10^{-3}[s]$, are shown in Figures 2.2 and 2.3. The employed discretization works perfectly, as the numerical results coincide very closely with our theoretical ones (especially in the case of the theoretical limit cycle in Figure 2.2, left).

Note that a Hamiltonian function can be constructed from a set of points along any desired close curve on the plane (without self-intersection). A simple fit can be made on this set of points (e.g., least squares method), returning a high-degree polynomial form representing the Hamiltonian function. This function will be differentiable (by construction), and we can ensure $H(X,Y) > 0 (\forall X, Y)$ by adding a constant; the Hamiltonian can then be directly used in our model.

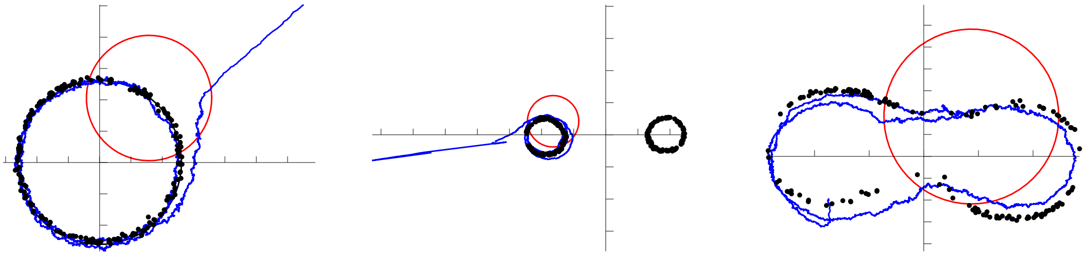

Figure 2.2 – Numerical simulation for $N = 200$ agents, $\rho = 1$, $\sigma = 0.07$ and $M = 4$. The black dots show the final position of the agent at time $T = 50[s]$, while the blue line gives the trajectory of one arbitrary agent (with its observation range in red). The black circle (hidden below the swarm of agents) gives the theoretically computed limit cycle. This shows the exactitude of Eq.(2.10), even for finite swarms.
Left: Harmonic oscillator Hamiltonian function $H(X,Y) = \frac{X^2+Y^2}{2}$.
Center: Cassini ovals Hamiltonian function $H(X,Y) = ((X-1)^2 + Y^2) \cdot ((X+1)^2 + Y^2)$, with $\rho = 0.4$, showing closed ovals without connections (see Yates (1947)).
Right: Same Hamiltonian function as the center figure, with $\rho = 0.8$, presenting one connected orbit around both attractors.

2.3 Robotic implementation

2.3.1 Braitenberg control mechanism

The actual adaptation of our MCD dynamics is implemented on the model of a *Braitenberg control mechanism* (BCM) Braitenberg (1984). In the BCM, the speed of the robot's motor(s) is reactuated at discrete timesteps, solely based on the output value(s) of a series of sensors.

In our case, we use cylindrical robots, equipped with eight light sensors (s0,s1,...,s7) evenly distributed along their circular perimeter and two driving motors (left and right), as pictured in Figure 2.4. The robot's movement evolves on the plane, with a light source located at the origin.

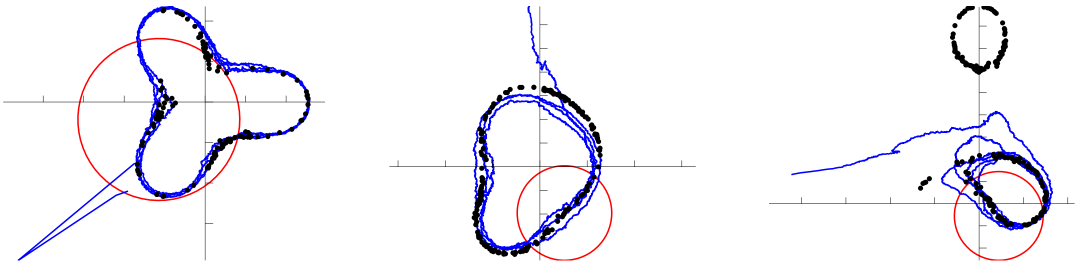

Figure 2.3 – Numerical simulation for $N = 200$ agents, $\rho = 1$, $\sigma = 0.07$ and $M = 4$, until time $T = 25[s]$ (left) or $T = 50[s]$ (center and right). In red, the observation range of a randomly picked representative agent.
Left: Hamiltonian function with three attracting poles $H(X,Y) = ((X-1)^2 + Y^2)\cdot((X+\frac{1}{2})^2 + (Y-\frac{\sqrt{3}}{2})^2)\cdot((X+\frac{1}{2})^2 + (Y+\frac{\sqrt{3}}{2})^2)$.
Center: Asymmetric Hamiltonian function $H(X,Y) = (((X-\frac{1}{2})^2 + Y^2)\cdot((X+\frac{1}{2})^2 + (Y-\frac{\sqrt{3}}{2})^2)\cdot((X+\frac{3}{4})^2 + (Y+\frac{\sqrt{27}}{4})^2))^{\frac{1}{3}}$.
Right: Hamiltonian function $H(X,Y) = (((X-1)^2 + Y^2)\cdot((X+1)^2 + Y^2)\cdot(X^2 + (Y-4)^2))^{\frac{1}{3}}$, resulting in two disconnected orbits.

The light source serves as the origin **O** in the mathematical model, acting as an attractor for the robots, while also being the center of the limit cycle the robots will ultimately arrange and circulate on. Our goal is to let a swarm of robots arrange and circulate in a circle around the light source, following a similar control mechanism to Eq.(2.1), with the Hamiltonian function of the Hopf oscillator. This choice of circular trajectories allows us to compare the behavior of an agent swarm (with analytical results) and a robotic swarm.

The light sensors gather the following information:

1. $\mathbf{N}_\rho(\mathbf{t})$: the number of instantaneous neighbors in a fixed circular range around each robot ($N_\rho(t) \geq 1\ \forall t$ as every robot always detects itself),

2. $\{\mathbf{S_0}(\mathbf{t}), \mathbf{S_1}(\mathbf{t}), \ldots \mathbf{S_7}(\mathbf{t})\}$: the normalized light intensity ($\in [0;1]$, 1 for the sensor(s) receiving the most light) measured on each sensor.

The gathered information enables us to update the velocities at discrete timesteps according to the rule:

$$\begin{array}{rcccc} V_R(t+1) & = & \alpha \cdot N_\rho(t) & + & \beta \cdot \left(\overbrace{S_0(t) + \sum_{i=5}^{7} S_i(t)}^{=:S_L(t)} - \overbrace{\sum_{i=1}^{4} S_i(t)}^{=:S_R(t)} \right) \\ V_L(t+1) & = & \alpha \cdot N_\rho(t) & + & \beta \cdot \left(S_R(t) - S_L(t) \right), \end{array} \tag{2.12}$$

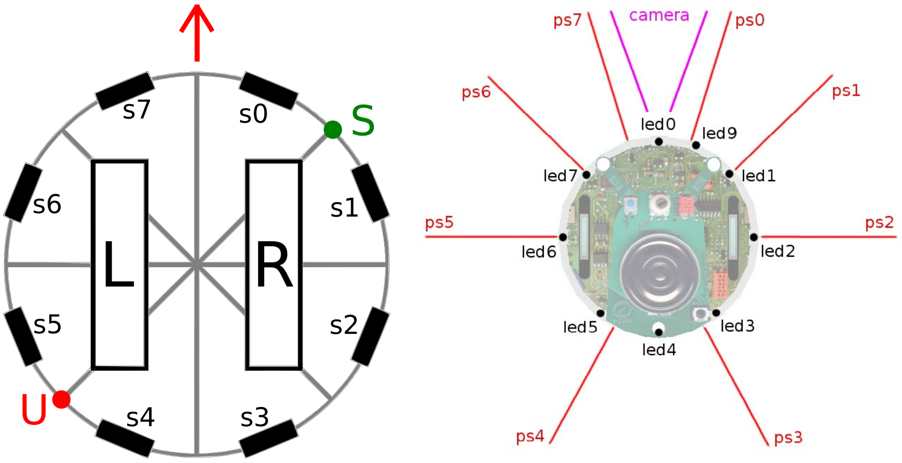

Figure 2.4 – Left: Theoretical robot, seen from above. Note the 8 sensors evenly distributed on the perimeter of the robot's body and the two motors L and R. The point S (resp. U) shows the stable (resp. unstable) facing direction of the light source in the BCM. Right: Actual e-puck robot in the same position; the 8 proximity sensors (ps0,ps1,...,ps7) are nearly evenly distributed on the perimeter.

where α and β are two positive parameters, controlling the translation/rotation velocities. This pair of controls in Eq.(2.12) effectively adapts Eq.(2.1) (in Cartesian coordinates) to a robotics paradigm, in terms of left/right motor speeds (speed and heading). In Eq.(2.12), we reduce the number of sensors to two by grouping them into the left group (S_L) and the right group (S_R).

The first term $\alpha \cdot N_\rho(t)$ accounts for the forward speed of the robot, and the other term regulates the heading. Indeed, when $\alpha = 0$, the speeds have the same norm but opposite signs, implying that the robot can only turn around its main axis. In this case, the robot stabilizes with the light source facing S, i.e., with the light source at the same distance from sensors 0 and 1, with $S_L(t) \equiv S_R(t) \Rightarrow V_L(t) = V_R(t) = 0$. This ending position is the only stable steady state; when the light source is facing the point U, at the same distance from sensors 4 and 5, it is unstable.

When the light initially stands on the left of the robot (i.e., facing sensors 5, 6, 7, or 0), $V_L(t)$ will exceed $V_R(t)$ (as $S_L(t) > S_R(t)$). In this configuration, the robot will turn on its axis until the light faces the point S. The same argument holds when the light initially stands on the right of the robot.

When the first term in Eq.(2.12) (the forward speed) is **constant and positive**, this control mechanism drives the robot to the light source to turn around it. The robot constantly moves forward, keeping the light source facing S, thereby creating a rotating trajectory around the light source.

The radius of the resulting orbit will be directly proportional to α, and inversely proportional to β: an increase in α results in a larger distance covered before the next heading update (and hence, a larger orbit). Conversely, an increase in β induces a sharper heading adaptation (and hence, a smaller orbit). For a fixed β, the radius of the limit cycle depends only on α.

In our case, we fix α and β, thus letting the forward speed be proportional to the number of instantaneous neighbors. This forces the orbit to shrink when few neighbors are detected, and increase in the other configuration, mimicking the MCD dynamics. While in the mathematical model of Section 2.2, the parameters ρ and M selected the limit cycle's radius, here ρ, α, and β contribute to the orbit selection. Accordingly, the parameter M will be adjusted by an ad-hoc combination of α and β.

Assuming the swarm of robots is large enough to ensure local communications, the proposed BCM will let the swarm converge to a consensual orbit and circulate on it at a constant speed. This convergence does not depend on the initial position and heading of the robots. As the central light is a global attractor, robots will also never drive away from it.

2.3.2 Physical implementation on e-puck robots

The formerly exposed BCM has been implemented on the open-hardware e-puck robot specifically designed for experimental swarm robotics Mondada et al. (2006) . The e-puck is a cylindrical robot, of approximately 70 millimeters in diameter, with 8 infrared (IR) proximity sensors (emitter and receptor) located nearly evenly on its perimeter (see Figure 2.4). Each sensor is composed of an IR emitter and a receptor, and can be used passively (only the receptor, to sample ambient light), or actively (emitter/receptor, for proximity search or message exchanges).

Our implementation uses only IR sensors (passively and actively, alternately), and the two motors. Each timestep is separated into five phases:

1. **Message broadcasting**: Each robot first broadcasts a message to all neighboring robots via IR (20-40 cm of range, depending on the angles of the emitter/receptor sensors). The message contains its ID, and the number of agents that have been counted at the previous timestep $N_\rho(t-1)$.

2. **Message reading**: The received messages are read to measure $N_\rho(t)$, the number of detected neighbors. A filtering step also allows detection of robots that were in range in the previous steps, but whose messages were not received (to correct possible miscommunication between robots). A memory of the detection of the other robots in the last 5 steps is maintained, and a *majority window algorithm (MWA)* is applied to correct for robots not being correctly detected. The filtered value $N'_\rho(t)$ is thereby constructed.
   The MWA counts as a neighbor any robot that has been in range at least 3 times in the last 5 timesteps, or that has just been detected during the present timestep. The

number of neighbors can only be underestimated, as we use an unmodulated light source (on a continuous current), and the IR communication between the e-pucks are modulated. This means that no false positives can occur in the communication among the robots, and only false negatives (undetected neighbors) can happen. To try and reduce the influence of non-detection of neighbors, we artificially force the number of neighbors at time t to be bounded below by $(N_\rho(t-1)-1)$. This mechanism ensures a smooth behavior of the speeds of the motors, by avoiding large jumps in the number of neighbors over time. We define $V_\rho(t)$ to be the set of the values $N_\rho(t-1)$ received from the neighbors at time t. Then the final value $N_\rho(t)$à is defined as:

$$N_\rho(t) := \max\left(N_\rho(t-1)-1, \frac{N'_\rho(t)+\sum_i V_\rho(t)_i}{N'_\rho(t)+1}\right). \tag{2.13}$$

3. **Light source sampling**: The intensity of the light source is passively sampled on each of the eight IR sensors to obtain $\{\bar{S}_0(t), \bar{S}_1(t), \ldots \bar{S}_7(t)\}$. The normalized values are then computed as $S_i(t) = \bar{S}_i(t) \,/\, \max_i \{\bar{S}_i(t)\}$ for $i = 0, 1, .., 7$.

4. **Velocity feedback**: With the data gathered, the velocity of each motor is computed and updated following Eq.(2.12), with $\alpha = 100$ and $\beta = 20$, and a base speed of 100:

$$\begin{cases} V_R(t+1) = 100 + 100 \cdot N_\rho(t) + 20 \cdot (S_L(t) - S_R(t)) \\ \\ V_L(t+1) = 100 + 100 \cdot N_\rho(t) + 20 \cdot (S_R(t) - S_L(t)). \end{cases} \tag{2.14}$$

The speeds here are given in *steps/second.* 1000 steps correspond to one full rotation of a wheel, whose diameter is approximately 41mm. A speed of 500 steps/s corresponds to $\frac{500}{1000} \cdot \pi \cdot 41 \approx 64.4\,[mm/s]$.

5. **Avoidance mechanism**: A proximity search is performed on each sensor to detect obstacles; collision avoidance is implemented by adapting the motors' velocities. The mechanism used is a standard Braitenberg-inspired collision avoidance mechanism. It has been designed to avoid collisions between e-puck robots, but cannot guarantee

collision avoidance with the light source. Its pseudo-code is given in Algorithm 1.

```
Data: $\alpha$ = 100;

// Something ahead, stop for this timestep
if obstacle_front() then
    VR(t+1) = 0;
    VL(t+1) = 0;
end
// Something ahead slightly left/right, turn the other direction
if obstacle_front_right() then
    VL(t+1) = VL(t+1) - $\alpha$;
end
if obstacle_front_left() then
    VR(t+1) = VR(t+1) - $\alpha$;
end
// Something left/right, turn slightly the other direction
if obstacle_right() then
    VL(t+1) = VL(t+1) - $\alpha$/2;
end
if obstacle_left() then
    VR(t+1) = VR(t+1) - $\alpha$/2;
end

right_motor(VR(t+1));
left_motor(VL(t+1));
```

Algorithm 1: Avoidance mechanism

Figure 2.5 summarizes the robot's main loop.

Different noise sources are inherent to this robotic implementation. First, the motors' noise: each robot can have a slightly different speed from its programming (the e-puck motors sometimes miss some motor steps, thus changing their forward speed and heading). Second, the sensors' noise in sampling the light source can also slightly change the robot's heading in the BCM. Finally, we must account for the noise in the number of neighbors, as they change its forward speed in the BCM. This final source is the biggest source of noise in the BCM. All of these noise sources add up, letting the robots follow noisy trajectories, as expected from the mathematical model of Eq.(2.1). We follow the assumption that these three noise sources are similar, in terms of behavior to the two independent WGN sources from the mathematical model. Indeed, the superposition of multiple independent noise sources can be simplified to a WGN source, by the central limit theorem (see Gillespie (1992), sect. 1.6).

With the IR sensors acting as the neighbors' detection mechanism, we can express the following expected theoretical results. On the limit cycle, each robot has three neighbors in average (himself and the two nearest neighbors). This is due to the small range, and the fact that the

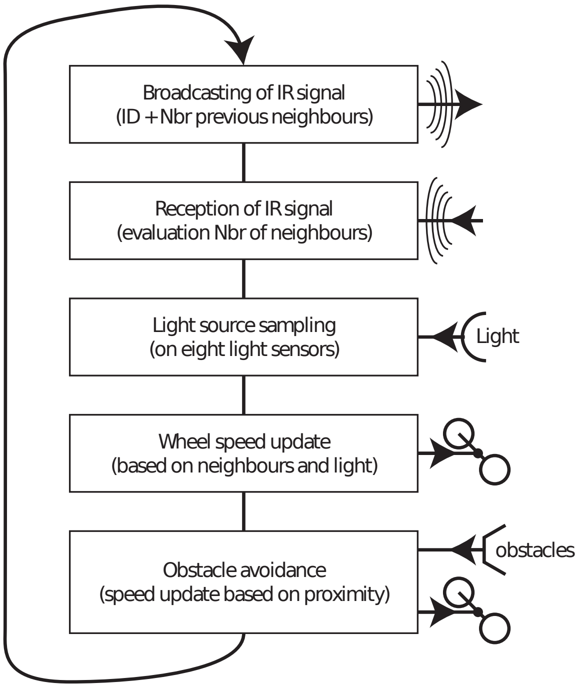
Broadcasting of IR signal
(ID + Nbr previous neighbours)
Reception of IR signal
(evaluation Nbr of neighbours)
Light source sampling
(on eight light sensors)
Light
Wheel speed update
(based on neighbours and light)
Obstacle avoidance
(speed update based on proximity)
obstacles

Figure 2.5 – Schematic of the robot's main programming loop.

robots also block the IR rays; thus, only the closest neighbors can be detected. As on the limit cycle, the robots always have the light at $\frac{\pi}{2}$ on their right, so the value of the sensors can also be estimated. Indeed, sensors 1 and 2 are closest to the light source, and approximately at the same distance. Their values will most likely be around 1. Sensors 0 and 3 will also have nearly the same values, and the other sensors will not receive any light, so that:

$$\Delta S := S_R - S_L \approx S_1 + S_2 + S_3 - S_0 \approx 2.$$

This allows us to consider the average speeds on the limit cycle as being constants, and to rewrite the BCM on the limit cycle as:

$$\begin{cases} V_R = 3\alpha + 2\beta \\ \\ V_L = 3\alpha - 2\beta. \end{cases} \tag{2.15}$$

A relation between these speeds and the **interaxial distance** e of the robots, leads to the radius of the limit cycle

$$\mathscr{L}_{\alpha,\beta} = \frac{e}{2}\frac{V_L + V_R}{V_L - V_R} = \frac{3\alpha \cdot e}{4\beta} \tag{2.16}$$

The angular speed can also be expressed as

$$\omega_{\alpha,\beta} = \frac{V_L - V_R}{e} = \frac{4\beta}{e}.$$

2.3.3 Dictionary theoretical model-robotic implementation

A formal proof of the convergence of our BCM would be very difficult to provide; this is why we chose to illustrate that our BCM exhibits the same characteristic behavior as the mathematical model of Sect.2.2, whose convergence we have formally proven. To better link the model and the robotic implementation, Table 2.1 illustrates the translation of these main characteristics between the theoretical and robotic control mechanisms.

Characteristic of the MCD dynamics	Theoretical Control Mechanism	Robotic Control Mechanism
Attraction/Repulsion with respect to the origin	Symmetric part of the dynamical matrix $\mathbb{V}$. **Control parameter**: M, ρ	Forward speed in the Braitenberg control mechanism. **Control parameter**: α, ρ
Rotation around the origin	Anti-symmetric part of the dynamical matrix $\mathbb{V}$. **Control parameter**: ω, ρ	Heading correction in the Braitenberg control mechanism. **Control parameter**: β, ρ
Attraction to the limit cycle	$U'[H,t]$ term in the symmetric part of the dynamical matrix $\mathbb{V}$. **Control parameter**: ρ	Transmission of $N_\rho(t-1)$ to/from neighbors, and filtering step of $N_\rho(t)$. **Control parameter**: ρ, majority window size
Repartition on the limit cycle	Noise sources $dW(t)$. **Control parameter**: σ	Robotics noise sources (motors imprecisions, communications errors, environmental noise, etc.). Avoidance mechanism.

Table 2.1 – Theoretical and robotics implementations of the main control mechanisms in our model, and their respective control parameter(s).

The explicit expression of the limit cycle in both cases is also summarized, to show how both depend on their control parameters

$$\mathscr{L}_{\rho,M} = \frac{\rho}{\sqrt{2-2\cos(\pi/M)}} \qquad\qquad \mathscr{L}_{\alpha,\beta} = \frac{3\alpha\cdot e}{4\beta}.$$

In the BCM, we see that our initial choice of setting α and β fixes the radius of the limit cycle (and the angular speed on it). If we choose a larger swarm of robots, we should not see a difference in the radius as long as we do not change these two control parameters. Theoretically, we could see the swarm trying to arrange on a circle whose perimeter is too small for all the robots to fit. This means that we should see α and β as functions of N, to be sure that all robots can fit on the consensual limit cycle. We should have the perimeter of the limit cycle at least larger than N times the diameter d of one robot:

$$2\pi\cdot\mathscr{L}_{\alpha,\beta} = 2\pi\cdot\frac{3\alpha\cdot e}{4\beta} \geq N\cdot d.$$

This result from the BCM matches the mathematical model, where the radius of the limit cycle depends only on the fraction of neighbors M and the radius of observation ρ. In the mathematical model, changing the swarm number does not change the limit cycle's radius either.

2.3.4 Experimental validation

To demonstrate the convergence of our BCM regardless of the initial conditions, tests were carried out with a swarm of eight robots, from 25 different (random) initial situations (positions and headings of the robots). The choice of these initial conditions was made to experimentally validate the inter- and intra-convergence variability. The headings changes in similarly located robots in different initial conditions (e.g., experiments 3 and 17) show how the control mechanism can achieve convergence to a consensual orbit with initial conditions close or far from the final orbit. The agents were placed systematically in a 200 × 200 cm rectangular horizontal arena. The initial positions and headings of the robots are shown in Figure 2.6, along with the position of the IR source, which remains unchanged during the experiments. Each experiment lasted from 1 to 4 minutes; long enough to let the robots rearrange from their initial positions to the limit cycle, and then maintain the limit cycle.

The tracking step allowed us to obtain the position of each robot through all of the 25 experiments. Figure 2.7 shows the tracking step applied to the videos, while Figure 2.8 shows the resulting tracked trajectories. Details on the multi-agent tracking tool developed can be found in Appendix A.

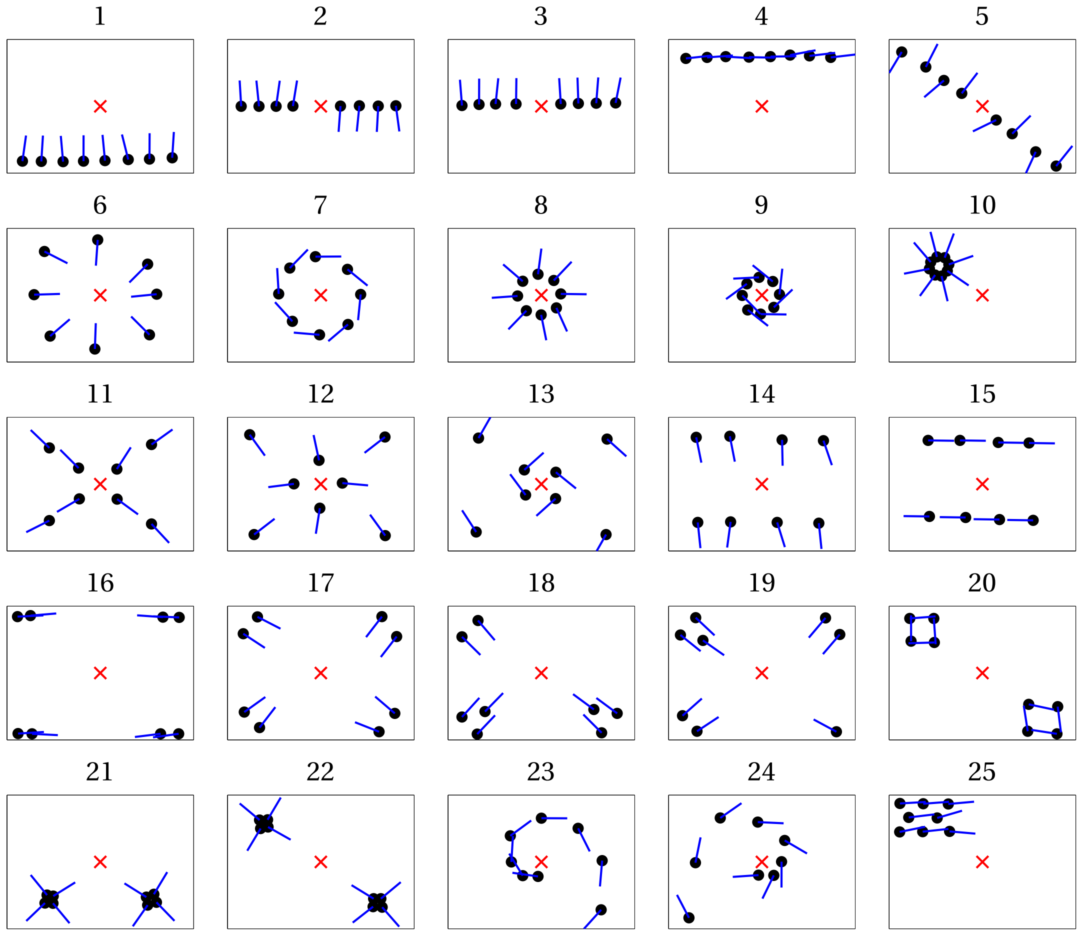

Figure 2.6 – Initial positions and headings of the eight robots in each of the 25 experiments. Each circle corresponds to a robot, and the corresponding line denotes the heading. The center cross represents the position of the light source.

2.3.5 Experiment Results

Data extracted from tracking has been used to quantitatively assess convergence, based on the following measures:

1. Mean and standard deviation of each robot's radius in the last 15% of each experiment (empirically found to be in the limit cycle regime for every initial situation).
2. Mean and standard deviation of each robot's angular speed in the same time window.

The extracted data are shown in Figure 2.9 for each experiment, where these averages and standard deviations are pictured for each robot on the left side, and as one average for the whole swarm on the right. It is worthwhile to note the very low fluctuations on the average radius and angular speeds for the swarm, through the whole set of initial conditions.

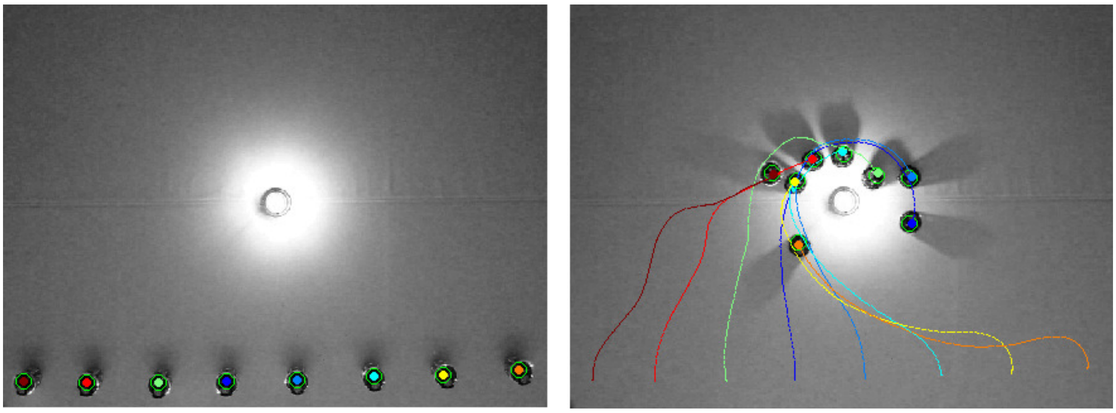

Figure 2.7 – Left: A randomly selected initial condition assuming eight aligned equally spaced agents in the inferior working space region. The IR radiation source is located at the center of the rectangular arena.
Right: Respective agents' control mechanism and their mutual interactions. It is important to observe that the proposed Kalman filter (see Appendix A) is capable of determining the position of an agent with high precision independently of lighting conditions and other agents' positions.

As a measure of the uniformity of the robots' dispersion on the limit cycle, we now recall the order parameter (see Acebrón et al. (2005a)) for a group of N oscillators on $\mathbb{R}^2$ in polar coordinates:

$$\mathscr{R}(t) = \left| \frac{1}{N} \sum_{i=1}^{N} r_i(t) \cdot e^{i\theta_i(t)} \right|, \tag{2.17}$$

which takes a real positive value. Note that if all the oscillators share the same phase $\theta_i(t)$ (and the same radii) at a given time, the value for $\mathscr{R}(t)$ will be high. Conversely, if all the phases of the oscillators are uniformly distributed over $[0:2\pi]$, and if their radii are the same, $\mathscr{R}$ will vanish.

In this research, we used information on the position in the last 15% of each run to determine the phase of each robot through time, and compute $\mathscr{R}(t)$ for the swarm. Figure 2.10 reports the average in this time window (along with the standard deviation) for each experiment.

Remark: The positions of robots that got stuck against the IR source during an experiment are shown in the initial configurations plot in Figure 2.6, even though their data was not used in the analysis. Over the 25 experiments, 15 robots got stuck, with a maximum of 2 stuck robots for one initial condition (7.5% of unusable data). As the IR source is an attractive point, and because of the collision avoidance mechanism used, the robots sometimes change their course and end up hitting the light source. A robot in this situation can not get back to the

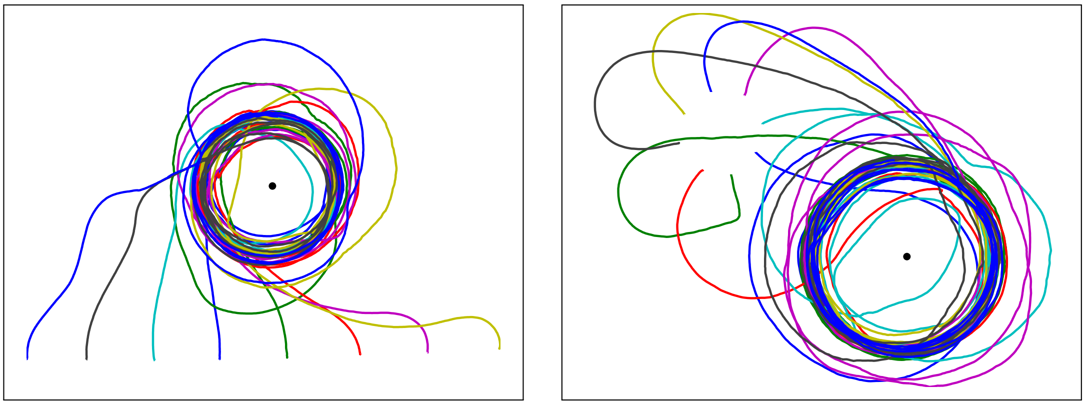

Figure 2.8 – Full extracted trajectories of the eight robots through the duration of experiments, for initial conditions 1 (left) and 6 (right).

limit cycle, and stays at the same spot with 0 velocity until the end of the experiment. In the mathematical model of Sec. 2.2, agents can leave the attractor only because of the noise source. Our robots can not do the same, due to the physical presence of the IR source blocking their path.

This issue could not be solved by using a different collision avoidance mechanism, as avoiding a light source, solely with the use of the IR sensors is impossible (at short range, the IR sensors are saturated by the light source). This result conforms to our expectations, as it fits the theoretical predictions as well as the underlying Eq.(2.1).

2.3.6 Comparison with the theoretical results

Theoretical results derived in Sect. 2.3.2 lead to the following limit cycle radius and angular speed (with the e-puck robot's interaxial distance $e = 52[mm]$):

$$\mathcal{L}_{\alpha,\beta} = \frac{3\alpha \cdot e}{4\beta} = \frac{(100+3\cdot 100)\cdot 52}{4\cdot 20} = 260\,[mm] \qquad \omega_{\alpha,\beta} = \frac{4\beta}{e} = \frac{4\cdot \frac{20}{1000}\cdot 41\pi}{52} \approx 0.198. \tag{2.18}$$

These results very closely match our experimental results, where the average radius of the limit cycle over the 25 experiments is $\overline{\mathcal{L}_{\alpha,\beta}} := 252.7\,[mm]$, and the average angular speed is $\overline{\omega_{\alpha,\beta}} := 0.197$.

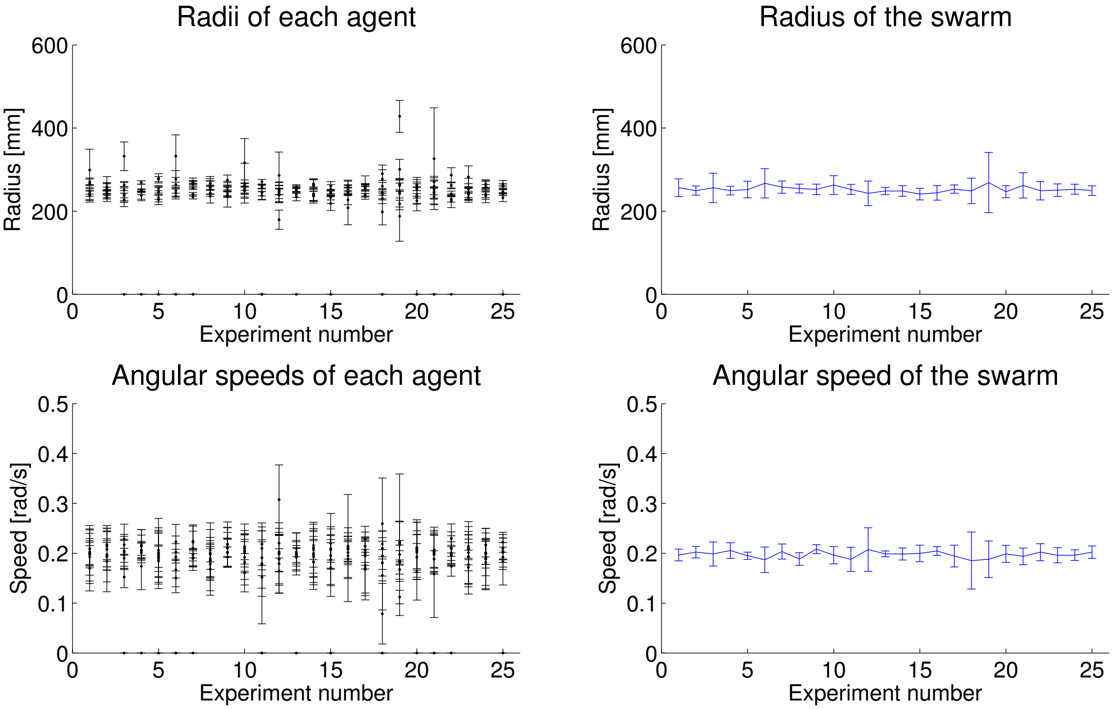

Figure 2.9 – Average radius/angular speed in the last 15% of each experiment. Left: For each robot. Right: Averaged for the whole swarm.

2.3.7 Generalization to other Hamiltonian functions

The choice of a BCM limits the characteristics of the Hamiltonian functions that can be adapted to a hardware implementation. The scope of this research was not to study the limit of validity of our model; other types of control mechanism may adapt to general Hamiltonian functions. Nevertheless, the BCM described here for the case of the harmonic oscillator ($H(x, y) = \frac{1}{2}(x^2 + y^2)$) can be extended to more complex Hamiltonian functions. For example, one can obtain Cassini oval-like curves by placing the robots in an environment with two light sources. Using exactly the same control mechanism of Eq.(2.12), we obtain a swarm behavior similar to the mathematical case with the Cassini ovals Hamiltonian function. Depending on the observation range ρ of the robots, cases with one connected consensual orbit or two separated orbits can arise. This time, robots sample the ambient light coming from both light sources, acting as the two focal points from the Cassini Ovals Hamiltonian function.

Tests have not yet been carried out on an actual swarm of robots, but numerical results are shown in Figure 2.11. These results are obtained by simulating Eq.(2.12) with $dt = 0.1s$, on a swarm of 100 robots starting with random positions and headings on the plane. The two light sources are positioned at $(\pm 100, 0)$, and WGN sources are added to the (exact) gathered

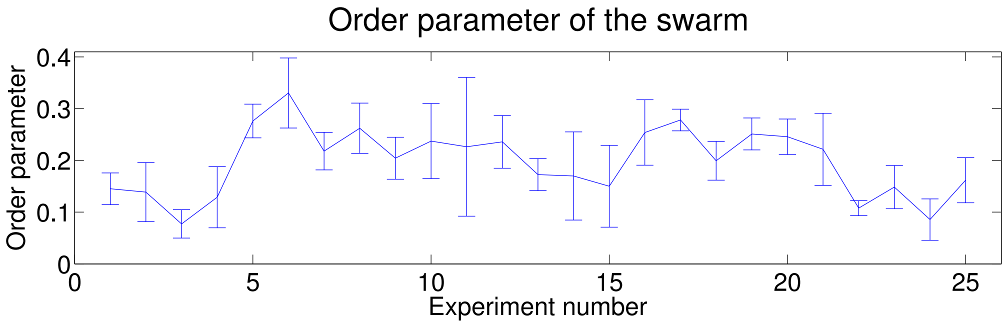

Figure 2.10 – Order parameter $\mathscr{R}$ of the swarm for each initial situation, averaged over the last 15% of each experiment.

information to simulate the noise actual robots would experience:

$$\begin{cases} V_R(t+1) = \alpha \cdot N_\rho(t) + \beta \cdot (S_L(t) - S_R(t) + \sigma_l dW_R(t)) \\ V_L(t+1) = \alpha \cdot N_\rho(t) + \beta \cdot (S_R(t) - S_L(t) + \sigma_l dW_L(t)) \end{cases} \tag{2.19}$$

Empirically chosen values for the WGN sources are $\sigma_l = 0.05$ for the light source sampling, and $\sigma_N = 0.5$ for the number of instantaneous neighbors ($\tilde{N}_V(t) := N_V(t) + \sigma_N dW_N(t)$).

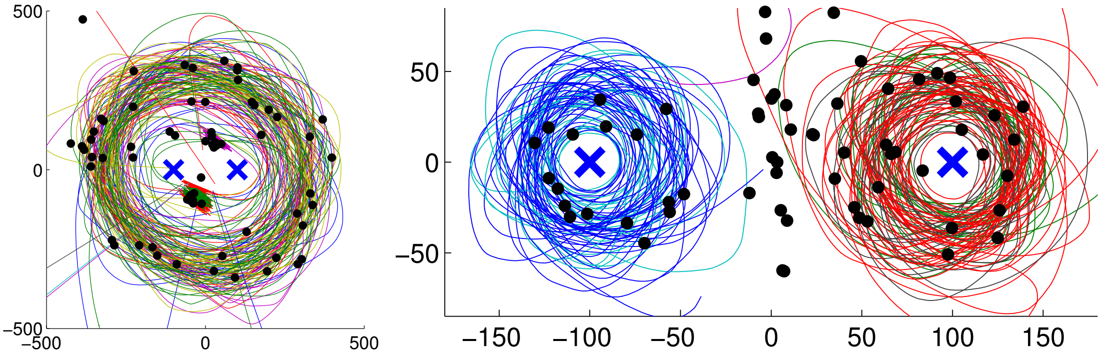

Figure 2.11 – Numerical simulation of the BCM on a swarm of 100 robots, with two light sources located at $(\pm 100, 0)$.
With an observation range of $\rho = 100$, the swarm consensually rotates around both light sources (left), whereas a smaller range of $\rho = 10$ lets the swarm split into two sub-swarms rotating around each light source (right). The trajectory of 10 randomly selected robots are shown, along with the final position of all robots as black dots.

2.4 Conclusion

For a whole class of interacting autonomous agents evolving in an environment subject to noise or external perturbations, we have been able to perform an analytical characterization corroborated by an extensive set of simulation experiments and ultimately to implement the control mechanism on a swarm composed of eight e-puck robots. The possibility to simultaneously complete these complementary approaches on the same class of control mechanisms is exceptional, and originates from the simplicity of the underlying dynamics (i.e., MCD dynamics). However, despite its simplicity, our modeling framework incorporates a number of basic features rendering it generic, namely: non-linearities in the control mechanism; finite range interactions between agents; self-organization mechanisms leading to dynamic consensual spatio-temporal patterns; and environment noise, which corrupts ideal trajectories and sensor measurements. Beyond the pure pedagogic insights offered by this class of models, the results provide strong evidence that built-in stability of the control mechanism and the resilient behavior observed during the actual implementation open the door for more elaborate implementations. The modeling framework exposed here is more than a mere class of models; it offers a constructive method to deduce generalized classes of fully solvable agent dynamics. In particular, extension of the MCD dynamics via the introduction of Hamiltonian functions, involving more degrees of freedom, will allow analysis of the robots' evolution in higher dimension (from planar to 3-D spaces).

2.5 New Contributions of Chapter 2

- The mixed canonical-dissipative (MCD) dynamic introduced in Chapter 1 is successfully converted into a Braitenberg-inspired control mechanism (BCM), thus bridging the gap between the theory and the real robotic world. Experimental validation on a swarm of 8 e-puck robots is presented.
- **Publication**: This chapter is reproduced from the journal paper Sartoretti et al. (2014a), with slight modifications to fit the present dissertation.

Leader-Based (Hard) Control Part III

3 Leader-Follower Control Mechanism for Planar Robots Evolving in Formation

Summary

Leader-based control has been extensively studied in swarm robotics, where it often is an easily implementable type of swarm control. Leader-followers models can be viewed as a degenerate case of heterogeneous swarms (one leader, and $N-1$ regular agents). In this chapter, which is mostly added for completeness, we propose a simple class of models based on the Braitenberg-type dynamic already studied in Chapter 2. We build on the column formation studied in Krishnanand and Ghose (2005), and propose a control mechanism enabling a swarm of robots to follow a leader while remaining in a triangular platoon formation. The described control mechanism can be implemented on mobile robots, and only uses locally gathered information via their infrared sensors.

3.1 Problem Statement

We consider a swarm of robots containing one leader and $N-1$ followers. The swarm is initially in formation, and our aim is to construct a control mechanism enabling the robots to follow the leader while remaining in formation. The control mechanism should only use local information, gathered by the robots using their infrared sensors. The use of leader-follower models has been extensively used in robotics, and provides a convenient method to externally control a swarm in real-time (Desai et al. (1998)). As an introductory example, we first recall the column formation from Krishnanand and Ghose (2005), on which we then build to obtain the triangular-shaped formation movement.

3.2 Introductory Example: Robotic Train

[1] *[...]We first consider a swarm of mobile robots initially positioned in a single file. Our aim is to allow the whole swarm to move in formation, the first robot acting as the swarm's leader, while the others follow in its path. To this aim, we let each regular mobile robot act as a differential-motored, two-sensored, light-attracted Braitenberg vehicle Braitenberg (1984). This vehicle regularly updates the speed of its left (resp. right) motor proportionally to the intensity of the light read by its right (resp. left) sensor. In other words, each of our regular robots consistently adapts its course to drive toward the brightest light source its sensors can detect. To let the robot move in formation, we attach a light at the rear of each robot. Therefore, each regular robot will be attracted toward the robot directly in front of it in the file. Hence, each agent (except for the last one in the file) acts as a (local) leader for the next agent in the file. Similarly, each regular robot simultaneously acts as a follower, attracted by the previous robot in the file. This effectively enables us to build a "robot train," whose path the first agent in line (i.e., the leading robot) controls.[...]*

3.2.1 Braitenberg Control Mechanism

Formally, we respectively write $V_L(t)$ and $V_R(t)$ the speeds of the left and right motors at timestep t. Similarly, we respectively write $M_L(t)$ and $M_R(t)$ the light intensities read on the left and right sensors at timestep t. We use the normalized values $S_{L,R}(t)$, obtained by computing $S_{L,R} = \frac{M_{L,R}(t)}{\max(M_L(t),M_R(t))}$. With this, we express the speed update rule as, in a similar manner as in the previous chapter (see Eq.(2.14)):

$$\begin{cases} V_L(t+1) = V(t+1) + \beta \cdot (S_R(t) - S_L(t)), \\ \\ V_R(t+1) = V(t+1) + \beta \cdot (S_L(t) - S_R(t)). \end{cases} \tag{3.1}$$

In Eq.(3.1), $V(t+1)$ stands for the forward speed of each robot, and $\beta \in \mathbb{R}^+$ is a parameter governing the rotation speed of the robots. We let each robot adapt its current forward speed $V(t+1)$ in order to keep up with the robot in front of itself in the line. More specifically, each robot aims at remaining at a given distance from the its local leader. To achieve this, we implement a simple proportional controller on each robot's speed:

$$V(t+1) = \frac{D(t)}{D_0} \cdot V_{\text{Leader}}, \tag{3.2}$$

with $D(t)$ the measured distance from the local leader, D_0 the goal distance from the local leader, and V_{Leader} the speed of the swarm's leader (assumed constant).

---

[1] Italic text in the present section is reproduced from the conference paper Sartoretti (2015).

3.2.2 Numerical Simulations

To simulate our robotic swarm, we consider the robots as e-puck robots (see Chapter 2). As a reminder, e-puck robots are cylindrical mobile differential robots, equipped with 8 proximity sensors. These sensors are nearly uniformly distributed along the robots' perimeter. For the sake of the numerical simulations, we consider the sensors to be uniformly distributed along the robots' perimeter. Figure 2.4 illustrates the real and theoretic shape of the mobile robots considered here.

Here, the e-puck robots with their 8 sensors are used to model 2-sensored attractive Braitenberg vehicles. This is achieved by aggregating their sensors into two groups (left and right), namely

$$\begin{cases} S_R &= S_0 + S_1 + S_2 + S_3 \\ \\ S_L &= S_4 + S_5 + S_6 + S_7. \end{cases} \tag{3.3}$$

To model the ubiquitous randomness of the environment and sensors' actuators, we add noise to our control mechanism. White Gaussian Noise (WGN) sources are added to the difference $S_R(t) - SL(t)$, with an empirically selected variance $\sigma = 0.05$:

$$\begin{cases} V_L(t+1) = V(t+1) + \beta \cdot (S_R(t) - S_L(t) + \sigma W(t)), \\ \\ V_R(t+1) = V(t+1) + \beta \cdot (S_L(t) - S_R(t) - \sigma W(t)). \end{cases} \tag{3.4}$$

Figure 3.1a illustrates the initial state of the 10 robots, and 3.1b-3.1d display a selection of consecutive states of the swarm. In this run, the leading robot is scripted to follow a horizontal figure eight. This pattern is a robust test for the swarm's resistance to turns induced by the leader. Indeed, this figure eight consists of two consecutive full rotation with opposite orientations. Each robot reacts to the change of direction of its leader after a short delay. With time, these delays add up, and lead to a large difference of paths between the front and the rear robots in the file. If the rotation speed β in the Braitenberg dynamics Eq.(3.4) is not adequately chosen, a turn induced by the leader can jeopardize the swarm's cohesion. This requires us to further investigate the swarm's stability (i.e., the swarm's capacity to remain flocked, mainly when the leader changes direction).

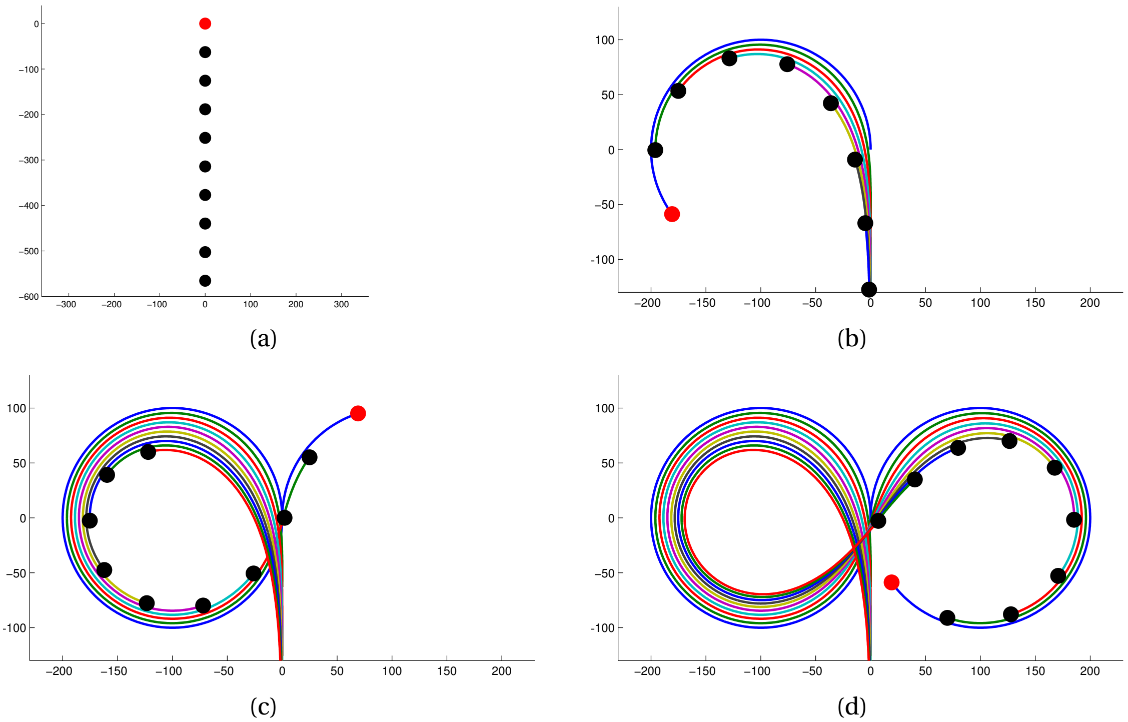

(a) (b) (c) (d)

Figure 3.1 – a: Initial state of a swarm of 10 robots (1 leader [in red] and 9 followers) following the dynamics of Eq.(3.2). All robots are initially facing upward. b-d: Selected consecutive states of the swarm through time. During this run, the leader follows a horizontal scripted figure eight, while the rest of the train follows in its path. Distances are displayed in millimeters.

3.2.3 Stability Analysis

The forward speed updating rule given in Eq.(3.2) allows the followers to match the leader's speed. The main issue with keeping the formation arises when the leader takes a turn. To remain in formation, the followers must be able to take a turn as sharp as their leader.

A robot's sharpest turn occurs when one of its sensors measures no light (i.e., for instance $S_L(t) = 0$ induces the sharpest right turn). When this occurs, we have $S_R(t) - S_L(t) = 1 \big(= -(S_L(t) - S_R(t))\big)$, implying that the differential between both motors will be 2β. Assuming that the robot's forward speed remains close to V_{Leader}, the resulting minimal radius the robot can follow is:

$$\rho_{\min} = \frac{e}{2}\frac{V_L + V_R}{V_L - V_R} = e\frac{V_{\text{Leader}}}{2\beta}, \tag{3.5}$$

with e the interaxial distance of the robot. Knowing the radius $\rho_{\min}$ of the sharpest possible turn taken by the leader, Eq.(3.5) determines the threshold value β_c in Eq.(3.1) (i.e., any $\beta > \beta_c$

ensures swarm cohesion during turns):

$$\beta_c = \frac{e}{2}\frac{V_L + V_R}{V_L - V_R} = e\frac{V_{\text{Leader}}}{2\rho_{\min}}. \tag{3.6}$$

Figure 3.2 displays the end state of an unstable swarm (i.e., where the formation control mechanism cannot keep the swarm in formation), with $\beta = 32 < 43.19 = \beta_c$. Notice how the last 3 agents are unable to follow the leader during its turn, and ultimately leave the swarm.

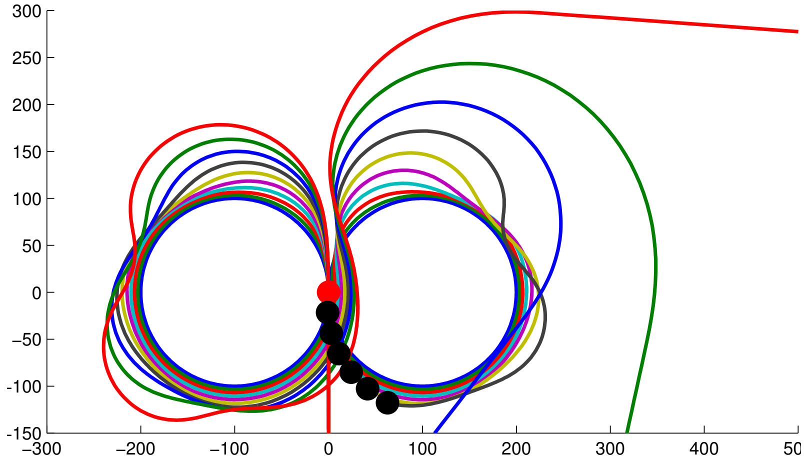

Figure 3.2 – End state of a swarm of 10 robots (1 leader [in red] and 9 followers) following the dynamics of Eq.(3.2) at $T = 60[s]$. During this run, the leader follows a horizontal scripted figure eight, while the rest of the train follows in its path. The choice of $\beta = 32 < 43.19 = \beta_c$ does not enable all robots to remain in formation while they follow the leader. Three robots (red, blue and green lines) ultimately leave the swarm. Distances are displayed in millimeters.

Even in stable swarms, regular robots follow slightly different paths than the leader (this, because of the delays between the leader's and the followers' turns), but cohesion still remains.

3.3 Triangular Formation

3.3.1 First Layer - 4 Robots

Building on the previous section, we shall now allow the robots to move together in more complex formations. Although the same method can be used to obtain almost arbitrary shape (limited only by the positions of the sensors along the robot's perimeters), we here focus on triangular-shaped platoons. The basic idea is to now have each robot permanently keep its local leaders at selected angles from its own heading. The resulting control mechanism is the sum of (slightly modified) Braitenberg-type control mechanisms Eq.(3.4).

The layer 0 of the triangular pyramid (i.e., the top of the triangle) is always occupied by the leader agent (robot 1). The first layer is then composed of 3 robots ($i = 2, 3, 4$), one behind the leader, and the two others on its sides. Robot 3 steadily updates its position in order to remain at the south of the leader. Robots 2 and 4 try to keep the leader at an angle of approximately $\frac{\pi}{4}$ on their right/left respectively. The situation is summarized in Figure 3.3.

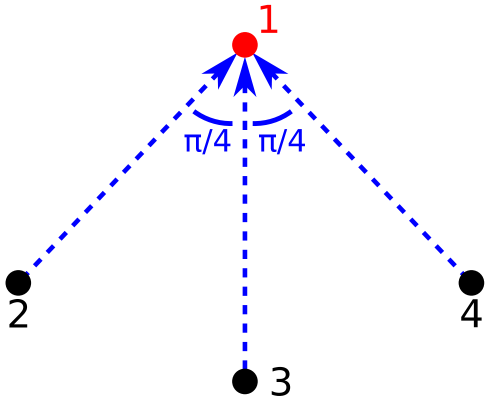

Figure 3.3 – Triangular one-layered formation for 4 robots: 1 leader (in red) and 3 followers (in black). The blue lines represent the angle at which each follower wishes to keep the leader from its heading. All robots are facing upward.

To construct the control mechanism of robots 2 and 4, we simply modify the sensor aggregations as:

$$(2)\begin{cases} S_R &= S_1 + S_2 + S_3 + S_4 \\ S_L &= S_5 + S_6 + S_7 + S_0. \end{cases} \qquad (4)\begin{cases} S_R &= S_7 + S_0 + S_1 + S_2 \\ S_L &= S_3 + S_4 + S_5 + S_6. \end{cases} \tag{3.7}$$

We finally let each follower's control mechanism be given by Eq.(3.4), with the sensor groups given by Eq.(3.7). This control produces a triangular-shaped formation progression of the swarm, driven by the leader. As before, the stability of the formation depends on the parameter β, and its stability analysis is similar, since the robots are basically following the same control mechanism. Simulation results are presented in Figure 3.4.

3.3.2 Extra Layers

Building on this idea of individual sensor groups, we can enlarge the triangular formation. The next step requires to add 5 robots ($i = 5, 6, 7, 8, 9$). One possibility to stabilize the formation is to let the new robots' control mechanisms depend on more than one local leader. Figure 3.5 illustrates the leader-follower relations between agents during formation movement.

To obtain control mechanisms allowing a robot to remain in formation with respect to more than one leader, we adapt Eq.(3.4). As an illustration, consider robot 6. This robot must stay

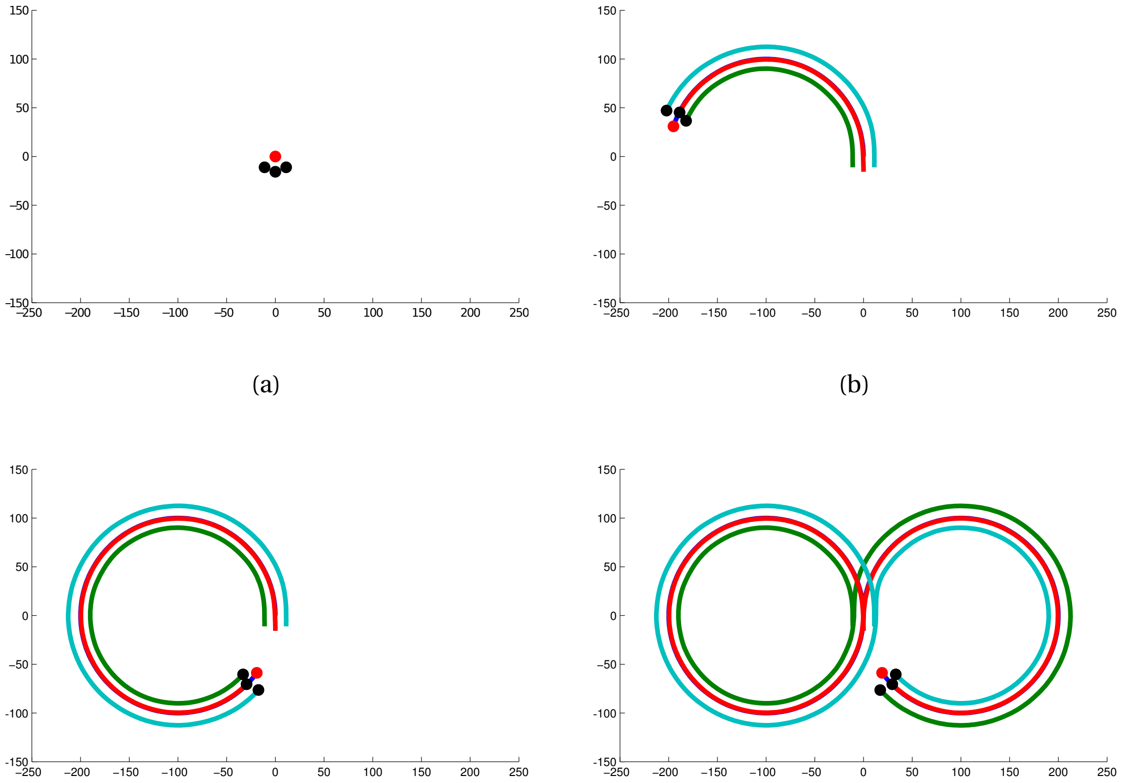

(a) (b)

(c) (d)

Figure 3.4 – a: Initial state of a swarm of 4 robots (1 leader (in red) and 3 followers) in a one-layered triangular formation. All robots are initially facing upward. b-d: Selected consecutive states of the swarm through time. During this run, the leader follows a horizontal scripted figure eight, while the rest of the train follows in its path. The forward speed of the leader is 12.19 [cm/s], and $\beta = 40 > \beta_c = 32.3$. Distances are displayed in millimeters.

behind robot 2, while keeping robot 3 at its right with an angle $\frac{\pi}{4}$. To this aim, we define the two following sensor groups:

$$(2)\left\{\begin{array}{lcl} S_{R,2} & = & S_0+S_1+S_2+S_3 \\ \\ S_{L,2} & = & S_4+S_5+S_6+S_7. \end{array}\right. \qquad (3)\left\{\begin{array}{lcl} S_{R,3} & = & S_1+S_2+S_3+S_4 \\ \\ S_{L,3} & = & S_5+S_6+S_7+S_0. \end{array}\right. \tag{3.8}$$

Basically, we now simply add the couple of control mechanisms obtained from Eq.(3.4) for

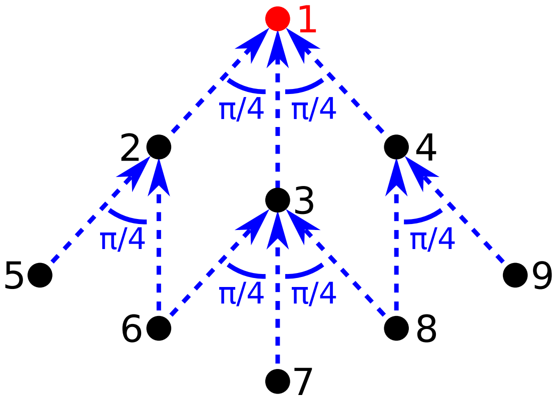

Figure 3.5 – Triangular two-layered formation for 9 robots: 1 leader (in red) and 8 followers (in black). The blue lines represent the angle at which each follower wishes to keep its leading robots from its heading. All robots are facing upward.

each of these sensor groups:

$$\begin{cases} V_L(t+1) = V(t+1) + \beta \cdot (S_{R,2}(t) + S_{R,3}(t) - S_{L,2}(t) - S_{L,3}(t)), \\ V_R(t+1) = V(t+1) + \beta \cdot (S_{L,2}(t) + S_{L,3}(t) - S_{R,2}(t) - S_{R,3}(t)). \end{cases} \tag{3.9}$$

Introducing Eq.(3.8) in Eq.(3.9), we observe that by adding the values from each sensor groups, some sensor values vanish. We finally obtain the global left/right sensor groups for robot 6:

$$\begin{cases} S_R & = & S_1 + S_2 + S_3 \\ S_L & = & S_5 + S_6 + S_7. \end{cases} \tag{3.10}$$

Along the same lines, we can derive the control mechanism foir robot 8, from its relative position to robots 3 and 4. Having all the individual sensor groups, we finally use Eq.(3.4) to obtain the global formation movement.

Figure 3.6 shows the initial state and a selection of consecutive states of the swarm, in a run where the leader agent follows a figure of eight. Here, the swarm also remains in formation during the turns, since the parameter $\beta = 40 > \beta_c = 32.3$.

Remark: the basic idea behind this triangular formation movement opens to more complex geometries, where robots depend on more than a couple of leaders. However, appropriate modification of Eq.(3.2) would be required for robots whose leaders are behind them.

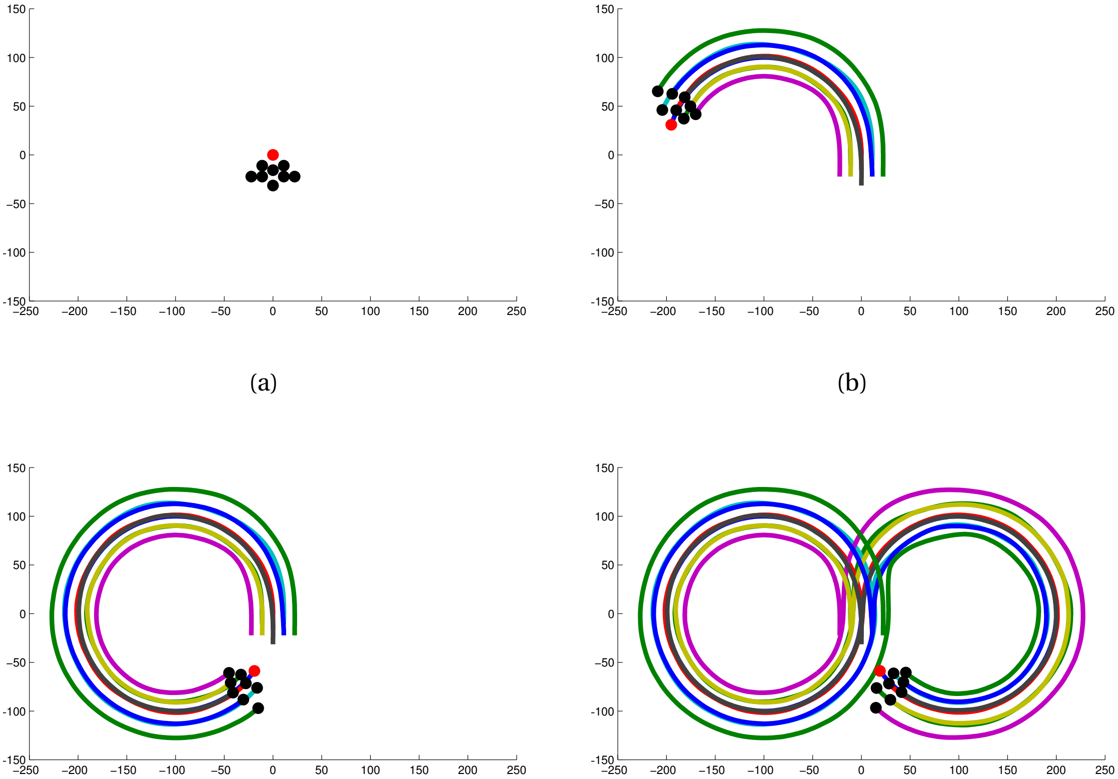

(a) (b)

(c) (d)

Figure 3.6 – a: Initial state of a swarm of 9 robots (1 leader [in red] and 8 followers) in a two-layered triangular formation. All robots are initially facing upward. b-d: Selected consecutive states of the swarm through time. During this run, the leader follows a horizontal scripted figure eight, while the rest of the train follows in its path. The forward speed of the leader is 12.19 [cm/s], and $\beta = 40 > \beta_c = 32.3$. Distances are displayed in millimeters.

3.4 New Contributions of Chapter 3

- In this chapter, we consider robotic platoon formations driven by a **visible leader**. Based on Chapter 2, we construct a control mechanism for the collective evolution of triangular platoons. This control parameter only relies on local information delivered by infrared sensors. For such swarms, a simple theoretical analysis enables to analytically fix the value of the Braitenberg rotation speed, to guarantee swarm cohesion.

4 Nonlinear filtering and heterogeneous swarms of autonomous agents - An exactly solvable model

Summary

We consider slightly heterogeneous swarm of agents controlled by one hidden leader. By hidden, we mean in this work that an external observer of the swarm cannot distinguish the leader from the regular agents. We study the global dynamics by using a newly established connection binding multi-agents dynamics and nonlinear optimal state estimation (nonlinear filtering). For a whole nonlinear class of mutual interactions, we are able to exactly characterize the resulting swarm dynamics. Our leader-follower dynamics are interpretable as a feedback particle filtering problem which itself is similar to a finite-dimensional, nonlinear filter problem originally proposed by V. E. Beneš. The state estimation problem can be explicitly solved as it merely uses a change of probability measure on an Ornstein-Uhlenbeck process. The agents interactions, driven by common observations of the randomly corrupted leaders position, correspond to the innovation kernel that underlies any Bayesian filter. Numerical results fully corroborate our theoretical findings and intuition.

4.1 Introduction

Among the vast and steadily increasing amount of literature devoted to the dynamics of a large number of mutually interacting autonomous agents, analytically solvable models stylizing some aspects of reality are welcome Hongler et al. (2014); Eftimie (2012); Bellomo and Dogbe (2011); Bertin et al. (2006). Despite specific features inherent in analytical approaches, these contributions enhance our understanding of the emergence of collective phenomena like synchronization, aggregation, pattern formation, behavioral phase transitions, fashion trend formation, and others. Most analytical studies focus on the dynamics of homogeneous swarms (i.e., those involving identical agents). Either the agents local rules are given and the ultimate goal is to analytically derive the emerging collective patterns or inversely, given a collective behavior, the goal is to unveil the agents local rules and their interactions. Purely homogeneous swarms are however rather scarcely encountered in reality.

In this chapter, we focus our attention on slightly heterogeneous populations in which one special agent (we call it the *leader*) is able to drive the whole swarm towards a desired objective Wang et al. (2011). Several types of leaders can be distinguished depending on the ways they affect their fellows. Either the leader is external and hence is explicitly recognized by ordinary agents of the swarm Couzin et al. (2005); Aureli and Porfiri (2010)), or it acts as a *shill* who appears ordinary to its fellows while in fact obeying a hidden master Faria et al. (2010); Gribovskiy et al. (2010); Wang and Guo (2008). Besides very particular models Sartoretti and Hongler (2013d,b), there is generally little hope for an analytical investigation of the collective behavior of a shill- or leader-infiltrated (and hence heterogeneous) swarm. The objective of this chapter is to unveil a class of dynamical models for which this investigation can be achieved.

Our source of inspiration is taken from the realm of estimation problems. In noise filtering, one considers the evolution of a stochastically driven system $\mathscr{S}$, monitored by an observer $\mathscr{O}$, which is itself delivering noisy information. The filtering goal at time t is to construct the best possible estimation of the state $\mathscr{S}$ by processing information delivered only from $\mathscr{O}$ up to time t. The filtering process is achieved via *sequential Bayesian* steps. Specifically, one starts with a *prediction step* to estimate the relevant conditional probability density function (pdf) based on the $\mathscr{S}$-dynamics, and then one updates this pdf based on the $\mathscr{O}$-dynamics. For linear $\mathscr{S}$-evolutions driven by White Gaussian Noise (WGN) and $\mathscr{O}$-measurements also corrupted by WGN, the filtering problem is completely solvable, and its explicit solution is known as the *Kalman-Bucy filter*. Indeed, due to linearity and Gaussian driving noise, both the prediction and the updating steps preserve their Gaussian character. Therefore the underlying filtering problem remains finite-dimensional as all operations are expressible via means and covariances only. For nonlinear evolution, the Gaussian character is lost, generally leading to infinite-dimensional problems. Analytical treatments are then precluded and only numerical approaches are feasible. One numerical method is given by particle filters, specifically *feedback particles algorithms* (FPA) Yang et al. (2013). These algorithms are directly based on dynamics of randomly interacting particles and can therefore be identified with specific agents dynamics. The FPA prediction step is achieved by attributing the $\mathscr{S}$-dynamics to a homogeneous swarm of agents. The updating process, realized by mutual agents interactions will globally minimize, in real time, the Kullback-Leibler distance between the $\mathscr{S}$ pdf and the swarm empirical distribution. In this chapter, we view the $\mathscr{S}$-dynamics as playing the role of a leader evolving among a homogeneous swarm of N ordinary agents. When $N \to \infty$, this dynamic is reducible to a *mean-field game* Pequito et al. (2011); Guéant et al. (2011) with here an infinitesimally short time horizon, (as only real time updating – excluding smoothing – is realized). The FPA offers, therefore, a natural framework to construct leader driven swarms of agents. As a natural consequence, solvable filtering problems, like the Kalman-Bucy case, provide directly solvable heterogeneous swarms dynamics. Here, our intention is to construct a class of multi-agents models which simultaneously keep the associated FPA finitely dimensional and yet escape from the pure Gaussian world. The idea on which we base our construction, is to consider a class of "Girsanov-changes" of probability measures applied to Ornstein-Uhlenbeck dynamics (i.e., linear dynamics with Gaussian noise sources). Here one considers the class of Girsanov changes of measures studied in Taylor (1989); Hongler (1981); Dai Pra (1991); Beneš (1981); Daum (1985).

We organize the chapter as follows: in section 2, the explicit connection between the filtering problem and the driving of a swarm of agents infiltrated by a leader is exposed. In section 3, we introduce our specific example of non-Gaussian interacting agents, controlled by a leader and for which the associated FPA is analytically solvable. Finally, in Section 4, we report numerical experiments to illustrate our analytical findings.

4.2 Multi-Agent Dynamics and Feedback Particle Filtering

Consider a swarm of N Brownian agents $\mathscr{A}_i$, $i = 1, 2, \cdots, N$, and one additional leader agent $\mathscr{A}$ with dynamics:

$$\begin{cases} dX_i(t) = f(X_i(t))\,dt + \mathscr{K}\left(X_i(t), \vec{X}(t), dZ(t)\right) + \sigma dW_i(t), \\ \text{leaders dynamics} \begin{cases} dY(t) = f(Y(t))\,dt + \sigma dW(t), \\ dZ(t) = hY(t)dt + \sigma_o dW_y(t), \end{cases} \end{cases} \tag{4.1}$$

where $h > 0$ is a constant, $f : \mathbb{R} \to \mathbb{R}$, $dW_i(t)$, $dW(t)$ and $dW_y(t)$ are mutually independent WGN processes and the vector $\vec{X}(t) = (X_1(t), X_2(t), \cdots, X_N(t))$ describes the dynamic state of the N homogeneous agents. The *leader* agent $Y(t)$ affects the dynamics of the $X_i(t)$ via the interaction kernel $\mathscr{K}\left(X_i, \vec{X}, dZ\right)$. We emphasize that the leader's dynamics $Y(t)$ itself is independent from the swarms state $\vec{X}(t)$. Agents are only able to observe the corrupted leaders position $Z(t)$, (the leader effectively hides its real position $Y(t)$ from the other fellows).

In Eq.(4.1), we focus our attention on the class of interaction kernels:

$$\mathscr{K}\left[X_i(t), \vec{X}(t), dZ(t)\right] = v\left(X_i(t), t\right) \otimes \left\{ dZ(t) - \underbrace{\frac{h}{2}\left[X_i(t) + \frac{1}{N}\sum_{k=1}^{N} X_k(t)\right] dt}_{\mathscr{G}[X_i(t), \vec{X}(t)]} \right\}, \tag{4.2}$$

where the coupling strength $v = v(X_i(t), t)$ is a positive convex function in $X_i(t)$ and where, due to the presence of multiplicative WGN processes, we define $\otimes$ to denote the Stratonovich interpretation of the underlying stochastic integrals Jazwinski (1970). In Eq.(4.2), $\mathscr{G}\left[X_i(t),\vec{X}(t)\right]$ is a consensual position given by the average between agent $\mathscr{A}_i$'s position and the whole swarm barycenter. The interaction kernel relates the position increment $\mathscr{G}dt$ with the leader's unveiled position increment $dZ(t)$ and weights this stimulus with the coupling strength ν. The assumptions on ν imply that $\mathscr{K}\left[X_i(t),\vec{X}(t),dZ(t)\right]$ tends, in real time, to steadily reduce the distance between $\mathscr{G}\left[X_i(t),\vec{X}(t)\right]dt$ and $dZ(t)$. Although the multiplicative factor $\nu(X_i(t),t)$ in Eq.(4.2) remains yet undetermined, its complete specification can be fixed by introducing a cost structure. In general, one requires that for some running cost functional $\mathscr{J}\left[\mathscr{K},X_i(t),\vec{X}(t),\mathscr{Z}(t),t\right]$ and final cost $\Psi\left(X_i(T),\vec{X}(T),dZ(T)\right)$ at time horizon T, the interaction $\mathscr{K}$ minimizes the associated optimization problem. Formally, the interaction kernel (and hence ν) would be the unique minimizer over a set $\mathbb{K}$ of admissible controls, namely:

$$\begin{aligned}&\mathscr{K}\left[X_i(t),\vec{X}(t),dZ(t)\right]\\&=\min_{K\in\mathbb{K}}\left\{\left(\int_t^T\mathscr{J}\left[K,X_i(s),\vec{X}(s),dZ(s),s\right]ds\right)+\Psi\left(X_i(T),\vec{X}(T),dZ(T)\right)\right\}.\end{aligned}\tag{4.3}$$

The coupled set of Eqs.(4.1), (4.2) and (4.3) can be interpreted as a multi-player differential game Bensoussan et al. (2013). For large populations, one can use the empirical density $P^{(N)}(x,t)$ to construct the mean-field posterior density $P(x,t\,|\,\mathscr{Z}(t),x_0)$:

$$P^{(N)}(x,t)dx=\frac{1}{N}\sum_{n=1}^{N}\mathbf{1}\left\{X_n(t)\in[x,x+dx]\right\}\approx P(x,t\,|\,\mathscr{Z}(t),x_0)dx,\tag{4.4}$$

where the condition $\mathscr{Z}(t)$ stands for the information history of the process Z until time t and x_0 for the common initial location of the whole swarm. In the $N\to\infty$ limit, we have:

$$\lim_{N\to\infty}\frac{1}{N}\sum_{k=1}^{N}X_k(t)=\int_{\mathbb{R}}x'P(x',t\,|\,\mathscr{Z}(t),x_0)dx'=\mathbb{E}\left\{X(t)\,|\,\mathscr{Z}(t)\right\}.\tag{4.5}$$

The Fokker-Planck equation which governs this mean-field posterior density reads (with a self explaining abuse of notation for $\mathscr{K}$):

$$\begin{aligned}\frac{\partial}{\partial t}P(x,t\,|\,\mathscr{Z}(t),x_0)&=-\frac{\partial}{\partial x}\left\{\left[f(x)+\mathscr{K}\left(x,\mathbb{E}\left\{X(t)\,|\,\mathscr{Z}(t)\right\}\right)\right]P(x,t\,|\,\mathscr{Z}(t),x_0)\right\}\\&\quad+\frac{\sigma^2}{2}\frac{\partial^2}{\partial x^2}P(x,t\,|\,\mathscr{Z}(t),x_0).\end{aligned}\tag{4.6}$$

Note that Eqs.(4.6) and (4.3) define in a forward/backward coupling, a so called differential *mean-field game problem.*

Feedback particles filters. For vanishing forward time horizon (i.e., $T = t$) in Eq.(4.3), a simpler situation arises (the backward in time coupling becomes trivial) and the minimization is reduced to solving an Euler-Lagrange variational problem (ELP) for $\Psi(x,\mathbb{E}\{X(t) \mid \mathcal{Z}(t)\})$. Choosing the objective criterion Ψ as the Kullback-Leibler distance d_K:

$$\begin{cases} \Psi(x,\mathbb{E}\{X(t)\},dZ(t)) := d_K\left\{P(x',t \mid \mathcal{Z}(t),x_0);Q(x,t \mid x_0)\right\}, \\[2ex] d_K\left\{P(x',t \mid \mathcal{Z}(t),x_0);Q(x,t \mid x_0)\right\} := \int_{\mathbb{R}} P(x',t \mid \mathcal{Z}(t),x_0)\left\{\ln\left[\frac{P(x',t \mid \mathcal{Z}(t),x_0)}{Q(x',t \mid x_0)}\right]\right\}dx', \end{cases} \tag{4.7}$$

with $Q(x,t \mid x_0)$ being the transition probability density of the diffusion process $Y(t)$ defined in Eq.(4.1) we find the ELP:

$$\begin{cases} -\frac{\partial}{\partial x}\left\{\frac{1}{P(x,t \mid \mathcal{Z}(t),x_0)}\frac{\partial}{\partial x}\left[P(x,t \mid \mathcal{Z}(t),x_0)v(x,t)\right]\right\} = \frac{h}{\sigma^2}, \\[2ex] \lim_{|x|\to\infty} P(x,t \mid \mathcal{Z}(t),x_0)v(x,t) = 0, \end{cases} \tag{4.8}$$

which leads to:

$$\begin{cases} v(x,t) = \frac{h}{\sigma_o^2 P(x,t \mid \mathcal{Z}(t),x_0)}\left\{\int_{-\infty}^{x}\left[\mathbb{E}\{X(t) \mid \mathcal{Z}(t)\} - x'\right]P(x',t \mid \mathcal{Z}(t),x_0)dx'\right\}, \\[2ex] \mathbb{E}\{X(t) \mid \mathcal{Z}(t)\} = \int_{-\infty}^{+\infty} x' P(x',t \mid \mathcal{Z}(t),x_0)dx'. \end{cases} \tag{4.9}$$

Eqs.(4.1) and (4.2), together with $v(x,t)$ given in Eq.(4.9) produce a nonlinear continuous time feedback particle filter. This allows for a direct reinterpretation of the leader-based dynamics in terms of a stochastic filtering problem. A class of examples is detailed in the next section.

It is worthwhile noting that the leader influences the swarm through the variance σ_o (and the parameter h), and not only through its position. As σ_o grows, the agents uncertainties of the actual leader's position increase. Consequently the coupling strength $v(x,t)$ decreases, the agents variances increase and the swarm tends to form a widespread group of agents around the leader. Alternatively, small values for σ_o allow for very compact swarm formation.

4.3 Finite Dimensional Filtering with Weber Parabolic Functions

Let us now introduce a specific filtering problem, which will be related to the control of the multi-agents dynamics. The nonlinear filtering problem is to estimate the value of the one-dimensional state $Y(t)$, at time t, given a set of measurements prior to t: $\mathscr{Z}(t) = \{Z(s) \mid 0 \leq s \leq t\}$. We will treat hereafter time-continuous measurements and assume that the leader state $Y(t)$ – starting at position y_0 – evolves according to the stochastic differential equation:

$$\begin{aligned} dY(t) &= \overbrace{\left\{ \frac{d}{dy} \left[\log \mathscr{Y}_B(y) \right] \Big|_{y=Y(t)} \right\}}^{:=f_B[Y(t)]} dt + dW(t), \\ Y(0) &= y_0 \end{aligned} \tag{4.10}$$

in which $W(t)$ is the standard Brownian motion and where $\mathscr{Y}_B(y)$ is the Weber parabolic function, which solves the ordinary differential equation:

$$\frac{d^2}{dy^2} \mathscr{Y}_B(y) = \left[\frac{y^2}{4} + \left(B - \frac{1}{2} \right) \right] \mathscr{Y}_B(y) \tag{4.11}$$

with B a control parameter. From the definition of $f_B[Y(t)]$, we easily see that

$$\frac{d}{dy} f_B(y) + f_B^2(y) = \frac{\frac{d^2}{dy^2} \mathscr{Y}_B(y)}{\mathscr{Y}_B(y)} = \frac{y^2}{4} + \left(B - \frac{1}{2} \right). \tag{4.12}$$

This leads to a Beneš type of finite-dimensional filtering problem (a fully analytical treatment of filtering problems in the Beneš class can be found in Daum (1985)). In the sequel, we impose the parameter range $B \in \mathbb{R}^+$ which ensures the positivity of $\mathscr{Y}_B(y)$ $(\forall\, y \in \mathbb{R})$. For $B \in [0, 1/2]$, we further observe that the generalized potential $-\log\left[\mathscr{Y}_B(y)\right]$ is locally attractive near the origin and asymptotically repulsive for $|y| \to \infty$. In the parameter range $B > 1/2$, the potential is systematically repulsive $\forall\, y \in \mathbb{R}$ (Hongler (1981)). Figure 4.1 shows the shape of $\mathscr{Y}_B(y)$ and $f_B(y)$ for different values of the control parameter B.

For $B = 0$ and $B = 1$ respectively, we obtain linear dynamics:

$$\left\{ \begin{array}{lllll} \mathscr{Y}_0(y) & = & e^{-\frac{1}{4}y^2} & \Rightarrow & f_0(y) = -\frac{1}{2} y \\[2ex] \mathscr{Y}_1(y) & = & e^{+\frac{1}{4}y^2} & \Rightarrow & f_1(y) = +\frac{1}{2} y. \end{array} \right. \tag{4.13}$$

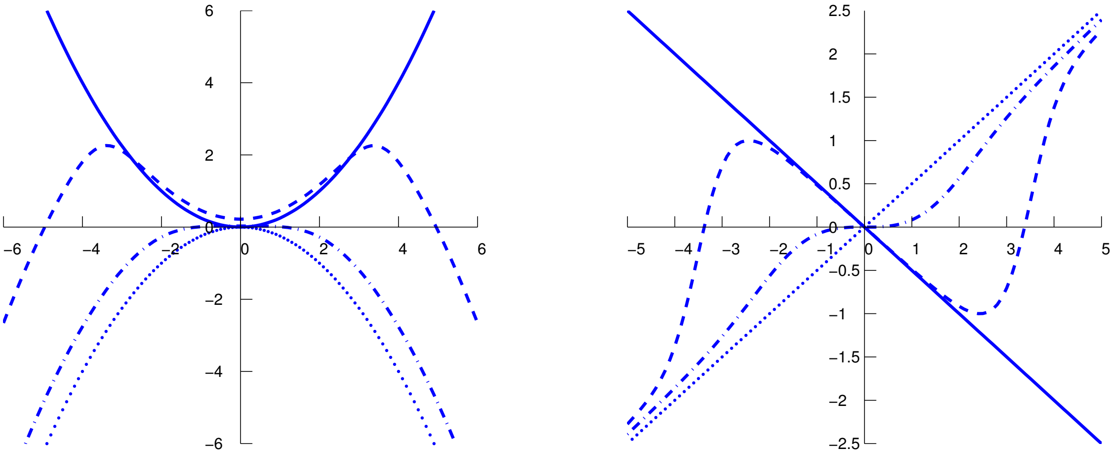

Figure 4.1 – Shape of $\mathscr{Y}_B(y)$ (left) and $f_B(y)$ (right) for $B = 0$ (plain line), $B = 0.01$ (stripped line), $B = 0.5$ (stripped-dotted line) and $B = 1$ (dotted line). For $B = 0$, the filtering problem is linear and the dynamics are stable. For $B = 1$, the filtering problem is again linear but with unstable dynamics. In between, we have a nonlinear filtering problem and the conditional probability density changes – with increasing B – from unimodal to bimodal and back to unimodal.

Using the framework introduced in Daum (1985), the continuous time filter is given by the normalized probability density $P(y, t|\mathscr{Z}_t)$ of observing $Y(t) := y$ conditioned on the set of measurements up to time t, $\mathscr{Z}(t)$, and can be written as:

$$P(y,t) := P(y,t \,|\, \mathscr{Z}(t)) = \frac{\mathscr{Y}_B(y) \cdot e^{-\frac{(y-m)^2}{2s}}}{\mathscr{J}_0(m,s,B)} \tag{4.14}$$

(computational details are given in Appendix B) with $\mathscr{J}_0(m, s, B)$ the normalization function:

$$\mathscr{J}_0(m,s,B) = 2\sqrt{\frac{\pi s}{2+s}} \left[\sqrt{\frac{2+s}{2-s}} \right]^B e^{\frac{m^2 s}{2(4-s^2)}} \cdot \mathscr{Y}_B\left(\frac{2m}{\sqrt{4-s^2}} \right). \tag{4.15}$$

(see Appendix B). The measurement *dependent* quantities $m := m(Z(t); t)$ are given by

$$m = m(Z(t);t) = \frac{\tanh(pt)}{p} \left[h \int_0^t \frac{\sinh(ps)}{\sinh(pt)} dZ(s) + \frac{p y_0}{\sinh(pt)} \right] \tag{4.16}$$

and similarly, the measurement *independent* quantities $s := s(t)$ reads:

$$s = s(t) = \frac{1}{p}\tanh(pt) \tag{4.17}$$

with the definition $p = \sqrt{h^2 + \frac{1}{4}}$.

With this expression for $P(y,t)$, we have the conditional mean:

$$\langle Y_t \rangle := \mathbb{E}(Y_t | \mathcal{Z}(t)) = \frac{4m}{4-s^2} + \frac{2s}{\sqrt{4-s^2}} f_B\left[\frac{2m}{\sqrt{4-s^2}}\right] \tag{4.18}$$

and after tedious elementary manipulations, we have the conditional variance:

$$var(Y_t) := \mathbb{E}((Y_t - \langle Y_t \rangle)^2 | \mathcal{Z}(t)) = \frac{2s}{2+s} + \frac{4s^2}{4-s^2}\left\{\frac{m^2}{4-s^2} + B - f_B^2\left(\frac{2m}{\sqrt{4-s^2}}\right)\right\}. \tag{4.19}$$

Remark: For the linear cases $B = 0$ and $B = 1$ from Eq.(4.13), we consistently find the following classical results:

$$P(y,t) = \frac{\exp\left\{-\frac{((2+s)y-2m)^2}{4s(2+s)}\right\}}{\sqrt{2\pi\frac{2s}{2+s}}}, \qquad \langle Y_t \rangle = \frac{2}{2+s}m, \qquad var(Y_t) = \frac{2}{2+s}s \tag{4.20}$$

for $B = 0$ and

$$P(y,t) = \frac{\exp\left\{-\frac{((2-s)y-2m)^2}{4s(2-s)}\right\}}{\sqrt{2\pi\frac{2s}{2-s}}}, \qquad \langle Y_t \rangle = \frac{2}{2-s}m, \qquad var(Y_t) = \frac{2}{2-s}s \tag{4.21}$$

for $B = 1$. As predicted by the linear version of the feedback filter, when $B = 0$ and $B = 1$ the coupling strength $v(x,t)$ reduces to the standard **state independent** Kalman gain:

$$v(x,t) = v(t) = \frac{h}{\sigma^2} var(Y_t). \tag{4.22}$$

4.4 Numerical Results

Numerical results are obtained by simulating (4.1) for a finite swarm of agents and one leader. Thanks to the consistency of the estimator (see Yang et al. (2013)), one can still use the results from the mean-field analysis for a large enough N. In this case $P(y,t)$ must be fitted to the empirical histogram of the agents' position at time t to find the values for m and s. The control $v(x,t)$ can then be computed from its integral expression in Eq.(4.9), while $\langle Y \rangle_t$ can be computed from Eq.(4.18). The derivative $\frac{d}{dx}v(x,t)$ is computed by using the relation $\frac{\frac{d}{dx}P(x,t)}{P(x,t)} = f_B(x) + \frac{x-m}{s}$, which can be written as:

$$\frac{d}{dx}v(x,t) = \frac{h}{\sigma^2}(\langle Y \rangle_t - x) - v(x,t) \cdot \left(f_B(x) - \frac{x-m}{s} \right). \tag{4.23}$$

Note that this natural fitting strategy used to estimate $P(y,t)$ is – computationally – very costly. Extensive numerical computations have shown that $v(x,t)$ can safely be computed from Eq.(4.9) when directly using the empirical histogram of the agents' position instead of the fitted function in Eq.(4.14). The derivative $\frac{d}{dx}v(x,t) \simeq \frac{v(x+h,t)-v(x,t)}{h}$ is computed by selecting a sufficiently small value h.

Numerical results in linear cases.

Figures 4.2 and 4.3 show in red the time evolution of the noisy leader's unveiled position. The mean value from the swarm of agents (likewise, the output of the feedback particle filter) produces the smooth blue curve. As the agents' control is updated based on the unveiled position of the leader, a small delay can be observed between the leader's movements and the swarm's reactions. The filter performs well: as expected, the swarms barycentric position is nearly always closer to the actual position of the leader than to the unveiled position. This means that the control on the agents leads to a better approximation of the actual leaders position.

Numerical results in nonlinear cases.

We now consider the parameter range $0 < B < 0.5$ where the dynamics of the leader is nonlinear and exhibits an attractive potential in the central region (i.e., around the origin) and a repulsive potential for $|x| \gg 0$. Between these two regions, the potential changes from attractive to repulsive and the agents experience strong nonlinear dynamics. Note that the dynamics in the attractive region is meta-stable, and a leader starting within this region ultimately escapes to infinity.

During the sojourn time of the leader in the attractive region, the close-by agents undergo quasi linear dynamics. They stay in this attractive region and self-arrange in the vicinity of the

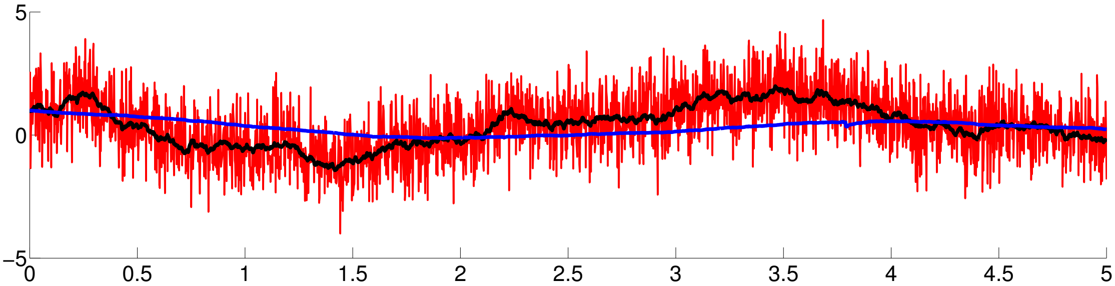

Figure 4.2 – Leader's position $Y(t)$ from Eq.(4.10) (black), along with its unveiled position $\mathcal{Z}(t)$ (red), for $B = 0$, $\sigma = h = 1$ and $t \in [0;5]$. In blue the mean value $\langle Y \rangle_t$ measured from a swarm of $N = 1000$ agents. The particles start with $Y_i(0) = x_0 = 1\ \forall i$, while $Z(0) = Y(0) = x_0$.

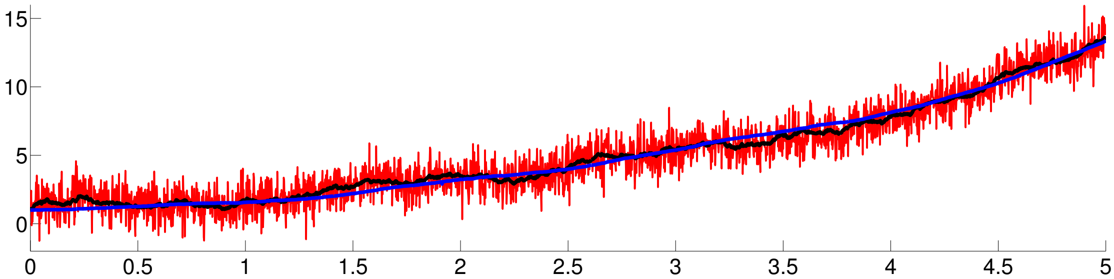

Figure 4.3 – Leader's position $Y(t)$ from Eq.(4.10) (black), along with its unveiled position $\mathcal{Z}(t)$ (red), for $B = 1$, $\sigma = h = 1$ and $t \in [0;5]$. In blue the value $\langle Y \rangle_t$ measured from a swarm of $N = 1000$ agents. The particles start with $Y_i(0) = x_0 = 0.1\ \forall i$, while $Z(0) = Y(0) = x_0$.

leaders position to empirically build the a posteriori distribution $P(y,t)$. As soon as the leader escapes from the attractive region, the other agents start feeling their barycentric control and ultimately follow the leader outside the attractive region. The barycenter of an infinite swarm follows the leaders position with nearly no delay; but in our case, as $N < \infty$ agents, a delay can possibly be observed between the exit times of the leader and the agents. Figures 4.4 and 4.5 show the results of a representative numerical simulation for $N = 1000$ agents, with a very narrow and shallow attractive region ($B = 0.49$). Observe the explicit delay between the exit times of the leader and the swarm for $\sigma = 5$ in Figure 4.5.

4.5 Conclusion

Heterogeneous multi-agent systems are notoriously difficult to describe analytically, especially if the underlying dynamics is intrinsically nonlinear. In this note, we present a class of dynamics from which explicit and fully analytical results can be derived. The core of our construction relies on recent approaches that have been obtained in the realm of nonlinear estimation problems. The so-called particle filter method – commonly used to tackle nonlinear estimation problems - can be reinterpreted as a general leader-follower problem in

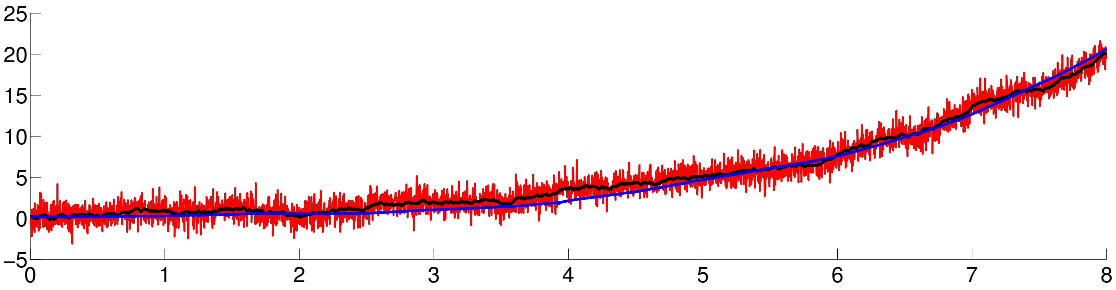

Figure 4.4 – Leader's position $Y(t)$ from Eq.(4.10) (black), along with its unveiled position $\mathscr{Z}(t)$ (red), for $B = 0.49$, $\sigma = h = 1$ and $t \in [0;8]$. In blue the value $\langle Y \rangle_t$ measured from a swarm of $N = 1000$ agents. The particles start with $Y_i(0) = x_0 = 0.2\ \forall i$, while $Z(0) = Y(0) = x_0$.

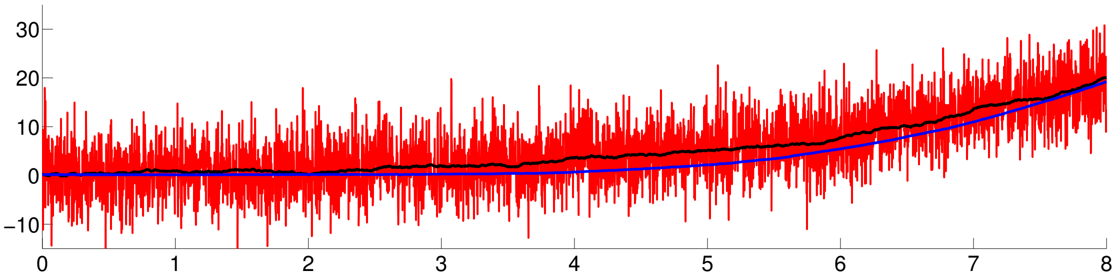

Figure 4.5 – Leader's position $Y(t)$ from Eq.(4.10) (black), along with its unveiled position $\mathscr{Z}(t)$ (red), for $B = 0.49$, $\sigma = 5$, $h = 1$ and $t \in [0;8]$. In blue the value $\langle Y \rangle_t$ measured from a swarm of $N = 1000$ agents. The particles start with $Y_i(0) = x_0 = 0.2\ \forall i$, while $Z(0) = Y(0) = x_0$.

which a swarm of interacting agents try to follow a leader whose unveiled position is corrupted by noise. In stochastic filtering, only finite-dimensional problems can possibly be solved analytically. When linear dynamics is driven by Gaussian noise, all relevant probability distributions remain Gaussian, and hence calculations can be limited to the first two moments (Kalman-Bucy filter). The intimate connection existing between multi-agent systems and estimation problems show that, for nonlinear dynamics, analytical results are in general hopeless. However, for one class of non-Gaussian finite-dimensional filtering problems – pioneered by Beneš – explicit analytical models are available. It is therefore natural to study how the Beneš' class enables us to construct nonlinear solvable multi-agents systems, as is done here. The core analytical tools leading to solvable finite-dimensional filtering problems rely on an underlying Riccati equation that we explicitly solved (in the scalar situation) via Weber parabolic cylinder functions. Using these special functions, we are able to answer two open questions originally formulated in Daum (1985) (our Eq.(4.18) answers Daum's open question 2, and our class of nonlinear dynamics answer Daum's open question 6). Our multi-agent class of dynamics enables us to explicitly observe how a leader can control the spreading factor of the agents around its position by tuning the strength of the observation noise.

4.6 New Contributions of Chapter 4

- We present an analytically tractable case of hard control of a swarm by a **hidden** leader. By tuning one control parameter, the leader is able to influence the repartition of the swarm around its own position.
- To achieve this goal, we use a recent stochastic filtering algorithm (feedback particle filtering). Beside the Kalman-Bucy case (linear dynamic), we also consider a class of exactly solvable nonlinear estimation problems.
- **Publication**: This chapter is reproduced from the conference paper Sartoretti et al. (2014b), with slight modifications to fit the present dissertation.

Shill-Based (Soft) Control

Part IV

5 Soft Control of Self-Organized Locally Interacting Brownian Planar Agents

Summary

This contribution is addressed to the dynamics of heterogeneous interacting agents evolving on the plane. Heterogeneity is due to the presence of an unfiltered externally controllable fellow, a shill, which via mutual interactions ultimately drives (i.e. soft controls) the whole society towards a given goal. We are able to calculate relevant dynamic characteristics of this controllable agent. This opens the possibility to optimize the soft controlling of a whole society by infiltrating it with a properly designed shill. Numerical results fully corroborate our theoretical findings.

5.1 Introduction

The *Soft Control* of a swarm of interacting agents consists in introducing an externally controllable agent into an homogeneous swarm of autonomous agents. By suitably chose the externally controllable fellow, one ultimately can (softly) control the whole swarm. While her dynamics differs, the controllable infiltrated agent, often referred to as the *Shill* (SH), is detected by the other fellows as being an ordinary member of the society. The SH's influence can be used to stimulate specific positive features to the whole group (optimal driving to targets, enhancement of flocking capability, extra energy scavenging, etc. Sartoretti and Hongler (2013d); Wang et al. (2011); Wang and Guo (2008)). Alternatively the SH's presence may destroy the overall swarm's coherence Sartoretti and Hongler (2013d). Soft control is also commonly used in ethology, by introducing robotic shills in societies of animals, see for instance Gribovskiy et al. (2010); Halloy et al. (2007); Faria et al. (2010).

In the sequel, we consider an homogeneous swarm of Brownian agents following a planar mixed canonical-dissipative dynamics as introduced in Sartoretti and Hongler (2013b). After showing how the agents asymptotically converge to (and circulate on) a self-selected closed annular orbits on $\mathbb{R}^2$, we then introduce a SH agent into the swarm. We then use the SH's presence to soft control the angular speed of the whole society.

5.2 Interacting Diffusion Processes on $\mathbb{R}^2$

For $\overline{\mathbf{X}}(t) = (\mathbf{X}_1(t), \mathbf{X}_2(t), \cdots, \mathbf{X}_N(t)) \in \mathbb{R}^{2N}$ with $\mathbf{X}_k(t) = (x_{1,k}(t), x_{2,k}(t)) \in \mathbb{R}^2$, our class of dynamics is given by a collection of N mutually interacting planar Brownian agents evolving according to a set of Stochastic Differential Equations (SDE) on $\mathbb{R}^{2N}$:

$$\begin{cases} d\mathbf{X}_k(t) = dt\left[\mathscr{A}_k(t) - \Lambda\left(\mathscr{L}_{k,\rho}(t) - \mathscr{H}(\mathbf{X}_k)\right)\right] \triangledown \mathscr{H}(\mathbf{X}_k) + \sigma\, d\mathbf{W}_k(t), \\ \\ \mathbf{X}_k(0) = \mathbf{X}_{0,k}, \end{cases} \tag{5.1}$$

where $\sigma, \Lambda \in \mathbb{R}^+$ are control parameters, and the definitions of the dynamical inputs are:

i) **the Hamiltonian function**$\mathscr{H}(x_1, x_2) : \mathbb{R}^2 \mapsto \mathbb{R}^+$ are used to define a family of closed, non-intersecting, planar curves with equations given by $[\mathscr{H}(x_1, x_2) - R] = 0$, $\forall\ R > 0$. We note $\triangledown\mathscr{H}(\mathbf{X}_k) = \left.\begin{pmatrix} \frac{\partial}{\partial_{x_1}}\mathscr{H}(x_1, x_2) \\ \frac{\partial}{\partial_{x_2}}\mathscr{H}(x_1, x_2) \end{pmatrix}\right|_{\mathbf{X}_k}$

ii) **the tangent dynamical map at the origin**. In absence of noise source ($\sigma \equiv 0$), the origin is a singular point of Eq.(5.1) and its associated linear map $\mathscr{A}_k(t)$:

$$\mathscr{A}_k(t) = \begin{pmatrix} \frac{N_{k,\rho}(t)}{N} - \frac{1}{M} & \frac{N_{k,\rho}(t)}{N} \\ \\ -\frac{N_{k,\rho}(t)}{N} & \frac{N_{k,\rho}(t)}{N} - \frac{1}{M} \end{pmatrix} \tag{5.2}$$

where $M \in [1, N] \subseteq \mathbb{R}^+$ is a control parameter and $(N_{k,\rho}(t)/N)$ is the fraction of the total swarm detected by agent a_k in the neighborhood $\mathscr{D}_{k,\rho}(t)$ defined as:

$$\mathscr{D}_{k,\rho}(t) = \left\{\mathbf{X} \in \mathbb{R}^2 \mid \|\mathbf{X} - \mathbf{X}_k(t)\|_2 \leq \rho\right\} \tag{5.3}$$

iii) **the self-adaptive Hamiltonian level**. The scalar quantity:

$$\mathscr{L}_{k,\rho}(t) := \frac{1}{N_{k,\rho}(t)} \sum_{i \in V_{k,\rho}(t)} \mathscr{H}(\mathbf{X}_i)$$

where $N_{k,\rho}(t)$ has been defined in ii). The summation extends over the agents' set $V_{k,\rho}(t) := \left\{i \mid \mathbf{X}_i \in \mathscr{D}_{k,\rho}(t)\right\}$

iv) **the noise sources**. $d\mathbf{W}_k(t) = \big(dW_{1,k}(t), dW_{2,k}(t)\big)$ are $2N$ independent standard White Gaussian Noise (WGN) processes

Proposition 1. *For $t \to \infty$, the dissipative dynamics Eq.*(5.1) *reaches a stationary regime characterized by the time-invariant probability product measure:*

$$P_s(\bar{\mathbf{x}})\,d\mathbf{x} = [P_s(\mathbf{x})\,d\mathbf{x}]^N \quad \text{with} \quad P_s(\mathbf{x})\,d\mathbf{x} = \mathcal{Z}^{-1}\exp\left\{-\frac{\Lambda}{\sigma^2}\left[\mathcal{L}_{s,\rho} - \mathcal{H}(\mathbf{x})\right]^2\right\}d\mathbf{x}. \tag{5.4}$$

where $\mathcal{Z}$ is the normalization factor, and $\mathcal{L}_{s,\rho}$ is the stationary Hamiltonian level curve statistically reached by the agents.

Proof of Proposition 1.

We first write the Fokker-Planck equation (FPE) associated with the diffusion process of Eq.(5.1):

$$\partial_t P(\bar{\mathbf{x}}, t|\bar{\mathbf{x}}_0) = -\nabla\cdot\left\{\left[\mathscr{A}(t)\nabla\mathcal{H}(\mathbf{x}) - \nabla V_\rho\left(\bar{\mathbf{x}}, t\right)\right]\cdot P(\bar{\mathbf{x}}, t|\bar{\mathbf{x}}_0) - \frac{\sigma^2}{2}\nabla P(\bar{\mathbf{x}}, t|\bar{\mathbf{x}}_0)\right\}, \tag{5.5}$$

with $\mathscr{A}(t)$ the $(2N \times 2N)$ block-simplectic matrix

$$\mathscr{A}(t) := \begin{pmatrix} A_1(t) & & 0 \\ & \ddots & \\ 0 & & A_N(t) \end{pmatrix}, \qquad \text{with } A_k(t) = \begin{pmatrix} 0 & \frac{N_{k,\rho}(t)}{N} \\ -\frac{N_{k,\rho}(t)}{N} & 0 \end{pmatrix}$$

The dissipative component of the drift is derived from the time-dependent generalized potential $V_\rho\left(\bar{\mathbf{x}}, t\right)$, which reads as:

$$V_\rho\left(\bar{\mathbf{x}}, t\right) = \sum_{k=1}^{N}\left\{\overbrace{\left[\frac{N_{k,\rho}(t)}{N} - \frac{1}{M}\right]}^{:=\mathscr{R}_{k,\rho}(t)} + \frac{\Lambda}{2}\left[\mathcal{L}_{k,\rho}(t) - \mathcal{H}(\mathbf{X}_k)\right]^2\right\}\nabla\mathcal{H}(\mathbf{x}). \tag{5.6}$$

The parameters $\mathscr{R}_{k,\rho}(t)$ and $\mathcal{L}_{k,\rho}(t)$ in Eq.(5.6) implicitly depend on the agents' configurations, implying that Eq.(5.5) is effectively a nonlinear FPE. The potential $V_\rho\left(\bar{\mathbf{x}}, t\right)$ is globally attractive on $\mathbb{R}^{2N}$ (i.e $V_\rho\left(\bar{\mathbf{x}}, t\right) \to \infty$ for $\|\bar{\mathbf{x}}\| \to \infty$). Global attraction on $\mathbb{R}^{2N}$ in Eq.(5.1) together with the WGN driving forces imply that the diffusive dynamics is **ergodic**. Hence, it exists an unique invariant measure $P_s(\bar{\mathbf{x}})$ implying that both $\mathscr{R}_{k,\rho}(t)$ and $\mathcal{L}_{k,\rho}(t)$ asymptotically converge towards stationary (time-independent) values $\mathscr{R}_{k,s,\rho}$ and $\mathcal{L}_{k,s,\rho}$. Moreover, as Eqs.(5.5) and (5.6) are invariant under permutations of the agents labeling, we shall have $\mathscr{R}_{k,s,\rho} =: \mathscr{R}_{s,\rho}$ and $\mathcal{L}_{k,s,\rho} =: \mathcal{L}_{s,\rho}$ $(\forall\, k)$. Dissipation drives the system to its minimal energy configuration, leading to the specific values $\mathscr{R}_{s,\rho} \equiv 0$ and to $\lim_{t\to\infty}\mathscr{A}(t) = \mathscr{A}_s$ with:

$$\mathscr{A}_s := \begin{pmatrix} A_s & & 0 \\ & \ddots & \\ 0 & & A_s \end{pmatrix}, \qquad \mathscr{A}_s = \begin{pmatrix} 0 & \frac{1}{M} \\ -\frac{1}{M} & 0 \end{pmatrix}.$$

Observe that the gradient $\bigtriangledown V_\rho\left(\overline{\mathbf{x}}, t\right)$ is systematically orthogonal to the antisymmetric component $\mathscr{A}(t) \bigtriangledown \mathscr{H}(\mathbf{x})$. This remains true in the stationary regime $\mathscr{A}_s$, allowing us to write the stationary solution of the FPE Eq.(5.5) in the *product-form* $P_s(\overline{\mathbf{x}})$:

$$\begin{aligned} &P_s(\overline{\mathbf{x}}) = [P_s(\mathbf{x})]^N = \left[\mathscr{N}^{-1} e^{\{-V_{s,\rho}(\mathbf{x})\}}\right]^N, \\ &V_{s,\rho}(\mathbf{x}) = +\tfrac{\gamma}{2}\left[\mathscr{L}_{s,\rho} - \mathscr{H}(\mathbf{x})\right]^2 \end{aligned} \tag{5.7}$$

with $\overline{\mathbf{x}} = (\mathbf{x}_1, \mathbf{x}_2, \cdots, \mathbf{x}_N) \in \mathbb{R}^{2N}$, $\mathbf{x}_k \in \mathbb{R}^2$. In Eq.(5.7), $\mathbf{x} \in \mathbb{R}^2$ stands for one representative agent in the swarm. The product form of $P_s(\overline{\mathbf{x}})$ explicitly shows that our dynamics propagates chaos, validating the use of a mean-field (MF) approach, where the behavior of a single agent of the swarm effectively reflects the global dynamics.

Here the stationary regime of the single representative agent $\mathbf{X}(t) = (x_1(t), x_2(t))$ is characterized by the invariant probability density $P_s(\mathbf{x})$:

$$0 = -\bigtriangledown\left\{\left[\mathscr{A}_s \bigtriangledown \mathscr{H}(\mathbf{x}) - \bigtriangledown V_{s,\rho}(\mathbf{x})\right] \cdot P_s(\mathbf{x})\right\} + \frac{\sigma^2}{2} \triangle P_s(\mathbf{x}), \tag{5.8}$$

Auto-consistency of the nonlinear FPE here implies:

$$\frac{N_{s,\rho}}{N} = \int_{\mathbf{x} \in D_{s,\rho}} P_s(\mathbf{x})\, dx_1\, dx_2 \left(= \frac{1}{M}\right) \tag{5.9}$$

where here $D_{s,\rho}$ is the stationary representative agent's neighborhood.

□

Corollary 1. *For the harmonic oscillator's Hamiltonian function*

$$\mathscr{H}(x_1, x_2) = 1/2\,(x_1^2 + x_2^2), \tag{5.10}$$

and with $\Lambda \to \infty$, the stationary probability measure converges to a uniform distribution of the agents on the limit cycle. Indeed, the angular speed of each agent on the limit cycle is proportional to the local density of its neighbors. This mechanism helps spread the agents on

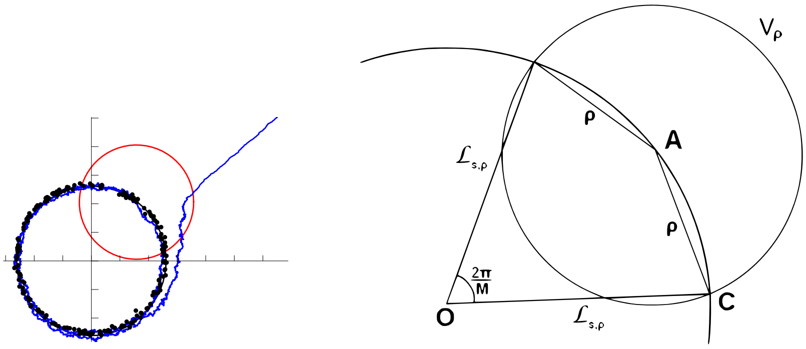

Figure 5.1 – Left: An example run with $N = 100$ agents, and a range $\rho = 1$. In black, the theoretic limit cycle, and in blue the positions through time of one agent.
Right: Geometric explanation of the computation of $\mathscr{L}_{s,\rho}$: In the stationary regime, each agent has in average $\frac{N}{M}$ agent in her neighborhood. Since the agents are uniformly distributed on the limit cycle, the number of neighbors is directly correlated with the arc length contained within the neighborhood of each agent. Thus, each agent's range exactly encompasses an arc of $\frac{2\pi}{M}$, and the rule of cosine in the triangle OAC leads to the result of Eq.(5.11).

the limit circle, and its action only stops once the swarm is uniformly distributed.

In the stationary regime, each agent has in average $\frac{N}{M}$ agent in her neighborhood. Since the agents are uniformly distributed on the limit cycle, the number of neighbors is directly correlated with the arc length contained within the neighborhood of each agent. Thus, each agent's range exactly encompasses an arc of $\frac{2\pi}{M}$, and the rule of cosine in the triangle OAC (see Figure 5.1) finally leads to:

$$\mathscr{L}_{s,\rho} = \frac{\rho}{\sqrt{2 - 2\cos(\frac{\pi}{M})}}. \tag{5.11}$$

5.3 Swarm Soft Controlling - Harmonic oscillator Hamiltonian

Now we focus on cylindrically symmetric configurations involving the Hamiltonian Eq.(5.10), and for these cases we generalize Eq.(5.1) by allowing the agents to self-adapt their circulation velocities. This can be achieved by replacing the nominal matrix $\mathscr{A}_k(t)$ in Eq.(5.2) by $\mathbb{A}_k$:

$$\mathbb{A}_k = \begin{pmatrix} \frac{N_{k,\rho}(t)}{N} - \frac{1}{M} & \omega_k(t)\,\frac{N_{k,\rho}(t)}{N} \\ -\omega_k(t)\,\frac{N_{k,\rho}(t)}{N} & \frac{N_{k,\rho}(t)}{N} - \frac{1}{M} \end{pmatrix}, \tag{5.12}$$

where the now adaptive angular velocity $\omega_k(t)$ of agent a_k obeys to the relaxation dynamics:

$$\begin{cases} \dot{\omega}_k(t) = \gamma_1 \cdot \left[\langle \omega \rangle_{k,\rho}(t) - \omega_k(t) \right] + \gamma_2 \cdot \left[\Omega - \omega_k(t) \right], \qquad \omega_k(0) = \omega_{0,k}, \\ \\ \langle \omega \rangle_{k,\rho}(t) := \frac{1}{N_{k,\rho}(t)} \sum_{j \in V_{k,\rho}(t)} \omega_j(t), \end{cases} \tag{5.13}$$

with $\gamma_i > 0$ $(i = 1,2)$, and Ω the natural angular speed toward which all agents are constantly drawn.

Remark. The set of ordinary differential equations in Eq.(5.13) describes an autonomous, systematically dissipative linear dynamical system. Accordingly, the unique resulting attractor is here given by $\lim_{t \to \infty} \omega_k(t) = \Omega, \quad \forall k$.

5.3.1 Inhomogeneous swarm - Shill soft controlling mode

Let us now introduce an externally controllable agent, to be called the *shill* (SH) agent, into the swarm. Agent SH is, without loss of generality, taken as a_1 and we assume that we can fix $\omega_1(t) \equiv \omega_s$. Regarding the radial dynamics, we assume that SH behaves as an ordinary agent. In presence of SH, the swarm is heterogeneous, thus precluding analytical approaches for general parameter ranges. Nevertheless, for limiting regimes, we will now see that our dynamics still lend itself to an approximate analytical treatment.

We assume in Eq.(5.1) that the signal to noise ratio (SNR) $(\Lambda/\sigma^2) << 1$. In absence of SH, the stationary regime of the homogeneous swarm uniformly distributes the agents along the arcs of a narrow annular ring with radius $\mathscr{L}_{s,\rho}$. The agents circulate with a common angular velocity $\omega_k \equiv \Omega$. Let us now introduce SH into the swarm.

We shall consider the cases where $\omega_s > \Omega$ (the other possibilities can be discussed along the same lines). Taking into account the presence of SH in the swarm, our goal is to first show that for $\langle \omega \rangle_{k,\rho}(t)$ in Eq.(5.13) can be approximately expressed as a convex combination of ω_s and ω_k:

$$\langle \omega \rangle_{k,\rho}(t) \simeq \begin{cases} \frac{\omega_s + (\frac{N}{M} - 1)\omega_k(t)}{N/M} & \text{when} \quad SH \in V_{k,\rho}(t), \\ \\ \omega_k(t) & \text{otherwise.} \end{cases} \tag{5.14}$$

To heuristically derive Eq.(5.14), we assume that at initial time $t = -\infty$, we have an homogeneous population involving N agents. At time $t = 0^-$, this homogeneous swarm has reached its stationary regime, i.e. the agents are confined in a ring close to the cycle $\mathscr{L}_{s,\rho}$ and their stationary circulation has the common angular velocity $\omega_k \equiv \Omega$. For times $t \geq 0^+$, we switch on SH's action by imposing $\omega_1(t) \equiv \omega_s > \Omega$. Via mutual interactions, SH is able to enhance the a_k's angular velocities for $k = 2, \dots, N$. Therefore, besides the intrinsic dissipation mechanism given in Eqs.(5.1) together with Eqs.(5.12) and (5.13), the a_k's ($k = 2, \dots, N$) do effectively scavenge rotational energy from SH and ultimately an energy balance will be reached.

For large populations N, we assume SH's influence to be **quasi-adiabatic**. That is to say, we assume that the a_k's distribution on the limit cycle $\mathscr{L}_{s,\rho}$ remains essentially unaltered. Since we choose SH's angular speed $\omega_s \equiv \omega_1 > \Omega$ and because SH itself circulates with high probability inside the thin annulus $\mathscr{L}_{s,\rho}$, SH periodically crosses the $V_{k,\rho}(t)$ for $k = 2, 3, \dots, N$. During the SH's transit time inside $V_{k,\rho}(t)$, interaction with SH enhances ω_k. Conversely, when SH lies outside $V_{k,\rho}(t)$, then ω_k freely relaxes towards Ω. To be consistent with the adiabatic energy exchange assumption, the SH's influence on ω_k during one $V_{k,\rho}(t)$ over-crossing has to remain small. At a given time t, and for a tagged a_k ($k = 2, 3, \dots, N$), two configurations are alternatively realized depending on whether SH belongs to $V_{k,\rho}(t)$ or not:

i) SH $\notin V_{k,\rho}(t)$: only regular neighbors surround a_k. Their individual speed very slightly differs from $\omega_k(t)$. These differences are due to SH leaving the neighboring a_k's $V_{k,\rho}(t)$ at different successive times. Some of the neighbors of a_k will have an angular velocity slightly higher than $\omega_k(t)$ (*the rapids*), while others will have a slightly lower angular velocities (i.e. *the slows*). SH's constant rotation, always leaves a wake of agents with a slight angular velocity enhancement in SH's trail. Constant rotation implies that the rapids and slows are approximatively spatially distributed symmetrically with respect to a_k and close to the cycle $\mathscr{L}_{s,\rho}$. Since the a_k's neighbors present in $V_{k,\rho}(t)$ are approximately uniformly distributed on the cycle $\mathscr{L}_{s,\rho}$, on average the numbers of *rapids* and *slows* are identical. Hence, the average speed of the agents in $V_{k,\rho}(t)$ is approximately $\omega_k(t)$ (i.e. the *rapids* approximately compensate for the *slows*).

ii) SH $\in V_{k,\rho}(t)$: here we invoke the fact that a_k has in average $\frac{N}{M}$ neighbors. Using i) for the $\frac{N}{M} - 1$ regular neighbors of a_k and taking into account SH's presence, the weighted average of the angular velocities leads to the first line in Eq.(5.14).

Using Eq.(5.14) into Eq.(5.13) enables to write:

$$\dot{\omega}_k(t) = \begin{cases} \left(\gamma_1 \frac{M}{N} + \gamma_2\right) \cdot \left[\overbrace{\frac{\gamma_1 \frac{M}{N}\omega_s + \gamma_2 \Omega}{\gamma_1 \frac{M}{N} + \gamma_2}}^{\nu_1} - \omega_k(t) \right] & \text{when} \quad SH \in V_{k,\rho}(t) \\ \gamma_2 \cdot \left[\underbrace{\Omega}_{\nu_2} - \omega_k(t)\right] & \text{otherwise.} \end{cases} \tag{5.15}$$

For an ultra-fast relaxation regime $\gamma_k \to \infty$ ($k = 1, 2$), Eq.(5.15) implies:

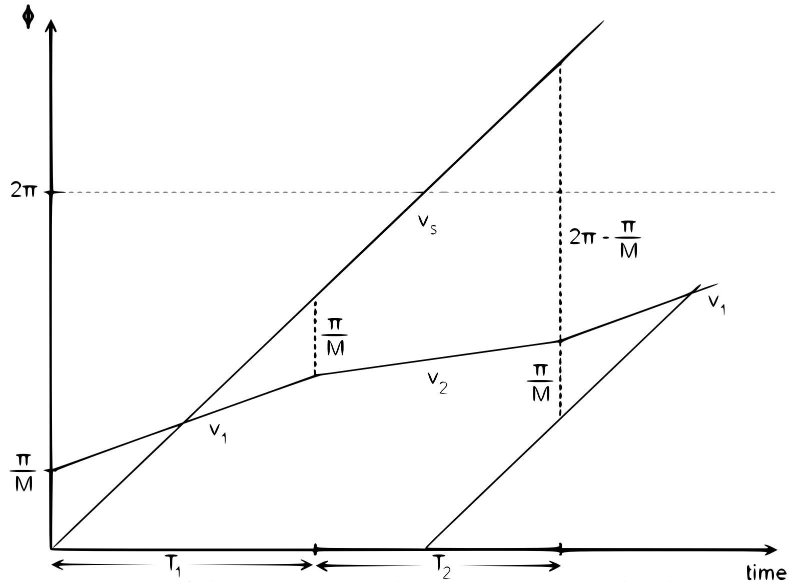

Figure 5.2 – Computation of the time intervals T_1 and T_2 spent by the agents in each of the states of Eq.(5.16). The state 1 starts when SH enters the agent's range (that is when their phase differs by $\frac{\pi}{M}$ in one direction), and lasts until they differ by $\frac{\pi}{M}$ in the other direction. Then, the time interval T_2 lasts until SH re-enters the agent's range, that is when their phases differ of $\frac{2M-1}{M}\pi$.

$$\omega_k(t) \simeq \begin{cases} v_1 & \text{when SH in } V_{k,\rho}(t), \\ v_2 & \text{otherwise.} \end{cases} \tag{5.16}$$

Now, we can calculate the time spend into the alternative states of Eq.(5.16). To this aim consider Figure 5.2, where we sketch the approximative resulting behavior for an arbitrary agent k together with SH.

In view of Figure 5.2, we now can write:

$$\begin{cases} \frac{2\pi}{M} + T_1 \cdot v_1 = T_1 \cdot \omega_s & \Rightarrow \quad T_1 = \frac{2\pi}{M(\omega_s - v_1)}, \\ \frac{pi}{M} + T_2 \cdot \omega_s = T_2 \cdot v_2 + \frac{2M-1}{M}\pi & \Rightarrow \quad T_2 = \frac{(2M-2)\pi}{M(\omega_s - v_2)}. \end{cases} \tag{5.17}$$

Hence, on a single time period $T = T_1 + T_2$, the resulting weighted average angular velocity yields:

$$\omega_{ave} = \frac{T_1 \cdot v_1 + T_2 \cdot v_2}{T_1 + T_2} = \underbrace{\frac{\gamma_2 N}{\gamma_1 + \gamma_2 N}}_{\alpha(N,\gamma_1,\gamma_2)} \cdot \Omega + \underbrace{\frac{\gamma_1}{\gamma_1 + \gamma_2 N}}_{\beta(N,\gamma_1,\gamma_2)} \cdot \omega_s.$$

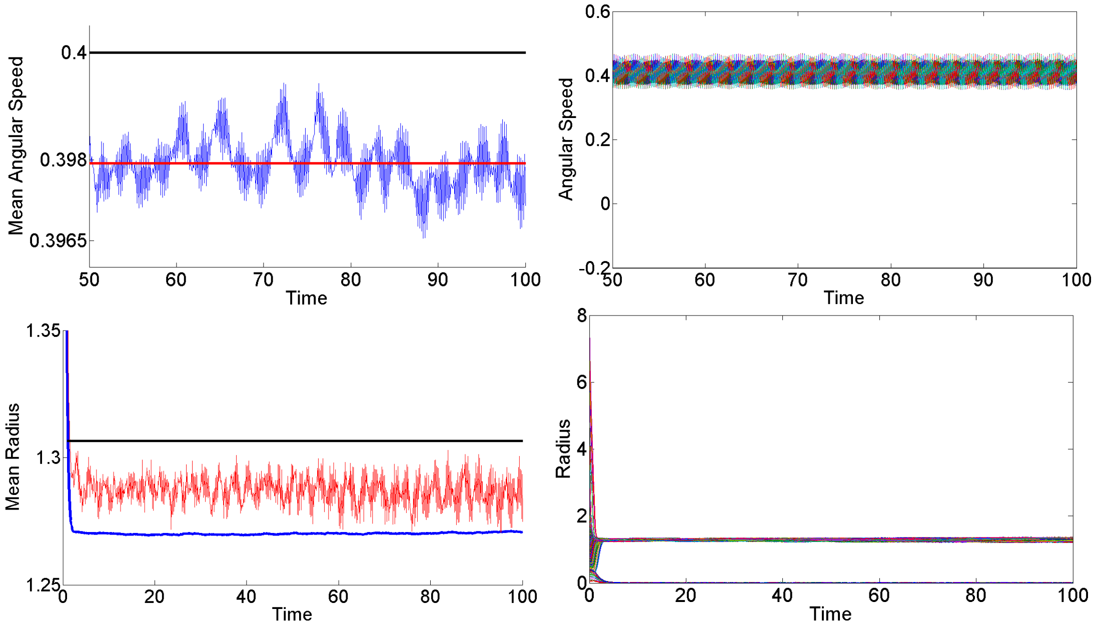

Figure 5.3 – Top left: In blue, the average angular speed of the regular agents, with in red its average over the period $t \in [50;100]$. In black, the expected value $\omega_{ave} = 0.4$. right: Individual angular speeds of each agent as a function of time. Bottom left: In blue the average radius of the regular agents, and in red the radius of SH. In black, the expected value $\mathscr{L}_{s,\rho} \simeq 1.31$. right: Individual radii of each agent as a function of time.

Note that $\alpha(N,\gamma_1,\gamma_2)+\beta(N,\gamma_1,\gamma_2) = 1$ and $\left[\alpha(N,\gamma_1,\gamma_2)/\beta(N,\gamma_1,\gamma_2)\right] = N(\gamma_2/\gamma_1)$. Hence, we consistently observe that $\lim_{N\to\infty}\alpha(N,\gamma_1,\gamma_2) = 1$, showing that the SH's relative influence is reduced with the population size N.

Figure 5.3 shows numerical results for a swarm of $N = 2000$ agents for time $t \in [0;100]$ with $M = 4$. Input parameters are

$$\left.\begin{array}{lllllllll} \sigma & = & 0.5 & \rho & = & 1 & \Omega & = & -0.2 \\ \gamma_1 & = & 40 & \gamma_2 & = & 1 & \omega_s & = & 31.4 \end{array}\right\} \Rightarrow \omega_{ave} = 0.4.$$

Note that some agents end up in the vicinity of the origin. These agents will asymptotically with time converge to the limit cycle $\mathscr{L}_{s\rho}$, and to the theoretic consensual angular speed ω_{ave}, but that can not be seen in the small time window of these simulations. Despite these agents, the average values for the radius and the angular speed of the swarm exactly match the theoretical values.

5.4 Conclusion

The intrinsic swarm's heterogeneity due to the presence of a shill fellow into an otherwise homogeneous swarm agents offers, in general, little hope for analytically deriving the dynamical features of the global population. However for the present mixed canonical-dissipative dynamics with agent-dependent angular speed, we are able to show how reliable analytical approximations can be derived. Being able to quantitatively appreciate the shills presence, it then offers the possibility to select the optimal shills characteristics. Our analytical approach is fully corroborated by a set of numerical simulations involving large populations of magnitude order of 10^3 individuals.

5.5 New Contributions of Chapter 5

- Building on Chapter 1, we introduce a **hidden** shill (i.e., infiltrated agent), able to soft control the swarm's circulation on the limit ring. For this heterogeneous swarm situation, we are able to analytically estimate the resulting swarm dynamic.
- **Publication**: This chapter is reproduced from the journal paper Sartoretti and Hongler (2013c), with slight modifications to fit the present dissertation.

6 Soft Control of Swarms - Analytical Approach

Summary

We analytically study the collective dynamics of mutually interacting heterogeneous agents evolving in a random environment. Our formal framework consists of a collection of N scalar drifted Brownian motions (BM) diffusing on $\mathbb{R}$. The mutual interactions are introduced via a ranked-based, real-time mechanism always endowing the laggard (i.e the agent with the leftmost position) with an extra positive drift. The extra drift generates a net tendency for any agents not to remain the laggard of the society. For well chosen individual and extra laggard's drifts, the agents organize with time to flock towards a tight and stable traveling spatial pattern. For a population of $(N-1)$ identical agents and an "atypical" fellow (called hereafter the shill), we are able to analytically discuss the dynamics. In particular we exhibit how a single turbulent shill, stylized here by a ballistic diffusion process, can destroy the cohesion of a swarm. Conversely, we also analytically show how a single shill is able to safely pilot a whole swarm to avoid an obstacle, via interactions with its fellows. A series of simulations experiments comfort our analytical findings.

6.1 Introduction

The capability of a collection of interacting stochastic agents to exhibit an emergent collective behavior (i.e *flocking behavior*) even in random environments stimulates a strong research activity devoted to both experimental and theoretical modeling approaches. For suitable range of mutual interactions, flocking (phase) transitions are observed, namely the self-organized capability to create finite and persistent spatio-temporal patterns Banner et al. (2005); Yates et al. (2009); Chatterjee and Pal (2010); Dosseti (2012); Pal and Pitman (2008); Ichiba et al. (2011); Bialek et al. (2012).

Agents societies can be composed of either dynamically homogeneous or heterogeneous individuals requiring for each case drastically different approaches. For large and **homogeneous** population of agents, the classical statistical mechanics concepts and in particular the

mean-field description (MF) directly offers an appropriate tool to analytically discuss the global dynamics. In the MF description, one basically assumes that the behavior of the global society can be characterized by the dynamics of a single representative agent which feels its fellows' interactions via an effective external field. In most circumstances however, homogeneity fails, and therefore a growing attention is now paid to **heterogeneous** populations. Heterogeneity occurs typically when one or several masked agents, that we shall from now on refer to as **shills**, exhibit leaders or troublemakers behaviors. These shills are not recognized by the regular agents which see them as ordinary fellows, leaving the interaction rules between them unchanged. The presence of shills can strongly alter the ultimate evolution of the whole society and it is the central goal here to analytically study this problematic.

Our approach involves assemblies of interacting stochastic agents in which a single shill exhibits a different individual behavior. All agents, including the shill, interact with their fellows with fixed given rules. The paradigmatic vision of this situations has been currently explored in ethology where one fake individual is introduced among schools of fishes, cockroaches, newborn chicken, etc. The shill is able to ultimately pilot the whole population Gribovskiy et al. (2010); Faria et al. (2010); Vaughan et al. (2000). This basic mechanism also referred as the **soft control** of a population Jing and Lin (2010); Wang et al. (2011, 2009); Wang and Guo (2008) is the core of our present research. Since heterogeneous societies preclude MF approaches, rather few analytical results are yet available. Recent mathematical models of heterogeneous **rank-based interacting Brownian motions** (RBM), introduced in finance Banner et al. (2005); Chatterjee and Pal (2010); Pal and Pitman (2008); Ichiba et al. (2011), will be used in the sequel to analytically approach the soft control problematic. We shall **analytically show** how a **troublemaker can break the cohesion** of an initially tight swarm and **how a single agent can efficiently incitate its fellows to achieve a preassigned task**.

The chapter is organized as follows: we first recall in section 2 relevant properties of RBM, also known in economy as the **Atlas models**. In section 3, we use the RBM's framework to show how a troublemaker is able to smash an initially tight swarm. Our individual dynamics are one-dimensional diffusion processes with piecewise constant drifts except for the shill, which will be assumed to be driven by a **ballistic process with quadratic variance in time**. The ballistic noise is itself generated by a simple non-Gaussian diffusive stochastic process with nonlinear drift. In section 4, we address the dual soft control problem in which a shill is used to steer the whole collection of RBM's towards slots that are drilled through an obstacle board.

6.2 Rank-Based Brownian Motions - Atlas Model

Our approach makes extensive use of recent results Ichiba et al. (2011), that we now briefly summarize. Let us consider a collection of N interacting agents diffusing according to the class of processes:

$$\mathrm{d}Y_i(t) = \left(\sum_{k=1}^{N} g_k 1_{Q_k(i)}\{Y(t)\} + \gamma_i + \gamma\right)\mathrm{d}t + \sigma_i \mathrm{d}W_i(t),$$

$$Y_i(0) = y_i,\ t \in \mathbb{R}^+, \tag{6.1}$$

where $Y(t) = (Y_1, Y_2, \cdots, Y_N) \in \mathbb{R}^N$ and $\mathrm{d}W_i(t)$ are N independent standard White Gaussian Noise processes (WGN) processes. The indicator function 1_{Q_k} in Eq.(6.1) effectively generates mutual interactions. The effective, time-dependent drift component g_k entering into the drifts $(g_k + \gamma_i + \gamma)$ of the N Brownian motions on $\mathbb{R}$, is **rank-based.** Namely, it is instantaneously adjusted according to the position (i.e. the rank) occupied by each agent with respect to the remaining $(N-1)$ fellows. The constant drift components γ_i are name-based, i.e. they are definitely assigned to each individual agent (γ_i is time-independent). Finally, a constant drift component γ can be added, which is common to all agents. Accordingly Eq.(6.1) describes a collection of N diffusion processes having piecewise deterministic drifts. The somehow simpler situation obtained when $\gamma_i \equiv 0\ \forall i$ has been thoroughly studied Pal and Pitman (2008).

In the sequel and without loss of generality, we systematically choose γ to be the (average) barycentric speed of the swarm. This is achieved, provided one has:

$$\sum_{k=1}^{N} [g_k + \gamma_k] = 0. \tag{6.2}$$

For future use, we introduce the following notations and definitions:

1. We write

   $$\bar{Y}(t) = \frac{1}{N}\sum_{k=1}^{N} Y_k(t), \qquad \bar{Y} \in \mathbb{R}, \tag{6.3}$$

   for the barycenter position. The set Σ_N stands for the set of all the permutations of $\{1, 2, ..., N\}$. It is proven Ichiba et al. (2011) that, for almost every initial conditions and when the set of constraints

   $$\sum_{k=1}^{l} [g_k + \gamma_{p(l)}] < 0 \tag{6.4}$$

   are fulfilled for all possible permutations $p = (p(1), ..., p(N)) \in \Sigma_N$, and $\forall l \in \{1, ..., N-1\}$, then the N deviations processes:

   $$\tilde{Y}_i(t) = [Y_i(t) - \bar{Y}(t)] \tag{6.5}$$

converge to stationary probability measures. Note that Eq.(6.4) yields therefore a set of $(N-1)\times|\Sigma_N| = N!\,(N-1)$ constraints to be verified.

2. When all constraints in Eq.(6.4) are fulfilled, the dynamics given by Eq.(6.1) then converges to a **tight swarm** described by a **stationary multi-variate process** characterizing the $(N-1)$-gap processes

$$\Xi_i(t) = [Y_{i+1}(t) - Y_i(t)]. \tag{6.6}$$

The associated probability density $\psi(z)$, $z \in \mathbb{R}_+^{N-1}$ can be written as a sum-of-product-of-exponential form:

$$\psi(z) = \left(\sum_{p\in\Sigma_N}\prod_{k=1}^{N-1}\lambda_{p,k}^{-1}\right)^{-1}\sum_{p\in\Sigma_N}\exp\left(-\langle\lambda_p, z\rangle\right) \tag{6.7}$$

with the parameters explicitly given by

$$\lambda_p = \left(\lambda_{p,k}\right)_{k=1}^{N-1} \qquad \lambda_{p,k} = \frac{-4\sum\limits_{l=1}^{k}\left(g_l + \gamma_{p(l)}\right)}{\sigma_k^2 + \sigma_{k+1}^2}. \tag{6.8}$$

Remark. It is worth observing that the diffusion coefficients σ_i do not enter into the set of tightness constraints given in Eq.(6.4). However, the σ_i's do enter into the parameters Eq.(6.7) characterizing the stationary probability measure.

6.3 How Does a Super-Diffusive Fellow Smash Tightness

We first investigate how a single "turbulent" fellow can destroy the cohesion of a tight swarm. To this aim, we use the RBM formalism introduced in section (6.2). We consider a configuration involving $(N-1)$ identical mutually interacting RBM's, referred from now on as the regular agents, interacting with a single fellow, the **shill**, say agent number one, which is itself driven by a **ballistic diffusion process** (remember from Eq.(6.1) that the $(N-1)$ regular agents are driven by independent WGN's). The ballistic process, to be introduced below, exhibits a variance $\propto\ t + \beta t^2$ with a **ballistic parameter** $\beta \geq 0$ a constant. For $\beta = 0$, the shill simply behaves as a regular fellow and therefore, in this $\beta = 0$ limit, our global dynamics reduces to a standard version of Eq.(6.1). We set the specific parameters: $g_N = (N-1)\,g$ and $g_k = -g$ for $1 \leq k \leq N-1$. In addition, we shall further assume that:

i) $\sum_{i=1}^{N}\gamma_i = 0$,

ii) $\max\limits_{1\leq i\leq N}\gamma_i < g$.

The couple of constraints i) and ii) imply that the Eq.(6.4) is fulfilled. Indeed, we directly verify that :

$$-g+\gamma_{p(1)}<0, \quad -2g+\gamma_{p(1)}+\gamma_{p(2)}<0, \quad \cdots$$

$$-(N-1)\,g+\sum_{k=1}^{N-1}\gamma_{p(k)}<0. \tag{6.9}$$

Hence, for $\beta=0$, our collection of agents behaves as a tight swarm enjoying a stationary joint probability law for the inter-distance between successive agents.

Let us now focus on $\beta>0$. Now, the shill $Y_1(t)$ behaves as a **turbulent fellow** which interacts with the remaining $(N-1)$ regular fellows. Specifically the dynamics of $Y_1(t)$ is chosen to be described by:

$$\mathrm{d}Y_1(t)=\left(\sum_{k=1}^{N} g_k \mathbb{1}_{Q_k(i)}\{Y(t)\}+\gamma_1+\gamma\right)\mathrm{d}t+\mathrm{d}Z(t),$$

$$Y_1(0)=y_1 \quad t\in\mathbb{R}^+, \tag{6.10}$$

where the process $\mathrm{d}Z(t)$ is a **super-diffusive ballistic noise generator** introduced in Hongler M. O. and Blanchard (2006); Hongler M. O. and Rodriguez (2012):

$$\mathrm{d}Z(t)=\left\{\beta\tanh\left[\beta Z(t)\right]\right\}\mathrm{d}t+\mathrm{d}W(t), \quad Z(t=0)=0. \tag{6.11}$$

The non-Gaussian Markov diffusion process $Z(t)$ given in Eq.(6.11) is fully characterized by its transition probability density $\mathscr{P}(z,t\mid 0)$ which simply reads:

$$\mathscr{P}(z,t\mid 0)=\frac{\left(\mathscr{P}_+ + \mathscr{P}_-\right)(z,t\mid 0)}{2}=\frac{e^{-\frac{\beta^2}{2}t}}{\sqrt{2\pi t}}e^{\frac{(x\pm\beta t)^2}{2t}}, \tag{6.12}$$

with average $\langle Z(t)\rangle=0$ and variance $\langle Z^2(t)\rangle=t+\beta^2t^2$.

The simple form given in Eq.(6.12) suggests the existence of an alternative representation for the ballistic noise $Z(t)$. Indeed, writing $BM_{\pm\beta}(t)$ for the Brownian motions with $\pm\beta$ constant drifts, we observe that the transition probability for the process $Z(t)$ can be rewritten as $Z(t) = \mathscr{B} BM_{\pm\beta}(t)$ where $\mathscr{B}$ is a symmetric Bernoulli r.v., taking the values ± 1 with equal probability $1/2$. Hence, one realization of the $Z(t)$ consists first in choosing with probability $1/2$ one among the couple processes $BM_{\pm\beta}(t)$, and then follow the realization of the selected process (see example 2 in Rogers and Pitman (1981) and Hongler M. O. and Blanchard (2006); Hongler M. O. and Rodriguez (2012)).

We now come back to the dynamics jointly involving a turbulent fellow given by Eq.(6.10) and $(N-1)$ regular agents described by Eq.(6.1). We then view the $(N-1)$ regular agents as being **infiltrated** by a **the shill** $Y_1(t)$.

Now we have to investigate the values of β enabling the swarm to remain tight (i.e. if a stationary probability measure for the intervals between successive agents exists). In view of the representation given in Eq.(6.12), for each realization of the noise source $Z(t)$, we effectively deal with a standard RBM model with a re-normalized name-based drift of $Y_1(t)$, namely $\gamma_1 \mapsto \gamma_1 \pm \beta$ depending on the outcome of $\mathscr{B}$. Accordingly, to infer on the tightness of the swarm, we simply have to separately examine Eq.(6.4) for the couple of outcomes $\pm\beta$.

Realization $+\beta$. Let us define $\gamma = \frac{\beta}{N}$, $\gamma_1 = \frac{N-1}{N}\beta$ and $\gamma_i = -\gamma = -\frac{\beta}{N}$ for $2 \leq i \leq N$. The constraints Eq.(6.6) are required for the swarm to be tight. This yields, for $l = 1$ and $p = (1, 2, 3..., N)$, to the most critical constraint:

$$g_1 + \gamma_{p(1)} < 0 \quad \Rightarrow \quad -g + \frac{N-1}{N}\beta < 0$$

$$\Leftrightarrow \quad \beta < \frac{N}{N-1} g. \tag{6.13}$$

Provided that Eq.(6.13) holds, the swarm remains tight when the Z_t noise induces a $+\beta$ extra drift.

Realization $-\beta$. The same reasoning applied to the $-\beta$ case yields:

$$\gamma = -\frac{\beta}{N} \quad \gamma_1 = -\frac{N-1}{N}\beta \quad \gamma_i = \frac{\beta}{N} \quad (2 \leq i \leq N). \tag{6.14}$$

The critical constraint arises when $l = 1$ and $\gamma_p := \left(\frac{\beta}{N}, ..., \frac{\beta}{N}, -\frac{N-1}{N}\beta\right)$ with:

$$-g + \frac{\beta}{N} < 0 \quad \Leftrightarrow \quad \beta < N \cdot g. \tag{6.15}$$

This implies that for $\beta < N \cdot g$, the swarm remains tight when the Z_t noise induces a $-\beta$ extra drift.

The previous considerations can be summarized by observing that when the constraints

Eq.(6.13) are fulfilled, so are also those given in Eq.(6.15). This suggests to distinguish an alternative **"semi"-tight regime** which arises when the constraints Eq.(6.15) alone are fulfilled. In this "semi"-tight case, the swarm exhibits a tight configuration when the $-\beta$ realization is achieved and is not tight for the other alternative $+\beta$. This intrinsic asymmetry can be easily understood as our RBM dynamics only pushes the laggard towards the others. Hence, regarding the tightness, the shill is obviously less influential when the $-\beta$ extra drift is realized.

6.3.1 Spatial Dispersion of the Agents

The extra $\pm\beta$-drifts due to the super-diffusive process driving the shill dynamics obviously affect the spatial dispersion of the swarm. Since all noise sources (including the $dZ(t)$ process) have zero average, the barycenter of the whole population will remain unchanged by the presence of $dZ(t)$. However, due to the presence of the shill, an initial single-modal cluster of agents will, as time increases, be split into two separately evolving population subgroups. According to the $\pm\beta$ realization taken by $dZ(t)$, the overall effect of the shill will steer the swarm either towards the negative or positive direction; this generates the formation of two distinct clusters. Each cluster has an individual barycentric velocity: $\gamma = \frac{\gamma_1}{N} = \frac{\pm\beta}{N}$; this guarantees that the average barycenter remains unchanged.

Specifically, whenever the shills drift assumes the value $-\beta$, the shill has an overall propensity to stay at the rear of the swarm. Accordingly, all regular agents will, with high probability, be endowed with the rank-based drift $-g$. Hence the regular agents possess a clear tendency to be driven toward the negative direction on $\mathbb{R}$. Conversely, in presence of the $+\beta$ realization, the shill is very likely to belong to the group of leaders. This imposes to the remaining $(N-1)$ regular fellows to equally share, with alternations, the rank-based drift of $(N-1)\,g$ which drives the laggard. Therefore, with the $+\beta$ realization, the whole population is driven towards the positive direction of $\mathbb{R}$. We now can isolate three regimes depending on the strength β.

a) $\beta < \beta_c := \frac{N}{N-1} g$. In this regime, the shill is able to steer the whole population in one of the two possible directions while remaining itself attached to the swarm. In other words, a stationary probability measure exists for the distance between the agents (i.e. all agents evolve in a single flock). Note however that the presence of the shill breaks an initially uni-modal spatial repartition into a **bi-modal repartition**.

For three agents (i.e. one shill and two regular fellows), the resulting spatial repartition obtained by simulation is shown in Figure 6.1. In Figures 6.1 and 6.2, the shills position is represented in black, the others being displayed in grey.

b) $\beta_c \leq \beta < g \cdot N$. Here the strength of the ballistic noise precludes to reach a global stationary state for the inter-distance processes between the N agents. Indeed, the renormalized drift associated with the $+\beta$ realization of $dZ(t)$ (i.e. $\hat{\gamma}_1 = \gamma_1 + \beta$), violates the constraint Eq.(6.13). However, for the $-\beta$ realization, the constraint for $\hat{\gamma}_1 = \gamma_1 - \beta$ is fulfilled, implying that the shill remains flocked with its $(N-1)$ remaining fellows. An experiment with β chosen in this range, shows the spatial repartition in Figure 6.2 (left).

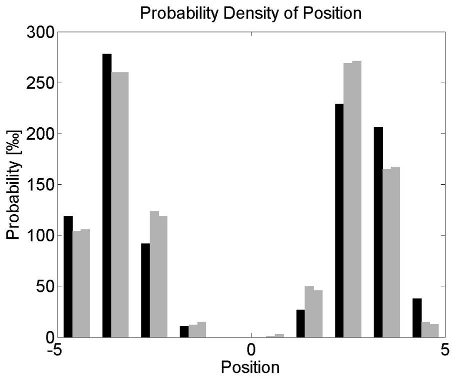

Figure 6.1 – Probability of spatial repartition of the agents at $t_{end} = 10$, numerical computation over 10^3 runs, with $N = 3$, $g = 1$, $\beta = 1.1 < \beta_c = \frac{3}{2}$.

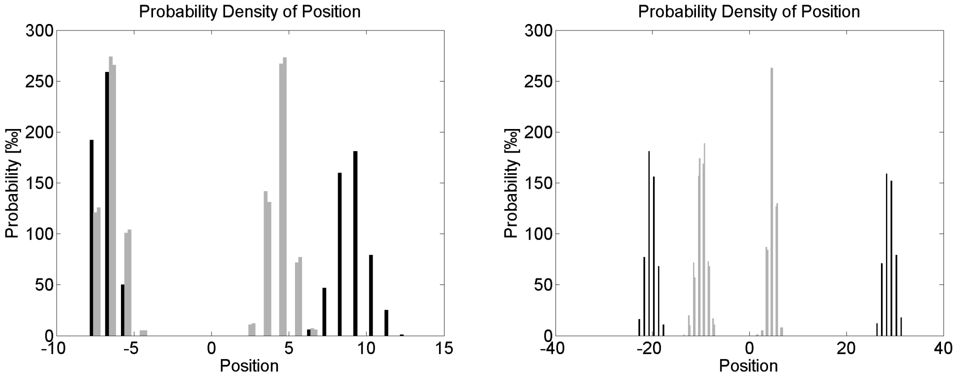

Figure 6.2 – Left: End position distribution at $t_{end} = 10$, with $N = 3$, $g = 1$, $\beta = 2 > \beta_c$.
Right panel: Probability density of the position at $t_{end} = 10$ for $N = 3$, $g = 1$, $\beta = 4 > N \cdot g$. Both numerical computations include 10^3 runs.

> c) Finally, for $\beta > g \cdot N$, the shill becomes highly turbulent (i.e., with a large ballistic noise variance) and the tightness constraints are never fulfilled. The shill escapes from the flock and the resulting spatial repartition is typically shown in Figure 6.2 (right).

For all choices of the ballistic strength β, the numerical results intimately match the analytical predictions. In particular, the shill escapes from the flock when the critical ballistic strength $\beta = \beta_c$ is reached (for the $+\beta$ realization, or when $\beta = N \cdot g$ for the $-\beta$ realization of $dZ(t)$. In these non-stationary regimes, the shill quits the $(N - 1)$- regular tight swarm with velocity $\mathcal{V}(\beta) \propto \beta$.

6.3.2 Distance Between Successive Agents

Complementary to the tightness constraints, let us now briefly discuss the stationary probability measure which characterizes the distances between successive agents. To this aim, we shall choose β to ensure the existence of a global stationary regime (i.e. ensures tightness), namely $0 \leq \beta < \beta_c = \frac{N}{N-1} g$.

Note however that using the results derived in Ichiba et al. (2011), heterogeneous diffusion constants can also be analytically discussed. The distances separating consecutive agents defined in Eq.(6.6) can be explicitly computed by using the results summarized in section (6.2). For agent $Y_1(t)$ and in view of the extra β-drift induced by the shill ballistic driving, we are now led to define a couple of name-based drifts vectors as:

$$\gamma^{\pm} = \pm \begin{pmatrix} \frac{N-1}{N}\beta & -\frac{\beta}{N} & \cdots & -\frac{\beta}{N} \end{pmatrix}. \tag{6.16}$$

The fulfillment of the tightness constraints given in Eq.(6.4) ensures that the $\lambda_{p,k}$ from Eq. (6.8) are strictly positive ($\forall\, p, k$). Hence, it results a couple of stationary probability densities (one for each realization $+\beta$ and $-\beta$), characterizing the inter-distance process $\Xi(t)$ (see Eq.(6.6)):

$$\begin{aligned} &\mathbb{P}\left\{z \leq \Xi(t) \leq z + dz \mid \pm\beta \text{ is realized}\right\} = \mathbb{P}_{\pm\beta}(z)\, dz \\ &= \left(\sum_{p \in \Sigma_N} \left(\prod_{k=1}^{N-1} \lambda^{\pm}_{p,k} \right)^{-1} \right)^{-1} \sum_{p \in \Sigma_N} \exp\left(- \left\langle \lambda^{\pm}_{p}, z \right\rangle \right) dz. \end{aligned} \tag{6.17}$$

The complete stationary probability density then reads:

$$\mathbb{P}(z) = \frac{1}{2}\left[\mathbb{P}_{+\beta}(z) + \mathbb{P}_{-\beta}(z) \right]. \tag{6.18}$$

6.4 Using a Shill to Guide the Collective Crossing of Obstacles

The shill $Y_1(t)$ of section (6.3) has so far been viewed as a mere trouble maker. However, for specific tasks to be achieved, a shills presence might become truly beneficial. Indeed, the presence of a shill can **softly control a swarm towards a preassigned target**.

To concretely illustrate this alternative view point, let us, once again, consider a collection of $(N-1)$ identical drifted Brownian (regular) agents and one shill, say $Y_1(t)$, all diffusing on $\mathbb{R}$. From now on, we shall represent the evolution on $\mathbb{R}^2$ with the time being identified with the x-axis, and positions with the y-axis. At time $t = 0$, all N agents start at location $y_i(0) = 0$, $1 \leq i \leq N$. We may think of agents running on the x-axis with constant unit speed, as we therefore identify the x-axis with time. At the x-location T (see Figure 6.3), we introduce a solid wall (i.e. the obstacle) in which two-slots are drilled. The global objective for the N agents is to try to avoid the fatal collisions with the wall by traveling trough one of the couple of slots. The two slots have width W and are symmetrically drilled at the ordinates $\pm D$, see Figure 6.3 for a sketch of the configuration.

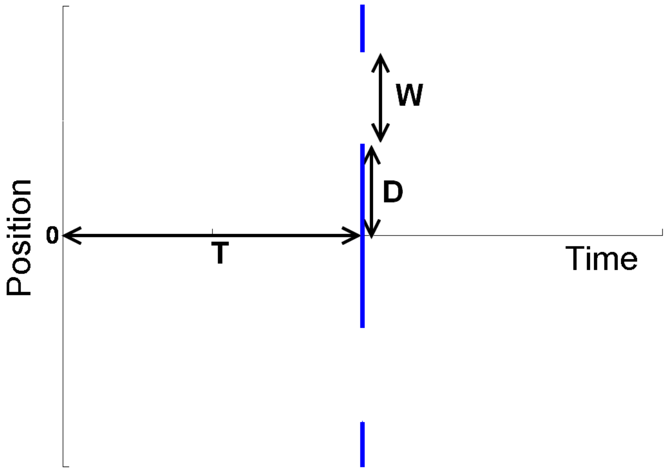

Figure 6.3 – Initial configuration for the soft control problem. The agents start their diffusion at $\left(t_0, y_0\right) = (0,0)$.

In absence of shill, one has an homogeneous swarm (all agents are dynamically identical) and the N-swarm proceeds according to the rule defined in Eq.(6.1). As a consequence, the wall will be hit with high probability as, at time T, the probability density of the positions will be given by a collection of N centered Gaussians (we basically have N Brownian motions with constant drifts having their mean barycenter located at zero). As seen in section (6.3), the presence of a super-diffusive shill $Y_1(t)$ may strongly modify this nominal $\beta = 0$ picture. Indeed $Y_1(t)$, with suitable parameters β and g is able to steer the whole swarm with high preference to one of the slots. This basic and simple idea can be made fully quantitative as discussed below. In our simulations, we set $\beta = 0$ once the slots are crossed. Therefore, the global swarm continues its nominal path with a tight configuration after the obstacle.

6.4.1 Optimal Barycentric Driving for Suitable Choice of β

First, we select the $Y_1(t)$ parameters to ensure global tightness. This is achieved by defining $\beta < \beta_c = \frac{N}{N-1}g$. For a single realization of the $Z(t)$ noise, we already know that the average barycentric y-speed of the swarm is $\frac{\pm\beta}{N}$. Hence, at time T, the group barycenter reaches the y-position located at $\frac{\pm\beta T}{N}$. The center of the slots being located at $\pm\left(D + \frac{W}{2}\right)$, we therefore naturally require:

$$\frac{\pm\beta T}{N} = \pm\left(D + \frac{W}{2}\right) \quad \Leftrightarrow \quad \beta_{opt} := \frac{\left(D + \frac{W}{2}\right)\cdot N}{T}. \tag{6.19}$$

The choice β_{opt}, does not yet ensure that the shill $Y_1(t)$ itself remains attached to the flock. This second requirement can be achieved provided one has:

$$\frac{\left(D+\frac{W}{2}\right)\cdot N}{T} = \beta_{opt} < \beta_c = \frac{N}{N-1}g$$

$$\Leftrightarrow g > \frac{\left(D+\frac{W}{2}\right)\cdot (N-1)}{T} =: g_c. \tag{6.20}$$

This choice of the couple parameters β_{opt} and $g > g_c$ now jointly ensures that i) the barycenter is steered towards one of the slots centers and ii) $Y_1(t)$ remains tightly attached to the swarm. The overall swarm's y-dispersion is itself dependent on the diffusion constants σ_i, which were here taken as ($\sigma_i := \sigma \ \ \forall i$).

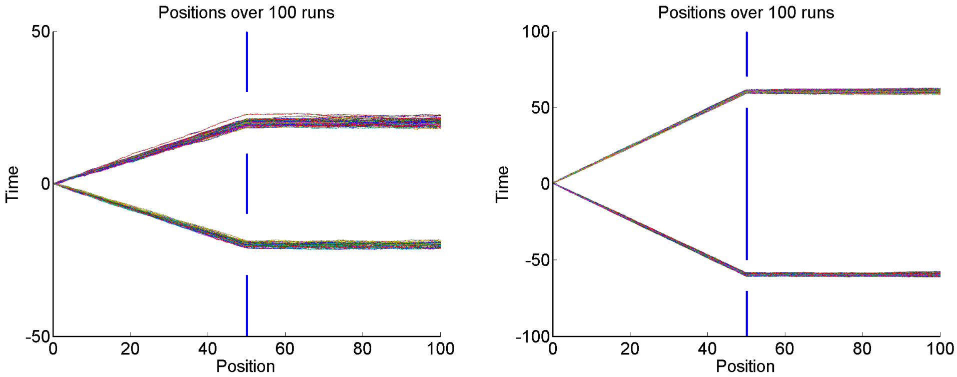

Figure 6.4 – Left panel: $N = 10$ agents, $W = 20$ and $D = 10$. Right panel: $N = 20$ agents, $W = 20$ and $D = 50$.

6.4.2 Adjusting the Spatial Dispersion Resolution for a Given Drift g

When the drift g is fixed, the ballistic component β cannot always be chosen to simultaneously ensure tightness and the collective drive into one of the slots. Keeping the barycentric driving $\beta = \beta_{opt}$, as defined in Eq.(6.19), three different scenarii are now possible:

a) $\beta = \beta_{opt} < \beta_c$. In this case, the shill nicely steers the group towards one of the slots while staying attached to the flock, as we already established in section 6.4.1.

b) $\beta = \beta_{opt} \geq \beta_c$. Here, $Y_1(t)$ escapes from the $(N-1)$-flock with a constant drifting velocity. Two sub-cases have to be distinguished, i) drift $\beta - g$ resulting when $+\beta$ is realized by $dZ(t)$ and conversely ii) drift $(N-1)\,g - \beta$ for the alternative $-\beta$ case. In both cases, the regular agents evolve with an average drift γ_{ave} which reads:

$$\gamma = \begin{cases} \frac{\beta}{N} = \frac{(\beta-g)\cdot 1+(N-1)\cdot\gamma_{ave}}{N} & \text{for } +\beta \\ -\frac{\beta}{N} = \frac{((N-1)g-\beta)+(N-1)\gamma_{ave}}{N} & \text{for } -\beta \end{cases}$$

$$\Leftrightarrow \gamma_{ave} = \begin{cases} \frac{g}{N-1} \\ -g \end{cases} . \tag{6.21}$$

c) $\beta = \beta_{opt} \geq \beta_c < N{\cdot}g$. Here, the shill remains attached to the flock for the $-\beta$ realization of $dZ(t)$, but escapes otherwise. This then leads to a mix of cases a) and b) depending on whether $+\beta$ or $-\beta$ is realized.

The computation of γ_{ave} from case b) shows that with g fixed such that $\beta_{opt} \geq \beta_c$, the shill escapes from the flock (hence, no stationary probability measure exists). The remaining $(N-1)$ regular fellows evolve with average speed γ_{ave} (which is β-independent). Whatever the values taken by β, the shill is never able to drive the swarm through one of the slots, the swarm's speed being only **g-dependent** if the shill is not attached to the swarm.

So far, only the swarm's directions has been considered. Obviously, the dispersion is also a determinant feature for efficient slots crossings. Here, not only g but the ratio $\frac{g}{\sigma}$ will be determinant. Clearly for small g values, the swarm dispersion will exhibit a clear tendency to exceed the slots widths, altering therefore the overall efficiency.

6.4.3 Multi-slots Configurations

So far, we did consider the capability of a shill to steer the swarm through a couple of slots. For multi-slots configurations, the shill construction used before naturally suggests to define more general shills to steer swarms in many different directions. This is achievable by replacing the ballistic noise driving the shill with more complex stochastic processes. Doing so however, the shill dynamics cannot be anymore represented by a simple diffusive stochastic differential equation like Eq.(6.11). As an illustration, consider a three symmetrical slots configuration for which one is naturally driven to introduce the following noise source:

$$dZ(t) = \begin{cases} \beta \tanh\left(\beta Z(t)\right) dt + dW(t) & \text{with prob. } \frac{2}{3}, \\ dW(t) & \text{with prob. } \frac{1}{3}. \end{cases} \tag{6.22}$$

The shill dynamics is taken as before, namely with probability $\frac{2}{3}$ it steers the swarm towards the positive or negative slots with ballistic parameter β and with probability $\frac{1}{3}$, it behaves as a regular agent driving the swarm on a centered path, see Figure 6.5.

For arbitrary number of slots and configurations, one can generalize our construction by suitably adjusting the properties of the noise source driving the shill.

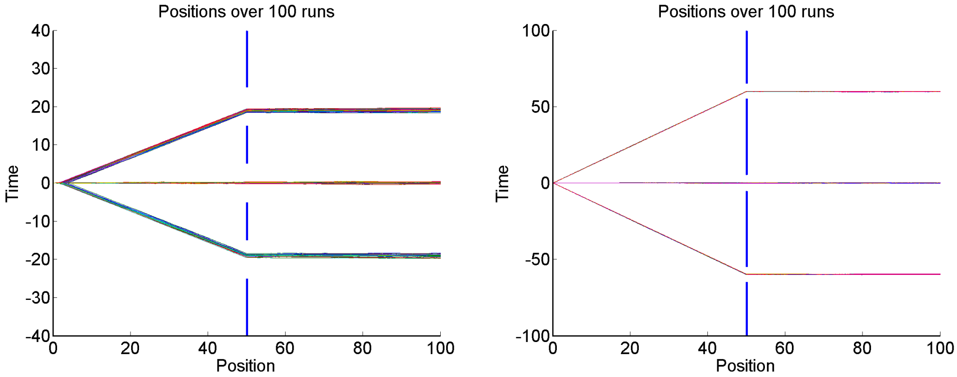

Figure 6.5 – Trajectories for β and g optimal, with $N_d = 3$ doors, under different conditions for the position/width of the doors.

6.5 Conclusion

It is a true challenge, to analytically discuss the swarm dynamics of heterogeneous interacting agents. Due to heterogeneity, ordinary analytical tools like the mean-field approach are to be ruled out a priori. Hence besides simulation experiments, very little hope remains for rigorous theoretical results. We think particularly to modeling approaches relying on statistical mechanics and phase transitions to explain the emergence of self-organized spatio-temporal patterns (i.e *flocking*). However as our research intends to show, facing inhomogeneous swarms problems, complete hope for analytical results should not be abandoned. The theoretical analysis, when achievable, definitely offers sources of inspiration for new and unexpected research axis.

In our present contribution, we barely scratched the wealth of analytical possibilities. Indeed, swarm heterogeneity has numerous origins, affecting the individual drifts and/or the variances, modeling the sensitivity of each agent to the external random environment. In parallel, heterogeneity can either be systematic, thus implying that each agent behaves differently, or can be limited to one or only a few individuals who exhibit singular behaviors. In the latter configuration, the emergent swarm dynamics can be affected, sometimes even strongly, by the exotic behavior of this (or these) individual(s). The influence of the exotic fellow(s) can hence be viewed as a *soft control* mechanism, either harmful or beneficial. The exotic insiders, acting as leaders (or as *shills* in economy) are not detected to be singular by the other fellows, offering the (politically frightening possibility!) to drive large swarms towards global goals known only to the manipulators. A formal analytical approach (complemented with simulations) to this general problematic is a truly fascinating challenge.

Further works include analysis of multiple shills influence, leading to the separation of the initial swarm into multiple flocks, one shill soft-controlling each flock. Generalization in two or three dimensions would also provide more realistic applications.

6.6 New Contributions of Chapter 6

- Based on rank-based Brownian motions (Hybrid Atlas Model [HAM]) dynamic, we are once again able to analytically discuss the soft control of a swarm. The shill's dynamics tune a swarm's behavioral phase transition. Either flocked, semi-flocked or incoherent swarm evolutions emerge.

- We use this model to visit the many facets offered by swarm soft control (visible/invisible shill, constructive/destructive soft control).

- **Publication**: This chapter is reproduced from the conference paper Sartoretti and Hongler (2013d), with slight modifications to fit the present dissertation.

Strongly Heterogeneous Swarms Part V

7 Interacting Brownian Swarms: Some Analytical Results

Summary

*We consider the dynamics of swarms of scalar Brownian agents subject to local imitation mechanisms implemented using mutual rank-based interactions. For appropriate values of the underlying control parameters, the swarm propagates tightly and the distances separating successive agents are iid exponential random variables. Implicitly, the implementation of rank-based mutual interactions, requires that agents have infinite interaction ranges. Using the probabilistic size of the swarm's support, we analytically estimate the critical interaction range below that flocked swarms cannot survive. In the second part of the paper, we consider the interactions between two flocked swarms of Brownian agents with finite interaction ranges. Both swarms travel with different barycentric velocities, and agents from both swarms indifferently interact with each other. For appropriate initial configurations, both swarms eventually collide (*i.e.*, all agents interact). Depending on the values of the control parameters, one of the following patterns emerges after collision: (i) Both swarms remain essentially flocked, or (ii) the swarms become ultimately quasi-free and recover their nominal barycentric speeds. We derive a set of analytical flocking conditions based on the generalized rank-based Brownian motion. An extensive set of numerical simulations corroborates our analytical findings.*

7.1 Introduction

Elementary models of multi-agents swarms often rely on the assumption that all individuals obey identical dynamical rules. This hypothesis of agents' homogeneity significantly simplifies the mathematical modeling and its treatment. In particular, for large swarms, homogeneity enables analytical discussions based on the mean-field (MF) approach. In the MF approach, the effects of mutual interactions are aggregated into an external effective force field, driving the dynamic of a single randomly picked agent, whose behavior reflects the whole society's evolution. Homogeneity is, however, rarely encountered in actual situations. A natural question is to then ask how heterogeneity between agents affects and/or possibly destroys the potential emergence of collective (*i.e.*, flocking) dynamics. In the presence of heterogeneity, analytical approaches are more difficult as, *a priori*, the MF approach cannot be directly employed. In multi-agent swarms, heterogeneity can manifest itself in many different forms and degrees. It may concern the individual dynamics of each agent and/or the way agents interact with their fellows. An extreme heterogeneous situation is realized when, due to its specificities, a single agent is actually leading the entire swarm Couzin et al. (2005); Sartoretti et al. (2014b); Han et al. (2006); Sartoretti and Hongler (2013d,c). In this paper, we focus on comparatively low heterogeneities encountered when only the individual dynamics differ but not the interacting rules. For this case, a paradigmatic and pioneering example is the Kuramoto synchronization of heterogeneous phase oscillators for which the role of heterogeneity can, to a certain extent, be analytically discussed Strogatz (2000); Acebrón et al. (2005b). More recently, models based on rank-based drifted Brownian motion (RBM) Pal and Pitman (2008), and, in particular, the so-called Hybrid Atlas Model (HAM) Ichiba et al. (2011), offer another possibility to analytically discuss the heterogeneous swarm dynamics, without relying on the MF approach. In the sequel, we shall basically use the HAM modeling framework to study a new type of global heterogeneity. This is achieved when two sub-swarms are forced to mutually interact. Each sub-swarm, formed by homogeneous agents, is initially tightly flocked and obeys specific collective dynamics. The global society formed by the union of the two sub-swarms is clearly heterogeneous. This example depicts a situation where two distinct sub-swarms (agents of each sub-swarm are different) interact via a local competition mechanism (here, agents systematically try to catch their leaders in a finite observation range). In this paper, we are able to analytically characterize the post-collisional outputs. Depending on external control parameters (individual sub-swarm dynamics, strength of competition), we observe that the post-collisional situation can either be a single tight swarm or a segregation into the nominal sub-swarm.

The paper is organized as follows: In Section 7.2, we introduce the microscopic agent's dynamic and link it to RBMs. In Section 7.3, relying on the HAM theory, we derive the flocking conditions for single swarms composed of scalar agents interacting via imitation. The mutual interactions are effectively of long-range types (*i.e.*, each agent can observe all leaders independent of their distance). For a finite number of tightly flocked agents, the (scalar) inter-distance between successive fellows is a stationary random variable, and, hence, so is the size of the swarm extension. This enables us to define a characteristic stationary swarm extension. In Section 7.4, we consider a couple of sub-swarms, initially well separated on the real line and with different average barycentric speeds. As the positive barycentric velocity of the leftmost sub-swarm is chosen, larger than the one of the rightmost sub-swarm, collision is unavoidable. For large but finite observation ranges of the sub-swarm (*i.e.*, range larger than the sub-swarm characteristics of each sub-swarm extension derived in Section 7.3), we study the asymptotic post-collisional behavior of the whole system. The conditions for either the emergence of a global flocking swarm or quasi-freedom of the sub-swarms are approximatively derived. All analytical findings are tested and corroborated by simulation experiments. Concluding remarks, along with perspectives, are finally presented in Section 7.5.

7.2 Flocking of Interacting Brownian Agents

We consider a swarm of N Brownian agents $\mathscr{A}_j$, $j = 1, 2, \cdots, N$, diffusing on $\mathbb{R}$. Agent $\mathscr{A}_i$ follows the dynamic:

$$dX_i(t) = d_{U,i}(\vec{X}(t), t)dt + \sigma dW_i(t), \quad X_i(0) = x_{i,0}, \tag{7.1}$$

where $\vec{X}(t) = (X_1(t), X_2(t), \cdots, X_N(t))$ and $dW_i(t)$ $(i = 1, .., N)$ are independent White Gaussian Noise (WGN) sources. The set of individual drifts $d_{U,i}(\vec{X}(t), t)$ for $i = 1, 2, \cdots, N$ are rank-dependent interactions that are defined as follows:

(i) In real-time, agent $\mathscr{A}_i$ counts the (time-dependent) number $N_{U,i}(t)$ of leading fellows located within an *observation interval* U, namely the number of $\mathscr{A}_k$ for $k \neq i$ that are located in $R_{U,i}(t)$ with:

$$R_{U,i}(t) := \{x \in \mathbb{R} \mid 0 < x - X_i(t) \leq U\}. \tag{7.2}$$

(ii) The $\mathscr{A}_i$-rank-based drift in Equation (7.1) is then determined by:

$$d_{U,i}(\vec{X}(t), t) := \alpha \frac{N_{U,i}(t)}{N}, \quad i = 1, 2, \cdots, N, \tag{7.3}$$

with $\alpha \in \mathbb{R}_+$ a velocity scale factor.

According to Equation (7.1), agent $\mathscr{A}_i$ is positively accelerated by its leaders located in $R_{U,i}(t)$ but ignores the presence of its followers. These types of dynamics generically model imitation mechanisms; a typical example for the diffusion of innovation is shown in Hongler et al. (2015).

For very large swarms (*i.e.*, when $N \to \infty$), we may define an agent probability density $\rho(x, t \mid x_0)$ at position x at time t. Adopting a mean-field (MF) approach, $\rho(x, t \mid x_0)$ obeys a (nonlinear) Fokker–Planck parabolic partial differential equation (pde):

$$\begin{cases} \partial_t \rho(x, t \mid x_0) = \mathscr{F} \rho(x, t \mid x_0), \\ \mathscr{F}(\cdot) := \frac{\sigma^2}{2} \partial_{x,x}(\cdot) - \alpha \partial_x \left[\int_0^U \rho(y + x, t \mid x_0) dy \, (\cdot) \right]. \end{cases} \tag{7.4}$$

For $U = \infty$, the model can be analytically investigated, and its solution behaves as a flocked swarm of agents that propagate like a soliton wave Hongler et al. (2015); Jourdain and Malrieu (2008); Hongler et al. (2014). Conversely, for small U, a first order expansion of Equation (7.4) yields Burgers' equation, that can be analytically solved via the well known Hopf–Cole (logarithmic) transformation Jourdain and Malrieu (2008). In this small U regime, $\rho(x,t)$ exhibits a diffusive behavior that asymptotically vanishes with time. Qualitatively, when U is very small, the agents mutual interactions are not strong enough to sustain a cooperative soliton dynamic pattern. By introducing a decreasing distance-dependent modulation on rank-based drifts, it has been showed that a bifurcation point, controlled by the distance decay rate, exists that separates both propagating regimes Hongler et al. (2015, 2014).

In general, however, the joint nonlocal and nonlinear characteristics of Equation (7.4) precludes direct analytical characterization of this bifurcation point. Alternative approaches then have to be found. In the present paper, focusing on Equation (7.1) with $N < \infty$, we shall use available results for rank-based Brownian motions Pal and Pitman (2008); Ichiba et al. (2011) to approximately estimate the observation range required to generate a soliton-like propagation.

7.2.1 Rank-Based Brownian Motions (RBMs)

For calculation convenience, we now consider the dynamics of Equation (7.1) with respect to the swarm's barycenter. That is to say, Equation (7.3) becomes:

$$\begin{cases} d_{U,i}(\vec{X}(t),t) := \alpha \frac{N_{U,i}(t)}{N} - \gamma, \\ \\ \gamma := \frac{1}{N}\sum_{l=0}^{N-1} \alpha \frac{l}{N} = \alpha \frac{N-1}{2N} \quad \text{(average barycentric drift)}. \end{cases} \tag{7.5}$$

In other words, agents $\mathscr{A}_i$, $i = 1, 2, \cdots, N$ counts, in real time, the number of its leaders $\mathscr{A}_k$ with $k \neq i$. It then updates its drift $d_{U,i}(\vec{X}(t),t)$ as given in Equation (7.5), where γ is the average drift velocity of the swarm. Since the WGN in Equation (7.1) achieves unbounded realizations, the ability for all $\mathscr{A}_i$'s to exactly count the number of their leaders effectively requires an infinite observation range U.

By construction, one can verify that the stability conditions:

$$\sum_{k=1}^{l} \left[\alpha \frac{k-1}{N} - \gamma\right] = \frac{\alpha}{2N} l \cdot [l - N] < 0 \qquad \forall 1 \leq l < N \tag{7.6}$$

are verified, meaning that the laggards have a systematic average tendency to catch up with the leaders.

The rank-based drifts effectively implement a stylized gravity model, where the set of conditions for Equation (7.6) ensures the existence of a stationary probability measure for the RBM. This stationary regime corresponds to a tight propagating swarm that effectively behaves like a soliton propagating wave. Moreover, Banner et al. (2005); Pal and Pitman (2008) established that in this stationary state, the inter-distances between successive agents are independent, λ_l-exponentially distributed random variables with:

$$\lambda_l = \frac{\alpha}{N\sigma^2} l \cdot [N-l], \quad l = 1, 2, \cdots, N-1. \tag{7.7}$$

Since the swarm's stationary size is the sum of $(N-1)$ independent exponentially distributed r.v.'s, it defines a hypoexponential probability distribution $\mathscr{H}(x)$ with density:

$$d\mathscr{H}(x) = \sum_{l=1}^{N-1} \lambda_l e^{-\lambda_l x} \left(\prod_{l=1, k \neq l}^{N-1} \frac{\lambda_k}{\lambda_k - \lambda_l} \right) dx. \tag{7.8}$$

Accordingly, the average size of the swarm $\mu_S(N)$ and its corresponding variance $\sigma_S(N)$ behave as follows:

$$\begin{cases} \mu_S(N) = \int_0^\infty x \, d\mathscr{H}(x) = \sum_{l=1}^{N-1} \lambda_l^{-1} = \frac{N\sigma^2}{\alpha} \sum_{l=1}^{N-1} \frac{1}{l(N-l)} \approx_{N\to\infty} \frac{2\sigma^2}{\alpha} \log(N), \\ \sigma_S^2(N) = \int_0^\infty (x-\mu_S)^2 d\mathscr{H}(x) = \sum_{l=1}^{N-1} \lambda_l^{-2} \approx_{N\to\infty} \frac{\sigma^4}{\alpha^2} [\frac{\pi^2}{3} + 4\frac{\log(N)}{N}] \to_{N\to\infty} \frac{\sigma^4\pi^2}{3\alpha^2}. \end{cases} \tag{7.9}$$

The coefficient of variation $cv_S^2 := \frac{\sigma_S^2(N)}{\mu_S^2(N)}$, which measures the stochasticity of the swarm's size, vanishes in the mean-field limit $(N \to \infty)$. Observe that, in the mean-field limit, the agents' density $\rho(x, t)$ of the RBM directly coincides with Burgers' dynamics for $U = \infty$. This leads to a tight soliton-like propagation density with infinite support. This is consistent with Equation (7.9), where the swarm's size slowly diverges for $N \to \infty$.

7.3 Heuristic Characterization of the Observation Threshold Leading to Cooperative Dynamics

Consider the nominal dynamics Equation (7.1) and now assume finite observation ranges (*i.e.*, $0 < U < \infty$). Due to the unboundedness of the WGN, an exact ranking procedure is therefore not strictly possible. A non vanishing probability (decreasing with increasing U's) exists to find outlying leaders (*i.e.*, located beyond the observation range of some of their followers). While the average swarm size $\mu_S(N)$ from Equation (7.9) is valid only when $U = \infty$, we postulate that it can still be used to approximately characterize the minimal observation range $U_c < \infty$ required to sustain a tight swarm. Indeed, whenever $U < U_c$, it is highly probable that some agents cannot determine their respective ranks. These outlying agents will underestimate their instantaneous drifts (from their incomplete observations), ultimately leading to their escape from the bulk. Outlying agents always escape the swarm from the rear, leading with time to an effective "evaporation".

For consistency, the initial conditions $X_i(0)$, to be drawn from a probability measure with finite support Ω_0, namely $X_{i,0} \in \Omega_0$ with $\Omega_0 = [l, r] \subset \mathbb{R}$ and length$(\Omega_0) = r - l \leq \mu_S(N)$ must be restricted. Let us now define a characteristic relaxation time $\tau_{\text{relax}} = \frac{\mu_S(N)}{\sigma^2}$ that corresponds to the time needed by the stochastic processes to diffuse over the interval of length μ_S. For observation ranges $U > \mu_S$ and initial conditions $X_{i,0} \in \Omega_0$, all N agents mutually interact at time $t = 0$, and, therefore, correctly determine their relative ranks. We assume that this will remain true with high probability, for times $0 < t < \tau_{\text{relax}}$. In other words, we expect that the initially tight swarm is likely to remain flocked for $t \leq \tau_{\text{relax}}$, effectively a metastable state. For asymptotic times, however (*i.e.*, $t \gg \tau_{\text{relax}}$), the swarm's tightness will be destroyed. Indeed, for any finite U, outliers will ultimately escape the attraction generated by the bulk of the remaining swarm. Therefore, our heuristic postulates that the characteristic observation range, separating these two regimes, $U_c = \mu_S(N)$. The actual validity of these simple heuristics have been tested in several numerical experiments that are reported in Figures 7.1 and 7.2.

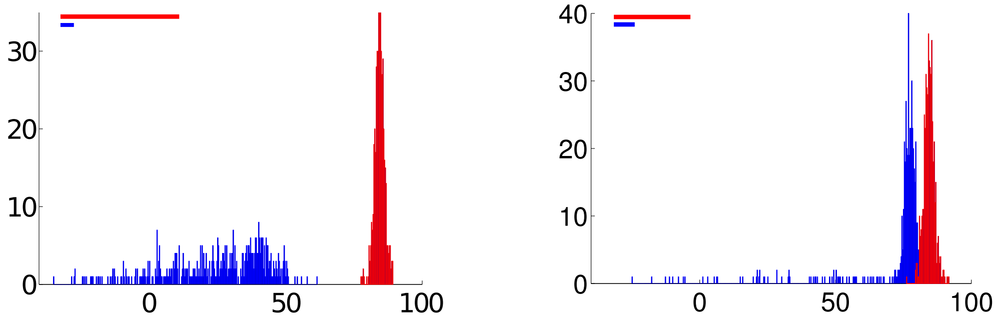

(a)

(b)

Figure 7.1 – End probability distribution $P(x, T)$ at time $T = 200 > \tau_{\text{relax}} = \frac{\mu_s}{\sigma^2} = \frac{13.58}{1^2}$ of swarms of $N = 500$ agents, with respect to U. Here, all agents initially start at $x_0 = -15$. **(a): tight swarm for $U = 3U_c = 3\mu_S$ (red) and "diffusive evaporating" swarm for $U = \frac{U_c}{3}$ (blue). (b): tight swarm for $U = 2U_c$ (red) and "diffusive evaporating" swarm for $U = \frac{U_c}{2}$ (blue). The respective observation ranges U are depicted at the top of each figure.**

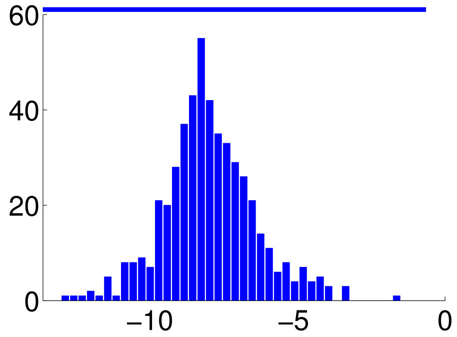

Figure 7.2 – End probability distribution $P(x,T)$ at time $T=\tau_{\text{relax}}=13.58$ of a swarm of $N=500$ agents, initially starting at $x_0=-15$. The observation range $U=U_c=\mu_S$ is depicted at the top of the figure. Notice that the evaporation (*i.e.*, destruction of swarm tightness) does not start before the relaxation time τ_{relax}.

7.4 Interactions between Collinear Colliding Swarms

In this section, we investigate the mutual interactions between two initially distinct swarms $\mathscr{S}_1$ and $\mathscr{S}_2$ composed of $\mathscr{A}_{1,k}$, $k=1,2,\cdots,N_1$ respectively $\mathscr{A}_{2,j}$, $j=1,2,\cdots,N_2$ agents driven by rank-based interactions. Initially, we let all agents from $\mathscr{S}_1$ be randomly positioned with $X_{0,1}\in[l_1,r_1]:=\Omega_1$; similarly, for $\mathscr{S}_2$, we assume that $X_{0,2}\in[l_2,r_2]:=\Omega_2$. Assume non-overlapping supports $\Omega_1\bigcap\Omega_2=\emptyset$ with $r_1<l_2$ (interval Ω_1 is located on the left of Ω_2) and finite observation ranges U such that $U<l_2-r_1$). Accordingly, at time $t=0$, agents from $\mathscr{S}_1$ do not interact with agents from $\mathscr{S}_2$ and *vice versa.* We further assume that initially the swarm $\mathscr{S}_k$ with $k=1,2$ has an average barycentric drift velocity $d_k>0$ and that $d_1>d_2$. This implies that the $\mathscr{S}_1$-agents will, on average, catch and ultimately overcome their $\mathscr{S}_2$-fellows. Therefore, for large times, the $\mathscr{S}_1$-agents exhibit a net tendency to become $\mathscr{S}_2$-leaders. Qualitatively, after a $\mathscr{S}_1$-$\mathscr{S}_2$ collision, the following dynamic features occur:

(i) $\mathscr{S}_1$-agents become leaders and thus are less influenced by (or possibly almost independent from) $\mathscr{S}_2$-agents. This implies that, with time, $\mathscr{S}_1$-agents will exhibit a net tendency to recover their nominal drifts (*i.e.*, the drifts realized before the collision).

(ii) $\mathscr{S}_2$-agents feel the presence of their leaders from $\mathscr{S}_1$ and, therefore, have a net tendency to increase their drifts.

Therefore, depending on the values of the population sizes N_1 and N_2 and drifts d_1 and d_2, two alternative situations emerge:

(a) Mutual capture of swarms. After collision, $\mathscr{S}_1$ and $\mathscr{S}_2$ aggregate into a global tight swarm $\mathscr{S}_{\text{glob}}$. The average barycentric drift d_{glob} of $\mathscr{S}_{\text{glob}}$ is larger than d_2. Thus, in this case, mutual interactions generate an increase in the average velocity of the global population.

(b) Quasi-asymptotic freedom of swarms. After collision, and for asymptotic times, the swarms $\mathscr{S}_1$ and $\mathscr{S}_2$ evolve almost without interactions (quasi-free swarm evolutions). In the quasi-free regime, $\mathscr{S}_1$ and $\mathscr{S}_2$ recover their respective initial individual barycentric velocities d_1 and d_2.

In the sequel, the implementation of the velocity condition $d_1 > d_2$ is realized by considering two distinctive rank-based dynamics: (i) The Hybrid-Atlas model (HAM) introduced by T. Ichiba *et al.* Ichiba et al. (2011) and (ii) a new modified HAM model (MHAM). For both cases, we analytically estimate the threshold values of the relevant control parameters that lead to either outcome (a) or (b).

7.4.1 Colliding Swarms Driven by Hybrid Atlas Models

In this first situation, we assume that the swarms $\mathscr{S}_1$ and $\mathscr{S}_2$ are populated by slightly different types of agents. Agents $\mathscr{S}_1$ and $\mathscr{S}_2$ share a common rank-based drift, given in Equation (7.1), but we endow the $\mathscr{S}_1$s with an extra systematic constant drift $\Gamma_1 > 0$:

$$d_{U,i}(\vec{X}(t),t) = \alpha \frac{N_{U,i}(t)}{N} + \mathbb{1}_{\{i \leq N_1\}}\Gamma_1, \tag{7.10}$$

with $N = N_1 + N_2$.

This ensures that $\mathscr{S}_1$-agents, on average, initially travel faster than $\mathscr{S}_2$-agents, and, therefore, $d_1 > d_2$. Since the initial $\mathscr{S}_1$-support Ω_1 is located on the left of Ω_2, a $\mathscr{S}_1$-$\mathscr{S}_2$-collision is unavoidable. At this point, we emphasize that when $U = \infty$, the global heterogeneous society $\mathscr{S}_{\text{glob}} = \mathscr{S}_1 \cup \mathscr{S}_2$, when subject to the dynamics given by Equation (7.1), is a special case of HAM dynamics Ichiba et al. (2011). In Ichiba et al. (2011), the authors derive the set of combinatorial stability conditions that ensure the existence of a tight swarm stationary state. Heuristically speaking, one has to explicitly verify that, in all possible ranking configurations, the agents $\mathscr{S}_1$ and $\mathscr{S}_2$ are systematically driven by attractive drifts directed toward the barycenter of $\mathscr{S}_{\text{glob}}$.

For $U < \infty$, the hypotheses in Ichiba et al. (2011) are not strictly realized (since the perfect ranking determination would indeed require $U = \infty$). Along the same lines as in Section 7.3, we assume that for large enough but finite U, the agents' ranking in $\mathscr{S}_{\text{glob}}$ during collision remains approximately unaffected. Accordingly, the HAM tightness conditions also remain approximately valid in $\mathscr{S}_{\text{glob}}$, during collision. The average barycentric drift of $\mathscr{S}_{\text{glob}}$, during collision and when $\mathscr{S}_1$ is ahead of $\mathscr{S}_2$, reads:

$$\gamma_{HAM} = \frac{1}{N}\left(\sum_{i=1}^{N_1}(\alpha\frac{i-1}{N}+\Gamma_1)+\sum_{i=N_1+1}^{N}\alpha\frac{i-1}{N}\right) = \frac{(-1+N)\alpha+2N_1\Gamma_1}{2N}. \tag{7.11}$$

Therefore, the recentered rank-based drift $d_{U,l}(\vec{X}(t),t)$ of agent $\mathscr{A}_l$ from $\mathscr{S}_{\text{glob}}$, in this configuration, becomes:

$$d_{U,i}(\vec{X}(t),t) = \alpha\frac{N_{U,i}(t)}{N} + \mathbb{1}_{\{i\le N_1\}}\Gamma_1 - \gamma_{HAM}, \qquad l = 1,2,\cdots,N-1. \tag{7.12}$$

According to Ichiba et al. (2011), the set of combinatorial tightness stability conditions for HAM dynamics, under any permutation $\mathbf{p}\in\Sigma_N$ of the $N = N_1 + N_2$ agents read as:

$$\sum_{k=1}^{l}\left[\alpha\frac{k-1}{N}+\mathbb{1}_{\{\mathbf{p}(k)\le N_1\}}\Gamma_1-\gamma_{HAM}\right]\overset{!}{<}0, \qquad \begin{array}{l}\text{for } l=1,2,\cdots,N-1,\\ \forall\mathbf{p}\in\Sigma_N,\end{array} \tag{7.13}$$

where $\overset{!}{<}$ expresses the necessary condition.

To check the validity of Equation (7.13), it is sufficient to focus on the most critical agent configuration. This configuration is realized when all faster agents take the ranks $1,...,N_1$ (*i.e.*, when $\mathscr{S}_1$ is ahead of $\mathscr{S}_2$). This corresponds to the choice $l = N_1$ in Equation (7.13), under the permutation $\mathbf{p} = (1,2,...,N)$, where:

$$\sum_{j=0}^{N_1-1}\left[\alpha\frac{j}{N}+\Gamma_1\right] = -\frac{N_1N_2(\alpha-2\Gamma_1)}{2N}. \tag{7.14}$$

To ensure that this sum is negative (i.e., outcome (a): both societies remain flocked together), one must finally have:

$$\Gamma_1 < \frac{\alpha}{2}. \tag{7.15}$$

Remark that the condition in Equation (7.15) does not depend on the individual swarm sizes N_1 and N_2, with our specific choice of agent drifts Equation (7.10).

7.4.2 Colliding Swarms Driven by Modified Hybrid Atlas (MHAM) Dynamics

Here, we assume that the N_1 agents from $\mathscr{S}_1$ follow the dynamics of Equation (7.1), with $\alpha = \tilde{\alpha}_1 > 0$ and similarly, $\mathscr{S}_2$ is subject to the same dynamics but with $\alpha = \tilde{\alpha}_2 < \tilde{\alpha}_1$. From now on and without loss of generality, we focus only on the $\tilde{\alpha}_2 = 1$ and $\tilde{\alpha}_1 = \rho$. As before, we initially configure the system so that swarm $\mathscr{S}_1$ and $\mathscr{S}_2$ do not interact at time $t = 0$ (*i.e.*, $X_{0,1} = [l_1, r_1] = \Omega_1$, $X_{0,2} = [l_2, r_2] = \Omega_2$, $\Omega_1 \cap \Omega_2 = \emptyset$ and the common observation range U is such that $U > l_2 - r_1$). When $\rho > 1$, we have $d_1 > d_2$ and **we look for a critical ratio ρ_c under which a tight swarm survives a $\mathscr{S}_1$-$\mathscr{S}_2$ collision**. To this aim, let us consider a "post-colliding" configuration realized when $\mathscr{S}_1$ is completely ahead of $\mathscr{S}_2$. In term of stability, this configuration is the most critical: $\mathscr{S}_1$-agents can only escape from $\mathscr{S}_2$ via this configuration. Therefore, the $\mathscr{S}_{\text{glob}}$ tightness has to be checked under this specific configuration.

Accordingly, whenever the stability conditions from Ichiba et al. (2011) are verified under this critical configuration, they will also be verified under any other configuration. Therefore, the tightness of $\mathscr{S}_{\text{glob}}$ only depends on this critical configuration. Formally, we now rewrite Equation (7.5) for $\mathscr{S}_{\text{glob}}$ and verify whether the stability requirements given by Ichiba et al. (2011) are fulfilled for this critical case. In this case, the recentered dynamics read:

$$\begin{cases} d_{U,k}(\vec{X}(t),t) = \begin{cases} \rho\frac{N_{U,k}(t)}{N} - \gamma_{MHAM} & \text{for} \quad k \le N_1, \\ \frac{N_{U,k}(t)}{N} - \gamma_{MHAM} & \text{otherwise.} \end{cases} \\ \gamma_{MHAM} = \frac{\rho}{N}\sum_{k=1}^{N_1}\frac{k-1}{N} + \frac{1}{N}\sum_{k=N_1+1}^{N}\frac{k-1}{N} = \frac{\rho N_1(N_1-1)+N_2(2N_1+N_2-1)}{2N^2}. \end{cases} \tag{7.16}$$

From Ichiba et al. (2011), the stability conditions for $\mathscr{S}_{\text{glob}}$ read:

$$\sum_{k=1}^{l}\left[(1+\mathbb{1}_{\{k\le N_1\}}(\rho-1))\cdot\frac{k-1}{N} - \gamma_{MHAM}\right] \overset{!}{<} 0, \quad \forall 1 \le l \le N-1. \tag{7.17}$$

The most critical condition is realized for $l = N_1$ (this condition tests whether the distance between $\mathscr{S}_1$ and $\mathscr{S}_2$ remains stationary). It reads:

$$\sum_{k=1}^{N_1}\left[\rho\frac{k-1}{N} - \gamma_{MHAM}\right] = \frac{N_1 N_2 (N_2 - 1 - N_1(\rho-2) + \rho)}{2N^2} \overset{!}{<} 0, \tag{7.18}$$

implying that the critical threshold ρ_c ($\rho < \rho_c$ implies outcome (a), i.e., both societies remain flocked together) finally reads:

$$\rho_c = 1 + \frac{N}{N_1 - 1}. \tag{7.19}$$

Notice that for $N_1 = 1$, ρ_c cannot possibly exist (*i.e.*, $\rho_c = \infty$). The first agent has no drift, since it never observes any leader. Therefore, a society of one leader cannot possibly drive a swarm. Instead a single leader always remains flocked with $\mathscr{S}_2$. For $N_1 = N_2$, Figure 7.3 shows the critical value ρ_c. When $N \to \infty$, ρ_c asymptotically converges toward $\rho_c = 3$. Figure 7.4 shows the behavior of ρ_c as a function of the proportion $\frac{N_1}{N}$ (faster agents in $\mathscr{S}_{\text{glob}}$), for $N \to \infty$ agents. For $N \to \infty$ and $\frac{N_1}{N} \to 1$, $\rho_c \to 2$.

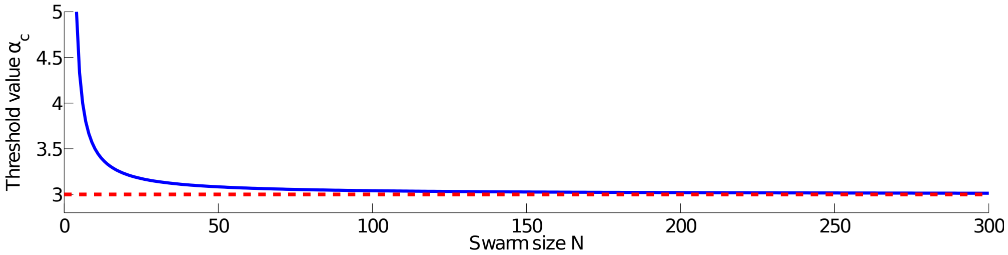

Figure 7.3 – Value of the critical threshold ρ_c, with regard to the swarm size N of the HAM, when $N_1 = N_2$. The asymptotic value $N \to \infty$ of $\rho_c = 3$ is depicted in red.

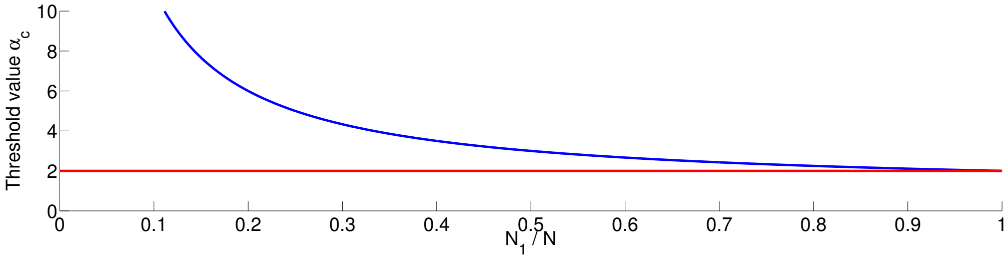

Figure 7.4 – Value of the critical threshold ρ_c, with regard to the proportion N_1/N of fast agents in the HAM, when $N \to \infty$.

7.4.3 Numerical Simulations

We consider two different cases, both with $N_1 = N_2 = 250$ agents. In both simulations, the society $\mathscr{S}_1$ starts with all agents located at $x_{0,1} = -15$, while agents from $\mathscr{S}_2$ start at $x_{0,2} = +15$. The common observation range U is selected large enough ($U > \max(\mu_{S,1}, \mu_{S,2})$), and $\sigma = 1$. For the experiments, we vary ρ, in order to compare i) a case in which both societies remain flocked together with ii) a case leading to the quasi-freedom behavior.

Figure 7.5 shows one realization in which $\rho < \rho_c$, allowing both societies to remain flocked. The left plot shows the final distribution of agents from both societies, as $\mathscr{S}_1$ leads $\mathscr{S}_2$. In the right plot of Figure 7.5, we show the average barycentric speeds of both societies. Notice how $\mathscr{S}_1$ is initially accelerated as its agents interact with those from $\mathscr{S}_2$. Later, when $\mathscr{S}_1$ has overcome $\mathscr{S}_2$, agents from $\mathscr{S}_2$ get an extra drift due to interactions with $\mathscr{S}_1$. This finally enables both societies to evolve at the same average barycentric speed (and therefore to remain flocked).

In Figure 7.6, we show the same scenario, for one realization with $\rho > \rho_c$ (quasi-freedom regime). In the right plot, we still notice the initial drift gained by $\mathscr{S}_1$ as its agents interact with those from $\mathscr{S}_2$. Once $\mathscr{S}_1$ has overcome $\mathscr{S}_2$, agents from $\mathscr{S}_2$ get an extra drift, that is not large enough to keep both societies flocked together. The extra drift gained by $\mathscr{S}_2$ finally vanishes, once $\mathscr{S}_1$ exits the observation range of the agents from $\mathscr{S}_2$. Finally, $\mathscr{S}_1$ and $\mathscr{S}_2$ recover their nominal speeds.

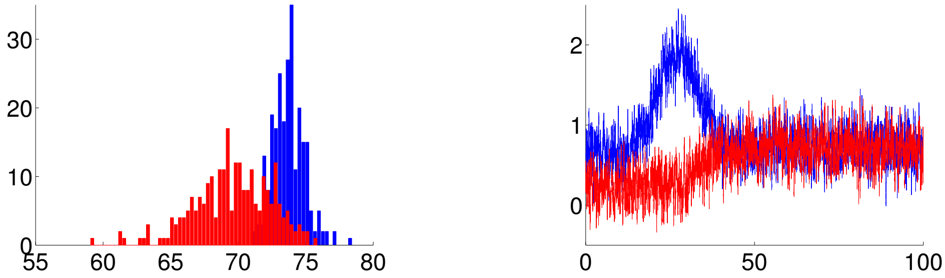

(a) (b)

Figure 7.5 – Final distributions $P_{1,2}(x,T)$ and average barycentric speeds $v_{1,2}(t)$ for one realization, in which both societies that start at $x_{0,\{1,2\}} = \mp 15$ achieve flocking. Here, $\rho = 2.5 < \rho_c$, $U = 20 > U_c = 5.4$, $\sigma = 1$ and $N_1 = N_2 = 250$ agents. (**a**)**: distribution of the agents from $\mathscr{S}_1$ (blue) and $\mathscr{S}_2$ (red), at ending time $T = 100$. (b): average barycentric speed of each society, with respect to time.**

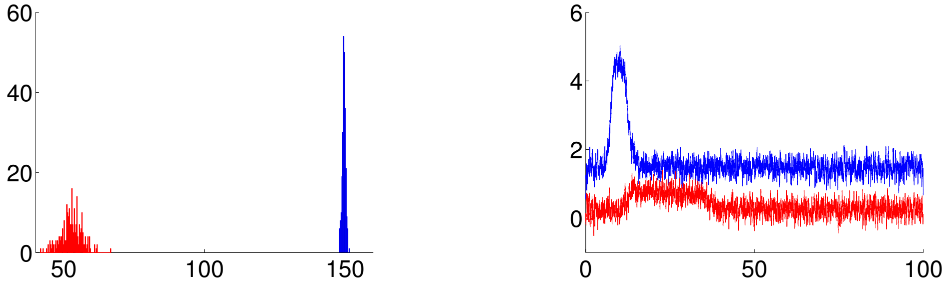

(a) (b)

Figure 7.6 – Final distributions $P_{1,2}(x,T)$ and average barycentric speeds $v_{1,2}(t)$ for one realization, in which both societies that start at $x_{0,\{1,2\}} = \mp 15$ do not achieve flocking. Here, $\rho = 6 > \rho_c$, $U = 20 > U_c = 2.26$, $\sigma = 1$ and $N_1 = N_2 = 250$ agents. (**a**)**: distribution of the agents from $\mathscr{S}_1$ (blue) and $\mathscr{S}_2$ (red), at ending time $T = 100$. (b): average barycentric speed of each society, with respect to time.**

7.5 Conclusions and Perspectives

Tightly flocked swarms of agents are externally perceived as plastic (*i.e.*, deformable) macroscopic bodies with dynamics resulting from the compromise between the individual evolutions, and the nature and range of the mutual interactions. Having macroscopic bodies at hand, basic physics naturally suggests the questions: (i) how such do solid bodies mutually interact; (ii) what emerges after collisions, and (iii) what type of information can we get from studying the results of the collisions? The discussion of collisions presents some similarities with the physics of solitons' interactions where the underlying nonlinearities precludes the superposition principle to be be invoked. We show here that the rank-based Brownian dynamics is one possible approach to explore, in a partly analytical way, some of the challenging questions related to swarm interactions.

7.6 New Contributions of Chapter 7

- Building again on the Hybrid Atlas Model (HAM), we consider the interactions between two Brownian agents swarms. We are able to analytically discuss the possible outcomes of the swarms' collision. This model simultaneously connects the micro- and macroscopic descriptions of swarms.

- **Publication**: This chapter is reproduced from the published journal paper Sartoretti and Hongler (2016), with slight modifications to fit the present dissertation.

8 Distributed Planar Manipulation in Fluidic Environments

Summary

We present a distributed control mechanism allowing a swarm of non-holonomic autonomous surface vehicles (ASVs) to synchronously arrange around a rectangular floating object in a grasping formation; the swarm is then able to collaboratively transport the object to a desired final position and orientation. We analytically consider the problem of synchronizing the ASVs' arrival at the object, with regard to their initial random positions. We further analytically construct a set of acceptable trajectories, allowing the transport of the grasped object to its final desired position. Numerical simulations illustrate the performance of the presented control mechanism. We present experimental results, to demonstrate the feasibility and relevance of our strategy.

8.1 Introduction

As robotic swarm sizes can vary over time, we are interested in developing scalable control mechanisms, that can adapt to any swarm size, and that are resistant to single robot failures. In some cases, scalability can be obtained via the use of a distributed control framework, where the global swarm's behavior is distributed among all agents. The robustness of the resulting distributed swarm strategy can then be increased by adding redundancy in the number of agents performing each role.

In this paper, we address the problem of transporting an object in a fluidic environment, using a swarm of autonomous non-holonomic robots. We build on Sartoretti et al. (2014a) to devise a distributed Braitenberg-inspired control mechanism, allowing the autonomous surface vehicles (ASVs) to move along smooth trajectories only as they approach, grasp and manipulate a rectangular object.

Previous works have successfully achieved decentralized manipulations of large objects by swarms of ground robots. In Fink et al. (2008), the decentralized manipulation of an Lshaped object held under caging is obtained by first having the team surround the object of interest and then transporting it by collectively pushing it along the desired direction. Manipulation is achieved through careful composition of artificial potential fields. More recently, a decentralized control mechanism allowing the manipulation of a general-shaped object by a swarm of gripping robots evolving on the ground is presented in Habibi et al. (2015). However, when considering a swarm of ASVs, new challenges arises, due to the decreased friction and the non-negligible inertial effects. Closely related to the present work, in Feemster et al. (2006), the authors devise a decentralized control mechanism allowing a swarm of tugboats to rotate a larger object, by collaboratively using their individual torques. Using tugboats attached to a larger vessel, the authors successfully devise and implement a control mechanism enabling the vessel's manipulation in Esposito (2008); Esposito et al. (2008).

The main contribution of this work is the construction of a set of acceptable trajectories, allowing a swarm of ASVs to transport an object from any given initial state (position, given orientation) toward any desired final state, under conditional closure (CC). The presented distributed control mechanism then allows the swarm of ASVs to collaboratively grasp the object under CC, and to collectively transport it toward its final desired state.

The outline of this paper is as follows: in Section 8.2, we briefly presents the considered problem. In Section 8.3, we define the two main phases of our control mechanism, and present numerical results. Section 8.4 is devoted to our experimental results, while Section 8.5 discusses of the future perspectives.

8.2 Problem Statement

We consider a swarm of N autonomous robotic ASVs evolving on a still body of water, initially positioned at random. A large vessel, represented by a rectangular object on the water surface, is initially positioned at a position that we define as the origin $\mathbf{O} = (0,0)$ of the swarm's global frame of reference. Without the loss of generality, we will assume that the vessel is positioned so that its length lays on the X-axis. The goal for the robotic swarm is to first regroup on one side of the vessel, facing the vessel (namely, on the side where $y > 0$), and then to push the vessel toward a final position $\{x_f, y_f\}$, with a final orientation h_f. We separate the control mechanism into two phases, namely the approach and the push phases.

Each ASV is modeled as a differential autonomous robot, evolving on a two-dimensional plane. Each robot is then assigned a specific target point T_i $(1 \leq i \leq N)$, which it aims for during the approach phase. The target points $T_2, ..., T_{N-1}$ are uniformly distributed along the central axis of the vessel, while T_1 and T_N are placed at each end of the vessel. This allows the swarm, once positioned near their target points, to hold the vessel under conditional closure (CC) (see Fig.8.1) Pereira et al. (2002). A robot starting on the bottom half-plane $\{y < 0\}$ must first move around the vessel. Once on the other half-plane $\{y > 0\}$, the ASV must then gradually change its course to approach the vessel perpendicularly to its side.

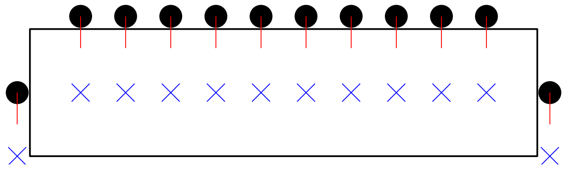

Figure 8.1 – Example of conditional closure (CC), where the pushing ASVs (black dots) are able to translate and rotate the vessel, with constraints on the translation direction and the rotation pivot. The target points are depicted as blue crosses, and the ASVs' heading vectors as red segments).

Once each ASV in the swarm has reached the vicinity of its target, the vessel is held under CC. In this position, the robots can only translate the vessel towards the half-plane $\{y \geq 0\}$. Furthermore, any rotation applied to the vessel under CC cannot have its pivot point within the vessel. Therefore, the rotation radius (distance between the barycentric position of the vessel, and the pivot point) must be at least $\frac{S_x}{2}$ (i.e., half the length of the vessel). These constraints define a set of allowed translations and rotations, which the swarm can apply to the vessel under CC. The objective then is to devise a distributed control strategy to enable the swarm to maintain CC while manipulating the vessel to the desired position $\{x_f, y_f\}$, with desired orientation h_f, given its initial position/orientation $x_0 = y_0 = h_0 = 0$.

8.3 Planar Manipulation Under Conditional Forced Caging

8.3.1 Distributed Approach and Grasp

We first define a general Braitenberg control mechanism Braitenberg (1984) allowing an ASV to move at a constant speed, keeping a given point $T = \begin{pmatrix} Tx \\ Ty \end{pmatrix}$ at a given angle ϕ from its heading. The angle ϕ defines the desired difference between the angular position of a robot, and its heading h. For example, when $\phi = \frac{\pi}{2}$, the ASV simply revolves around the point T (i.e., T is the instantaneous center of rotation for the ASV, remaining at an angle of $\frac{\pi}{2}$ from the ASV's heading). Fig. 8.2 illustrates the situation at a given time and depicts the various relevant quantities.

With these quantities, both motor speeds are updated as follows:

$$\begin{cases} V_{L,i}(t+1) & = S_{1,i} + \beta \cdot \cos\left[h_i(t) - \alpha_i(t) + (\frac{\pi}{2} - \phi_i(t))\right], \\ V_{R,i}(t+1) & = S_{1,i} - \beta \cdot \cos\left[h_i(t) - \alpha_i(t) + (\frac{\pi}{2} - \phi_i(t))\right], \end{cases} \tag{8.1}$$

with $\alpha = \arctan\left(\frac{y_i - Ty_i}{x_i - Tx_i}\right)$, (x_i, y_i) the position of the robot when its motor speeds are updated

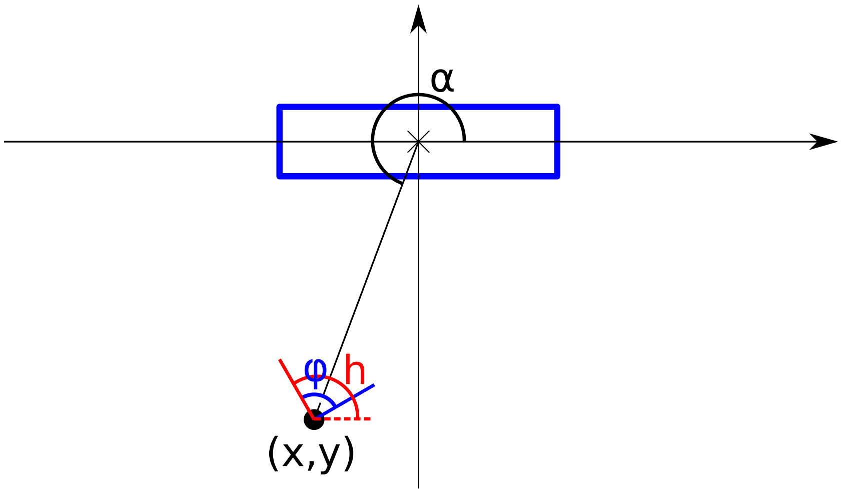

Figure 8.2 – Illustration of the system and the relevant quantities needed for the Braitenberg control mechanism. Here, $T = \mathbf{O} = (0,0)$. The vessel (blue rectangle) and an ASV (black dot) located at position (x, y). The heading h of the ASV is illustrated in red, and its angular position α in black. A desired angle ϕ, defining the desired difference between α and h, is depicted in blue.

and $S_{1,i}$ its (constant) approach speed. The control mechanism defined in Eq.(8.1) allows a robot to rotate around the origin point in a clockwise direction for $\phi = \frac{\pi}{2}$, and in a counter-clockwise direction for $\phi = 3\frac{\pi}{2}$. We want to allow robots starting in the half-plane $\{x > 0\}$ to rotate in the counter-clockwise direction, to reach their destination faster. To achieve this, we let $D \in \{0,1\}$ denote each robot's direction of rotation (clockwise (0) or counter-clockwise (1)). An ASV starting in the half-plane $\{x < T_i\}$ is assigned $D = 0$, and an ASV starting at initial position $x_{0,i} \geq T_i$ receives $D = 1$. A correction is then made to the control mechanism of Eq.(8.1) to encompass this rotation direction, by changing $\phi_i(t) \to \phi_i(t) + D\pi$.

To obtain a spiral-shaped motion from the initial position of the robot until its perpendicular approach to the vessel's side, we now let ϕ depend on the angular position of each robot. We want $\phi \approx \frac{\pi}{2}$ when the robot is in the lower half-plane $\{y < 0\}$ (i.e., pure rotation around the origin point). We then want ϕ to gradually decrease toward $\phi = 0$, as α approaches $\frac{\pi}{2}$ (i.e., pure attraction to the origin point). We let ϕ exponentially decrease, as α approaches $\frac{\pi}{2}$:

$$\phi_\sigma(\alpha) = \frac{\pi}{2}\left(1 - \exp\left(-\frac{arcmin(\alpha, \frac{\pi}{2})}{\sigma}\right)\right), \tag{8.2}$$

where $\sigma^2 \in \mathbb{R}^+$ controls the rate of exponential decay. We write $arcmin(\theta_1, \theta_2)$ as the minimal angle difference between θ_1 and θ_2:

$$arcmin(\theta_1,\theta_2) := \min\begin{pmatrix} mod(\theta_1-\theta_2, 2\pi) \\ mod(\theta_2-\theta_1, 2\pi) \end{pmatrix}.$$

We finally incorporate $\phi_\sigma(\alpha)$ into Eq.(8.1) to obtain the final control mechanism for our robotic swarm. Note how $\phi_\sigma(\alpha)$ must also be corrected with regard to D, to obtain suitable dynamics for both turning directions:

$$\begin{cases} V_{L,i}(t+1) & = S_{1,i} + \beta\cdot\cos\left[h_i(t) - \alpha_i(t) + \frac{\pi}{2} + D\pi - (2D-1)\phi_\sigma(\alpha_i(t))\right], \\ \\ V_{R,i}(t+1) & = S_{1,i} - \beta\cdot\cos\left[h_i(t) - \alpha_i(t) + \frac{\pi}{2} + D\pi - (2D-1)\phi_\sigma(\alpha_i(t))\right], \end{cases} \tag{8.3}$$

Computation of the Approaching Speeds

Using the control mechanism from Eq.(8.3), a robot starting at any given initial position moves along a spiral-shaped trajectory toward its given target point T. We now want all robots to converge to their targets T_i within a desired given time T_{goal}. The correct synchronization of the arrival times allows the robots to start pushing the vessel all at once.

We need to estimate the length of the path a robot will move along during its approach, given its initial position (x_0, y_0). To do this, we approximate the trajectories created by the Braitenberg control mechanism of Eq.(8.3) as exponential spirals. We express a spiral as a function of the radius of each point of the spiral with respect to its angular position. To simplify the expression, we rotate the frame of reference, and measure the angular position θ of the spiral's points starting from the angle $\frac{\pi}{2}$. In our case, our spirals are defined for any angular position $\theta \in [0;\pi]$, where, because of symmetries, robots cannot move more than half a circle around their target point. Using the relation for $\phi_\sigma(\alpha)$, we now approximate our spiral as:

$$r(\theta) := r_\pi\left(1-\exp\left(-\frac{\theta}{\sigma}\right)\right). \tag{8.4}$$

The typical shape of the spiral, with $r_\pi = 1$, is depicted in Fig. 8.3. In our case, we need to let each robot compute r_π, from its initial position (r_0, θ_0), where $\theta_0 = arcmin(\alpha_0, \frac{\pi}{2})$. This is achieved by putting r_0 and θ_0 in Eq.(8.4), and by extracting r_π. We finally find:

$$r_\pi = \frac{r_0}{1-\exp\left(-\frac{\theta_0}{\sigma}\right)}. \tag{8.5}$$

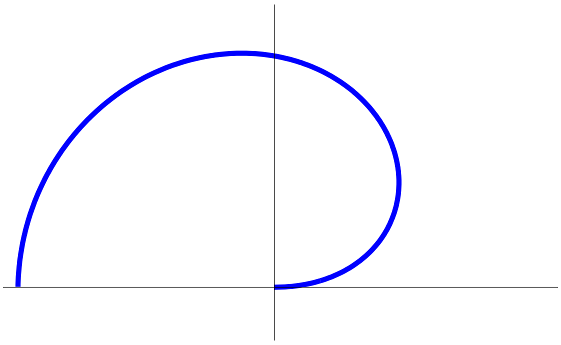

Figure 8.3 – Typical shape of the spiral of Eq.(8.4), with $r_\pi = 1$. Here, we make the substitution $\theta = arcmin(\alpha, \frac{\pi}{2})$, meaning that both axes are simply switched.

With the expression of the spiral for the trajectories' shapes, we can now obtain the trajectories lengths from the initial position of each robot. The initial angular and radial positions of each robot are first computed with respect to their target point:

$$\begin{cases} r_0 = \sqrt{(x_0 - T_x)^2 + (y_0 - T_y)^2} \\ \\ \theta_0 = arcmin(\arctan \frac{y_0 - T_y}{x_0 - T_x}, \frac{\pi}{2}). \end{cases}$$

We then compute the length of the spiral following Eq.(8.4), from the initial position to the target point, as:

$$L_i(r_0, \theta_0) = \int_0^{\theta_0} \sqrt{r(\theta)^2 + \left(\frac{d}{d\theta} r(\theta)\right)^2}\, d\theta,$$

which yields a lengthy but exact result, given by Eq.(8.6).

$$\begin{aligned} L_i(r_0,\theta_0) \quad = \quad & r_0 \left(\tfrac{1}{e^{\theta_0/\sigma}-1} + 1\right) \left(\left(1 - \frac{\sigma^2 \log\left(\sqrt{\sigma^2+1}+1\right)}{\sqrt{\sigma^2+1}} \right) - e^{-\frac{\theta_0}{\sigma}} \sqrt{\sigma^2 \left(e^{\theta_0/\sigma} - 1\right)^2 + 1} + \right. \\ & \left. \frac{\sigma^2 \log\left(e^{-\frac{\theta_0}{\sigma}} \left(\sigma^2 \left(1 - e^{\theta_0/\sigma}\right) + \sqrt{\sigma^2+1}\sqrt{\sigma^2 \left(e^{\theta_0/\sigma}-1\right)^2+1}+1\right)\right)}{\sqrt{\sigma^2+1}} - \sigma \sinh^{-1}\left(\sigma - \sigma e^{\theta_0/\sigma}\right) \right). \end{aligned} \tag{8.6}$$

With this analytical expression for the trajectory length of an ASV starting at any initial position, we are able to adapt the individual speeds $S_{1,i}$ of each ASV. We let the approach speed of each ASV depend on its trajectory length $L_i(r_0, \theta_0)$ in order to let the ASVs meet their target point in the vicinity of a desired time T_{goal}:

$$S_{1,i} = S_{1,i}(r_0,\theta_0) = \frac{L_i(r_0,\theta_0)}{T_{\text{goal}}}. \tag{8.7}$$

Link with Brownian Swarms

Eq.(8.3), defining our Braitenberg control mechanism, can be translated into a multi-agent swarm dynamic, expressed in terms of differential equations. We identify the ASVs as Brownian agents, evolving on the plane $\mathbb{R}^2$, and following the dynamic expressed in polar coordinates:

$$\begin{cases} dr_i(t) = -S_{1,i} \cdot \exp\left(-\frac{arcmin(\alpha_i(t),\frac{\pi}{2})}{\sigma}\right), \\ d\alpha_i(t) = (2D-1)\frac{S_{1,i}}{r_i(t)}\left(1-\exp\left(-\frac{arcmin(\alpha_i(t),\frac{\pi}{2})}{\sigma}\right)\right). \end{cases} \tag{8.8}$$

Noise can be added to this dynamic, in order to encompass the actuators and sensors' errors, by adding independent White Gaussian Noise sources on either or both state variables. This effectively allows us to express the swarm's dynamic as a set of N Stochastic Differential Equations (SDE). Conventional tools of dynamical systems theory can be used on the resulting nonlinear SDEs to study the probability distribution of the swarm's position during the approach.

Note that, similarly to the original Braitenberg control dynamics, the norm of the instantaneous speed of each agent remains constant through time:

$$v_i(t) = r(t)\frac{d}{dt}\alpha(t) + \frac{d}{dt}r(t) = S_{1,i} \qquad \forall t.$$

Fig. 8.4 illustrates the initial position and final position of a swarm of $N = 10$ robots following Eq.(8.8) without noise, up to time $T = 10$. Notice how the trajectories of the agents are very close to the spiral shapes created from Eq.(8.4).

8.3.2 Computation of the Manipulation Trajectories

Once the ASVs have achieved CC around the vessel, the pushing phase starts. During this second phase, the ASVs continue to follow Eq.(8.3), but adapt their forward speeds to translate/rotate the vessel. To manipulate the vessel by controlling the individual ASVs' forward speeds, we restrict the vessel's motion to circular arcs only, until it has achieved the desired

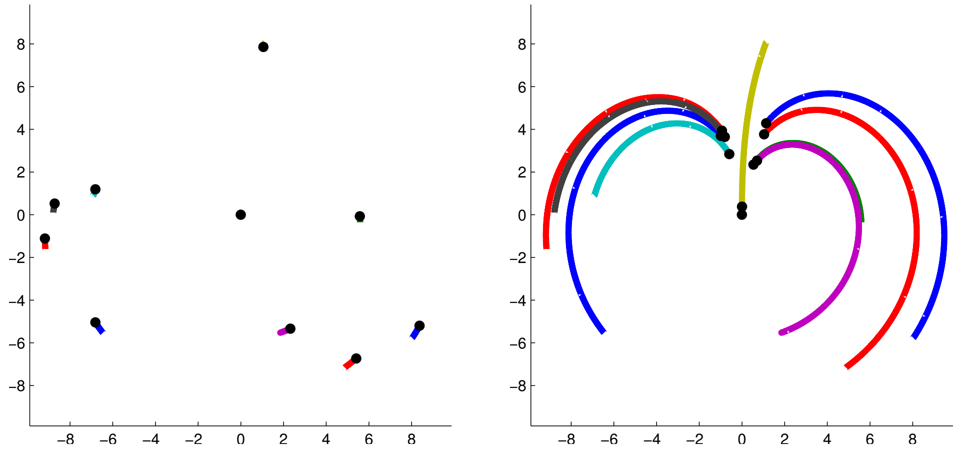

Figure 8.4 – Initial (left) and final (right) positions, and trajectories, of a swarm of $N = 10$ agents following Eq.(8.8) without noise. Here, $\sigma^2 = \frac{1}{2}$. Notice the trajectories following the spiral-shape of Eq.(8.4).

final position and orientation. By construction, we can show that from its initial position, two well chosen circular arcs always allow the vessel to end up at the desired final position given a desired orientation. We prove this by computing the centers of the two circles the vessel will be transported along. We let the vessel first travel an arc length α_1 around the center $\{C_{1,x}, C_{1,y}\}$ of a first circle C_1. It then travels an arc length α_2 around the center $\{C_{2,x}, C_{2,y}$ of a second circle C_2.

We first note that $C_{1,y} = 0$, since the vector $\{C_{1,x} - x_0, C_{1,y} - y_0\}$ must be perpendicular to the initial normal vector of the vessel. The normal vector of the vessel is defined as a unitary vector, perpendicular to the vessel's orientation (i.e., initially the normal vector of the vessel is $\{1,0\}$). This ensures that the vessel's normal vector is tangent to C_1, since its orientation faces the center of C_1. We then express the constraints within our system:

1. We know that after the first arc α_1, the orientation of the vessel is α_1. After the second arc, the final orientation must therefore verify:

$$h_f = \alpha_1 + \alpha_2. \tag{8.9}$$

2. Using the rotation matrix $M_\alpha = \begin{pmatrix} \cos(\alpha) & -\sin(\alpha) \\ \sin(\alpha) & \cos(\alpha) \end{pmatrix}$, we can compute the successive positions of the vessel after traveling along each of the two arcs. After the first arc, the

vessel ends up at the position $\{x_1, y_1\}$, with

$$\begin{aligned}\begin{pmatrix} x_1 \\ y_1 \end{pmatrix} &:= M_{\alpha_1} \cdot \begin{pmatrix} x_0 - C_{1,x} \\ y_0 - C_{1,y} \end{pmatrix} + \begin{pmatrix} C_{1,x} \\ C_{1,y} \end{pmatrix} \\ &= \begin{pmatrix} C_{1,x} \cdot (1 - \cos(\alpha_1)) \\ -C_{1,x} \cdot \sin(\alpha_1) \end{pmatrix}.\end{aligned} \tag{8.10}$$

From this intermediate position, the vessel then follows an arc length α_2 around the center of C_2. The final position must equal $\{x_f, y_f\}$, which gives us a second relation:

$$M_{\alpha_2} \cdot \begin{pmatrix} x_1 - C_{2,x} \\ y_1 - C_{2,y} \end{pmatrix} + \begin{pmatrix} C_{2,x} \\ C_{2,y} \end{pmatrix} = \begin{pmatrix} x_f \\ y_f \end{pmatrix}. \tag{8.11}$$

3. Finally, the vector $\{x_1 - C_{2,x}, y_1 - C_{2,y}\}$ must be perpendicular to the vessel's normal vector after the first arc. This condition, similar to the one raising $C_{1,y} = 0$, ensures that at $\{x_1, y_1\}$, the ASV is simultaneously on both circles C_1 and C_2.

$$\begin{aligned}\begin{pmatrix} x_1 - C_{2,x} \\ y_1 - C_{2,y} \end{pmatrix} \cdot \left(M_{\alpha_1} \cdot \overbrace{\begin{pmatrix} 1 \\ 0 \end{pmatrix}}^{\text{initial normal vector}} \right) &= \\ (C_{2,x} - C_{1,x}) \cdot \sin(\alpha_1) - C_{2,y} \cdot \cos(\alpha_1) = 0.&\end{aligned} \tag{8.12}$$

With these 4 equations, and 5 variables $\{\alpha_1, \alpha_2, C_{1,x}, C_{2,x}, C_{2,y}\}$, we are left with one degree of freedom. We choose to fix α_1, and to compute the values of the other variables accordingly. After solving Eqs(8.9)-(8.12), with α_1 fixed, we end up with:

$$\begin{cases} \alpha_2 &= h_f - \alpha_1 \\ C_{1,x} &= -\frac{1}{2} \csc\left(\frac{\alpha_1}{2}\right) \csc\left(\frac{\alpha_1 + \alpha_2}{2}\right) \left(x_f \cos\left(\alpha_1 + \frac{\alpha_2}{2}\right) + \right. \\ & \quad \left. y_f \sin\left(\alpha_1 + \frac{\alpha_2}{2}\right)\right) \\ C_{2,x} &= \frac{1}{2} \csc\left(\frac{\alpha_2}{2}\right) \csc\left(\frac{\alpha_1 + \alpha_2}{2}\right) \left(x_f \cos\left(\frac{\alpha_1}{2}\right) + \right. \\ & \quad \left. \sin\left(\frac{\alpha_1}{2}\right) (y_f \cos(\alpha_1 + \alpha_2) - x_f \sin(\alpha_1 + \alpha_2))\right) \\ C_{2,y} &= \cos\left(\frac{\alpha_1}{2}\right) \csc\left(\frac{\alpha_2}{2}\right) \left(x_f \cos\left(\frac{\alpha_1 + \alpha_2}{2}\right) + \right. \\ & \quad \left. y_f \sin\left(\frac{\alpha_1 + \alpha_2}{2}\right)\right) \end{cases} \tag{8.13}$$

Furthermore, we want to ensure that the initial push is made in the correct direction. Indeed, we could initially find $\alpha_1 > 0$ and $C_{1,x} > 0$. In this case, we would need to initially push the vessel towards $\{y > 0\}$, which is not allowed. To correct this move, we would simply rewrite $\alpha_1 = \alpha_1 - 2\pi$, meaning that the robots will push the vessel in the correct direction, but for a longer arc. Notice that this does not change the final position $\{x_1, y_1\}$ after the first arc. We must therefore check for these cases, and adapt α_1 accordingly:

$$\tilde{\alpha}_1 := \begin{cases} \alpha_1 - 2\pi & \text{if } \operatorname{sign}\alpha_1 = \operatorname{sign}C_{1,x}, \\ \\ \alpha_1 & \text{otherwise.} \end{cases} \tag{8.14}$$

Similarly, at the interface $\{x_1, y_1\}$ between both circles, we need to ensure that the trajectory is continuous. We also need to correct α_2 if its value would mean the movement must be instantly reverted when switching to the second arc. To obtain the condition, we set the frame of reference at the position $\{x_1, y_1\}$, with the orientation α_1:

$$\begin{pmatrix} \tilde{C}_{2,x} \\ \tilde{C}_{2,y} \end{pmatrix} = M_{-\alpha_1} \cdot \begin{pmatrix} C_{2,x} - x_1 \\ C_{2,y} - y_1 \end{pmatrix}.$$

We then check the same condition as in Eq.(8.15) (same sign between α_2 and $\tilde{C}_{2,x}$), to correct α_2:

$$\tilde{\alpha}_2 := \begin{cases} \alpha_2 - 2\pi & \text{if } \operatorname{sign}\alpha_2 = \operatorname{sign}\tilde{C}_{2,x}, \\ \\ \alpha_2 & \text{otherwise.} \end{cases} \tag{8.15}$$

Fig. 8.5 shows an incorrect trajectory corrected using this method, enabling us to obtain a smooth trajectory following only allowed translations/rotations under CC.

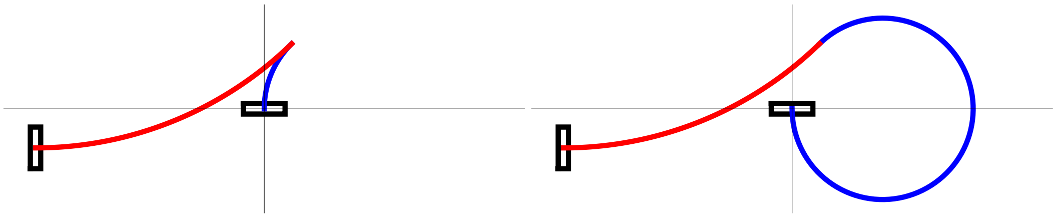

Figure 8.5 – Example trajectory where α_1 must be corrected (left), and the corrected trajectory using Eq.(8.15) (right). The initial and final states of the vessel are shown in black.

Computation of the Pushing Speeds

Once we find the centers of the circles C_1 and C_2 for an acceptable trajectory, we let the speed of each robot in the swarm depend on its distance to the center of the circle the vessel is traveling around. Namely, if we let $P(t) = \{P_x(t), P_y(t)\}$ be the instantaneous position of the barycenter of the caged vessel at time t, we let the speed of the robot i at time t be:

$$V_i(t) = \frac{||X_i(t) - C||}{||P(t) - C||} \cdot \overline{S_2}, \tag{8.16}$$

with C the center of the circle the vessel is currently travel along, and $\overline{S_2}$ the desired average speed of the vessel along the trajectory. Furthermore, we let the robots switch from $C = C_1$ to $C = C_2$ when $P(t) \approx \{x_1, y_1\}$ (Eq.(8.10)).

Optimal Trajectory in Fluidic Environment

For mobile robots evolving on the ground, a well-known result states that the shortest trajectory under constraint of maximal curvature, and with selected initial and final tangents, is a Dubins path Dubins (1957); Bui et al. (1994). Such a path always starts with a rotation with maximal curvature (i.e., $\frac{S_x}{2}$ in our case), followed by a forward motion, and finally by a second rotation with maximal curvature. This means that, on the ground at least, our circular trajectories are always sub-optimal (i.e., equal or longer than the corresponding Dubins path).

But since our ASVs evolve in a fluidic environment, a Dubins path can prove to be difficult to apply, due to the necessary rotations with maximal curvature. To apply a rotation with maximal curvature $\frac{S_x}{2}$ to our vessel, we would need to use one of the end ASVs (i.e., the ASVs caging the plank along its main axis) as the rotational pivot. This maneuver is easily managed on the ground, but proves to be harder on water, where the force exerted by the vessel on the pivot during the rotation will most likely move the pivot ASV. In this case, trajectories favoring rotation with smaller curvature can increase the transport precision under CC.

8.3.3 Numerical Results

Fig. 8.6 shows selected consecutive states in a run with $N = 10$ ASVs. In the simulation, we assume that the sum of the ASVs' weights is equal to the individual weight of the vessel. This helps synchronize the pushing, by preventing early arriving ASVs from being able to rotate the vessel too fast on their own. The push phase can therefore only start when the whole swarm is here to push the vessel together. The approach speeds of the ASVs are computed to synchronize their arrival around $T_{\text{goal}} = 30\,s$. The arc length around the first circle is selected to be $\alpha_1 = 1$, and the trajectory is computed in order to position the ASV at $\{x_f, y_f, h_f\} = \{55, -95, 0.1\}$.

To better reflect reality, we add noise to the exact angular position of the agents at each timestep, and add individual noise on their (x, y) position when it is updated in Eq.(8.3). The noise sources are all White Gaussian Noise sources, with an individual variance of 0.05. The control mechanism of Eq.(8.3) is updated at 50 Hz. Notice that the arrival of the ASVs to the vessel is very well synchronized.

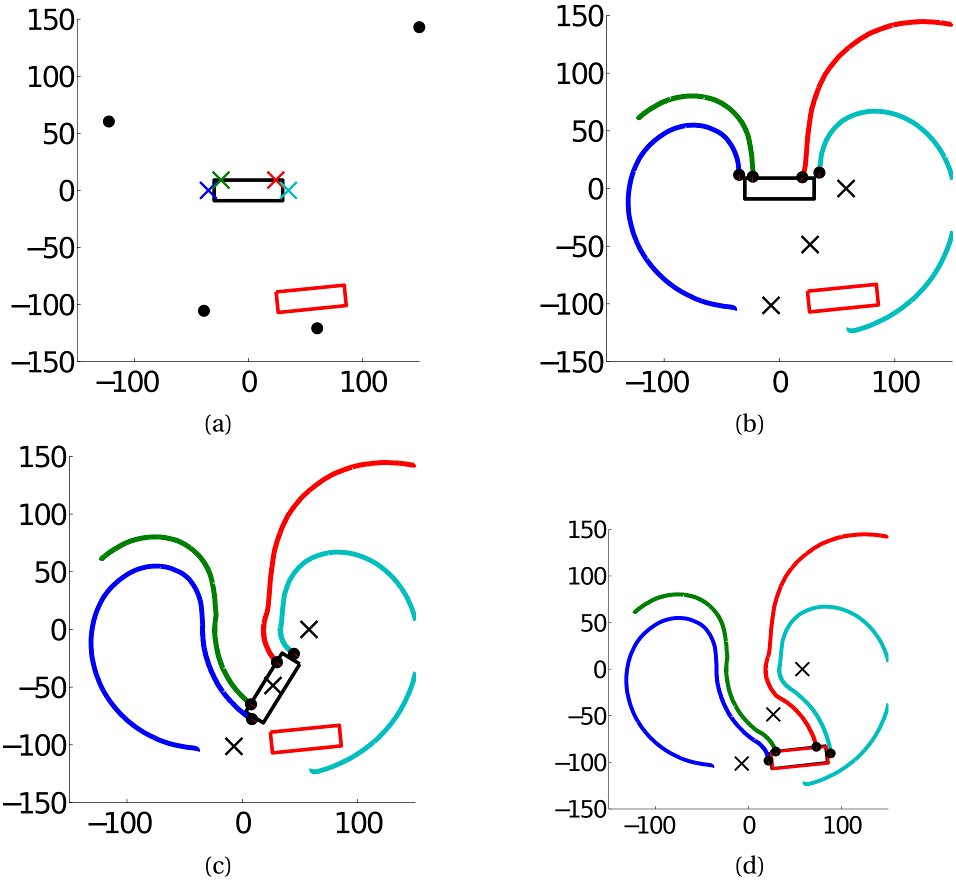

(a)

(b)

(c)

(d)

Figure 8.6 – Selected successive states of the system during a numerical simulation of the approach and push phases. Here, a swarm of $N = 4$ ASVs (black dots) push the large vessel (black rectangle) towards the final position $\{x_f, y_f, h_f\} = \{55, -95, 0.1\}$ (red rectangle).

Fig. 8.7 show the complete trajectories followed by a swarm of $N = 8$ ASVs to transport the vessel to its final state, from its initial state $\{x_0, y_0, h_0\} = \{0, 0, 0\}$. The considered trajectories allow the plank to be transported to any position, even on the half-plane $\{y > 0\}$, as illustrated in Fig. 8.7b.

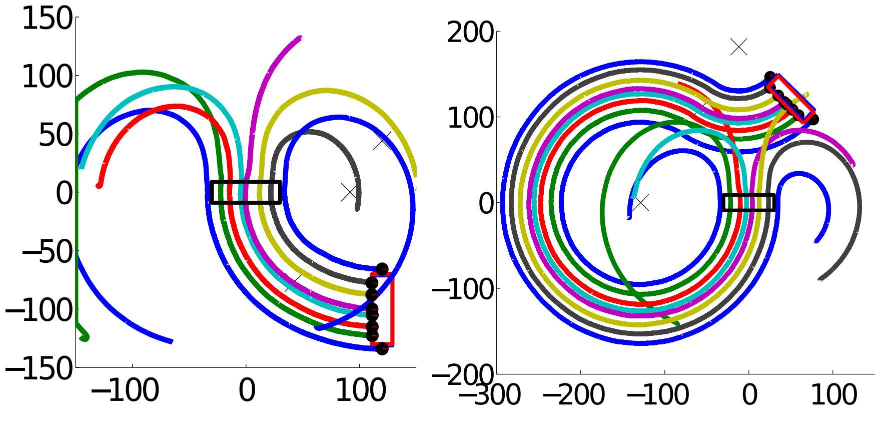

(a) (b)

Figure 8.7 – Complete trajectories of a swarm of $N = 8$ ASVs (back dots), moving a vessel to its final position (red rectangle). The vessel is initially positioned at $\{x_0, y_0, h_0\} = \{0, 0, 0\}$. The two circles' centers, and the intermediate switching point, are depicted as black crosses.

8.4 Results

8.4.1 Experimental Setup

In this section we evaluate the proposed control mechanism employing our indoor laboratory experimental testbed : multirobot Coherent Structure Testbed (mCoSTe). The mCoSTe is an indoor laboratory experimental testbed that consists of a $3m \times 3m \times 1m$ flow tank and a fleet of micro-autonomous surface vehicles (mASVs). The mASVs are differential drive surface vehicles, approximately 12 cm long, equipped with a micro-controller board, XBee radio module, and an inertial measurement unit (IMU). Localization for the mASVs and the vessel being manipulated is provided by an external motion capture system.

The considered control mechanism was successfully implemented on a swarm of $N = 4$ mASVs, evolving on still water. The boats are tracked in real time by a collection of overhead cameras, and their positions, headings, speeds and heading derivatives are read at a frequency of $20\,Hz$. The role of the vessel is played by a floating plank of $40\,cm \times 15\,cm$, with fins at both ends of its length, limiting its movement along its main axis.

Since the boat propellers' rotation speeds cannot be linearly translated into a forward speed (as opposed to wheeled mobile robots), Eq.(8.2) is used to control the boats' headings during the approach phase. The boats' headings and forward speeds are updated at a frequency of $10\,Hz$, using the gathered tracking data. A couple of controllers acting on the boats' headings (PD controller) and forward speeds (P controller) are also updated at $10\,Hz$ to ensure a proper application of the underlying dynamic.

During the approach, the optimal approach speed of each boat is updated at each iteration ($dt = 0.1\,s$), to synchronize the arrival of all the boats. The targets are re-attributed at each iteration, to ensure a minimal probability of collision between the boats. The targets are attributed to the nearest boats to minimize path crossings between boats. The push phase only starts when all the boats are arranged in CC around the plank. This stop phase is needed, since a single early arriving boat can move the light plank easily, which would have a harmful effect on the approach of the other boats.

Once the CC is obtained, the desired final state of the plank $\{x_f, y_f, h_f\}$ is computed in the current frame of reference of the plank. The resulting trajectory is computed to transport the plank toward the desired position under CC. During the push phase, the 2 pushing boats control the plank's orientation along the computed trajectory, ensuring the plank faces the current circle center. The end boats, caging the plank along its x axis, remain in the plank's vicinity to correct its possible deviations along its main axis.

Once in range of the final position, all boats stop their motors. The plank continues its movement, driven by its inertia. Since the plank is held under CC, a stopping maneuver cannot be made by the boats to ensure the plank is stopped precisely on target.

8.4.2 Experimental Results

Fig. 8.8 presents successive states in an experimental run with $N = 4$ boats. During this experimental run, the following values are set for the parameters of the control mechanism:

$$\begin{cases} \sigma = 1 & T_{\text{goal}} = 80\,s \\ \alpha_1 = 1 & \{x_f, y_f, h_f\} = \{55, -95, 0.1\}. \end{cases}$$

The initial position of the boats (black dots) and the plank (black rectangle) is depicted in Fig. 8.8a, along with the targets along the plank's side (colored crosses). In Fig. 8.8b, the boats have just arrived to their targets, and have stopped to synchronize the beginning of the push phase. At this moment, the final position and orientation of the plank is computed from its current state (red rectangle), and the corresponding trajectory is computed. The two circle centers, along with the intermediate switching point, are computed (black crosses) (Fig. 8.8c). The boats then start moving the plank under CC along the computed trajectory, and switch once the plank has just passed the intermediate point (Fig. 8.8d). As soon as the final position is in range ($20\,cm$) of the plank, the boats stop their motors, and let the plank derive to its final position (Fig. 8.8e). The plank, still moving under its inertia, derives toward its final position (Fig. 8.8f).

Fig. 8.9 presents still frames from the video recording the run depicted in Fig. 8.8.

A series of experimental runs was performed to test the repeatability of the considered control mechanism. The minimal distance from the plank's center to the desired final position $\{x_f, y_f\}$ was computed for each run, along with the angle error at that precise instant. The

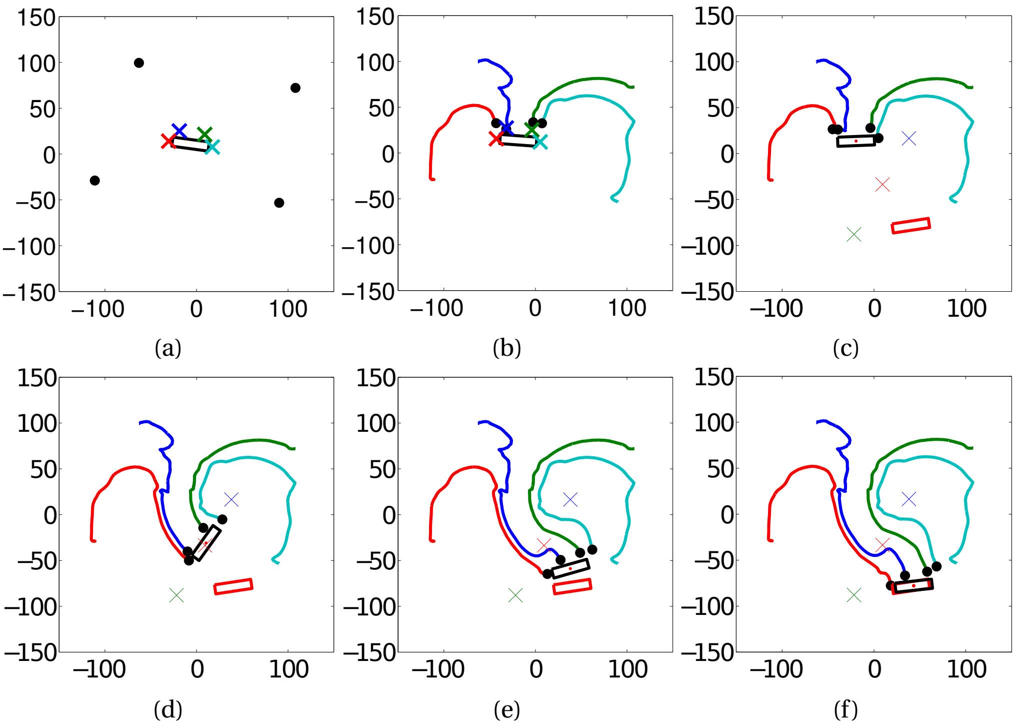

(a) (b) (c)

(d) (e) (f)

Figure 8.8 – Key successive states during an experimental run of the presented control mechanism with $N = 4$ boats. The trajectories (colored lines) of the boats (black dots), are depicted, along with the plank's current position (black rectangle) and its final desired state (red rectangle). During the approach phase, the boats' targets along the plank's side are plotted as colored crosses. During the push phases, the circle centers and intermediate switching points are illustrated as black crosses.

corresponding measured errors are illustrated in Fig. 8.10, along with their respective mean over the 12 experiments. The mean distance error and its standard deviation read $4.88\,cm \pm 1.8\,cm$, while the mean orientation error and its standard deviation read $-0.26\,rad \pm 0.44\,rad$.

8.5 Conclusions and Perspectives

The control mechanism presented in this paper is relevant to solve the problem of manipulating an object in a fluidic environment. It allows simple non-holonomic ASVs to distributively arrange and grasp an object under CC. Despite the fact that this grasping method reduces the set of acceptable translations and rotations, the object can always be transported to any position on the Euclidean plane. Numerical and experimental results are very good, as we test the manipulation of a rectangular object, representing a large vessel for instance.

The computed trajectories followed by the object toward its final position are known to be sub-optimal, compared to the corresponding Dubins path, but appear to be more stable on

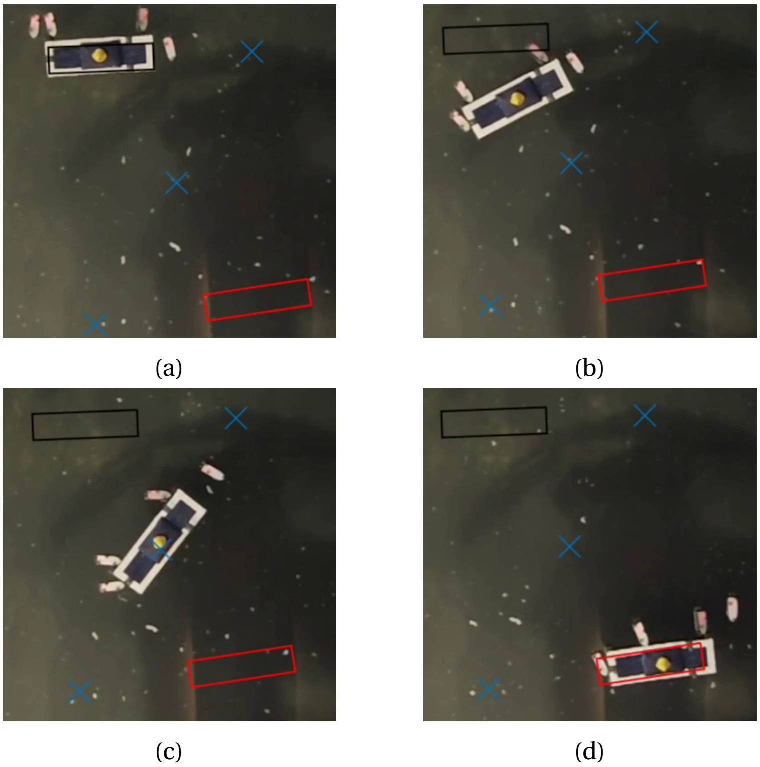

Figure 8.9 – Key successive states during an experimental run of the presented control mechanism with $N = 4$ boats. Initial position of the boat (black rectangle); final desired state (red rectangle). The circles centers, and the intermediate switching point, are depicted as blue crosses. Caging position obtained by the boats after the approach phase (8.9a). Start of the pushing phase (8.9b), switch between both circles (8.9c), and stopping point of the boats (8.9d).

the surface of a viscous fluid. Future works will include the comparison between object manipulation using both trajectories in terms of time consumption, stability during manipulation, and precision of final placement.

8.6 New Contributions of Chapter 8

- We devise a distributed control mechanism, enabling the manipulation of a floating object by a swarm of boats The fluidic environment constrains the set of admissible transport trajectories, which are analytically calculated. We numerically and experimentally validate the model, using a swarm of 4 robotic boats.

- This examplifies a case of distributed swarm dynamic, with *stigmergic interactions* (i.e., agents influence the environment, which itself affects their dynamics).

- **Publication**: This chapter is reproduced from the preprint version of the accepted

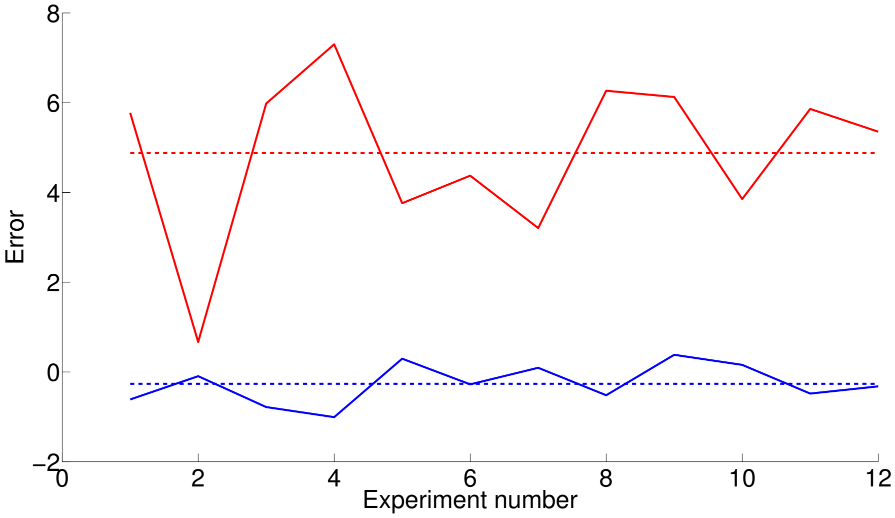

Figure 8.10 – Minimal error on the position (red) and corresponding error on the orientation (blue) during the 12 experimental trials. The respective mean errors are depicted as dotted lines.

conference paper Sartoretti et al. (2016), with slight modifications to fit the present dissertation.

Conclusion and Perspectives Part VI

Conclusion and Perspectives

Like many researchers, we developed during the last years a growing fascination for the emergence of collective spatio-temporal patterns in swarms of autonomous and heterogeneous agents. Even very elementary individual rules, supplemented with interactions with neighboring fellows (introducing intrinsic nonlinearities), can produce highly stable global patterns. This observation raises numerous challenging questions, which can be summarized into the key question $\mathscr{Q}$: *What individual dynamic and what type of interactions generate an a-priori given collective spatio-temporal behavior ?* Devoted to this topic, a rich and wide interdisciplinary literature corpus ranging from pure mathematics to actual experimentations is available. Too often, at least to our opinion, wide gaps remain open between pure theoretical studies and actual implementations. One of our basic goal in this work is to illustrate, via new elementary swarms models, how this gap can be bridged. Anybody addressing the question $\mathscr{Q}$ opens a rich Pandora box of challenging technical issues like: the role played by i) the dimensionality of the agents state space, ii) the range and the nature of mutual interactions, iii) the swarm heterogeneity, iv) the ubiquitous presence of noise in the agents dynamics, and still many others. The plurality of issues displayed in this short and surely non exhaustive list shows that universal answers to this key question cannot be expected. This leads very naturally to the strong temptation of focusing on specific case studies and to then proceed directly via computer simulation. Clearly, numerical simulations offer the possibility to virtually model any relevant situations, whereas imposing oneself the discipline of getting analytical descriptions creates strong limitations, which is often apprehended as a crippling drawback. Nevertheless and at the expense of reducing the modeling freedom, we opt to gain deeper scientific insights of swarm dynamics, that only come out when analytical approaches are consented. Adopting this methodological constraint for the modeling, we felt very soon the need to distinguish between homogeneous and heterogeneous swarms, being naturally aware that the later describe the generic situation. As always when highly complex system are to be discussed via an analytical approach, one has to get rid of refinements and simplify, idealize, stylize to ultimately come out with minimalist models. This lead us to start by considering homogeneous situations, therefore giving in to fully generic situations. As large homogeneous swarms of agents share some (but clearly not all) dynamic features with gas of interacting particles, we realize that analytical tools and concepts developed for statistical physics (and in particular the concept of mean-field dynamics) are very powerful - this is exemplified at several occasions in this work. Nevertheless, one has to be cautious. By essence, such statistical physics approaches inherently possess strong modeling limitations. Indeed, one should be aware that gas particles do not have autonomous decision capability, a feature that basically characterizes agents. Proceeding to higher complex issues, we then focus of heterogeneous swarms with relatively limited populations, a topic which, to the best of our knowledge, remains far less visited. Here again, our goal to propose analytical models lead us to introduce a new taxonomy step for slightly heterogeneous swarms. We separate dynamics subject to hard control dynamics where leaders drive the dynamics, and dynamics with soft control where singular infiltrated (shills) agents influence the whole population (shills are not perceived by their fellows as being singular). Among potential frameworks suitable for heterogeneous swarms, simplicity lead us to explore the possibilities to use recent mathematical results, obtained for rank-based Brownian motions and from feedback particle filtering. All swarms models studied so far share the characteristic that agents mutually interact directly. However, in numerous situations, agents interact stigmergically, that is to stay, they interact indirectly via their individual influences on their common environment. This is the topic approached in our last chapter where, again, the possibility to simultaneously perform the analytical, the simulation and the actual implementation approaches is illustrated using a small swarm of robotic boats.

A steadily growing demand to build partly (or fully) decentralized systems able to autonomously perform predefined complex tasks in changing environment stimulates a booming activity in swarm robotics research. To gain maturity and applicability in this area, it is more and more essential to minimize the relevant inter-agents information flows needed to reach collective goals and to maximize the resilience under randomness.

To our appreciation, the soft control approach and its fascinating connections with biological/ethological models is promised to a bright future. While, the idea that one or a group of controllable infiltrated agents can influence a whole society is a classical feature in politics, sociology and ethology, it still remains under-explored in the engineering of multi-agents systems. This new approach connecting living and engineering worlds brings together hard and soft sciences is an entirely new paradigm. Intertwining the influence of robots and animals is a domain that remains widely open.

Appendices Part VII

A Chapter 2 - Multi-agent tracking tool

To determine the states of every single agent in our experiments, we developed a multi-agent tracking tool based on computer vision techniques and the Kalman filter . This task was particularly challenging due to the very inhomogeneous lighting conditions in the acquired videos (mainly because of the central light source). This acquisition setup is composed of an overhead digital camera equipped with a wide angle lens (Canon EF-S 10-22mm f/3.5-4.5 USM, mounted on a Canon EOS 7D body) . Our multi-agent tracking tool has been developed in C++ using the GNU compiler collection (GCC 4.6.3) and standard computer vision algorithms included in the open source computer vision library (OpenCV, v. 2.3.1-7, http://opencv.org/).

The employed technique follows three steps:

1. The image foreground is extracted for further processing using a precomputed mean background.
2. The Gaussian scale-space representation of the extracted foreground $I_F(x,y)$ containing the agents was convolved with a Gaussian kernel, as $L(x,y,\sigma) = G(x,y,\sigma) * I_F(x,y)$, where, in a two-dimensional space, the Gaussian function is given by

   $$G(x,y;\sigma) = \frac{1}{2\pi\sigma^2} e^{-(x^2+y^2)/2\sigma^2} \tag{A.1}$$

   and σ is the standard deviation. The outcome of this convolution at a specific scale is strongly dependent on the relationship between the sizes of the blob structures in the image domain. Since our background is characterized by high pixel values and the blobs dimensions are known, every agent can be characterized by a local extrema of the resulting Gaussian scale-space representation $L(x,y,\sigma)$.
3. Assuming that the initial frame does not present any false positives, every single detected blob in the initial frame represents an agent (see Figure 2.7, left). The detected spatial locations of the agents are used as inputs for the Kalman filter Kalman (1960), where

the initial speeds of the agents are assumed to be zero. The estimates of the system states are based on the initial conditions and the sequence of the detected blobs along the experiments. Since the radius of the cylindrical robots are known, as well as their directions and linear speeds, a new measurement is easily casted as a good candidate input for the Kalman filter or as a new input for the designed regressive filter.

In this work, the agents are assumed to follow non-uniform translational motions, with a constant acceleration between consecutive frames. The uncertainties associated with the measurements of the positions induced by different lighting conditions are treated as white noise. The states x_k^i of the *i-th* agent at time k as well as the measurement z_k^i are described by linear SDE in the image domain:

$$\begin{cases} x_k^i = \Phi x_{k-1}^i + w_{k-1} \\ z_k^i = H x_k^i + v_k \end{cases} \tag{A.2}$$

where $x_k^i \in \Re^4$, $z_k^i \in \Re^2$.

w_{k-1} and v_k are WGN sources, respectively representing the process and measurement noises. They are assumed to be mutually statistically independent, and to be drawn from zero-mean multivariate Gaussian distributions with covariances Q and R. The covariances' matrices can be described as a function of the experimental parameters, such as the lighting variability across the experiments, the number of agents, etc. However, in our experiments, they were assumed to be constant. The evolution of the current state vector x_k^i over time is described by the transition matrix Φ derived from the non-uniform translational motion equations

$$\Phi = \begin{bmatrix} 1 & 0 & \Delta t & 0 \\ 0 & 1 & 0 & \Delta t \\ 0 & 0 & 1 & 0 \\ 0 & 0 & 0 & 1 \end{bmatrix}, \tag{A.3}$$

where Δt is equal to 0.1 s, as the videos were acquired at a constant frequency equal to 10 Hz, the time elapsed between consecutive frames was assumed to be constant.

H is a 2×4 transformation matrix that related the predicted state vectors x_k^i into the measurement domain:

$$H = \begin{bmatrix} 1 & 0 & 0 & 0 \\ 0 & 1 & 0 & 0 \end{bmatrix}. \tag{A.4}$$

Remark: The videos of all the experiments can be found online, at http://www.youtube.com/channel/UCCgwiDNHoyG9RJ2_pdyewmg.

B Chapter 4 - Details of Calculations

For the readers ease we introduce notations and collect formulas useful for the computation of the conditional probability density.

B.0.1 Collection of useful formulas

$$\sinh(x+y) = \sinh(x)\cosh(y) + \cosh(x)\sinh(y),$$

$$\cosh(x+y) = \cosh(x)\cosh(y) + \sinh(x)\sinh(y).$$

$$\int_{\mathbb{R}} e^{-ax^2-2bx-c}dx = \sqrt{\frac{\pi}{a}}e^{\frac{b^2-ac}{a}}, \qquad a>0$$

$$\int_{\mathbb{R}} \cosh[x\alpha]e^{-\frac{(x-\mu)^2}{\gamma}}dx = \sqrt{\pi\gamma}\cosh[\mu\alpha]e^{\frac{1}{4}\gamma\alpha^2} \tag{B.1}$$

$$\int_{\mathbb{R}} x\cosh[x\alpha]e^{-\frac{(x-\mu)^2}{\gamma}}dx = \sqrt{\pi\gamma}\left[\frac{\alpha\gamma}{2}\sinh(\mu\alpha) + \mu\cosh(\mu\alpha)\right]e^{\frac{1}{4}\gamma\alpha^2} \tag{B.2}$$

$$\int_{\mathbb{R}} x\sinh[x\alpha]e^{-\frac{(x-\mu)^2}{\gamma}}dx = \sqrt{\pi\gamma}\left[\frac{\alpha\gamma}{2}\cosh(\mu\alpha) + \mu\sinh(\mu\alpha)\right]e^{\frac{1}{4}\gamma\alpha^2} \tag{B.3}$$

From sections 9.24 and 9.25 of Gradshteyn and Ryzhik (1980), we extract:

$$\mathscr{D}_{-B}(x) = \frac{e^{-\frac{x^2}{4}}}{\Gamma(B)} \int_{\mathbb{R}^+} e^{-x\zeta - \frac{\zeta^2}{2}} \zeta^{B-1} d\zeta, \quad (\mathscr{R}(B) > 0) \quad \text{(see Gradshteyn and Ryzhik (1980), 9.241/2)} \tag{B.4}$$

$$\begin{cases} \mathscr{Y}_B(x) := \frac{1}{2}\left[\mathscr{D}_{-B}(x) + \mathscr{D}_{-B}(-x)\right] = \sqrt{\frac{2}{\pi}} \frac{e^{-\frac{x^2}{4}}}{\Gamma(B)} \int_{\mathbb{R}^+} \cosh(x\zeta) e^{-\frac{\zeta^2}{2}} \zeta^{B-1}\, d\zeta, \\ \frac{d^2}{dx^2}\left\{\mathscr{Y}_B(x)\right\} = \left[\frac{x^2}{4} + \left(B - \frac{1}{2}\right)\right] \mathscr{Y}_B(x), \quad (B \geq 0), \quad \text{(see Gradshteyn and Ryzhik (1980), 9.255/1)} \end{cases} \tag{B.5}$$

B.0.2 Quadratures

Let us define the couple of quadratures:

$$\mathscr{J}_i(m,s,B) = \int_{\mathbb{R}} x^i \mathscr{Y}_B(x) e^{-\frac{(x-m)^2}{2s}} dx, \;\; i = 0, 1. \tag{B.6}$$

0^{th}-order moment - $\mathscr{J}_0(m,B)$

Using the integral representation given in Eq.(B.5), we can write:

$$\begin{aligned} \mathscr{J}_0(m,s,B) &= \int_{\mathbb{R}} \left\{\mathscr{Y}_B(x) e^{-\frac{(x-m)^2}{2s}}\right\} dx \\ &= \sqrt{\frac{2}{\pi}} \frac{1}{\Gamma(B)} \int_{\mathbb{R}^+} \zeta^{[B-1]} e^{-\frac{\zeta^2}{2}} \left\{\int_{\mathbb{R}} \cosh(\zeta x) e^{-\frac{(x-m)^2}{2s} - \frac{x^2}{4}} dx\right\} d\zeta \\ \mathscr{J}_0(m,s,B) &= \sqrt{\frac{2}{\pi}} \frac{e^{-\frac{m^2}{2(2+s)}}}{\Gamma(B)} \int_{\mathbb{R}^+} \zeta^{[B-1]} e^{-\frac{\zeta^2}{2}} \left\{\int_{\mathbb{R}} \cosh(\zeta x) e^{-\frac{(2+s)}{4s}\left(x - \frac{2m}{2+s}\right)^2} dx\right\} d\zeta \end{aligned}$$

Now we use Eq.(B.1) with $\gamma = 4s/(2+s)$ and $\mu = 2m/(2+s)$ to get

$$\mathscr{J}_0(m,s,B) = 2\sqrt{\frac{2}{\pi}} \sqrt{\frac{\pi s}{(2+s)}} \frac{e^{-\frac{m^2}{2(2+s)}}}{\Gamma(B)} \int_{\mathbb{R}^+} \zeta^{[B-1]} e^{-\frac{\zeta^2}{2}\left[\frac{2-s}{2+s}\right]} \cosh\left[\frac{2m\zeta}{2+s}\right] d\zeta$$

Let us introduce the renormalization $\eta := \zeta\sqrt{\frac{2-s}{2+s}}$, which implies

$$\mathscr{J}_0(m,s,B) = \sqrt{\frac{2}{\pi}}2\sqrt{\frac{\pi s}{2+s}}\frac{e^{-\frac{m^2}{2(2+s)}}}{\Gamma(B)}\left[\sqrt{\frac{2+s}{2-s}}\right]^B \underbrace{e^{+\frac{m^2}{(4-s^2)}}e^{-\frac{m^2}{(4-s^2)}}}_{=1}\int_{\mathbb{R}^+}\eta^{[B-1]}\cosh\left[\frac{2m\eta}{\sqrt{4-s^2}}\right]e^{-\frac{\eta^2}{2}}\,d\eta. \tag{B.7}$$

Finally, using the definition Eq.(B.5), we end up with:

$$\mathscr{J}_0(m,s,B) = 2\sqrt{\frac{\pi s}{2+s}}\left[\sqrt{\frac{2+s}{2-s}}\right]^B e^{\frac{m^2 s}{2(4-s^2)}}\mathscr{Y}_B\left(\frac{2m}{\sqrt{4-s^2}}\right). \tag{B.8}$$

First order moment - $\mathscr{J}_1(m,s,B)$

From the definitions Eqs.(B.4) and (B.6), we can write:

$$\mathscr{J}_1(m,s,B) := \int_{\mathbb{R}}\left\{x\mathscr{Y}_B(x)e^{-\frac{(x-m)^2}{2s}}\right\}dx$$

From the previous equation and the definition of $\mathscr{J}_0(m,s,B)$ given in Eq.(B.6), we can write:

$$\frac{d}{dm}\mathscr{J}_0(m,s,B) \quad = \quad \int_{\mathbb{R}}\left\{\left[\frac{(x-m)}{s}\right]\mathscr{Y}_B(x)e^{-\frac{(x-m)^2}{2s}}\right\}dx = \frac{1}{s}\mathscr{J}_1(m,s,B) - \frac{m}{s}\mathscr{J}_0(m,s,B).$$

This is equivalent to the relation:

$$\mathscr{J}_1(m,s,B) = m\mathscr{J}_0(m,s,B) + s\left[\frac{d}{dm}\mathscr{J}_0(m,s,B)\right]. \tag{B.9}$$

Using Eqs.(B.8) and (B.9), the conditioned expectation reads:

$$\mathbb{E}(x|\mathscr{Z}_t) \quad = \quad \left.\frac{\mathscr{J}_1(m.b,B)}{\mathscr{J}_0(m,s,B)}\right|_t = m + s\left[\frac{d}{dm}\left(\log\{\mathscr{J}_0(m,s,B)\}\right)\right]\Big|_t = \frac{4}{4-s^2}m(z) + \frac{2s}{\sqrt{4-s^2}}f_B\left(\frac{2\,m(z)}{\sqrt{4-s^2}}\right) \tag{B.10}$$

Bibliography and Index Part VIII

Bibliography

A

Acebrón, J. A., Bonilla, L. L., Vicente, C. J. P., Ritort, F., and Spigler, R. (2005a). The kuramoto model: A simple paradigm for synchronization phenomena. *Reviews of Modern Physics*, 77(1):137–185. doi:10.1103/RevModPhys.77.137.

Acebrón, J. A., Bonilla, L. L., Vicente, C. J. P., Ritort, F., and Spigler, R. (2005b). The kuramoto model: A simple paradigm for synchronization phenomena. *Reviews of Modern Physics*, 77(1):137–185. doi:10.1103/RevModPhys.77.137.

Aldana, M., Dossetti, V., Huepe, C., Kenkre, V., and Larralde, H. (2007). Phase transitions in systems of self-propelled agents and related network models. *Physical Review Letters*, 98. doi:10.1103/PhysRevLett.98.095702.

Aureli, M. and Porfiri, M. (2010). Coordination of self-propelled particles through external leadership. *EPL*, 92(4). doi:10.1209/0295-5075/92/40004.

B

Baird, A. A., Kagan, J., Gaudette, T., Walz, K. A., Hershlag, N., and Boas, D. A. (2002). Frontal lobe activation during object permanence: Data from near-infrared spectroscopy. *NeuroImage*, 16(4):1120–1126. doi:10.1006/nimg.2002.1170.

Banner, A. D., Fernholz, R., and Karatzas, I. (2005). Atlas models of equity markets. *Ann. Appl. Prob. 15, 2296-2330*. doi:10.1214/105051605000000449.

Bellomo, N. and Dogbe, C. (2011). On the modeling of traffic and crowds: A survey of models, speculations, and perspectives. *SIAM Review*, 53(3):409–463. doi:10.1137/090746677.

Beneš, V. E. (1981). Exact finite dimensional filters for certain diffusion with nonlinear drifts. *Stochastics*, 5:65–92. doi:10.1080/17442508108833174.

Bensoussan, A., Frehse, J., and Yam, P. (2013). *Mean Field Games and Mean Field Type Control Theory*. Springer, New York, NY.

Berman, S., Halasz, A., Hsieh, M., and Kumar, V. (2009). Optimized stochastic policies for task allocation in swarms of robots. *IEEE Transactions on Robotics*, 25. doi:10.1109/TRO.2009.2024997.

Berman, S., Kumar, V., and Nagpal, R. (2011). Design of control policies for spatially inhomogeneous robot swarms with application to commercial pollination. In *2011 IEEE International Conference on Robotics and Automation*, pages 378–385, Piscataway, New Jersey,. IEEE. doi:10.1109/ICRA.2011.5980440.

Bertin, E., Droz, M., and Grégoire, G. (2006). Boltzmann and hydrodynamic description for self-propelled particles. *Physical Review E - Statistical, Nonlinear, and Soft Matter Physics*, 74(2). doi:10.1103/PhysRevE.74.022101.

Bialek, W., Cavagna, A., Giardina, I., Mora, T., Silvestri, E., Viale, M., and Walczak, A. M. (2012). Statistical mechanics for natural flocks of birds. *PNAS 13, vol. 109, 4786-4791*. doi:10.1073/pnas.1118633109.

Bonabeau, E., Dorigo, M., and Theraulaz, G. (1999). *Swarm Intelligence: From Natural to Artificial Systems*. Oxford University Press, New York, NY.

Braitenberg, V. (1984). *Vehicles: Experiments in Synthetic Psychology*. MIT Press, Cambridge, MA.

Brambilla, M., Ferrante, E., Birattari, M., and Dorigo, M. (2013). Swarm robotics: A review from the swarm engineering perspective. *Swarm Intelligence*, 7(1):1–41. doi:10.1007/s11721-012-0075-2.

Brambilla, M., Pinciroli, C., Birattari, M., and Dorigo, M. (2012). Property-driven design for swarm robotics. In *Proceedings of the 11th International Conference on Autonomous Agents and Multiagent Systems - Volume 1*, AAMAS '12, pages 139–146, Richland, SC. International Foundation for Autonomous Agents and Multiagent Systems. link to pdf file.

Bui, X.-N., Boissonnat, J.-D., Soueres, P., and Laumond, J.-P. (1994). Shortest path synthesis for dubins non-holonomic robot. In *Robotics and Automation, 1994. Proceedings., 1994 IEEE International Conference on*, pages 2–7 vol.1. doi:10.1109/ROBOT.1994.351019.

C

Chate, H., Ginelli, F., Gregoire, G., Peruani, F., and Raynaud, F. (2008). Modeling collective motion: Variations on the viczek model. *The European Physical Journal*, B64:451–456. doi:10.1140/epjb/e2008-00275-9.

Chatterjee, S. and Pal, S. (2010). A phase transition behaviour for brownian motions interacting through their ranks. *Prob. Theory Relat. Fields 147, 123-159*. doi:10.1007/s00440-009-0203-0.

Chavanis, P. H. (2008). Nonlinear mean-field fokker-planck equations. application to the chemotaxis of biological populations. *The European Physical Journal B*, 62(2):179–208. doi:10.1140/epjb/e2008-00142-9.

Couzin, I. D., Krause, J., Franks, N. R., and Levin, S. A. (2005). Effective leadership and decision-making in animal groups on the move. *Nature*, 433(7025):513–516. doi:10.1038/nature03236.

Cucker, F. and Smale, S. (2007a). Emergent behavior in flocks. *IEEE Transactions on Automatic Control*, 52(5). link to pdf file.

Cucker, F. and Smale, S. (2007b). On the mathematics of emergence. *Japanese Journal of Mathematics*, 2(1):197–227. doi:10.1007/s11537-007-0647-x.

D

Dai Pra, P. (1991). Stochastic control approach to reciprocal diffusion processes. *Applied Mathematics and Optimization*, 23(3):313–329. doi:10.1007/BF01442404.

Daum, F. E. (1985). Exact finite-dimensional nonlinear filters. *Proceedings of the 24th IEEE Conference on Decision & Control*, pages 1938–1945. doi:10.1109/TAC.1986.1104344.

Desai, J. P., Ostrowski, J., and Kumar, V. (1998). Controlling formations of multiple mobile robots. In *Proceedings - IEEE International Conference on Robotics and Automation*, volume 4, pages 2864–2869. doi:10.1109/ROBOT.1998.680621.

Dosseti, V. (2012). Cohesive motion in one-dimensionnal flocking. *Physica A: Math. Theor. 45*. doi:10.1088/1751-8113/45/3/035003.

Dubins, L. E. (1957). On curves of minimal length with a constraint on average curvature, and with prescribed initial and terminal positions and tangents. *American Journal of Mathematics*, 79(3):pp. 497–516. doi:10.2307/2372560.

E

Eftimie, R. (2012). Hyperbolic and kinetic models for self-organized biological aggregations and movement: A brief review. *Journal of mathematical biology*, 65(1):35–75. doi:10.1007/s00285-011-0452-2.

Esposito, J. (2008). Distributed grasp synthesis for swarm manipulation with applications to autonomous tugboats. In *Robotics and Automation, 2008. ICRA 2008. IEEE International Conference on*, pages 1489–1494. doi:10.1109/ROBOT.2008.4543412.

Esposito, J., Feemster, M., and Smith, E. (2008). Cooperative manipulation on the water using a swarm of autonomous tugboats. In *Robotics and Automation, 2008. ICRA 2008. IEEE International Conference on*, pages 1501–1506. doi:10.1109/ROBOT.2008.4543414.

F

Faria, J. J., Dyer, J. R. G., Clément, R. O., Couzin, I. D., Holt, N., Ward, A. J. W., Waters, D., and Krause, J. (2010). A novel method for investigating the collective behaviour of fish: Introducing 'robofish'. *Behavioral Ecology and Sociobiology 8, vol. 64, 1211-1218*. doi:10.1007/s00265-010-0988-y.

Feemster, M., Esposito, J., and Nicholson, J. (2006). Manipulation of large object by swarms of autonomous marine vehicles, part i: Rotational motions. In *System Theory, 2006. SSST '06. Proceeding of the Thirty-Eighth Southeastern Symposium on*, pages 205–209. doi:10.1109/SSST.2006.1619073.

Fernholz, R. (2002). *Stochastic Portfolio Theory*. Springer, New York.

Filliger, R. and Hongler, M.-O. (2005). Syphon dynamics – a soluble model of multi-agent cooperative behavior. *Europhysics Letters*, 70(3):285–291. doi:10.1209/epl/i2004-10492-x.

Fink, J., Hsieh, M., and Kumar, V. (2008). Multi-robot manipulation via caging in environments with obstacles. In *Robotics and Automation, 2008. ICRA 2008. IEEE International Conference on*, pages 1471–1476. doi:10.1109/ROBOT.2008.4543409.

Frank, T. D. (2005). *Nonlinear Fokker-Planck Equations*. Springer series in Synergetics. Springer: Complexity, New York, NY.

G

Gallay, O. and Hongler, M.-O. (2008a). Cooperative dynamics of loyal customers in queueing networks. *Journal of Systems Science and Systems Engineering*, 17(2):241–254. doi:10.1109/ICSSSM.2006.320780.

Gallay, O. and Hongler, M.-O. (2008b). Market sharing dynamics between two service providers. *European Journal of Operational Research*, 190(1):241–254. doi:10.1016/j.ejor.2007.06.018.

Gallay, O. and Hongler, M.-O. (2009a). Circulation of autonomous agents in production and service networks. *International Journal of Production Economics*, 120:378–388. doi:10.1016/j.ijpe.2008.01.012.

Gallay, O. and Hongler, M.-O. (2009b). Multi-agent adaptive mechanism leading to optimal real-time load sharing. In *Proceedings of MATHMOD 2009, 6th Vienna International Conference on Mathematical Modelling, Austria*. link to pdf file.

Gazi, V. and Fidan, B. (2007). Coordination and control of multi-agent dynamic systems: Models and approaches. In Şahin, E., Spears, W., and Winfield, A., editors, *Swarm Robotics*, volume 4433 of *Lecture Notes in Computer Science*, pages 71–102. Springer Berlin Heidelberg. doi:10.1007/978-3-540-71541-2_6.

Gazi, V. and Passino, K. M. (2004). A class of attractions/repulsion functions for stable swarm aggregations. *International Journal of Control*, 77(18):1567–1579. doi:10.1109/CDC.2002.1184277.

Gillespie, D. T. (1992). *Markov Processes*. Academic Press, Waltham, Massachusetts.

Gradshteyn, I. S. and Ryzhik, I. M. (1980). *Table of integrals series and products*. Academic Press.

Gribovskiy, A., Halloy, J., Deneubourg, J. L., Bleuler, H., and Mondada, F. (2010). Towards mixed societies of chickens and robots. *IEEE/RSJ 2010 International Conference on Intelligent Robots and Systems, Conference Proceedings pp. 4722-4728*. doi:10.1109/IROS.2010.5649542.

Guéant, O., Lasry, J.-M., and Lions, P.-L. (2011). Mean field games and applications. In *Paris-Princeton Lectures on Mathematical Finance 2010*, volume 2003 of *Lecture Notes in Mathematics*, pages 205–266. Springer Berlin Heidelberg. doi:10.1007/978-3-642-14660-2_3.

H

Habibi, G., Kingston, Z., Xie, W., Jellins, M., and McLurkin, J. (2015). Distributed centroid estimation and motion controllers for collective transport by multi-robot systems. In *Robotics and Automation (ICRA), 2015 IEEE International Conference on*, pages 1282–1288. doi:10.1109/ICRA.2015.7139356.

Halloy, J., Sempo, G., Caprari, G., Rivaullt, C., Asadpour, M., Ame, J. M., Detrain, C., Correl, N., Martinoli, A., and Mondada, F. (2007). Social integration of robots into groups of cockroaches to control self-organized choices. *Science*, 318(5853):1155–1158. doi:10.1126/science.1144259.

Hamann, H. and Wörn, H. (2008). A framework of space&time continuous models for algorithm design in swarm robotics. *Swarm Intelligence*, 2(2-4):209–239. doi:10.1007/s11721-008-0015-3.

Han, J., Li, M., and Guo, L. (2006). Soft control on collective behavior of a group of autonomous agents by a shill agent. *Journal of Systems Science and Complexity*, 19(1):54–62. doi:10.1007/s11424-006-0054-z.

Hongler, M.-O. (1981). Study of a class of nonlinear stochastic process - boomerang behavior of the mean. *Physica D*, 2:353–369. doi:10.1016/0167-2789(81)90014-2.

Hongler, M.-O., Filliger, R., and Gallay, O. (2014). Local versus nonlocal barycentric interactions in 1d agent dynamics. *Mathematical Biosciences and Engineering*, 11(2):303–315. doi:10.3934/mbe.2014.11.303.

Hongler, M.-O., Gallay, O., and Hashemi, F. (2015). Imitation's impact on the dynamics of long-wave growth. *Economic Modeling, (under revision)*.

Hongler, M.-O. and Ryter, D. M. (1978). Hard mode stationary states generated by fluctuations. *Zeitschrift für Physik B Condensed Matter and Quanta*, 31(3):333–337. doi:10.1007/BF01352359.

Hongler M. O., Filliger R., P. B. and Rodriguez, J. (2012). *On Stochastic Processes Driven By Ballistic Noise Sources*, chapter 1, pages 1–31. Ed. M. R. Adhikari.

Hongler M. O., R. F. and Blanchard, P. (2006). Soluble models for dynamics driven by a super-diffusive noise. *Physica A 370, 301-355*. doi:10.1016/j.physa.2006.02.036.

Hsieh, M. A., Kumar, V., and Chaimowicz, L. (2008). Decentralized controllers for shape generation with robotic swarms. *Robotica*, 26(5):691–701. doi:10.1017/S0263574708004323.

Hsieh, M.-A., Loizou, S., and Kumar, V. (2007). Stabilization of multiple robots on stable orbits via local sensing. In *Proceedings - IEEE International Conference on Robotics and Automation*, pages 2312–2317, Piscataway, New Jersey,. IEEE. doi:10.1109/ROBOT.2007.363664.

I

Ichiba, T., Papathanakos, V., Banner, A., Karatzas, I., and Fernholz, R. (2011). Hybrid atlas model. *Ann. Appl. Prob. 21(2) 609-644*. doi:10.1214/10-AAP706.

J

Jazwinski, A. H. (1970). *Stochastic Processes and Filtering Theory*. Academic Press.

Ji, Z., Wang, Z., Lin, H., and Wang, Z. (2009). Interconnection topologies for multi-agent coordination under leader-follower framework. *Automatica*, 45(12):2857–2863. doi:10.1016/j.automatica.2009.09.002.

Jing, H. and Lin, W. (2010). New strategy of the shill: 'consistent moving'. In *Control Conference (CCC), 2010 29th Chinese*, pages 4459–4464. link to pdf file.

Jourdain, B. and Malrieu, F. (2008). Propagation of chaos and Poincaré inequalities for a system of particles interacting through their CDF. *Annals of Applied Probability*, 18(5):1706–1736.

K

Kalman, R. E. (1960). A new approach to linear filtering and prediction problems 1. *Journal Of Basic Engineering*, 82(Series D):35–45. doi:10.1115/1.3662552.

Kernbach, S., editor (2013). *Handbook of Collective Robotics: Fundamentals and Challenges*. Pan Stanford Publishing, Singapore, Singapore.

Kernbach, S., Häbe, D., Kernbach, O., Thenius, R., Radspieler, G., Kimura, T., and Schmickl, T. (2013). Adaptive collective decision-making in limited robot swarms without communication. *International Journal of Robotics Research*, 32(1):35–55. doi:10.1177/0278364912468636.

Krishnanand, K. N. and Ghose, D. (2005). Formations of minimalist mobile robots using local-templates and spatially distributed interactions. *Robotics and Autonomous Systems*, 53(3-4):194–213. doi:10.1016/j.robot.2005.09.006.

L

Leonard, N. E. (2013). Multi-agent system dynamics: Bifurcation and behavior of animal groups. In *IFAC Proceedings Volumes (IFAC-PapersOnline)*, volume 9, pages 307–317, Amsterdam, Netherlands. Elsevier. doi:10.3182/20130904-3-FR-2041.00211.

Leonard, N. E., Paley, D. A., Lekien, F., Sepulchre, R., Fratantoni, D. M., and Davis, R. E. (2007). Collective motion, sensor networks, and ocean sampling. *Proceedings of the IEEE*, 95(1):48–74. doi:10.1109/JPROC.2006.887295.

Lerman, K., Martinoli, A., and Galstyan, A. (2005). A review of probabilistic macroscopic models for swarm robotic systems. In *Lecture Notes in Computer Science*, volume 3342, pages 143–152, New York, NY. Springer. doi:10.1007/978-3-540-30552-1_12.

M

Martinoli, A., Ijspeert, A. J., and Mondada, F. (1999). Understanding collective aggregation mechanisms: From probabilistic modelling to experiments with real robots. *Robotics and Autonomous Systems*, 29(1):51–63. doi:10.1016/S0921-8890(99)00038-X.

McKean Jr., H. P. (1966). A class of markov processes assocaietd with nonlinear parabolic equations. *Proc. Natl. Acad. Sci USA*, 56(6):1907–1911. link to pdf file.

Michini, M., Rastgoftar, H., Hsieh, M. A., and Jayasuriya, S. (2014). Distributed formation control for collaborative tracking of manifolds in flows. In *Proceedings of the American Control Conference*, pages 3874–3880. doi:10.1109/ACC.2014.6859204.

Mondada, F., Bonani, M., Raemy, X., Pugh, J., Cianci, C., Klaptocz, A., Zufferey, J.-C., Floreano, D., and Martinoli, A. (2006). The e-puck, a robot designed for education in engineering. *Robotics*, 1(1):59–65. link to pdf file.

Mondada, F., Martinoli, A., Correll, N., Gribovskiy, A., Halloy, J. I., Siegwart, R., and Deneubourg, J.-L.. (2011). A general methodology for the control of mixed natural-artificial societies. In Kernbach, S., editor, *Kernbach2013 of Collective Robotics*, pages 399–428. Pan Stanford.

N

Nourian, M., Caines, P., Malhamé, R., and Huang, M. (2010). Leader-follower cucker-smale type flocking synthesized via mean field stochastic control theory. In Angeles, J., Boulet, B., Clark, J., Kövecses, J., and Siddiqi, K., editors, *Brain, Body and Machine*, volume 83 of *Advances in Intelligent and Soft Computing*, pages 283–298. Springer Berlin Heidelberg. doi:10.1007/978-3-642-16259-6_22.

O

Olfati-Saber, R. (2006). Flocking for multi-agent dynamic systems: Algorithms and theory. *IEEE Transactions on Automatic Control*, 51(3):401–419. doi:10.1109/TAC.2005.864190.

P

Pal, S. and Pitman, J. (2008). One dimensional brownian particles with rank-dependent drifts. *Ann. Appl. Prob. 18 2179-2207*. doi:10.1214/08-AAP516.

Paley, D., Leonard, N., Sepulchre, R., Grunbaum, D., and Parrish, J. (2007). Oscillator models and collective motion. *IEEE Control Systems Magazine*, 27:89–105. link to pdf file.

Paley, D. A. and Leonard, N. E. (2006). Collective motion of self-propelled particles: Stabilizing symmetric formations on closed curves. In *45th IEEE Conference on Decision and Control*, pages 5067–5072. doi:10.1109/CDC.2006.377462.

Pequito, S., Aguiar, A., Sinopoli, B., and Gomes, D. (2011). Nonlinear estimation using mean field games. In *Network Games, Control and Optimization (NetGCooP), 2011 5th International Conference on*, pages 1–5. link to pdf file.

Pereira, G. A. S., Kumar, V., and Campos, M. F. M. (2002). Decentralized algorithms for multirobot manipulation via caging. *International Journal of Robotics Research*, 23:783–795. doi:10.1177/0278364904045477.

Pimenta, L. C. d. A., Pereira, G. A. S., Michael, N., Mesquita, R. C., Bosque, M. M., Chaimowicz, L., and Kumar, V. (2013). Swarm coordination based on smoothed particle hydrodynamics technique. *IEEE Transactions on Robotics*, 29:383–399. doi:10.1109/TRO.2012.2234294.

Prorok, A., Correll, N., and Martinoli, A. (2011). Multi-level spatial modeling for stochastic distributed robotic systems. *The International Journal of Robotics Research*, 30:574–589. doi:10.1177/0278364910399521.

R

Reynolds, C. W. (1987). Flocks, herds, and schools: A distributed behavioral model. *Computers (ACM)*, 21(4):25–34. doi:10.1145/37401.37406.

Rogers, L. C. G. and Pitman, J. W. (1981). Markov functions. *Ann. of Prob. 9(4), 573-582*. doi:10.1214/aop/1176994363.

S

Sabattini, L., Secchi, C., and Fantuzzi, C. (2012). Closed-curve path tracking for decentralized systems of multiple mobile robots. *Journal of Intelligent & Robotic Systems*, 71(1):109–123. doi:10.1007/s10846-012-9763-9.

Sartoretti, G. (2015). Leader-based versus soft control of multi-agent swarms. In *SWARM 2015 - International Symposium on Swarm Behavior and Bio-Inspired Robotics*. link to pdf file.

Sartoretti, G. and Hongler, M.-O. (2013a). Self-organized mixed canonic-dissipative dynamics for brownian planar agents. In *EUROCAST 2013 - International Conference on Computer Aided Systems Theory*, volume 1, pages 45–52. link to pdf file.

Sartoretti, G. and Hongler, M.-O. (2013b). Self-organized mixed canonical-dissipative dynamics for brownian planar agents. *Cybernetics and Physics*, vol. 2(no. 1):41–46. link to pdf file.

Sartoretti, G. and Hongler, M.-O. (2013c). Soft control of self-organized locally interacting brownian planar agents. In Moreno-Díaz, R., Pichler, F., and Quesada-Arencibia, A., editors, *Computer Aided Systems Theory - EUROCAST 2013*, volume 8111 of *Lecture Notes in Computer Science*, pages 45–52. Springer Berlin Heidelberg. doi:10.1007/978-3-642-53856-8_6.

Sartoretti, G. and Hongler, M.-O. (2013d). Soft control of swarms: Analytical approach. In *ICAART 2013 - Proceedings of the 5th International Conference on Agents and Artificial Intelligence*, volume 1, pages 147–153. link to pdf file.

Sartoretti, G. and Hongler, M.-O. (2016). Interacting brownian swarms: Analytical results. *Entropy*, 18, 27. doi:10.3390/e18010027.

Sartoretti, G., Hongler, M.-O., Elias de Oliveira, M., and Mondada, F. (2014a). Decentralized self-selection of swarm trajectories: From dynamical system theory to robotic implementation. *Swarm Intelligence*, vol. 8(no. 4):329–351. doi:10.1007/s11721-014-0101-7.

Sartoretti, G., Hongler, M.-O., and Filliger, R. (2014b). The estimation problem and heterogenous swarms of autonomous agents. In *SMTDA 2014 - Stochastic Modeling Techniques and Data Analysis International Conference*, volume 1. link to pdf file.

Sartoretti, G., Shaw, S., and Hsieh, M. A. (2016). Distributed planar manipulation in fluidic environments. In *ICRA 2016 - International Conference on Robotics and Automation*. IEEE Transactions. link to preprint pdf file.

Schwager, M., Michael, N., Kumar, V., and Rus, D. (2011). Time scales and stability in networked multi-robot systems. In *Proceedings - IEEE International Conference on Robotics and Automation*, pages 3855–3862, Piscataway, New Jersey,. IEEE. doi:10.1109/ICRA.2011.5979847.

Schweitzer, F. (2003). *Brownian Agents and Active Particles*. Springer, New York, NY.

Schweitzer, F., Ebeling, W., and Tilch, B. (2001). Statistical mechanics of canonical-dissipative systems and applications to swarm dynamics. *Physical Review E - Statistical, Nonlinear, and Soft Matter Physics*, 64(2 I):211101–211112. doi:10.1103/PhysRevE.64.021110.

Sepulchre, R., Paley, D. A., and Leonard, N. E. (2007). Stabilization of planar collective motion: All-to-all communication. *IEEE Transactions on Automatic Control*, 52(5):811–824. doi:10.1109/TAC.2007.898077.

Sepulchre, R., Paley, D. A., and Leonard, N. E. (2008). Stabilization of planar collective motion with limited communication. *IEEE Transactions on Automatic Control*, 53(3):706–719. doi:10.1109/TAC.2008.919857.

Song, P. and Kumar, V. (2002). A potential field based approach to multi-robot manipulation. In *Proceedings. ICRA 2002. IEEE International Conference on Robotics and Automation*, volume 2, pages 1217–1222. doi:10.1109/ROBOT.2002.1014709.

Strogatz, S. H. (2000). From kuramoto to crawford: Exploring the onset of synchronization in populations of coupled oscillators. *Physica D: Nonlinear Phenomena*, 143(1-4):1–20. doi:10.1016/S0167-2789(00)00094-4.

T

Tanner, H. G., Pappas, G. J., and Kumar, V. (2004). Leader-to-formation stability. *IEEE Transactions on Robotics and Automation*, 20(3):443–455. doi:10.1109/TRA.2004.825275.

Taylor, J. C. (1989). The minimal eigenfunctions characterize the Ornstein-Uhlenbeck process. *The Annals of Probability*, 17(3):1055–1062. doi:10.1214/aop/1176991256.

Tsiotras, P. and Castro, L. I. R. (2011). Extended multi-agent consensus protocols for the generation of geometric patterns in the plane. In *Proceedings of the 2011 American Control Conference*, pages 3850–3855, Piscataway, New Jersey,. IEEE. doi:10.1109/ACC.2011.5990927.

V

Vaughan, R., Sumpter, N., Henderson, J., Frost, A., and Cameron, S. (2000). Experiments in automatic flock control. *Robotics and Autonomous Systems 1, vol. 31, 109-117.* doi:10.1016/S0921-8890(99)00084-6.

Viczek, T., Czirok, A., Jacob, E. B., Cohan, I., and Schochet, O. (1995). Novel type of phase transitions in a system of self-driven particles. *Physical Review Letters*, 75:1226–1229. doi:10.1103/PhysRevLett.75.1226.

W

Wang, L. and Guo, L. (2008). Robust consensus and soft control of multi-agent systems with noises. *Journal of Systems Science and Complexity 3, vol. 21, 406-415.* doi:10.1007/s11424-008-9122-x.

Wang, X., Han, J., and Han, H. (2011). Special agents can promote cooperation in the population. *PLoS ONE 12, vol. 6.* doi:10.1371/journal.pone.0029182.

Wang, Y., Mao, X.-Z., and Liu, J.-P. (2009). Soft control for swarm systems with simple attraction and repulsion functions. *Proceedings of the 2nd International Conference on Intelligent Networks and Intelligent Systems, pp. 482-485.* doi:10.1109/ICINIS.2009.129.

Y

Yang, T., Mehta, P. G., and Meyn, S. P. (2013). Feedback particle filter. *IEEE Transactions on Automatic Control*, 58(10):2465–2480. doi:10.1109/TAC.2013.2258825.

Yates, C. A., Erban, R., Escudero, C., Couzin, I. D., Buhl, J., Kevrekidis, I. G., Mainia, P. K., , and Sumpter, D. J. T. (2009). Inherent noise can facilitate coherence in collective swarm motion. *PNAS 14, vol. 106, 5464-5469.* doi:10.1073/pnas.0811195106.

Yates, R. C. (1947). *A Handbook on Curves and their Properties.* National Council of Teachers of Mathematics, Reston, VA.

Z

Zhang, F. and Leonard, N. E. (2007). Coordinated patterns of unit speed particles on a closed curve. *Systems and Control Letters*, 56(6):397 – 407. doi:10.1016/j.sysconle.2006.10.027.

Zola, R. S., Lenzi, E. K., Evangelista, L. R., and Barbero, G. R. S. (2008). Exact solutions for a diffusion equation with a nonlinear external force. *Physical Review E*, 75(4). doi:doi:10.1016/j.physleta.2007.12.007.

Index

agents
  agent, **5**
  decision capability, **5**
  deliberative agent, **6**
  dynamic, **7**, **9**, 23, 39, 63, 73, 86, 96, 113
  nominal dynamic, **7**
  observation range, 88
  planar agent, **23**, 39, 62, 85, 86
  reactive agent, **6**
  state, **7**
  swarm, **7**
analytical results, **8**, 28, 42, 64, 78, 85, 130
ASV, *see* Autonomous Surface Vehicle
Autonomous Surface Vehicle, **125**

ballistic noise, **99**
barycenter, **24**, 97, 117
BCM, *see* Braitenberg control mechanism
Braitenberg control mechanism, **44**, 62, 127
Brownian agents, **8**, 14, 21, 38, 85, 95, 113, 131
Burger's equation, 114

Canon EOS 7D, 149
Cassini's ovals, 31, 56
CC, *see* Conditional Closure
Central Limit Theorem, 9, **49**
centralized dynamic, **7**
collision avoidance mechanism, 48
conditional closure, **126**
control mechanism, 125
  scalability, **125**
controller
  PID controller, 137
crowd
  crowd behavior, **4**, 13
  crowd control, **4**

decentralized dynamic, **7**, 14, 21, 23
decentralized manipulation, 125
diffusion process, **8**, 86, 96
drift, **9**, 97
Dubins path, **135**
dynamical systems, 131
  Fokker-Planck Equation, **9**, 12, 25, 40, 74, 88, 113
  mean-field approach, **9**, 12, 27, 39, 74, 88, 95, 113

e-puck mobile robot, **47**
estimation problem, 72
ethology, **4**, 14, 15, 85
experimental validation, 3, 52, 137
exponential spiral, **129**

FCFS, *see* First-Come, First-Serve (queueing systems)
Feedback Particle Filter, **75**
flocking, **8**, 13, 95, 98, 115
FPE, *see* Fokker-Planck Equation (dynamical systems)

game theory, 14, 74
  mean-field game, **74**
group
  coherent group, **3**
  cohesive group, **13**

  - group dynamics, **3**
- group description
  - macroscopic representation, 123
- group representation
  - macroscopic representation, **4**
  - microscopic representation, **4**, 123

- HAM, *see* Hybrid Atlas Model
- Hamiltonian function, 31, **39**, 86
- hard control, **11**, 72
- heterogeneous swarm, **9**, 14, 15, 71, 85, 95, 117
- homogeneous swarm, **9**, 12, 41, 85, 90, 95, 115, 125
- Hybrid Atlas Model, **96**, 118

- individuals, 3, *see also* agents
- interactions, **7**
  - global interactions, **7**, 73, 97
  - interaction network, **7**
  - local interactions, **7**, 13, 21, 90, 113
  - stigmergic interactions, **17**, 17, 140

- Kalman-Bucy filter, 72, 149
- Kullback-Leibler distance, **75**

- leader-based control, *see* hard control
- limit cycle, **28**, 52, 85, 88

- majority windows algorithm, **47**
- MAS, *see* multi-agent systems
- MCD, *see* mixed canonical-dissipative dynamic
- MF, *see* mean-field (dynamical systems)
- mixed canonical-dissipative dynamic, **23**, 39, 85
- multi-agent systems
  - emergent behavior, **5**, 13, 14, 21, 38, 95
  - heterogeneous MAS, *see* heterogeneous swarm
  - homogeneous MAS, *see* homogeneous swarm
  - multi-agent system, **7**
- MWA, *see* majority windows algorithm

- non-holonomic robot, 47, 125
- numerical simulations, **8**, 29, 43, 63, 79, 93, 95, 101, 116, 121, 131, 135

- order parameter, **54**
- ordinary differential equation, 90

- particle, **5**
- polar coordinates, 131
- potential landscape, **12**, 87
- potential-based dynamic, **12**

- queueing network, 13

- rank-based Brownian motions, **96**, 113
- robotics, 15
  - robotic implementation, 44
  - robotic shill, **12**, 15, 85
  - robotics control mechanism, **4**
  - swarm robotics, **4**, 14, 44, 137
- rules of Reynolds, **13**

- SDE, *see* stochastic differential equation
- sociology, **4**
  - crowd control, 103
- soft control, **11**, 15, 85, 96
  - constructive soft control, **11**, 15, 103
  - destructive soft control, **11**, 98
- soliton, 114
- special agents, **10**
  - leader, **10**, 14, 73
    - apparent leader, **10**
    - hidden leader, **10**, 72
  - shill, **11**, 15, 90, 95, 101
    - apparent shill, **11**, 101
    - hidden shill, **11**, 85, 90, 101
- stationary regime, 88
- stochastic differential equation, **8**, 23, 38, 86, 131, 150
- swarm control
  - planned control, **9**
  - real-time control, **9**
- swarm interactions, 111

- Weber parabolic function, **76**

WGN, *see* White Gaussian Noise
White Gaussian Noise, **9**, 21, 38, 63, 73, 97, 113, 131, 150
wild dogs, 12

Guillaume SARTORETTI

Born 01.10.1989 in Geneva (CH)
Nationality: Swiss
Address: 34 rue de la Servette, 1202 Genève
guillaume.sartoretti@gmail.com
(0041)79/584 46 08
https://www.researchgate.net/profile/Guillaume_Sartoretti

Education

April 2016	**PhD. from EPFL (Swiss Federal Institute of Technology), Switzerland** Title: *Control of Agent Swarms in Random Environments* Supervisor: Prof. Max-Olivier Hongler Enrolled in the "Robotics, Control and Intelligent Systems" Doctoral School
March 2012	Master of Science in Mathematics and Computer Science (University of Geneva)
June 2010	Bachelor of Science in Mathematics and Computer Science (University of Geneva)

Professional Experience

2012 - 2016	Teaching assistant for the Laboratory of Microengineering for Manufacturing (LPM), and the Laboratoire des Systèmes Robotiques (LSRO), *EPFL* (CH)
2013 - 2016	System administrator for the LPM laboratory, *EPFL* (CH)
2009 - 2012	IT support for students at the *University of Geneva* (CH)

Professional Activities

2015	Reviewer for the *International Conference on Intelligent Robots and Systems*.
2015	Session chair at the *First International Symposium on Swarm Behavior and Bio-Inspired Robotics*.
2014	Reviewer for the *International Conference on Robotics and Automation*.
2013	Session chair at the *International Conference on Agents and Artificial Intelligence*.

Invited Lectures, Seminars and Colloquia

2016	EPFL, Informal private presentation, DISAL laboratory, January 28th.
2015	Drexel University, Private presentation, SAS and GRASP laboratories, Sept. 29th.

Teaching

2012-2016	Teaching assistant, "*Vibrational Systems*", EPFL, course MICRO-300.
2012-2016	Teaching assistant, "*Practical Works in Manufacturing and Robotics*", EPFL, course MICRO-442.
2013-2015	Teaching assistant, "*Micro-informatics*", EPFL, course MICRO-315.
2013-2015	Teaching assistant, "*A guided tour for engineers in applied stochastic modeling*", EPFL, course MICRO-541.

Mentoring

2015-2016	Semester Project: Astrid Petitjean, “*Optimal dynamic component matching in flexible assembly lines*”.
2015-2016	Semester Project: Fabien Crépon, “*Optimal hedging stocks for random flexible production flows*”.
2013-2014	Semester Project: Fabianna Mantuano, “*Etude d’optimisation locale versus globale dans un flux de production*”.

Publications: Refereed Conference Papers

2016	G. Sartoretti, S. Shaw, and M. Ani Hsieh. Distributed planar manipulation in fluidic environments. In *ICRA 2016 - International Conference on Robotics and Automation*. IEEE Transactions.
2015	G. Sartoretti. Leader-based versus soft control of multi-agent swarms. In *SWARM 2015 - International Symposium on Swarm Behavior and Bio-Inspired Robotics.*
2014	G. Sartoretti, M.-O. Hongler, and R. Filliger. The estimation problem and heterogenous swarms of autonomous agents. In *SMTDA 2014 - Stochastic Modeling Techniques and Data Analysis International Conference*, volume 1.
2013	G. Sartoretti and M.-O. Hongler. Self-organized mixed canonic-disipative dynamics for brownian planar agents. In *EUROCAST 2013 - International Conference on Computer Aided Systems Theory*, volume 1, pages 45-52.
2013	G. Sartoretti and M.-O. Hongler. Soft control of swarms: Analytical approach. In *ICAART 2013 - Proceedings of the 5th International Conference on Agents and Artificial Intelligence*, volume 1, pages 147-153.
2012	G. Sartoretti, J.-L. Falcone, B. Chopard, and M. J. Gander. Decentralized method for trafic monitoring. In *ACRI 2012 - Cellular Automata for Research and Industry*, volume 1, pages 464-473.

Publications: Refereed Journal Papers and Book Chapters

2016	G. Sartoretti and M.-O. Hongler. Interacting brownian swarms: Analytical results. *Entropy*, 18, 27.
2014	G. Sartoretti, M.-O. Hongler, M. Elias de Oliveira, and F. Mondada. Decentralized self-selection of swarm trajectories: From dynamical system theory to robotic implementation. *Swarm Intelligence*, vol. 8(no. 4):329-351.
2013	G. Sartoretti and M.-O. Hongler. Soft control of self-organized locally interacting brownian planar agents. In *Lecture Notes in Computer Science*, pages 45-52. Springer Berlin Heidelberg.
2013	G. Sartoretti and M.-O. Hongler. Self-organized mixed canonical-dissipative dynamics for brownian planar agents. *Cybernetics and Physics*, vol. 2(no. 1):41-46.
2013	B. Barbieri, G. Sartoretti, J.-L. Falcone, B. Chopard, and M. J. Gander. Trafic prediction based on a local exchange of information. *Journal of Cellular Automata*, 8(5-6):429-441.
2012	G. Sartoretti, J.-L. Falcone, B. Chopard, and M. J. Gander. Decentralized method for trafic monitoring. In *Lecture Notes in Computer Science*, pages 464-473. Springer Berlin Heidelberg.